2014

Synthesis and Reactivity of HY Zeolite-Supported Rhodium Complexes

Artem D. Vityuk
University of South Carolina - Columbia

Recommended Citation

Vityuk, A. D.(2014). *Synthesis and Reactivity of HY Zeolite-Supported Rhodium Complexes.* (Doctoral dissertation). Retrieved from https://scholarcommons.sc.edu/etd/2694

SYNTHESIS AND REACTIVITY OF HY ZEOLITE-SUPPORTED RHODIUM COMPLEXES

by

Artem D. Vityuk

Bachelor of Science
D.I. Mendeleev University of Chemical Technology, 2006

Master of Science
D.I. Mendeleev University of Chemical Technology, 2008

Submitted in Partial Fulfillment of the Requirements

For the Degree of Doctor of Philosophy in

Chemical Engineering

College of Engineering and Computing

University of South Carolina

2014

Accepted by:

Michael D. Amiridis, Major Professor

Oleg S. Alexeev, Committee Member

Richard D. Adams, Committee Member

Andreas Heyden, Committee Member

Lacy K. Ford, Vice Provost and Dean of Graduate Studies

DEDICATION

To my parents…

There are no words that could fully express amount of support, inspiration and encouragement that my parents gave me during these years. With all of my heart – Thank you…

ACKNOWLEDGEMENTS

First of all, I would like to acknowledge my advisor Dr. Michael Amiridis. He is the person who gave me an opportunity to work on one of the most exciting research projects I have ever been involved in. His wise advice, scientific guidance and research directions allowed me to grow professionally throughout years at USC and open new horizons in catalysis. I also would like to emphasize the fantastic amount of motivation and support I have been receiving from him and, most importantly, his strong belief in me as in a researcher. I can not overstate the importance of such attitude and I will definitely remember Dr. Amiridis not only as a great research advisor but as one of the most kind, friendly and supportive people I have ever met in my life.

I would like to acknowledge Dr. Oleg Alexeev for all of his time and effort he invested in me. Today I can truly and confidently say that virtually all technical knowledge of heterogeneous catalysis and, especially, of its experimental part that I obtained during my stay at USC I learned from him. His firm principles of doing fundamental research "right", day-to-day discussions and, quite often, debates shaped me as a researcher. Among the key rules I learned from him which I am taking with me into my career are: be always critical about the experimental results, think creatively and never give up. I also would like

to thank him and his family for tremendous amount of help I received in situations outside the school. I will always remember him being near by when I needed him.

I would like to acknowledge Dr. Andreas Heyden for valuable discussions we had on topics of my research and on more general scientific matters. I enjoyed the “Advanced Mass-Transport” class which he taught and I loved being a Teaching Assistant in one of his classes later. Dr. Heyden is one of the most optimistic, positive and encouraging people I have ever met who could easily spark enthusiasm in occasions when things did not seem to go very well. Also, I would like to thank him for such dedication and passion for science that he has and which he conveys to students. I personally learned a lot from such attitude which basically tells me: “whatever you do – you should love doing it”.

I would like to acknowledge Dr. Richard Adams for a greatest expertise and precious suggestions he provided reviewing my work during the comprehensive exam and my pre-defense. I enjoyed reading Dr. Adams’ papers which elegantly show that rigorous organometallic chemistry and surface science could be combined to yield catalysts with exceptional properties. I sincerely thankful Dr. Adams for joining my committee which gave me an opportunity to get an opinion on my work of one of the world’s first experts in the field of organometallic chemistry.

I would like to acknowledge Dr. John Monnier for being such a charismatic person always ready to help and consult on quite complex scientific questions. To be honest, he is among few people I was lucky to work with who has such immense knowledge of heterogeneous catalysis fundamentals, its industrial applications and equipment design. I am very thankful Dr. Monnier for teaching me how to use VICI valves which I implemented in my very first catalyst testing station which I built. It is his approach to apply automatic control to testing units which enabled me to conduct research in a more efficient way.

I would like to acknowledge Dr. Christopher Williams for frequent and fruitful conversations we had regarding my research and, more specifically, spectroscopy applications in my project. I would like to recognize Dr. Williams ability to motivate and inspire for better work. Also, I will always remember our road trip from Columbia to Detroit which he organized in order to help students to attend the North American Catalysis Society Meeting (NAM) meeting. He is easily one of friendliest professors I encountered.

I would like to acknowledge Dr. Donna Chen and Dr. Michael Myrick for being great mentors. I would like to mention these professors as not only outstanding professionals and a few of the brightest people that I had chance to interact with but also as exceptional personalities. I will never forget Dr. Chen style of teaching which sparked my deep interest in Surface Science. Also, I was fascinated with Dr. Myrick's ability to explain the most complex concepts of Molecular Spectroscopy in simple and easily understandable terms when I took his class.

I would like to acknowledge research and administrative staff at Stanford Synchrotron Radiation Laboratory (SSRL), a national user facility operated by Stanford University on behalf of the U.S. Department of Energy, Office of Basic Energy Sciences. I am very thankful to Cynthia Patty for the help and assistance she provided during X-ray Absorption Measurements (XAS) that we performed at SSRL.

Additionally, I would like to thank all of the administrative and technical staff that helped me during my years at USC. More specifically, I am very thankful to: Marcia Rowen, Loretta Hardcastle, Vernon Dorrell, Brian Loggans, Chuck Holland and Pam Olszewski. Thank you all.

I also would like to express my gratitude to my close friends who supported me and were always ready to help in both research related issues or matters outside the school. I am very thankful to Elina, Chris, Behnam, Vasilis and Zahra for their help.

The funding from the University of South Carolina which made this research possible (ASPIRE grant 15510-12-29499) is gratefully acknowledged.

Lastly, I would like to acknowledge my parents. I realize that my dream to go to United States and pursue Ph.D. degree in the field I am most passionate about would never come true without their support and kind words. I am very thankful to them for their patience, love and care. I can’t thank you enough.

Thank you,

Artem

ABSTRACT

The growing interest towards design of heterogeneous analogs of highly active and selective homogeneous catalysts prompted researchers to invest significant efforts in understanding of synthetic pathways, structure, and activity of supported single-site metal complexes.

Synthesis of catalytically active organometallic species on solid supports with properties resembling those of their homogeneous counterparts could offer the opportunities to perform efficiently the solution organic reactions by utilizing flow instead of batch reactors and eliminate problems with separation of the expensive catalyst from reaction products. In this regard rhodium carbonyl complexes are viewed as very attractive candidates for heterogenization due to their extensive application as homogeneous catalysts for variety of industrially relevant liquid phase reactions.

Although several synthetic pathways have been offered in literature for the preparation of supported site-isolated mononuclear rhodium carbonyl species, there is clearly lack of knowledge on surface chemistry of such complexes. We were interested in molecular level understanding of transformations occurring in their coordination environment during the catalytic cycle and role and functions of the support during catalysis when using these materials.

We attempted to contribute to the field by investigating structural properties of well-defined Rh organometallic complexes attached to a zeolite framework and exploring their reactivity in several probe reactions. Our strategy was to prepare samples incorporating highly uniform and nearly molecular $Rh(CO)_2$ complexes anchored to a zeolite framework and to use the reactivity of the ligands in these complexes for the surface-mediated synthesis of important reaction intermediates. FTIR, EXAFS, and XPS spectroscopic measurements, as well as mass spectrometry and isotope labeling were used to monitor ligand exchange reactions and to understand the structure and composition of the species formed at the molecular level.

New results presented herein strongly suggest that dealuminated Y zeolites act as macroligands for grafted metal complexes and have at least two different types of binding sites capable of accommodating $Rh(CO)_2$ moieties. The fraction of these sites is a function of the Si/Al ratio of the support and $Rh(CO)_2$ complexes associated with these sites posses of remarkably different reactivity.

We developed a two-step pathway for the selective synthesis of well-defined and structurally uniform HY zeolite-supported $Rh(CO)(H)_x$ complexes under ambient conditions. The stability of these $Rh(CO)(H)_x$ species at elevated temperatures was addressed, as well as their surface chemistry in reactions with CO, C_2H_4, O_2, and N_2. $Rh(CO)(H)_x$ complexes were found to be catalytically active in both hydrogenation and dimerization of C_2H_4 at ambient conditions. While the role of the support was shown to be critical for the C-C bond formation reaction, it was possible to modify Rh coordination environment and suppress the dimerization pathway.

Furthermore, it was revealed that zeolite-supported rhodium dicarbonyl complexes could be used as model catalysts to probe the structure sensitive character of the NO + CO reaction.

TABLE OF CONTENTS

LIST OF TABLES

LIST OF FIGURES

CHAPTER 1. INTRODUCTION, MOTIVATION, LITERATURE REVIEW

1.1 INTRODUCTION

Catalysis plays a vital role in the production of chemicals, as evidenced by the fact that nearly 90% of world-wide chemical processes rely on at least one catalytic step [1]. A vast majority of industrial catalysts consist of supported metal nanoparticles which are capable of catalyzing many types of chemical reactions such as hydrogenation, isomerization, oxidation, and carbonylation, among others [1,2]. Unfortunately, many commercial catalysts are very complex and nonuniform in structure leading to low selectivity, reduced efficiency hindering detailed understanding of structure-catalytic properties relationships. In contrast, homogeneous catalysts are characterized by well-defined single active sites with unique coordination environment making them more selective and more specific compared to the conventional solid catalysts. Immobilization of organometallic complexes on high surface area porous supports is a strategy that allows to take the major advantages of homogeneous systems while avoiding technological difficulties associated with separation of the product from the catalyst in solution.

Although significant progress has been achieved recently in this field, the synthesis of exceptionally dispersed catalytic materials with well-defined active sites as well as molecular level characterization of their catalytic properties remain a major experimental challenge. More specifically, substantial gap in knowledge exists in understanding of ligands reactivity in supported complexes, mechanisms of their involvement in catalysis and role of the support. Understanding of these properties is a key to the development of new efficient alternatives to homogeneous catalysts on solid surfaces as well as important step towards building practical guidelines for rational catalyst design.

The following literature review summarizes the recent progress in the area of synthesis and reactivity of supported complexes.

1.2 MOTIVATION AND SIGNIFICANCE

Homogeneous catalysts offer a number of advantages over their heterogeneous counterparts. High concentration of active sites, accessibility of all active sites to reactants and tunable selectivity and and/or enantioselectivity are among key reasons making metal complexes so attractive for industrial applications. However, the use of homogeneous catalysts on commercial scale is limited due to the difficulties of their separation from reaction mixture, low recyclability and low thermal stability. These drawbacks can be eliminated by using supported catalysts. It is to meet the challenge of combining major advantages of homogeneous and heterogeneous catalytic systems in materials with enhanced performance in industrially relevant processes which remains strategic for researchers. As first steps in this direction it is critical to develop fundamental molecular-level understanding of structural properties of grafted complexes, reactivity of their coordination environment and establish functions of the support which could play a role of the inert back bone for anchored species or contribute to catalysis.

We focused on rhodium complexes because of their wide use as commercial catalysts and relatively well understood solution chemistry. Rhodium catalyzed homogeneous processes have significant industrial importance. For instance, production of aldehydes via hydroformylation of olefins is estimated at approximately 6.4 million metric tons per year while total capacity of methanol carbonylation which is a major pathway for the manufacturing of acetic acid is approaching 5 millions tons per year [3,4]. The prospect of transferring these processes from solution to solid surfaces is very promising for both economical and technological reasons. Although there are multiple patents on synthesis of immobilized rhodium complexes and their catalytic activity in commercial processes, so far there is only one industrially implemented technology involving $[Rh_2(CO)_2]^-$ bound to ion exchange resin which is used for the carbonylation of methanol [5,6].

This research is expected to advance the current understanding structure-catalytic properties relationships of supported rhodium complexes and, in a broader prospective, to build a foundation for the rational design of supported single-site catalysts with properties resembling those of organometallic solution chemistry analogs. The ultimate long term goal of this work is to define heterogeneous catalytic system with tunable catalytic properties where active sites are uniform in composition and distribution.

1.3 LITERATURE REVIEW

1.3.1 SYNTHETIC PATHWAYS TOWARDS SUPPORTED METAL COMPLEXES

Immobilization of organometallic complexes on solid supports implies attachment of these species to the surface through covalent or ionic bonds. Several strategies were offered to perform this step with three major ones defined as: anchoring of on functionalized solids, direct reaction with functional groups of the support [7,8] and encapsulating or encaging in the voids or pores of the support [9].

Interaction of transition metal complexes with preliminary functionalized supports is one of the most widely used methods to prepare single-site catalysts. The method implies coupling of the surface modified with certain functional groups with the precursor complex. Modification of the surface is conducted with ligand containing two functional groups X-L where X is chosen so as to react with surface hydroxyls (Cl, $SiCl_3$, $Si(OEt)_3$, $SiR'_2(OR)$) while L is a donor group such as alkylphosphines, arylphosphines or amines (PR_3, PAr_3, NH_2R) which interacts with the precursor complex [8]. The complex of interest normally posess reactivity towards L groups and react with them during the grafting procedure. It is important to note that supporting complex can loose ligands upon grafting or can remain structurally intact depending on its chemical properties (as well as on its electronic configuration and geometry). Among examples of successful application of this approach is immobilization of $Ru(NH_3)_4SO_3$ moiety on silica gel functionalized with 3-(l-imidazolyl)propyl groups [10]. It is suggested that properties of these complexes are very similar to those of the complexes in solution, since the immobilized complexes are separated from the support by more than two carbon atoms.

Support species can also be attached to surface through electrostatic interactions. Silica-tethered olefin polymerization catalysts was synthesized by grafting bis(cyclopentadienyl) dimethylzirconium (Cp_2ZrMe_2) on sulfonic acid functionalized SBA-15 [11]. Surface anionic functionalities were created by interacting of trimethylaluminum with anchored sulfonic groups. The subsequent reaction with Cp_2ZrMe_2 complex resulted in the formation of ionic pair: surface coordinated anion and an active metallocenium cation (Fig. 1.1). It was suggested that catalyst prepared in this way exhibit high stability and resistant to leaching of active species.

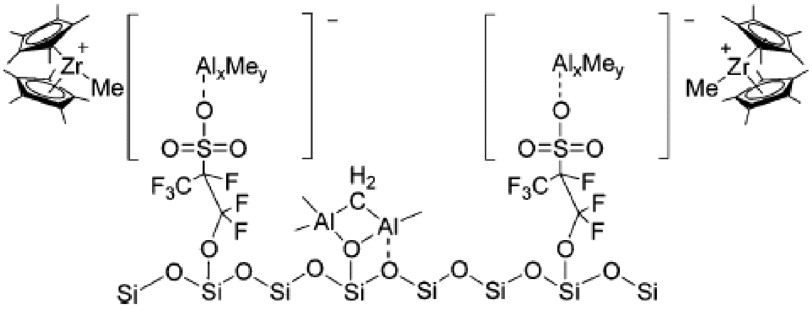

Figure 1.1 Bis(cyclopentadienyl) dimethylzirconium anchored on sulfonic acid functionalized SBA-15 [11].

Complexes electrostatically immobilized on different supports received substantial attention in literature. More specifically, complexes anchored to inorganic oxides and clays [210-214], ion-exchange resins [215,220, 221,229,231-233], dendrimers [237,258], heteropolyacids [261,267,273, 276,277], and zeolites [279,289,290,291] were reported.

Additionally, this method is used to anchor isolated metal ions via complexation. For instance, it was shown that surface of MCM-41 mesoporous silica functionalized with ethylenediamine, diethylenetriamine ligands efficiently bind Co(II) ions [12]. These species exhibited significant activity in oxygen binding and may find broad application in catalysis and gas separations.

Another example of a catalyst with high oxidation activity prepared by anchoring of metal complexes on functionalized supports is silica-anchored manganese Schiff-base complexes [13]. The grafting process involves seferal steps: at the fist stage MCM-41 surface is modified with 3-chloropropylsilane moieties which provide reactive Cl gproups. At the next step pentadentate ligands 3-[N,W-Bis-3-(3,5-di-tert-butylsalicylidenamino) propylamine (t-salpr) are grafted by partial nucleophilic displacement of chlorine of previously anchored species. Finally, Mn species are introduced by reacting surface t-salpr ligands with $Mn(acac)_2$ (Fig. 1.2).

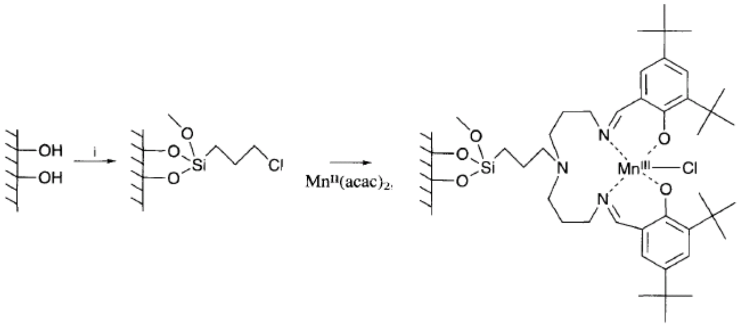

Figure 1.2 Manganese Schiff-base complexes anchored on MCM-41 [13].

Rhodium complexes supported on functionalized materials have also received significant attention in literature. For instance, homogeneously dispersed rhodium species were obtained by reaction of $[RhCl(CO)_2]_2$ and $RhCl_3$ with silica functionalized with chelating N-donor ligands [14]. The support was prepared by cohydrolysis of tetmethylorthoailicate and (3-aminopropyl)triethoxysilane following an acid-catalyzed sol-gel process (Figs. 1.3, 1.4).

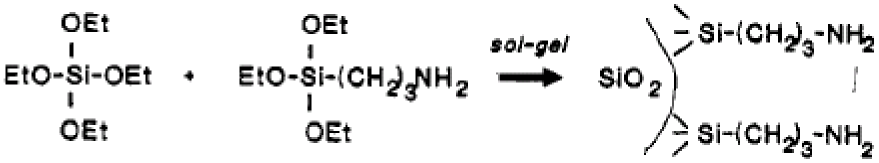

Figure 1.3 Procedure for the preparation of silica functionalized with N-donor groups [14].

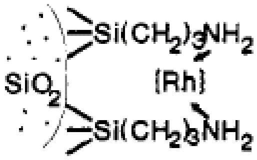

Figure 1.4 Rhodium complex anchored on silica functionalized with N-donor groups [14].

We note that using ligands with strong chelating properties such as amines or phosphines is a general and widely used strategy for immobilization of rhodium complexes. It is reported that reaction of $[RhCl(CO)_2]_2$ the surface of aminated and phosphinated MCM-41 material results in site-isolated $RhCl(CO)_2$

complexes with enhanced hydrogenation activity [15]. The support was modified by reaction of MCM-41 mesoporous silica with correspondent alkoxysilyl agents (Fig. 1.5). It is remarkable that no leaching was observed during the catalytic reaction in a liquid phase.

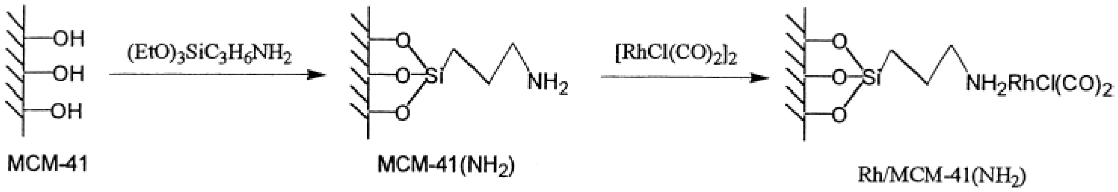

Figure 1.5 Anchoring of $RhCl(CO)_2$ complexes on MCM-41 treated with 3-aminopropyltriethoxysilane [15].

Coordination of rhodium complexes to the support through phosphine ligands was also successfully demonstrated. More specifically, diphosphino-functionalized MCM-41 material was shown to efficiently bind $RhCl(PPh_3)_3$ complexes which showed remarkable activity in hydrothiolation reaction of alkynes with thiols reaction (Fig. 1.6) [16].

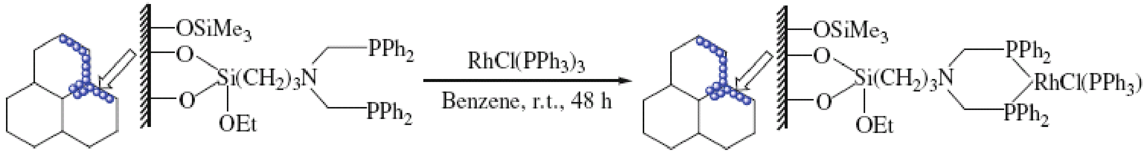

Figure 1.6. Anchoring of $RhCl(PPh_3)$ complexes on diphosphino-functionalized MCM-41 [16].

Another approach which is widely used to immobilize metal complexes on solid surfaces is a direct reaction of a precursor with functional groups of the support. It is recognized that acidic hydroxyl groups which cover surfaces of metal oxides are active enough to interact with different organometallic compounds. One of the methods of preparing well-defined supported-metal catalysts involves the protolysis of transition-metal allyl complexes with surface OH groups. Yermakov and coworkers synthesized and characterized a range of supported catalysts prepared in this way including Zr, Hf, Nb, Cr, Mo, W, Re, Ni, Pd, and Pt [17]. The anchoring mechanism is suggested to proceed through protonation of allyl ligands which leave as propane molecules followed by coordination of $M(C_3H_5)_x$ fragments to oxygen atoms of the support (Fig. 1.7) [17,18].

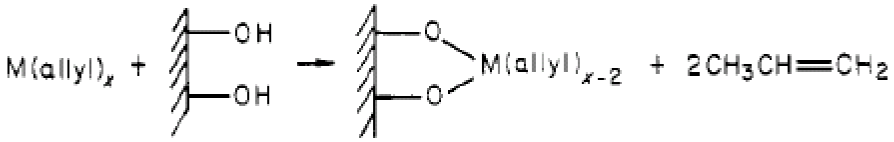

Figure 1.7 Interaction of $Rh(C_3H_5)_3$ complexes with silica [18].

It was shown that reactivity of surface hydroxyls depends on the nature of the support and degree of surface dehydroxylation. No reaction was observed for supports with highly nucleophilic hydroxyl groups (i.e., MgO) or with high hydroxyl coverage (i.e. not dehydroxylated Al_2O_3). Anchored species exhibited remarkable activity in hydrogenation of olefins and of arenes [19-21].

Although allyl ligands are considered among the most reactive towards surface hydroxyls, other alkyl functional groups can be used. For example,

$CH_3Rh(P(CH_3)_3)_2(CO)$ complex was shown to react irreversibly with dehydroxylated silica surface via displacement of methyl group which converts into methane upon complex chemisorption [22]. Supported complexes exhibited very rich surface chemistry including ligand substitution, oxidative addition of HCl and CH_3I, CO insertion, and reductive elimination (Fig. 1.8) [22,160,164].

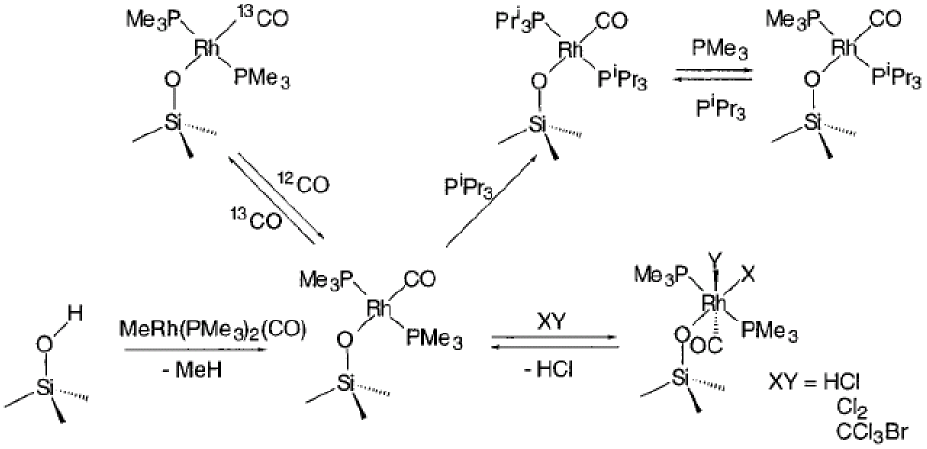

Figure 1.8 Surface chemistry of silica-supported $Rh(P(CH_3)_3)_2(CO)$ complexes [22].

Finally, it is worth noting that whole range of supported complexes were obtained by grafting perhydrocarbyl transition-metal complexes of ML_4 structure where M is Mo [23-25,187,188], Re [26-28,40,41], W [29-31], Ta [32-34], Ti [35-37], Zr [38] and L is tBu, tMe,Np. These species were synthesized by method described above which implies substitution of one of the M–C bonds by M–O moieties (Fig. 1.9). Anchored surface organometallic fragments were shown to possess high reactivity allowing for selective synthesis of important intermediates such as hydrides, carbenes or carbines, oxo and alkoxo species and were applied as catalysts in methathesis, polymerization and oxidation reactions [35,39].

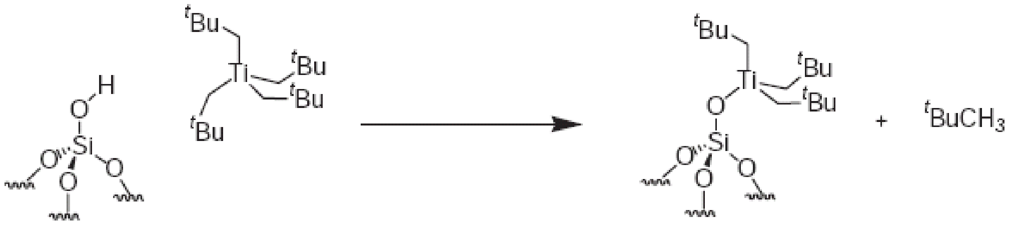

Figure 1.9 Grafting reactions of tetrakisneopentyl titanium on silica [36].

Alkyl ligands are not the only groups capable of reaction with surface hydroxyls. Methyltrioxorhenium (MTO) complexes can be heterogenized similarly by reaction of one of the “oxo” ligands with the support (Fig. 1.10). It is reported that loadings as high as 10 wt% can be reached on alumina [42]. Resulted catalyst exhibited high activity in cyclooctene metathesis already at room temperature.

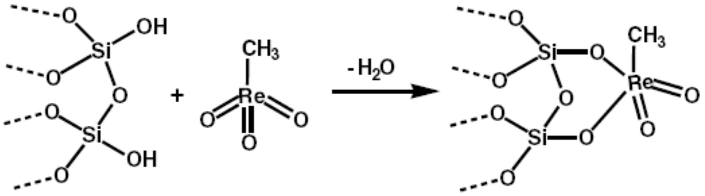

Figure 1.10 Grafting of methyltrioxorhenium (MTO) on silica [42].

Another group of ligands which are reactive towards surface hydroxyl groups and widely used in synthesis of supported single-site catalysts are β-diketones. These ligands include the following: acetylacetones (acac), dibenzoylmethane (dbm), benzoylacetone (ba), dipivaloylmethane (dpm), diisobutylmethane (dibm), trifluoroacetylacetone (tfac), hexafluoroacetylacetone (hfac), and others [43]. Due to strong chelating properties these ligands easily coordinate variety of transition metals. Among known complexes are Rh(I), Be(II), Mn(II), Co(II), Ni(II), Zn(II), Al(III), V(III), Fe(III), Cu(II), Pd(II), Pt(II) [44-50]. The mechanism of anchoring of such complexes to a solid surface involves protonation of β-diketone ligand by acidic hydroxyl group which leads to substitution of this ligand which leaves as stable diketone with surface oxygen atoms. However, it should be noted that multiple factors influence the reactivity of metal β-diketonate complexes. For instance, on supports with strong basic properties (MgO, CeO_2 etc.) only physisorption of complexes occurs. Similarly, for supports with weak acidic properties such as silica ligand exchange reactions do not occur, instead, complexes adsorb via hydrogen bonding [51-54]. The mechanism for binding in this case was suggested to be interaction between the surface silanols and the π-electron system of the β-diketone ligands. Remarkably, these materials exhibited unusual tendency to maintain monolayer dispersions even at high loadings of the complexes [55-57].

It is important to note that this synthetic approach can also be used to prepare molecularly dispersed metal oxide catalysts (Mo, Cu, V) [58]. The procedure involves grafting of transition metal acetylacetonate complexes ($Mn^+(acac)_n$) to the surface of a high-surface-area support followed by mild thermal treatment in oxygen [58]. In general, the preparation, characterization and catalytic properties of different types of supported metal acetyacetonate complexes such as $M^{+1}(acac)$, $M^{+2}(acac)_2$, $M^{+3}(acac)_3$ have been reported in the literature [195-206,208].

Covalent bonding to solid supports of metals derived from β-diketonate complexes is of particular interest. Gates and coworkers synthesized and characterized a whole family of structurally well-defined supported metal complexes derived from correspondent acetylacetonates [59-64]. It was reported, for instance, that $Au(CH_3)_2(acac)$ complexes react with the surface of partially dehydroxylated γ-Al_2O_3 resulting in anchored single-site $Au(CH_3)_2$ species (Fig. 1.11) [59].

Figure 1.11 Proposed structures of HY zeolite-supported $Au(CH_3)_2$ and $Ru(C_2H_4)_2(acac)$ complexes [59,60].

Similar approach was used to graft $Rh(C_2H_4)_2$ [64] and $Ru(C_2H_4)_2(acac)_2$ (Fig. 1.11) [60, 61] complexes on surfaces of Y and β zeolites. The precursor complexes $Rh(C_2H_4)_2(acac)$ and $Ru(C_2H_4)_2(acac)$ reacted with the surfaces of correspondent zeolites via displacement of one “acac” ligand. Grafted species exhibited high degree of structural uniformity and allowed a detailed characterization of structural properties of supported complexes and their reactivity. It was found that these species bind next to Al atoms of the zeolite and retained ethylene ligands posses high reactivity. More specifically, these ligands were shown to participate in ethylene dimerization reaction at ambient conditions. Synthesis of well-defined Y zeolite-supported $Ir(C_2H_4)_2$ species was also reported

[65]. Structural characterization revealed that supported iridium complexes are mononuclear and isostructural to grafted $Rh(C_2H_4)_2$ complexes. Interestingly, catalytic activity of supported Ir species in ethylene hydrogenation was found to be 35 times higher than activity of Rh analogs.

Although anchoring of metal complexes via their reaction with hydroxyl groups which terminate most of oxide supports is probably the major pathway of heterogenizing of homogeneous catalysts, other functional groups of the support can also be utilized. For instance, Lewis sites were shown to interact with variety of organometallic complexes resulting in strong covalent bonds. Iridium pincer complexes were successfully immobilized on alumina through binding of the electron donor group on a pincer ligand to a coordinatively-unsaturated surface Al sites (Fig. 1.12) [66]. These supported complexes were found to be highly effective as transfer-dehydrogenation catalysts.

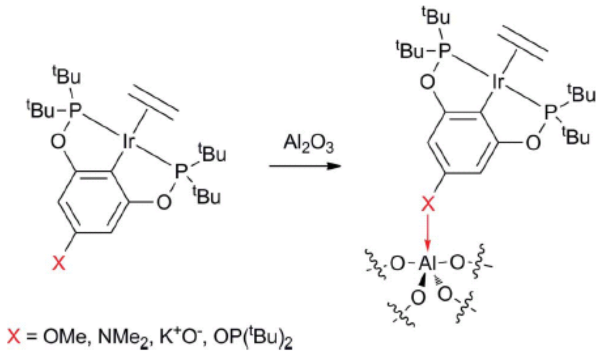

Figure 1.12 Anchoring of Ir pincer complexes on alumina [66].

Similar anchoring mechanism was suggested for ReO_4^- species immobilized on alumina. More specifically, it was found that interaction of Re_2O_7 with γ-Al_2O_3 results highly dispersed supported ReO_4^- species which do not react with hydroxyl groups but coordinate to Al Lewis sites [67]. This material exhibited high selectivity in olefin metathesis at temperatures of 0-100 ºC. Enhanced activity in olefin metathesis reaction was also reported for catalyst prepared by grafting of RhO_4 groups on γ-Al_2O_3 using NH_4RhO_4 complexes as precursors [68]. It was suggested that interactions between perrhenate and Lewis acid sites on alumina may play a key role in the activation of these catalyst for olefin metathesis.

Encapsulation of metal complexes in a framework of highly-ordered crystalline materials is another widely used strategy to synthesize catalytically active site-isolated species. Among major advantages of internal confinement of metal complexes are high degree of spatial isolation, low mobility at elevated temperatures and steric restrictions enabling shape-selective catalysis [69]. It was suggested that constrains imposed by walls of the material complexes are confined in significantly modify magnetic, electronic, and redox properties of encapsulated species [70-72].

Several methods have been developed for encapsulation of metal complexes inside the pore structure of zeolite. Flexible ligand method implies reaction of a ligand with metal cations already exchanged in zeolite framework. These ligands are usually small enough to penetrate into zeolite supercages through pores but resulted complexes are larger than pore openings and become essentially trapped inside the zeolite framework. This approach was initially offered by Herron and coworkers [73] to synthesize zeolite encapsulated bis(salicylaldehyde)ethylenediamine (salen) complexes of cobalt. The whole range of internally assembled salen complexes have been later reported including Fe(III) [74], Co(II) [78,298], Mn(II) [75,295,295-297], Rh(II) [76] and Pd(II) [77]. These complexes showed remarkable catalytic activity. For instance, cobalt Schiff base chelates incorporated in zeolite Y framework are capable of activating oxygen at ambient conditions [78]. Similar method was used to introduce vanadium oxide complexes VO(Saloph) where Saloph is N,N'-o-phenylenebis(salicylide naminato) in microporous zeolite NaY and mesoporous Al-MCM-41 materials. These species exhibited high activity and selectivity in the epoxidation of trans-stilbene and styrene [79]. Another example of the efficient oxidation single-site catalysts involves bis(picolinato) complexes of cobalt, nickel, and copper which were encapsulated in zeolite-Y and tested in the selective oxidation of phenol to catechol using H_2O_2 as mild oxidant (Fig. 1.13) [80].

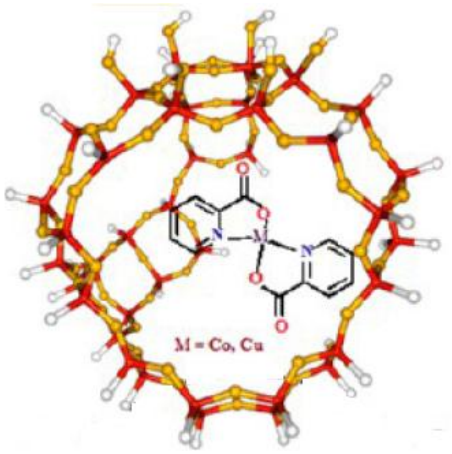

Figure 1.13 Structure of zeolite Y encapsulated metal picolinato complexes [80].

Encapsulated metal complexes with 2,2’-Bipyridine (bipy) [292,-294] and bis(oxazoline) [299,318,319] have also been reported.

“Ship-in-bottle” synthesis is another approach used to synthesize site-isolated metal complexes inside ordered materials. This method involves introduction of metal ions into the zeolite structure via ion exchange followed by treatment with appropriate ligands such as 1,2-dicyanobenzene [81-83] or carbon monoxide [69,84-86,88].

Single-site heterogeneous catalysts consisting of encapsulated complexes of Fe and Cu phthalocyanine prepared using “ship-in-bottle” method were shown active in methane to methanol and formaldehyde conversion at room temperature [89]. Interaction of carbon monoxide with zeolite-exchanged cations of transition metals results in mononuclear metal carbonyls or carbonyl clusters. If clusters are formed, their sizes are limited by the zeolite cage dimensions providing opportunity to control metal nuclearity under the reaction conditions [90, 91]. Similar approach can be used to modify coordination environment of already anchored complexes. For instance, reaction of encapsulated nickel carbonyl with phoshine ligands leads to the production of $Ni(CO)_3(PPhCHMe_2)$ complexes [87].

Encapsulation of small mononuclear carbonyl complexes by impregnation is possible. The encapsulation of carbonyl and subcarbonyl metal complexes has received a lot of attention in literature due to catalytic potential of these systems. For instance, it was demonstrated that $Mo(CO)_3$ complexes confined in supercages of Y zeolite (promoted with alkali metals) exhibit high activity in selective hydrogenation of 1,3-butadiene to cis-2-butene (Fig. 1.14). Although the catalyst was prepared by vapor deposition of $Mo(CO)_6$ complexes, these species experienced partial decarbonylation under the reaction conditions and $Mo(CO)_3$ complexes were found to be the active sites.

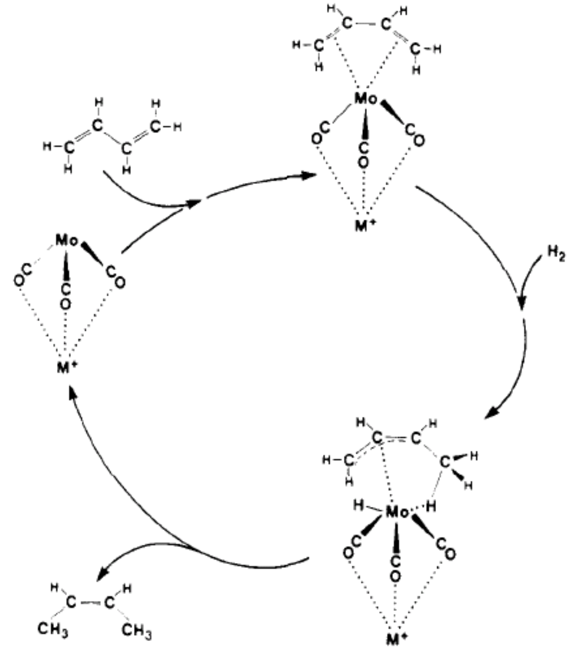

Figure 1.14 Proposed mechanism of 1,3-butadiene to cis-2-butene hydrogenation over Y zeolite-encapsulated $Mo(CO)_3$ complexes [92].

The sol-gel method is another approach for synthesis of encapsulated complexes and it implies crystallizing the zeolite or mesoporous silica around the preformed metal complex. The method is limited by range of complexes which are stable under the harsh conditions of support synthesis. This strategy was used to prepare NaX encaged [Ru($F_{16}P_c$)] species which exhibited high activity in oxidation of cyclohexane to cyclohexanone [321,324,337,338]. Sol-gel entrapment of $[Rh(COD)(\mu\text{-}Cl)]_2$ species into a silica modified with palladium nanoparticles was reported [340]. This system showed remarkable activity in arene hydrogenation. Active oxidation catalyst synthesized via sol-gel method was also reported. More specifically, copper complexes encapsulated in zeolites X and Y were shown to be more active in phenol oxidation (to p-benzoquinone, catechol and hydroquinone) than the homogeneous analog [339]

Finally, incorporation of metal cations in mesoporous sieve and zeolite matrices has received attention in literature as a novel pathway for synthesis of spatially isolated and uniformly distributed active sites. The idea of the method is to add a metal precursor to a synthesis gel during the templating process. Although these incorporated cations do not have stabilizing ligands as metal complexes have, sites which are accessible (not in the bulk) are capable to coordinate and activate reactants during the reaction.

In case of pure silica MCM-41 which has a neutral framework incorporation of $Al^{3+,}$ Ga^{3+} [93,94], Fe^{3+} [95,96,320] ions results in a negatively charged framework often compensated by protons. Consequently, such materials obtain acidic properties and bifunctional catalysis is allowed. In contrast, when Ti $^{4+}$ [97-100,342-344,346], V^{4+} [101-103], Sn^{4+} [106], Zr^{4+} [104,105], Mn^{4+} [135] ions are implanted, electroneutrality is maintained and more specific transformations are enabled. It is remarkable that materials obtained by this method found application in industrially important reactions. Mn^{3+} ions substituted in the framework of AlPO-36 exhibited high activity in oxidation of p-xylene to terephthalic acid [107,108]. Additionally, site-isolated Ti^{4+} sites incorporated in AlPO-5 were shown efficient in conversion of cyclohexene to adipic acid (Fig. 1.15) [109,110].

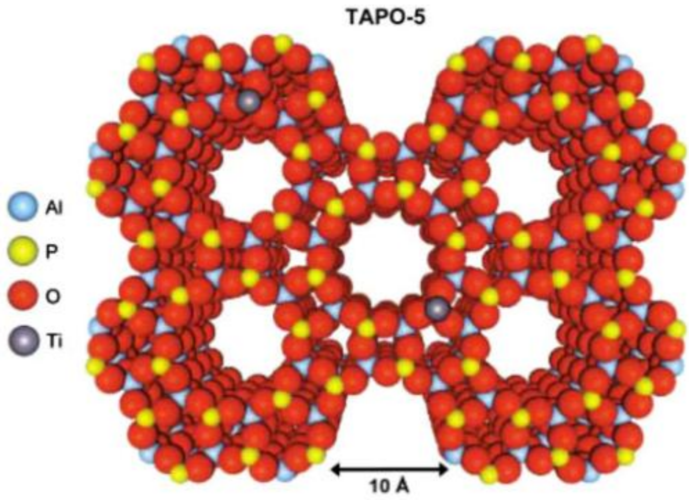

Figure 1.15 The structure of the AlPO-5 catalyst with framework-incorporated Ti^{4+} ions [109,110]

1.3.2 RHODIUM CARBONYLS SUPPORTED ON AMORPHOUS OXIDES

Highly dispersed supported rhodium catalysts have been the area of extensive research starting from the late 50th. Supported rhodium carbonyls are of particular interest mainly due to their enhanced activity in hydrogenation and carbonylation reactions. Besides, CO adsorption followed with infrared spectroscopy is widely used to characterize the surface of rhodium catalysts. It was established in pioneering work of Yang and Garland [111] that CO can be chemisorbed on Rh in three different bonding modes: linearly bonded form, gem-dicarbonyl form and bridged form (Fig. 1.16):

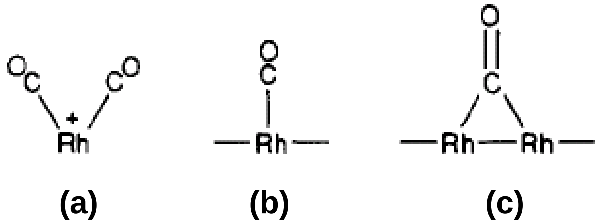

Figure 1.16 Bonding modes of CO chemisorbed on rhodium: (a) linearly bonded form, (b) gem-dicarbonyl (c) bridged form [111].

Furthermore, Yates and co-workers showed [112,113] that species (b) occur on isolated rhodium sites, while species (a) and (c) involve crystalline rhodium species. Several attempts were made to associate CO bonding mode on rhodium with rhodium oxidation state. Cavanagh proposed that form (a) may refer to oxidation state of rhodium higher than zero [114]. Primet studied CO adsorption on alumina-supported rhodium catalysts and zeolite using FTIR and XPS techniques and found that rhodium oxidation state in species (a) is +1 [115-117]. By date, it is generally accepted that rhodium gem-dicarbonyls are formed on single Rh atoms and these surfaces species are more pronounced for catalysts with high rhodium dispersion. Prins studied influence of CO chemisorption on the topology of rhodium supported on alumina using EXAFS and found that chemisorption of CO leads to significant decrease of Rh-Rh coordination number. They concluded that CO adsorption on metallic rhodium crystallites causes disruption of rhodium clusters yielding mononuclear species of type (a) [118]. The mechanism of rhodium crystallites break-up upon CO adsorption is not fully understood and several explanations were proposed including enhanced metal-support electronic interaction [119] and participation of surface hydroxyl groups [118].

Nature of the support substantially affects CO chemisorption behavior. It was reported that formation of rhodium gem-dicarbonyl occurs on alumina, silica, titania, magnesia [120]. Titania and silica supports allow for less dispersed rhodium species and favor formation of rhodium carbonyls species of type (b) and (c) while alumina favors formation of type (a) surface species [121]. On alumina-supported rhodium catalysts CO adsorption yields the following bands: 2101 cm^{-1} and 2035 cm^{-1} for type (a) species, 2060 cm^{-1} – 2070 cm^{-1} for type (b) and 1855-1870 cm^{-1} for bridged form (c) [111,115,122,123]. Although positions of these bands are slightly altered if alumina is replaced by other support, the general trend remains the same [124].

1.3.2 RHODIUM CARBONYLS SUPPORTED ON ZEOLITES

Since most of metal oxides are intrinsically nonuniform and characterized by high structural complexity, understanding of surface chemistry of rhodium species supported on such materials is hindered. In contrast, structurally ordered materials, such as zeolites, offer nearly uniform surface for the formation of well-defined active sites. Miessner investigated the surface chemistry and structural properties of dealuminated Y zeolite-supported rhodium carbonyl species [125,157]. It was reported that site-isolated $Rh(CO)_2$ species can be formed by exposure of 5-10 Torr of CO to highly dispersed supported rhodium particles. The crucial role of the support in stabilization of well-defined $Rh(CO)_2$ complexes can be understood by analyzing full width at half maximum (FWHM) values of v(CO) bands in FTIR spectra. More specifically, FWHM for CO adsorbed on rhodium supported on amorphous oxides is usually larger than 15 cm^{-1} but FWHM for rhodium carbonyls supported on highly dealuminated zeolite do not exceed 5-6 cm^{-1} indicating high degree of structural uniformity of surface species. It was proposed by Miessner group that $Rh(CO)_2$ species are located at cationic positions in the supercages near framework Al atoms. Since Al atoms in dealuminated Y zeolite are well-isolated, supported complexes do not interact with each other [125, 126]. Thus, dealuminated Y zeolite framework acts not only as bidentate ligand but also as matrix leading to effective isolation of rhodium sites [126].

Gates and coworkers used EXAFS spectroscopy and gave more detailed insight into the structural properties of Y zeolite-supported rhodium carbonyl complexes [63]. In order to avoid complications associated with Cl^- contributions in EXAFS spectra, different synthetic pathway was offered. More specifically, instead of using aqueous solutions of rhodium salts, chloride-free $Rh(CO)_2(acac)$ precursor was utilized. The principal advantage of this synthetic approach is that no high temperature pretreatment is required in order to cleave the ligands in a precursor. Interaction of precursor complex $Rh(CO)_2(acac)$ with dealuminated HY zeolite in pentane leads to protonation of “acac” group by acidic hydroxyls (Brønsted acid sites) and anchoring of $Rh(CO)_2$ fragments to the zeolite framework. EXAFS results as well as DFT calculations revealed that $Rh(CO)_2$

species are bonded to two oxygen atoms of zeolite and suggested to maintain 16 electron pseudo-square-planar geometry (Fig. 1.17).

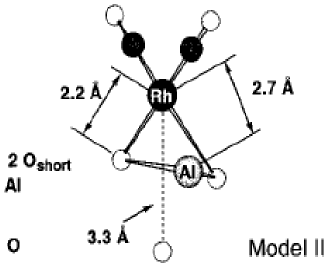

Figure 1.17 Simplified structural model for Y zeolite-supported $Rh^+(CO)_2$ complexes developed from EXAFS data analysis [63].

CHAPTER 2. SYNTHESIS AND CHARACTERIZATION OF HY ZEOLITE-SUPPORTED RHDOIUM CARBONYL HYDRIDE COMPLEXES

2.1 PREFACE

Fourier transform infrared (FTIR) and extended X-ray absorption fine structure (EXAFS) spectroscopic measurements, as well as results of mass spectrometry and isotope labeling experiments were used to characterize the species formed after grafting of a $Rh(CO)_2(acac)$ precursor on a highly dealuminated HY zeolite and during subsequent ligand exchange reactions. The results indicate that initially formed $Rh(CO)_2$ species on the surface of zeolite rapidly react with C_2H_4 to form $Rh(CO)(C_2H_4)$ complexes. Exposure of the latter to H_2 selectively yields $Rh(CO)(H)_x$ complexes characterized by a set of well-defined v_{CO} and v_{RhH} bands in their FTIR spectra. The hydride ligands in these $Rh(CO)(H)_x$ complexes can be displaced by CO or N_2 to form $Rh(CO)_2$ and $Rh(CO)(N_2)$ complexes, respectively. In contrast, C_2H_4 reacts with the hydrides, yielding C_2H_6 and an unstable Rh(CO) intermediate. The latter rapidly reacts with additional C_2H_4 from the gas phase to reform the original $Rh(CO)(C_2H_4)$ complex on the surface. The $Rh(CO)(H)_x$ species were found to be stable at room temperature under the flow of H_2 or He for an extended period of time.

However, the hydride ligands can be removed from these complexes at elevated temperatures.

2.2 INTRODUCTION

Rhodium is one of the most important metals in homogeneous and heterogeneous catalysis, with Rh complexes catalyzing a number of reactions of industrial importance primarily in the liquid phase, including hydroformylation, hydrogenation, hydrosilylation, dehydrogenation, and carbonylation [127-130]. The search for new heterogeneous Rh catalysts that will resemble the properties of their homogeneous analogs has constituted an active area of research for years. Such catalytic materials could offer not only easy separation of products from the catalyst but also the opportunity to perform more efficiently the same organic reactions in flow rather than in batch reactors.

For many of these reactions, it has been established that Rh complexes incorporating hydride ligands are key catalytically active species [127-130]. Such complexes have been identified in solution by FTIR and proton nuclear magnetic resonance (^{1}H NMR) measurements and have even been isolated as individual compounds stabilized with various organic ligands [131-134]. However, the selective synthesis of the heterogeneous analogs of these complexes is still a challenge. The formation of supported $Rh(CO)H_x$ complexes among other Rh surface species has been postulated in several literature reports based primarily on FTIR results [120,134,136-144]. In many of these reports, however, only v_{CO} vibrations have been taken into consideration, with the characteristic v_{CO} bands for the $Rh(CO)H_x$ species reported in a wide range of wavenumbers by different authors.

The formation of $Rh(CO)(H)$ or $Rh(CO)(H)_2$ species with a characteristic v_{CO} band located in the 2020-2030 cm^{-1} region was postulated first by Solymosi et al. [120] after exposure of MgO-, TiO_2-, SiO_2-, and γ-Al_2O_3-supported Rh samples to a CO_2/H_2 mixture at 100°C. Since terminal v_{CO} bands of □ γ-Al_2O_3-supported monocarbonyl Rh(CO) complexes had been observed by these authors in the 2060-2070 cm^{-1} region, it was suggested that the electron-donating properties of the hydride ligands in $Rh(CO)(H)_x$ species are responsible for the shift of the v_{CO} band to lower frequencies. Similarly, Worley et al. [136,137] have identified $Rh(CO)(H)_x$ species as key surface intermediates formed during the hydrogenation of carbon monoxide and carbon dioxide over TiO_2-, SiO_2-, and Al_2O_3-supported Rh catalysts at 210°C by the presence of the v_{CO} band in the 2020-2050 cm^{-1} region. Furthermore, these authors have shown that supported $Rh(CO)(H)_x$ complexes can also be formed in the absence of H_2 in the feed, with their formation attributed to an inverse hydrogen spillover effect. Ab initio molecular orbital calculations performed by the same group predict v_{CO} vibrations for gas phase Rh(CO)H species at approximately 2010 cm^{-1} and provide a qualitative support for the assignment of the v_{CO} band in the 2020-2050 cm^{-1} region to the surface $Rh(CO)(H)_x$ species [138]. However, neither of these groups was able to detect any bands attributable to the expected characteristic Rh-H vibrations of the surface $Rh(CO)(H)_x$ complexes.

It has been suggested that the lack of any $v_{Rh\text{-}H}$ bands in infrared spectra of supported $Rh(CO)(H)_x$ species can be explained either by their low intensity or by their superposition with more intensive v_{CO} bands. The ab initio calculations reported by Worley et al. [138] predict the appearance of in-plane and out-of-plane $v_{Rh\text{-}H}$ vibrations in the infrared spectra of gas phase Rh(CO)H complexes at approximately 1433 and 1643 cm^{-1}, respectively, with intensities comparable to those of the v_{CO} bands. However, this prediction is inconsistent with the majority of experimental FTIR results reported for various molecular Rh organometallic complexes incorporating hydride ligands which demonstrate the presence of the $v_{Rh\text{-}H}$ bands in the 2000-2200 cm^{-1} region [133,134]. Furthermore, the $v_{Rh\text{-}H}$ bands in FTIR spectra of RhH and RhH_2 complexes formed by the reaction of laser-ablated Rh atoms with H_2 and trapped in argon matrixes also appear in the same region [139]. While the last two examples indicate that the overlap of the v_{CO} and $v_{Rh\text{-}H}$ bands in spectra of supported $Rh(CO)(H)_x$ complexes is possible, the failure to detect the $v_{Rh\text{-}H}$ vibrations in the FTIR spectra of $Rh(CO)(H)_x$ species motivated the search for alternative assignments of the v_{CO} bands.

Iizuka et al. [140,141] for example, have reported the appearance of a new band at approximately 2040 cm^{-1} during hydrogenation of CO and CO_2 at 300°C over Al_2O_3-, ZrO_2-, and MgO- supported Rh catalysts. Since this band was also present upon exposure to CO and CO_2 without H_2 under similar experimental conditions, these authors have assigned it to the monocarbonyl Rh(CO) complex formed at low CO coverages. In this context, Miessner [142] has reported that a partial decarbonylation of $Rh^{I}(CO)_2$ species supported on highly dealuminated Y zeolites in a flow of diluted H_2 at 200-250°C results in the formation of reactive $Rh^I(CO)$ monocarbonyl species with a characteristic v_{CO} band at 2096 cm^{-1}. However, more recent DFT calculations do not support such assignments. For example, Rösch et all. [143] have reported that the v_{CO} band of monocarbonyl $Rh^I(CO)$ complexes formed on dealuminated Y zeolite and Al_2O_3 should appear at 2014 and 1984 cm^{-1}, respectively. Furthermore, the same authors have suggested that the v_{CO} bands at 2093 and 2061 cm^{-1}, which are located between the symmetric and asymmetric v_{CO} bands of dealuminated Y zeolite- and Al_2O_3-supported $Rh^I(CO)_2$ species, are most likely due to the formation of mixed $Rh^IH_2(CO)$ or $Rh^I(H)_2(CO)$ complexes incorporating either a dissociated or an undissociated H_2 molecule as an additional ligand. Along these lines, experimental results reported by Wovchko et al. [144] demonstrate that monocarbonyl $Rh^I(CO)$ complexes with a characteristic v_{CO} band at 2023 cm^{-1} can be formed by UV photolysis of $Rh(CO)_2$ species supported on dealuminated Y zeolite. Moreover, it has been shown that the $Rh^I(CO)$ complexes thus formed are coordinatively unsaturated and very reactive towards H_2, N_2, and O_2 even at room temperature, yielding a variety of Rh surface complexes with mixed ligands. In fact, $Rh(CO)(H_2)$ and $Rh(CO)(H)_x$ complexes thus prepared exhibit characteristic v_{CO} vibrations at 2096 and 2102 cm^{-1}, respectively [144]. However, these authors also failed to detect any $v_{Rh\text{-}H}$ vibrations in their spectra.

From the analysis of the available literature reports, it is also evident that the selective synthesis of supported $Rh(CO)(H)_x$ species has not been reported to date. Therefore, one can suggest that the difficulties with the selective synthesis and identification of supported $Rh(CO)(H)_x$ species by FTIR are most likely related to the nature of the catalytic materials used. Since conventional catalytic materials have been used most often for this type of research, a variety of surface species have been typically observed on their surfaces, because the Rh sites present in such materials are nonuniform in structure and composition. As a result, it is difficult to unambiguously identify the $Rh(CO)(H)_x$ species in these cases due to their low abundance and the relatively low intensity of the Rh-H stretching vibrations.

It is further evident that most recent advances in the preparation of supported Rh catalysts with well-defined and uniform Rh sites can assist in the selective synthesis of $Rh(CO)(H)_x$ species. For example, Goellner et al. [63] have demonstrated a one-step synthesis of HY zeolite-supported $Rh(CO)_2$ complexes. More specifically, it has been shown that $Rh(CO)_2(acac)$ complexes can react with the surface of dealuminated HY zeolite, resulting in the displacement of the (acac) ligand and the formation of site-isolated, well-defined $Rh(CO)_2$ species anchored inside the zeolite supercages. The uniform structure of these HY zeolite-supported $Rh(CO)_2$ complexes makes them excellent candidates for spectroscopic characterizations and offers the opportunity for the selective synthesis of supported $Rh(CO)(H)_x$ species.

In our current work, we explore the chemical properties of the $Rh(CO)_2$/HY materials in an effort to develop a pathway to the selective synthesis of HY zeolite-supported $Rh(CO)(H)_x$ species. FTIR and EXAFS spectroscopic measurements, as well as results of mass spectrometry and isotope labeling experiments were used to monitor ligand exchange reactions and to understand the molecular structure and composition of the species formed. The results presented herein demonstrate a relatively simple two-step pathway for the selective synthesis of well-defined and structurally uniform HY zeolite-supported $Rh(CO)(H)_x$ complexes under ambient conditions. Furthermore, the stability of these $Rh(CO)(H)_x$ species is addressed under the flow of He or H_2 at elevated temperatures, as well as their reactivity towards CO, C_2H_4, and N_2. In addition, catalytic properties of zeolite-supported $Rh(CO)(H)_x$ complexes were tested in a simple probe reaction of C_2H_4 hydrogenation and the results obtained confirm their importance for mechanisms describing hydrogenation of alkenes.

2.3 EXPERIMENTAL

2.3.1 REAGENTS AND MATERIALS

Dicarbonylacetylacetonato rhodium (I) $Rh(CO)_2(acac)$ (acac = $C_5H_7O_2$) (Strem, 98% purity) was used as supplied. n-Pentane (Aldrich, 99% purity) was refluxed under N2 in the presence of Na/benzophenone ketyl to remove traces of moisture and deoxygenated by sparging of dry N_2 prior to use. All glassware used in these steps was previously dried at 120°C. H_2, He, CO, and C_2H_4 (Airgas, all UHP grade) were additionally purified prior to their use by passage through oxygen/moisture traps (Agilent) capable of removing traces of O_2 and water to 15 and 25 ppb, respectively. ^{13}CO (Sigma Aldrich, 99%) and deuterium (Cambridge Isotopes, 99.8%) were used as received. A highly dealuminated HY zeolite (CBV760, Zeolyst International) with a Si/Al ratio of 30 (further denoted as HY30) was used as the support. The zeolite was calcined in O_2 at 300°C for 3 h, evacuated at 10-3 Torr and 300°C for 16 h, and stored in a glovebox (MBraun) filled with N_2 prior to use. The residual water and O_2 concentrations in the glovebox were kept below 0.1 ppm.

2.3.2 PREPARATION OF SUPPORTED SAMPLES

All syntheses and sample transfer procedures were performed with exclusion of air and moisture on a double-manifold Schlenk line and in a N2-filled MBraun glovebox. Supported samples were prepared by slurrying the $Rh(CO)_2(acac)$ precursor with the powder support in n-pentane under N_2 for 24 h at room temperature, followed by overnight evacuation at 25°C to remove the solvent. In each case, the $Rh(CO)_2(acac)$ precursor was added in the amount needed to yield samples containing 1 wt% Rh. The Rh weight loading was verified by inductively coupled plasma-mass spectrometry (ICP-MS) analysis (Galbraith Laboratories Inc.). The prepared samples were stored and handled in a glovebox filled with N_2 to prevent possible decomposition of supported species.

2.3.3 FTIR SPECTROSCOPY

A Nicolet Nexus 470 spectrometer equipped with a MCT-B detector cooled by liquid nitrogen was used to collect spectra with a resolution of 2 cm^{-1}, averaging 64 scans per spectrum. Each powder sample was pressed into a self-supported wafer with a density of approximately 20 mg/cm^2 and mounted in a home-made cell connected to a gas distribution manifold. The cell design allowed for the treatment of samples at different temperatures, while various gases flowed through the cell.

2.3.4 X-RAY ABSORPTION SPECTROSCOPY (XAS) MEASURMENTS

XAS spectra were collected at X-ray beamline 4-1 of the Stanford Synchrotron Radiation Laboratory (SSRL), Stanford Linear Accelerator Center, Menlo Park, CA. The storage ring electron energy was 3 GeV and the ring current was in the range of 345-350 mA.

XAS measurements were used to characterize the surface species formed after the impregnation of $Rh(CO)_2(acac)$ on the support and after exposure of samples to different treatments. Prior to these XAS measurements, each powder sample was pressed into a wafer inside a N_2-filled glovebox. The sample mass was calculated to give an absorbance of approximately 2.5 at the Rh K absorption edge. After the sample had been pressed, it was loaded into an EXAFS cell [145], sealed under N_2, and removed from the glovebox. The cell was connected to a gas distribution system and aligned in the X-ray beam. The cell design allows not only to handle samples without air exposure, but also to use the cell as a flow reactor. The XAS data were collected at room temperature in the transmission mode while different gases flowed through the cell, using a Si(220) double crystal monochromator which was detuned 30% to minimize the effects of higher harmonics in the X-ray beam. Samples were scanned at energies near the Rh K absorption edge (23220 eV). All spectra were calibrated with respect to Rh foil, the spectrum of which was collected simultaneously.

2.3.5 EXTENDED X-RAY ABSORPTION FINE STRUCTURE (EXAFS) DATA ANALYSIS

The EXAFS data were analyzed with experimentally determined reference files obtained from EXAFS data for materials of known structure. The Rh–Rh and Rh–Osupport interactions were analyzed with phase shifts and backscattering amplitudes obtained from EXAFS data for rhodium foil and Rh_2O_3, respectively. The Rh–C and Rh–O* contributions (where O* represents carbonyl oxygen) were analyzed with phase shift and backscattering amplitudes obtained from EXAFS data characterizing crystalline $Ru_3(CO)_{12}$, which has only terminal CO ligands. The transferability of the phase shifts and backscattering amplitudes for near neighbors in the periodic table has been justified experimentally [146]. The parameters used to extract these files from the EXAFS data are reported elsewhere [147]. The EXAFS data were extracted from the spectra with the XDAP software developed by XAFS Services International [148]. The EXAFS function for each sample was obtained from the X-ray absorption spectrum by a cubic spline background subtraction and normalized by dividing the absorption intensity by the height of the absorption edge. The final normalized EXAFS function for each sample was obtained from an average of six scans. The parameters characterizing both low-Z (O, C) and high-Z (Rh) contributions were determined by multiple-shell fitting with a maximum of 20 free parameters in r space (where r is the distance from the absorbing atom, Rh) and in k (wave vector) space over the ranges of $3.5 < k < 15.0$ Å-1 and $0.5 < r < 3.5$ Å with application of k^1 and k^3 weighting of the Fourier transform. The statistically justified number of free parameters (n), estimated from the Nyquist theorem [149,150], $n = (2\Delta k\Delta r/\pi) + 1$, where Δk and Δr are the k and r ranges used to fit the data, was approximately 23. The fit was optimized by use of a difference file technique [151,152], with phase- and amplitude-corrected Fourier transforms. The best fit parameters determined for each sample examined are summarized in Table 2.1. Standard deviations reported in Table 2.1 for the various parameters were calculated with the XDAP software, as described elsewhere [153]. Systematic errors are not included in the calculation of the standard deviations. The values of the goodness of fit (ε_ν^2) were calculated with the XDAP software as outlined in the Reports on Standards and Criteria in XAFS Spectroscopy [154]. The variances in both the imaginary and absolute parts were used to determine the fit quality [155].

2.3.6 MASS-SPECTROMETRY MEASURMENTS

Mass spectrometry (MS) measurements were used to monitor ligand exchange reactions between surface species and different gases and to identify the products released during such reactions. In a typical experiment, approximately 100 mg of the sample was loaded into a plug-flow micro reactor in a glovebox and the reactor was sealed to avoid air exposure. The reactor was subsequently connected to a gas distribution system equipped with mass flow controllers and an online Inficon Transpector 2 residual gas analyzer operating in a multi-ion detection mode. Before each experiment, the reactor was purged with He (100 ml/min) at 25°C and atmospheric pressure for 1 h to stabilize the baseline mass spectrometer signal. When this procedure was completed, various feeds (as specified in the text) were introduced into the reactor at 25°C and a flow rate of 100 ml/min. The feed and effluent compositions were routinely monitored with time on stream to detect species such as H_2 (m/z= 2), CO (m/z= 28), ^{13}CO (m/z= 29), CO_2 (m/z= 44), C_2H_4 (m/z= 26, 27, 28), and C_2H_6 (m/z= 30). The m/z values shown in brackets and listed in increasing order of their relative intensities and correspond to the most abundant lines in the fragmentation pattern of each species.

2.3.7 CATALYTIC MEASURMENTS

Catalytic activity measurements for the hydrogenation of C_2H_4 were performed in a quartz single-pass fixed-bed reactor at atmospheric pressure and room temperature. The temperature inside the reactor was monitored by a thermocouple extended into the catalyst bed. Samples in powder form (0.1 g) were loaded in a glovebox and the reactor was sealed to avoid air exposure. The total volumetric flow rate of the reactant mixture (608 Torr H_2/ 76 Torr C_2H_4/balance N_2) was held at 100 ml/min (1atm, 25°C), yielding a corresponding Gas Hourly Space Velocity (GHSV) of 6,000 h^{-1}. The feed and the reaction products were analyzed with an on-line gas chromatograph (HP 7890 A, Agilent) equipped with TCD and FID detectors and two capillary columns. A Rt-Alumina column (50m, 0.53 mm ID, Restek) was used for the analysis of hydrocarbons, while a Carboxen 1010 Plot column (30m, 0.53 mm ID, Supelco) was used for the analysis of hydrogen. In the absence of a catalyst, there was no measurable conversion of C_2H_4.

2.4 RESULTS AND DISCUSSION

When a $Rh(CO)_2$/HY30 sample prepared from the $Rh(CO)_2$(acac) precursor was exposed to H_2 at room temperature and atmospheric pressure, no visible changes in the FTIR spectra were observed. Furthermore, no new features were observed in the spectra even when the same experiment was performed at elevated temperatures. In this case, however, the v_{CO} bands at 2117 and 2053 cm^{-1} characterizing supported $Rh(CO)_2$ complexes progressively declined in intensity as the temperature was increased and completely disappeared from the spectra at approximately 300°C, indicating a complete decarbonylation of the $Rh(CO)_2$ species under these conditions. This process was also accompanied by an aggregation of the original site-isolated Rh cations into small clusters, as indicated by the increase in the Rh–Rh coordination number to approximately 4.0 shown in the EXAFS data for the sample treated in H_2 at 300°C (Table 2.1). These experiments clearly show that Rh carbonyl hydride complexes cannot be formed via the direct treatment of the $Rh(CO)_2$/HY30 sample with H_2. This result is further reinforced by DFT calculations predicting that the oxidative addition of H_2 to rhodium carbonyl complexes is thermodynamically unfavorable due to the presence of the initial substitution step on which the strong Rh–CO bond must be broken while only a weak Rh-(η^2-H_2) bond is formed instead [156].

Table 2.1 EXAFS structural parameters characterizing surface species formed after the treatment of the $Rh(CO)_2(acac)$/HY30 sample under different conditions.

Treatment	Shell	N	R (Å)	$\Delta\sigma^2$ (Å^2)	ΔE_0 (eV)	ε_v^2	k^1-variances (%)	
							Im.	Abs.
C_2H_4 at 25°C [a]	Rh–Rh	--	--	--	--	1.0	1.2	0.8
	Rh–C*	1.0	1.83	0.00262	-5.2			
	Rh–O*	1.1	2.97	0.00123	-4.8			
	Rh–C_{et}	2.1	2.15	0.00491	-0.7			
	Rh–$O_{support}$							
	Rh–O_s	2.6	2.21	0.00130	3.0			
	Rh–O_l	1.3	2.71	0.00171	-1.3			
C_2H_4 at 25°C followed by H_2 at 25°C [a]	Rh–Rh	--	--	--	--	1.4	0.8	0.6
	Rh–C*	0.9	1.84	0.00235	-7.5			
	Rh–O*	1.0	2.96	0.00067	-1.4			
	Rh–$O_{support}$							
	Rh-O_s	2.5	2.21	0.00184	-5.5			
	Rh-O_l	0.7	2.73	-0.00520	-6.1			
H_2 at 300°C [a]	Rh–Rh	4.0	2.67	0.00518	0.7	1.2	1.0	0.5
	Rh–$O_{support}$							
	Rh-O_s	1.5	2.07	0.00182	-8.9			
	Rh-O_l	1.4	2.80	0.00500	4.2			

Standard deviations in fits: N ± 20%, R ± 1%, $\Delta\sigma^2$ ± 10%, ΔE_0 ± 10%; N, coordination number; R, distance between absorber and backscatterer atoms; $\Delta\sigma^2$, Debye-Waller factor relative to the Debye-Waller factor of the reference compound; ΔE_0, inner potential correction accounting for the difference in the inner potential between the sample and the reference compound; ε_v^2, goodness of fit; the superscript * refers to carbonyl ligands, while the subscript $_{et}$ refers to

C_2H_4 ligands. [a] R-space fit ranges of $3.5 < k < 15.0$ Å^{-1} and $0.5 < r < 3.5$ Å; 23 allowed fitting parameters.

It has been reported previously that $Rh(C_3H_5)_2$ complexes grafted on SiO_2 can react with molecular hydrogen at room temperature to form SiO_2-supported $Rh(C_3H_5)H$ species and gaseous propane [20]. In contrast, it has also been reported that the similar treatment of $Rh(C_2H_4)_2$ species supported on HY30 zeolite results in the formation of gaseous ethane and the conversion of the original site-isolated Rh species into clusters incorporating approximately 3 Rh atoms [158]. While the former example suggests that the presence of alkene ligands in the precursor could be a prerequisite for the successful synthesis of supported Rh species incorporating hydride ligands, the latter clearly demonstrates the aggregation of Rh sites likely due to the unstable nature of Rh species formed under such conditions. One can further suggest that the aggregation of Rh could be minimized when more stable or less reactive ligands are present in supported Rh complexes in addition to alkene ligands. This points at the $Rh(CO)(C_2H_4)$ complex as a promising precursor for the formation of site-isolated $Rh(CO)H_x$ species.

2.4.1 SYNTHESIS OF SUPPORTED $Rh(CO)(C_2H_4)$ COMPLEXES

It has been shown previously that supported $Rh(CO)(C_2H_4)$ complexes can be formed via a two-step sequence of ligand exchange reactions [159]. More specifically, dealuminated Y zeolite-supported $Rh(C_2H_4)_2$ complexes prepared from a $Rh(C_2H_4)_2(acac)$ precursor can react with CO at room temperature and atmospheric pressure to yield supported rhodium dicarbonyl $Rh(CO)_2$ species. The carbonyl ligands of the latter were found to be reactive, with subsequent exposure to C_2H_4 under ambient conditions leading to the formation of mixed $Rh(CO)(C_2H_4)$ complexes [159]. The results described below show that the selective synthesis of dealuminated Y zeolite-supported $Rh(CO)(C_2H_4)$ complexes can also be achieved in one step.

Well-defined and site-isolated zeolite-supported $Rh(CO)_2$ complexes can be prepared directly from the $Rh(CO)_2(acac)$ precursor as described elsewhere [63]. These species exhibit a very specific infrared signature consisting of two very narrow v_{CO} bands at approximately 2117 and 2052 cm^{-1}, assigned to the symmetric and asymmetric v_{CO} vibrations of the carbonyl ligands, respectively. Moreover, the structure of these species has been established based on extensive EXAFS characterization measurements and confirmed by DFT calculations [63]. In particular, it has been shown that dealuminated Y zeolite-supported $Rh(CO)_2$ species retain the square-planar geometry of the $Rh(CO)_2(acac)$ precursor upon anchoring, with two oxygen atoms located in the T4 ring of the Y zeolite and coordinated to Al^{3+} cations representing the most probable binding sites for these species [63]. While such complexes were used in the past as convenient probes to identify specific locations of binding sites in the zeolite framework [63], it was generally assumed that their carbonyl ligands are unreactive [64].

A $Rh(CO)_2$/HY30 sample was prepared from the $Rh(CO)_2$(acac) precursor as described previously [63], and exposed to C_2H_4 flow at room temperature and atmospheric pressure, while FTIR spectra were collected to monitor changes in the surface species. As expected, the $Rh(CO)_2$/HY30 sample is characterized by two sharp bands in the v_{CO} region located at approximately 2117 and 2053 cm^{-1} (Fig. 2.1, spectrum 1), consistent with the presence of supported $Rh(CO)_2$ species. Upon exposure to the C_2H_4 flow, the v_{CO} band at 2117 cm^{-1} sharply declined in intensity (Fig. 2.1, insert) and completely disappeared from the spectrum after approximately 3 min on stream. During this process, the intensity of the v_{CO} band at 2053 cm^{-1} remained unchanged but the full width at half-maximum (FWHM) value increased from 6 to 10 cm^{-1} by the time the disappearance of the 2117 cm^{-1} band was completed (Fig. 2.1, spectrum 2).

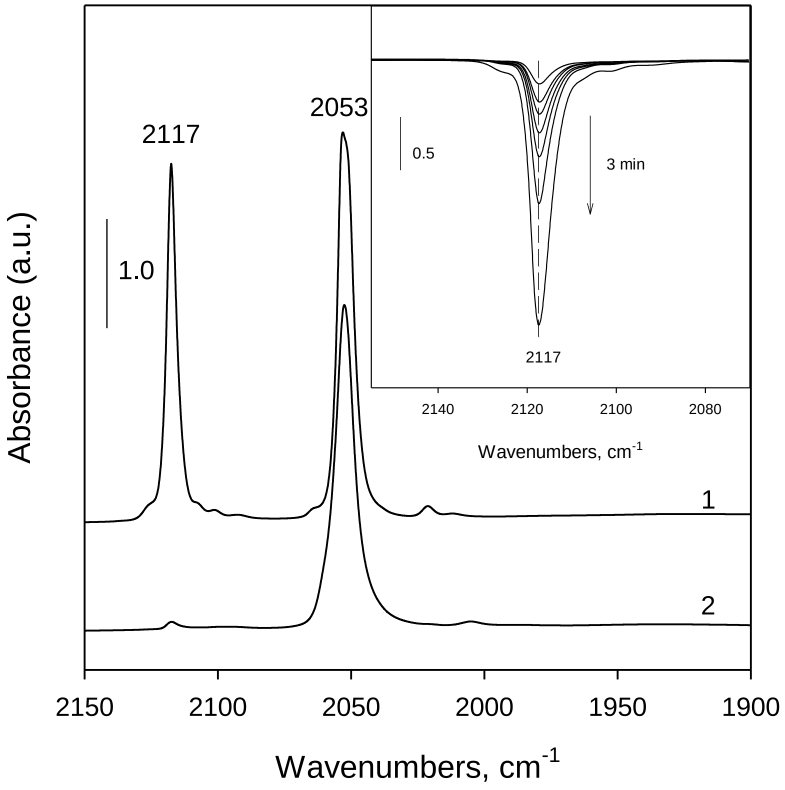

Figure 2.1 FTIR spectra in the ν_{CO} region of (1) a freshly prepared $Rh(CO)_2$/HY30 sample and (2) the same sample treated under the flow of C_2H_4 at room temperature for 3 min. The insert shows difference spectra illustrating the disappearance of the ν_{CO} band at 2117 cm^{-1} with time on stream.

When the sample was subsequently purged with He, new bands appeared in the spectra in the ν(C–H) region at 3094, 3070, 3021, and 2986 cm^{-1}, the ν(C=C) region at 1536 cm^{-1}, and the $\delta(CH_2)$ region at 1438 cm^{-1} (Table 2.2). All these new bands are consistent with those predicted by density functional theory (DFT) calculations and experimentally observed in various organometallic compounds of Rh incorporating π-bonded C_2H_4 ligands [161], indicating that C_2H_4 was coordinated to the Rh sites. The Rh complexes thus formed were evidently stable, as no changes in the FTIR spectra were observed for an extended period of time under He flow.

The square-planar 16-electron $Rh(CO)_2$ complex attached to two oxygen atoms of the zeolite framework [63] can potentially coordinate one additional C_2H_4 molecule without release of a carbonyl ligand. Depending on any changes occurring at the Rh-support interface during this process, the resultant species can either maintain the 16-electron count and the square planar geometry or be transformed to an 18-electron $Rh(CO)_2(C_2H_4)$ complex. The formation of the latter would likely also change the geometry, since the Rh cation is expected to be penta-coordinated in this case. Moreover, it is possible that carbonyl ligands in surface species thus formed may not be located in a cis position in respect to each other and, therefore, the FTIR signature of the $Rh(CO)_2$ species can be lost. Alternatively, it is also possible that the Rh-support interface remains unaffected during the process and one of the CO ligands is simply replaced by C_2H_4 so that the $Rh(CO)(C_2H_4)$ complex thus formed remains attached to two oxygen atoms of the support and is 16-electron and square-planar in nature. In order to differentiate between these possibilities, it is important to determine whether any CO ligands were released from the Rh complex.

While mass spectrometry measurements have been used in the past to monitor changes in the ligand environment of dealuminated Y zeolite-supported $Rh(CO)_2$ complexes prepared from the $Rh(C_2H_4)_2(acac)$ precursor upon exposure to C_2H_4 [159], the results reported are not convincing because it is virtually impossible to distinguish between CO and C_2H_4, both of which are characterized by a m/z ratio of 28. To resolve this issue, the $Rh(CO)_2$/HY30 sample in our case was first exposed to ^{13}CO to form supported $Rh(^{13}CO)_2$ species. The replacement of CO ligands by ^{13}CO in supported $Rh(CO)_2$ complexes proceeds to completion quickly, as indicated by the disappearance of the v_{CO} bands at 2117 and 2053 cm^{-1} and the appearance of two new bands at 2068 and 2005 cm^{-1} in the FTIR spectra (Table 2.2). The $Rh(^{13}CO)_2$/HY30 sample thus formed was first purged with He to remove any traces of CO and ^{13}CO from the system and subsequently exposed to a flow of C_2H_4 at room temperature and atmospheric pressure. The results obtained in this case were identical to those collected with $Rh(CO)_2$ species. For example, the v_{CO} band at 2068 cm^{-1} completely disappeared from the spectrum after approximately 3 min on stream; the band at 2005 cm^{-1} remained unchanged in intensity but became broader (FWHM 14 cm^{-1}); and new bands assigned to the v(C–H), v(C=C), and $\delta(CH_2)$ vibrations of C_2H_4 attached to Rh appeared in the FTIR spectra (Table 2.2), indicating that the reactivity of carbonyl ligands to C_2H_4 in $Rh(CO)_2$ and $Rh(^{13}CO)_2$ surface species is quite similar.

Table 2.2 Vibrational frequencies characterizing the surface species formed by adsorption of the $Rh(CO)_2(acac)$ precursor on the HY zeolite support and following subsequent treatments.

Sample	Treatment	Bands, cm^{-1}	Assignments	Suggested surface species
$Rh(CO)_2(acac)$/HY30	none	2117 2053	v_{CO} (sym) v_{CO} (asym)	$Rh(CO)_2$
$Rh(CO)_2(acac)$/HY30	C_2H_4 at 25°C for 3 min	3094 3070 3021 2986 2053 1536 1438	v_{CH} v_{CH} v_{CH} v_{CH} v_{CO} $v_{C=C}/\delta(CH_2)$ δ (CH_2)	$Rh(CO)(C_2H_4)$
$Rh(CO)_2(acac)$/HY30	^{13}CO pulse	2068 2005	v_{CO} (sym) v_{CO} (asym)	$Rh(^{13}CO)_2$
$Rh(CO)_2(acac)$/HY30	^{13}CO pulse followed by C_2H_4 for 3 min	3093 3074 3021 2987 2005 1530 1438	v_{CH} v_{CH} v_{CH} v_{CH} v_{CO} $v_{C=C}/\ \delta$ (CH_2) δ (CH_2)	$Rh(^{13}CO)(C_2H_4)$

Fig. 2.2 shows mass spectra of the reactor effluent recorded during the exposure of the $Rh(^{13}CO)_2$/HY30 sample to C_2H_4. When C_2H_4 was added to the He flow, the signal from this component (m/z=28) immediately appeared in the mass spectrum. The intensity of this signal increased progressively during the first 2.5 min on stream and remained constant thereafter. It should be noted that approximately 1 min was required to remove C_2H_4 completely from the system at the end of this experiment. Simultaneously with the appearance of C_2H_4, the signal from ^{13}CO (m/z=29) was also observed in the mass spectrum. This signal

displayed a sharp maximum and completely disappeared after approximately 2.5 min on stream, indicating that all ^{13}CO species released into the gas phase were purged from the system by that time. The presence of ^{13}CO in the reactor effluent provides unambiguous evidence that C_2H_4 indeed replaces ^{13}CO ligands in the $Rh(^{13}CO)_2$ surface species. Moreover, the complete temporal overlap of the release of ^{13}CO with the period required for C_2H_4 to reach its maximum concentration in the effluent further supports the previous conclusion. Finally, this conclusion is also reinforced by the FTIR results described above, providing clear evidence for the coordination of C_2H_4 on Rh sites.

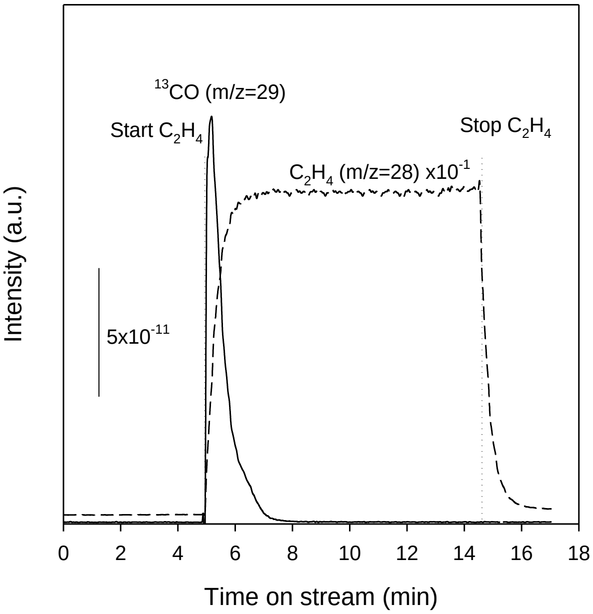

Figure 2.2 Mass spectra of the reactor effluent recorded during exposure of the $Rh(^{13}CO)_2$/HY30 sample to C_2H_4 at room temperature.

Literature examples, describing the reaction of the $Rh(CO)_2(acac)$ complex with alkenes either in solution or imbedded into a polymer matrix indicate that alkenes can replace only one CO ligand in the $Rh(CO)_2(acac)$ complex [162]. Moreover, infrared data reported by the same authors show that the $Rh(CO)(C_2H_4)(acac)$ complex is characterized by a single v_{CO} band at 2010 cm^{-1}, while the parent $Rh(CO)_2(acac)$ complex exhibits two bands in the v_{CO} region at 2081 and 2011 cm^{-1}, suggesting that the position of the remaining v_{CO} band (i.e., at 2011 cm^{-1}) in this complex is unaffected by the presence of the C_2H_4 ligand. Taking into account our experimental results described above and this literature example, we can safely infer that only one carbonyl ligand in HY zeolite-supported $Rh(CO)_2$ species can be replaced by C_2H_4, yielding $Rh(CO)(C_2H_4)$ complexes, with the group of infrared bands listed in Table 2.2 representing the characteristic FTIR fingerprint of these species.

The EXAFS data shown in Table 2.1 for the $Rh(CO)_2$/HY30 sample treated in C_2H_4 provide complementary information about the structure of the surface species formed. Based on XRD data reported elsewhere [163] for the $Rh(CO)_2(acac)$ precursor, the Rh–C and $Rh–O^*$ bond distances associated with two terminal CO ligands in this complex are 1.831 and 2.986 Å, respectively. EXAFS data reported previously [62] for $Rh(CO)_2$ species prepared from this precursor on different zeolites also confirm the presence of two terminal CO ligands in the surface species with average Rh–C and $Rh–O^*$ distances of 1.85 and 2.98 Å, respectively, suggesting that the carbonyl ligands remain intact following the impregnation step. The Rh K edge EXAFS data collected after exposure of the $Rh(CO)_2$/HY30 sample to C_2H_4 show the presence of Rh–C contributions with average coordination numbers of 1.0 and 2.1 at distances of

1.83 and 2.15 Å, respectively (Table 2.1). The first Rh–C contribution can be assigned to terminal carbonyl ligands. The corresponding Rh–O* contribution from the oxygen atoms of the CO ligands is observed with an average coordination number of 1.1 at a distance of 2.97 Å (Table 2.1). The distance of 2.15 Å characterizing the second Rh–C contribution is typical of Rh cationic complexes incorporating π-bonded alkenes as ligands [165]. The presence of such a contribution in the EXAFS spectrum of this sample provides strong evidence for the π-bonding of C_2H_4 to the Rh sites.

Consistent with the FTIR results, the EXAFS parameters (i.e., coordination numbers and bond distances) characterizing the $Rh(CO)_2$/HY30 sample exposed to C_2H_4 suggest that each Rh atom is coordinated to approximately one CO and one C_2H_4 ligand, indicating the formation of $Rh(CO)(C_2H_4)$ surface complexes. Since no Rh–Rh contributions were observed in the EXAFS spectrum, these complexes remain site-isolated. Furthermore, the $Rh(CO)(C_2H_4)$ species appear to strongly interact with the zeolite framework, as evidenced by the presence of Rh-$O_{support}$ (i.e., short (Rh–O_s) and long (Rh-O_l)) contributions characterized by average coordination numbers of 2.6 and 1.3 at average distances of 2.21 and 2.71 Å, respectively (Table 2.1). Among these Rh-$O_{support}$ contributions only the short one represents the Rh-support interface, indicating that the $Rh(CO)(C_2H_4)$ species are bound to approximately two oxygen atoms of the zeolite framework. While the average distance of 2.21 Å determined by EXAFS for this Rh-O_s contribution is somewhat longer than that typically observed for $Rh(CO)_2$ complexes (i.e., in the 2.05-2.19 Å range) formed on different supports (including zeolites) [62,166,167], it is fairly close to Rh-$O_{support}$ distances predicted by DFT calculations (i.e., 2.18-2.20 Å) for $Rh(CO)_2$ complexes bound to oxygen atoms connected to Al^{3+} sites in the four-ring (T4) or five-ring (T5) zeolite clusters [19]. Based on these results, we can conclude that the metal-support interface remains the same during the substitution of one carbonyl ligand in the surface $Rh(CO)_2$ complexes with C_2H_4.

2.4.2 SYNTHESIS OF SUPPORTED $Rh(CO)(H_x)$ SPECIES

When the $Rh(CO)(C_2H_4)$/HY30 sample was further exposed to the flow of pure hydrogen at room temperature and atmospheric pressure, significant changes were observed in the FTIR spectra with time on stream (Fig. 2.3). More specifically, the v_{CO} band at 2053 cm^{-1} declined in intensity, while a new band at 2091 cm^{-1} with a shoulder at 2096 cm^{-1} appeared in the spectra. The intensity of this band increased as a function of time and reached its maximum value when the band at 2053 cm^{-1} almost disappeared. This new band at 2091 cm^{-1} can be assigned to the v_{CO} vibration in a new surface species formed. Simultaneously with the changes observed in the v_{CO} region, the v_{CH} bands at 3093, 3074, 3021, and 2987 cm^{-1} characterizing the Rh-bound C_2H_4 ligands declined in intensity and eventually disappeared, while the appearance of C_2H_6 with a characteristic v_{CH} vibration at 2957 cm^{-1} was detected in the gas phase (spectra not shown for brevity). Finally, several new low intensity bands appeared in the 2170-2120 cm^{-1} region (Fig. 2.3) and their development coincided perfectly with the development of the 2091 cm^{-1} band.

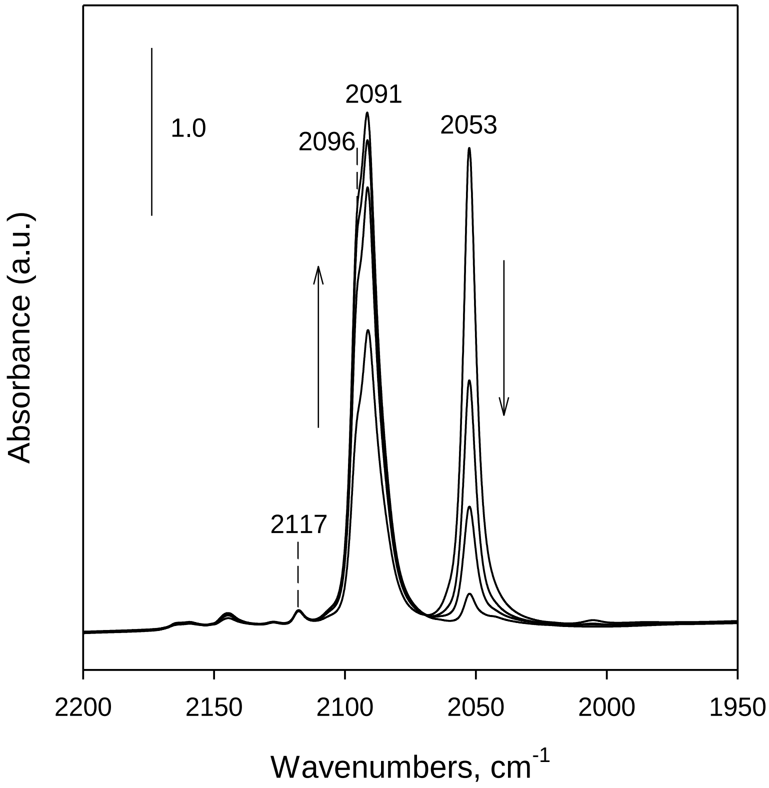

Figure 2.3 FTIR spectra recorded during exposure of the $Rh(CO)(C_2H_4)$/HY30 sample to the flow of H_2 at room temperature for 30 min. Arrows indicate the appearance and disappearance of ν_{CO} bands.

The formation of gas phase C_2H_6 during such a treatment was further verified in separate experiments using mass spectrometry measurements. The results shown in Fig. 2.4 confirm that hydrogenation of the C_2H_4 ligands in the zeolite-supported $Rh(CO)(C_2H_4)$ complexes by H_2 takes place at room temperature. This result is consistent with earlier reports [159,64] demonstrating the hydrogenation of the C_2H_4 ligands in zeolite-supported $Rh(C_2H_4)_2$ complexes by H_2 under similar conditions.

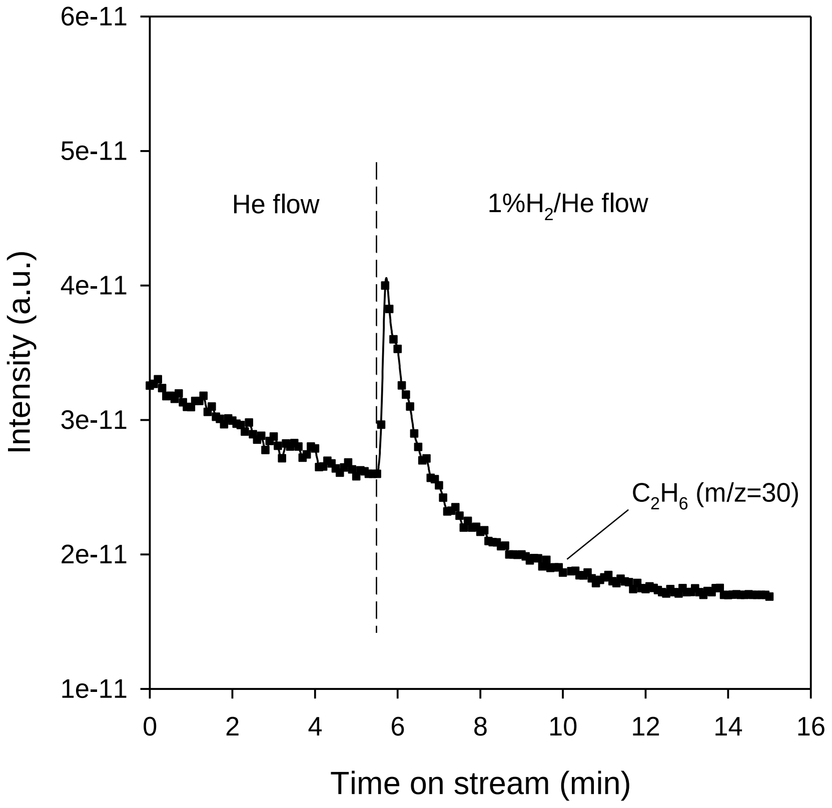

Figure 2.4 Mass spectrum of the gaseous effluent stream recorded during exposure of the Rh(CO)(C_2H_4)/HY30 sample to a 1% H_2/He flow at room temperature.

Experiments were also performed with ^{13}CO and D_2 in an effort to determine the nature and assign all new bands detected in the spectra (i.e., at 2091 cm^{-1} and in the 2170-2120 cm^{-1} region). Substitution of the CO ligands with ^{13}CO cannot be performed directly because all the new bands observed in Fig. 20 disappear immediately following a pulse of CO or ^{13}CO and Rh(CO)$_2$ (v_{CO} at 2117 and 2053 cm^{-1}) and Rh(^{13}CO)$_2$ (v_{CO} at 2068 and 2005 cm^{-1}) species are formed on the surface, respectively. Interestingly enough, the evolution of gas phase H_2 was observed in these experiments (confirmed by MS measurements), implying that the surface species formed after the treatment of $Rh(CO)(C_2H_4)$/HY30 with H_2 must incorporate some type of hydride ligands.

Alternatively, $Rh(^{13}CO)(C_2H_4)$ surface species (Table 2.2) were prepared first by CO-^{13}CO ligand exchange of the original $Rh(CO)_2$/HY30 sample followed by C_2H_4 treatment at room temperature, and were then exposed to the H_2 flow at room temperature and atmospheric pressure. The changes observed in the FTIR spectra during the H_2 treatment were similar to those described above for the $Rh(CO)(C_2H_4)$ species. More specifically, the characteristic vibrations of the C_2H_4 ligands disappeared with time on stream, consistent with their hydrogenation. The v_{CO} band at 2005 cm^{-1} characteristic of the $Rh(^{13}CO)(C_2H_4)$ species substantially declined in intensity, while a new band with a maximum at 2042 cm^{-1} and a shoulder at 2047 cm^{-1} was formed (Fig. 2.5, spectrum 2). The shape of this new band is nearly identical to that of the 2091 cm^{-1} band (with a shoulder at 2096 cm^{-1}) formed during the same experiment with $Rh(CO)(C_2H_4)$ species (Fig. 22, spectrum 1). Moreover, a further comparison of spectra shown in Fig. 2.5 for these two samples indicates that the main features of this new band (i.e., the maximum and the shoulder) are red-shifted by approximately 49 cm^{-1}, consistent with the CO-^{13}CO isotopic shift expected for surface species incorporating CO as a ligand. We can, therefore, conclude that the bands with maxima at 2091 and 2042 cm^{-1} observed in experiments with ^{12}CO and ^{13}CO, respectively, represent a CO ligand in a new environment. Furthermore, since the v_{CO} vibration of a zeolite-supported monocarbonyl Rh(CO) species is known to be at a much lower frequency [143], these results indicate that the Rh surface species characterized by the ν_{CO} bands at approximately 2091 and 2042 cm^{-1} incorporate some additional ligands.

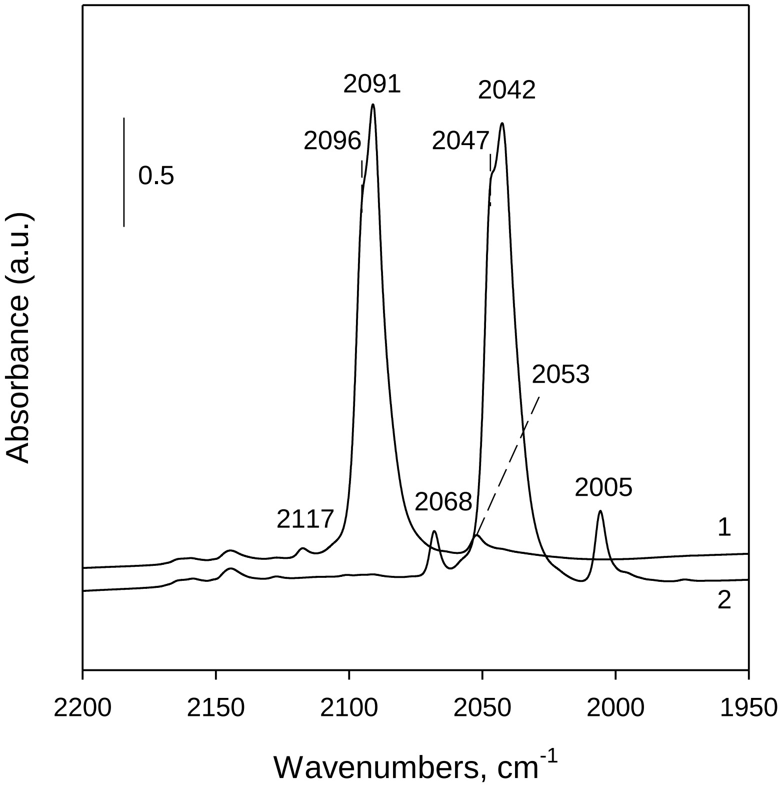

Figure 2.5 FTIR spectra of (1) Rh(CO)(C_2H_4)/HY30 and (2) Rh(^{13}CO)(C_2H_4)/HY30 samples treated in H_2 at room temperature for 30 min.

The results shown in Fig. 2.5 further indicate that the appearance of the new strong band in the ν_{CO} region during the H_2 treatment of zeolite-supported Rh(CO)(C_2H_4) and Rh(^{13}CO)(C_2H_4) complexes is accompanied by the appearance of several weak bands in the 2170-2120 cm^{-1} region. The position of these bands is exactly the same regardless of whether ^{12}CO or ^{13}CO is used.

When this region is plotted on a more sensitive scale (Fig. 2.6), at least four bands can be identified in the spectra with maxima at 2164, 2156, 2143, and 2129 cm^{-1}.

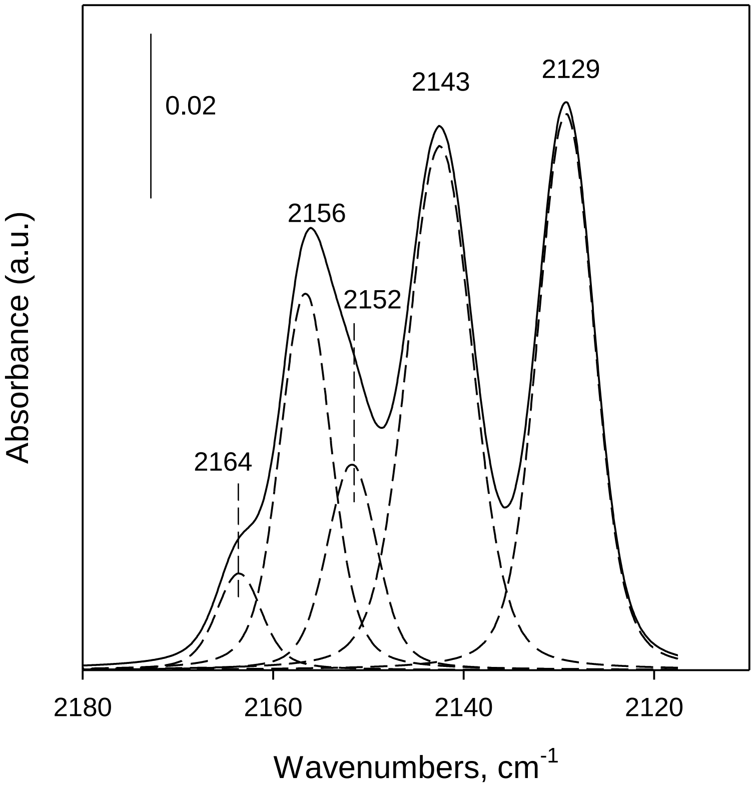

Figure 2.6 FTIR spectrum in the ν_{RhH} region of the surface species formed after the treatment of the Rh(CO)(C_2H_4)/HY30 sample with H_2 at room temperature for 30 min (solid line); deconvolution results also shown (dashed line).

Since all these bands fall into the range of wavenumbers characteristic of metal hydrides [168], their presence suggests the formation of rhodium carbonyl hydride Rh(CO)$(H)_x$ species. To further confirm such an assignment, the Rh(CO)(C_2H_4)/HY30 sample was exposed to H_2 for 30 min, purged with He, and subsequently exposed to a pulse of D_2. The intensity and position of the strong band at 2091 cm^{-1} remained unchanged after the pulse of D_2, confirming the assignment of this band to a v_{CO} vibration. However, the bands located at 2164, 2156, 2143, and 2129 cm^{-1} immediately disappeared from the spectrum, while four new bands appeared at 1564, 1553, 1541, and 1532 cm^{-1} (Fig. 2.7). The isotopic shift for each individual band was approximately 600 cm^{-1}, consistent with theoretical calculations and experimental results reported previously for the replacement of H by D in rhodium hydrides [169]. Overall, these ^{12}CO-^{13}CO and H_2-D_2 substitution experiments provide strong evidence for the formation of $Rh(CO)(H)_x$ species upon exposure of the HY zeolite-supported $Rh(CO)(C_2H_4)$ complexes to H_2 at room temperature. We can further infer that the chemical reaction between H_2 and C_2H_4 ligands provides a driving force for their formation.

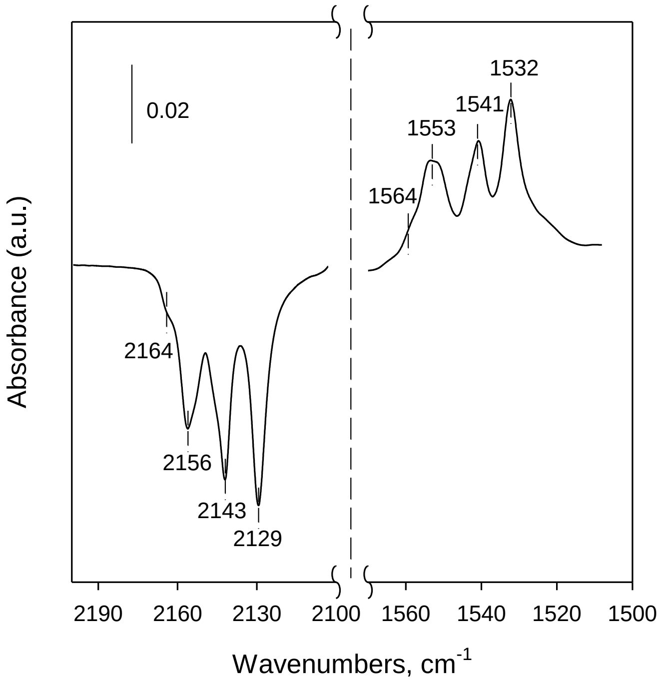

Figure 2.7 Difference FTIR spectrum illustrating changes in the v_{RhH} region after exposure of the $Rh(CO)(H)_x$ species to D_2.

2.4.3 STRUCTURE OF SUPPORTED $Rh(CO)(H_x)$ SPECIES

The Rh K edge EXAFS data (Table 2.1) collected for the $Rh(CO)(C_2H_4)$/HY30 sample treated in H_2 at room temperature provide a strong basis for elucidating the structure of the $Rh(CO)(H)_x$ surface species formed. The absence of any Rh–Rh contributions in the EXAFS spectra of this sample provides unambiguous evidence for the site-isolation and mononuclear nature of the supported rhodium complexes formed after the H_2 treatment. Furthermore, the presence of Rh–C and Rh–O* contributions with average coordination numbers of 0.9 and 1.0 at average distances of 1.84 and 2.96 Å, respectively, suggests that one carbonyl ligand is coordinated to each Rh atom in the surface species formed. In contrast, since no Rh–C contributions from π-bonded C_2H_4 ligands (expected at a distance of 2.15 Å) were observed in the spectra, it can be concluded that these ligands were removed during the H_2 treatment. This result provides a strong reinforcement for the FTIR and MS data, which also document the removal of the C_2H_4 ligands from the surface species in the form of C_2H_6. Finally, the Rh complexes formed on the surface remain attached to the zeolite framework, as evidenced by the presence of short (Rh–O_s) and long (Rh-O_l) contributions characterized by average coordination numbers of 2.5 and 0.7 at average distances of 2.21 and 2.73 Å, respectively (Table 2.1). Once again, since among these Rh-$O_{support}$ contributions only the short one represents the Rh-support interface, it is evident that the Rh species formed remain bound to approximately two oxygen atoms of the zeolite framework.

Overall, the EXAFS data show that the treatment of Rh(CO)(C_2H_4)/HY30 with H_2 at room temperature removes the C_2H_4 ligand, while the carbonyl ligand remains intact. At the same time, the metal-support interface remains unchanged after the loss of the C_2H_4 ligand, and the new surface complex continues to be bound to approximately two oxygen atoms of the zeolite framework. While hydride ligands cannot be identified by EXAFS, the FTIR and MS data discussed previously clearly indicate the presence of such ligands in the new complex, although the exact structure and composition of these hydride ligands needs to be further examined.

The FTIR spectrum in the v_{RhH} region, shown in Fig. 2.6 in a more sensitive scale, clearly has a complex band structure with four maxima. Deconvolution results shown in the same figure (dashed lines) indicate that in addition to the four bands present at 2164, 2156, 2143, and 2129 cm^{-1}, a fifth band can be also identified with a maximum at 2152 cm^{-1}. When the deconvolution procedure was also applied to the v_{CO} region of the same spectrum (Fig. 2.8), three bands were revealed at 2096, 2091, and 2086 cm^{-1}.

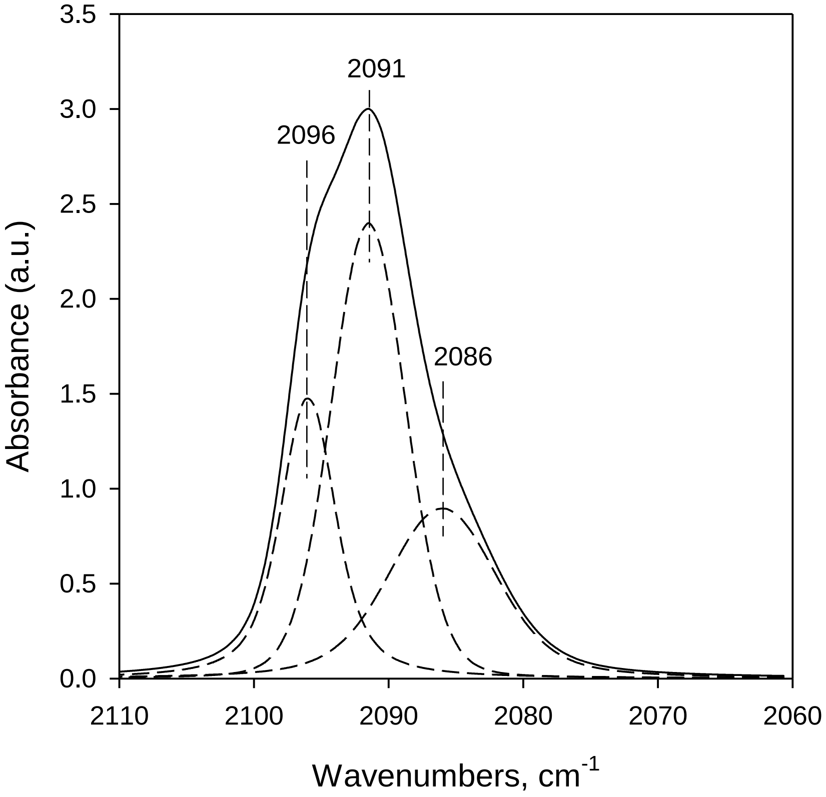

Figure 2.8 FTIR spectrum in the v_{CO} region of the surface species formed after the treatment of the $Rh(CO)(C_2H_4)$/HY30 sample with H_2 at room temperature for 30 min (solid line); deconvolution results also shown (dashed line).

A first interpretation of these results may be that a mixture of surface species incorporating different forms of hydrogen ligands was formed and previous literature reports may at first appear to support such a conclusion. For example, the v_{CO} bands at 2091 and 2096 cm^{-1} were observed previously after UV activation of zeolite-supported $Rh(CO)_2$ species in the presence of H_2 and were assigned to a mixture of Rh(CO)(H) and $Rh(CO)(H_2)$ species [144], with the latter incorporating molecular hydrogen as a ligand. While the synthesis of organometallic Rh complexes incorporating molecular hydrogen has been reported in previous publications [170-172], the number of such examples is fairly limited due to the lower stability of these species, as shown by DFT calculations [173]. Furthermore, organometallic complexes in which η^2-H_2 ligands are bound to the metal site, typically show the presence of several fundamental vibrations (i.e., v_{HH}, asymmetric and symmetric v_{MH2}, and δ_{MH2}) in their FTIR spectra at approximately 2690, 1570, 950, and 470 cm^{-1}, respectively [174]. While the symmetric v_{MH2} and δ_{MH2} bands cannot be detected in our case due to the strong absorption of the zeolite support in these regions, the anticipated v_{HH} and asymmetric v_{MH2} bands were not observed in our spectra. In addition, due to the analogy between the binding of molecular H_2 and C_2H_4 to metal sites in organometallic compounds, these ligands are known to participate in facile substitution reactions [170,172], with the $Rh(\eta^2$-$H_2)L$ complexes quantitatively transformed into $Rh(C_2H_4)L$ ones and vice versa. Moreover, organometallic complexes with η^2-H_2 ligands are not capable of catalyzing the hydrogenation of C_2H_4 at room temperature [174], since molecular H_2 must dissociate before this reaction can proceed. Mass spectrometry results discussed in section 3.4 show that when Rh(CO)(H)$_x$ surface species are treated with C_2H_4 a facile substitution process does not take place, but instead C_2H_6 is formed in the gas phase. Finally, results from experiments involving H-D exchange (Fig. 2.7) indicate that all major bands detected in the v_{RhH} region have counterparts in the v_{RhD} region with a isotopic v_{RhH}/v_{RhD} frequency ratio of 1.39 typical for metal hydrides [139] instead of a Rh(η^2-H_2)L type of species. Based on the above, we can conclude that the treatment of Rh(CO)(C_2H_4)/HY30 with H_2 at room temperature leads to the formation of Rh(CO)(H)$_x$ surface hydride species.

DFT calculations for unsupported Rh atoms with only hydride ligands attached predict that the split between the symmetric and asymmetric Rh-H stretching vibrations in a Rh(H)$_2$ dihydride species is approximately 50 cm^{-1}, with the asymmetric mode being the most intense one [139]. However, experimental FTIR results collected by the same authors for Rh(H)$_2$ species embedded in solid argon and neon matrixes show that the actual split between the two vibration modes is approximately 25 cm^{-1} [139]. Consistent with this result, two v_{RhH} bands with a split in the 15-30 cm^{-1} range have been also observed by others in FTIR spectra of different organometallic Rh complexes incorporating dihydride ligands [134,158]. Based on this information, two pairs of bands at 2164/2143 cm^{-1} and 2152/2129 cm^{-1} can be tentatively identified in the v_{RhH} region of our spectra (Fig. 2.6) and assigned to two distinct pairs of dihydride ligands coordinated to Rh sites. We can further infer that each pair of v_{RhH} bands has a counterpart in the v_{CO} region (Fig. 2.8). For example, the v_{RhH} bands at 2164 and 2143 cm^{-1} can be combined with the v_{CO} band at 2091 cm^{-1}, while the v_{RhH} bands at 2152 and 2129 cm^{-1} can be combined with the v_{CO} band at 2086 cm^{-1}. Such an assignment suggests that at least two types of $Rh(CO)(H)_2$ species were formed. The remaining v_{RhH} band at 2156 cm^{-1} does not have a pair in the v_{RhH} region, but it can be combined with the v_{CO} band at 2096 cm^{-1}. Such an assignment would be consistent with the presence of a third Rh(CO)(H) monohydride species on the support surface, which are expected to exhibit a single v_{RhH} vibration. Alternatively, the same two bands at 2156 and 2096 cm^{-1} can also be assigned to a $Rh(CO)(H)_2$ dihydride species in which the two hydride ligands are located trans to each other and, therefore, exhibit a single v_{RhH} stretching vibration. If this was the case however, resonance interactions between the v_{CO} and v_{RhH} vibrational modes would be expected, leading to a significant shift (~ 18-32 cm^{-1}) of the v_{CO} band upon H/D exchange [169]. Since our experimental data show no substantial changes in the v_{CO} region when hydride ligands were replaced for deuterium, we can assign the 2156 and 2096 cm^{-1} bands to the v_{RhH} and v_{CO} vibrations of a Rh(CO)(H) monohydride surface species, respectively. Furthermore, we can conclude that the CO and hydride ligands in the other two $Rh(CO)(H)_2$ complexes are located only in cis positions.

The $Rh(CO)(H)_x$ species formed on the zeolite surface appeared to be stable at room temperature under the flow of dry He for an extended period of time. Since these species incorporate hydride ligands and are bound to oxygen atoms of the zeolite framework (as indicated by EXAFS), Rh should be in the 3+ state in order to maintain the overall neutral charge. Since Rh^{3+} complexes do not exhibit square-planar geometry, we can further suggest that the geometry of the most abundant $Rh(CO)(H)_2$ complexes on the surface is pseudo-trigonal bipyramidal or even pseudo-octahedral if the support fills the empty coordination site on Rh to stabilize the latter geometry. In either case, the formation of several structural isomers can be reasonably expected, as shown in Fig. 2.9. Therefore, such isomers can be accountable for the two groups of bands observed in the v_{CO} and v_{RhH} vibration regions [175].

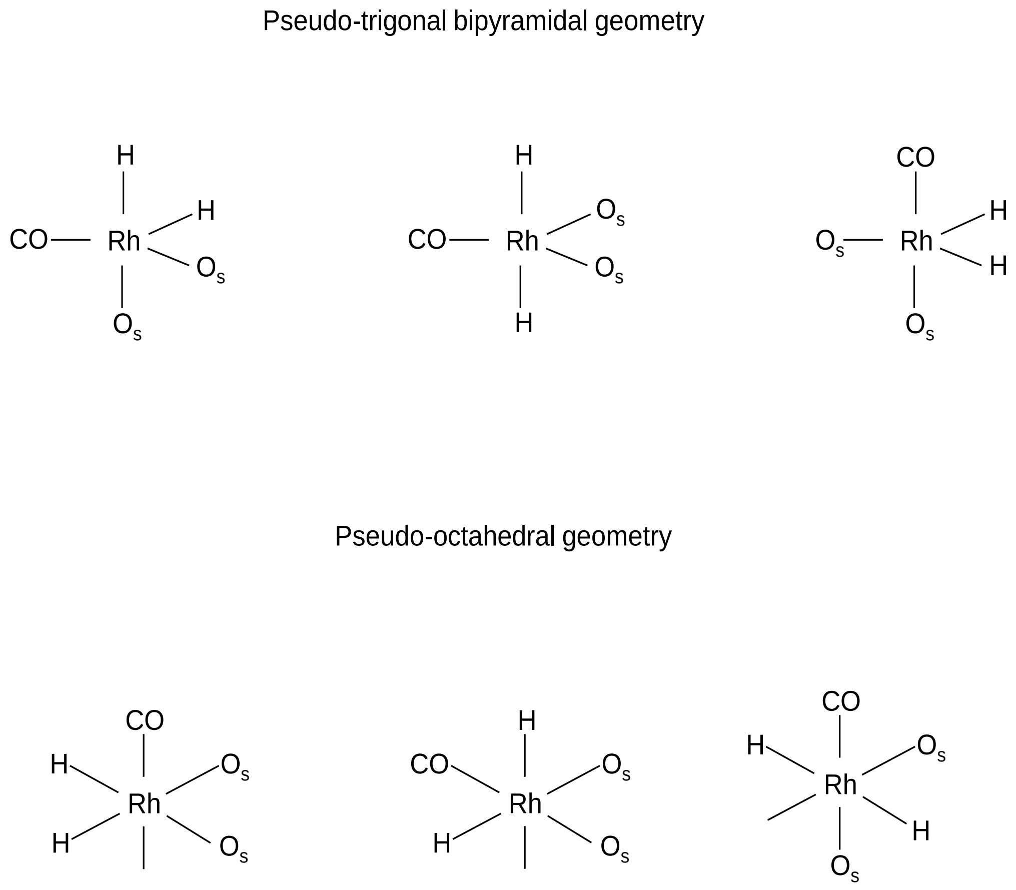

Figure 2.9 Possible isomers of HY zeolite-supported $Rh(CO)(H)_x$ species.

Finally, it has been suggested that oxygen atoms adjacent to Al^{3+} cations in the zeolite framework represent the most probable binding sites for Rh species [63]. While four such oxygen atoms are equally accessible and all of them are capable of coordinating Rh complexes, they are not all identical in terms of their electronic properties, providing a set of slightly different binding sites for the coordination of the Rh species. Moreover, since these oxygen atoms can be regarded as ligands for the Rh complexes, it is possible that small differences in their electronic properties could also influence the infrared vibrations in the ν_{CO} and ν_{RhH} regions.

The formation of the $Rh(CO)(H)_x$ complexes discussed above can be depicted as follows (Fig. 2.10). During the initial impregnation step, site isolated square-planar 16-electron $Rh^I(CO)_2$ complexes are formed on the zeolite framework from the $Rh(CO)_2(acac)$ precursor. Subsequent treatment of these complexes with C_2H_4 leads to the substitution of one CO ligand with C_2H_4 without any significant change at the metal support interface. The $Rh^I(CO)(C_2H_4)$ complexes thus formed, remain site isolated square-planar and 16-electron in nature. During the next H_2 treatment step, oxidative addition of hydrogen takes place. This leads to the oxidation of Rh^+ sites to Rh^{3+}, which is expected to assume octahedral geometry, yielding $Rh^{3+}(CO)(C_2H_4)(H)_2$ type complexes. Subsequent migration of one hydride ligand in this 18-electron complex leads to the formation of a 16-electron $Rh^{3+}(CO)(C_2H_5)(H)$ complex, which can further undergo reductive elimination of ethane (confirmed by MS measurements), yielding a highly reactive coordinatively unsaturated 14-electron $Rh^I(CO)$

complex. With H_2 present in the gas phase, this complex can be immediately converted into a 16-electron $Rh^{3+}(CO)(H)_2$ complexes via an oxidative addition of hydrogen. During this step, the formation of a smaller fraction of $Rh^{3+}(CO)(H)$ species may also take place. Such species could be bound to the zeolite framework slightly differently (Fig. 2.10) to maintain a 14-electron configuration. All steps leading to the formation of $Rh^{3+}(CO)(H)_x$ from $Rh^I(CO)(C_2H_4)$ are very fast with very short lifetimes for the corresponding intermediates, thus, making the detection of these intermediates impossible by our conventional FTIR measurements. As a result, while the $Rh^I(CO)(C_2H_4)$ starting and $Rh^{3+}(CO)(H)_x$ ending "points" of the scheme shown in Fig. 2.10 are strongly supported by experimental evidence, the intermediates shown are speculative in nature.

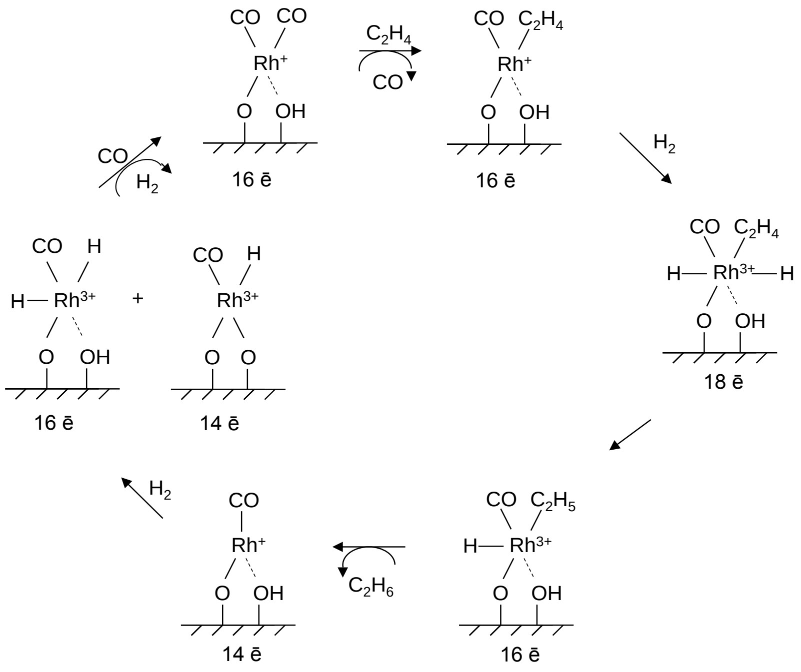

Figure 2.10 Schematic representation of the different steps involved in the formation of HY zeolite-supported $Rh(CO)(H)_x$ species.

2.4.4 REACTIVITY OF SUPPORTED $Rh(CO)(H_x)$ SPECIES TOWARDS CO, N_2, AND C_2H_4

While the FTIR spectrum of the $Rh(CO)(H)_x$ species remained unchanged under the flow of dry He, the v_{CO} and v_{RhH} bands assigned to these species (Fig. 2.3) disappeared immediately after the introduction of a short pulse of CO at room temperature. At the same time, two strong bands appeared in the v_{CO} region at 2117 and 2053 cm^{-1} and the resulting spectrum was identical to that of $Rh(CO)_2$ complexes shown in Fig. 2.1 (spectrum 1). This result indicates that $Rh(CO)(H)_x$ complexes can be rapidly converted to $Rh(CO)_2$ species via room temperature displacement of the hydride ligands by CO. To further confirm this conclusion, the same experiment was repeated with larger amounts of the $Rh(CO)(H)_x$/HY30 sample loaded into a reactor system, while the effluent was analyzed by mass spectrometry. A sharp MS signal from H_2 species (m/z=2) appeared immediately following exposure of this sample to a 1% CO/He mixture. This result complements the FTIR data and further demonstrates the presence and high lability of hydride ligands in the surface $Rh(CO)(H)_x$ complexes.

When the $Rh(CO)(H)_x$/HY30 sample was exposed to the flow of dry N_2 at room temperature, changes were once again observed in the FTIR spectra, but in this case the rate of change was much slower than that during exposure to CO. The final steady state spectrum obtained after approximately 12 h on stream is shown in Fig. 2.11 (spectrum 1). The intensity of the v_{CO} and v_{RhH} bands assigned to the $Rh(CO)(H)_x$ species declined substantially during this period, while new bands appeared at 2251, 2117, 2062, 2053, and 2014 cm^{-1}, indicating the formation of several new surface species. Consistent with literature reports [142,159], the two bands at 2251 and 2062 cm^{-1} can be assigned to the v_{NN} and v_{CO} stretching vibrations, respectively, of a $Rh(CO)(N_2)$ species. Furthermore, the relatively weak band at 2014 cm^{-1} can be assigned to a rhodium monocarbonyl Rh(CO) species [143], while the two relative strong bands at 2117 and 2053 cm^{-1} are characteristic of rhodium dicarbonyl $Rh(CO)_2$ complexes. These results suggest that nitrogen can replace the hydride ligands in the $Rh(CO)(H)_x$ species to form a new $Rh(CO)(N_2)$ complex. However, this process is slow and not selective, since a small fraction of $Rh(CO)(H)_x$ species remains on the surface even after 12 h of exposure, while additional surface species such as Rh(CO) and $Rh(CO)_2$ are also formed on the surface, the latter at significant amounts. Since the Rh(CO) complexes are coordinatively unsaturated, they can either coordinate N_2 to form more stable $Rh(CO)(N_2)$ complexes or participate in a redistribution of the CO ligands, yielding stable $Rh(CO)_2$ complexes and free Rh sites. In either case, the Rh(CO) complex can be considered a reaction intermediate.

Following subsequent treatment in H_2 at room temperature for 5 min, both $Rh(CO)(N_2)$ and Rh(CO) species disappeared from the surface, as indicated by the absence of the 2251, 2062, and 2014 cm^{-1} bands in the corresponding spectrum (Fig. 2.11, spectrum 2). At the same time, the v_{RhH} and v_{CO} bands assigned to the $Rh(CO)(H)_x$ species reappeared in the spectrum, indicating the formation of these species. This result suggests that at least in part, transformations between $Rh(CO)(N_2)$ and $Rh(CO)(H)_x$ species are reversible.

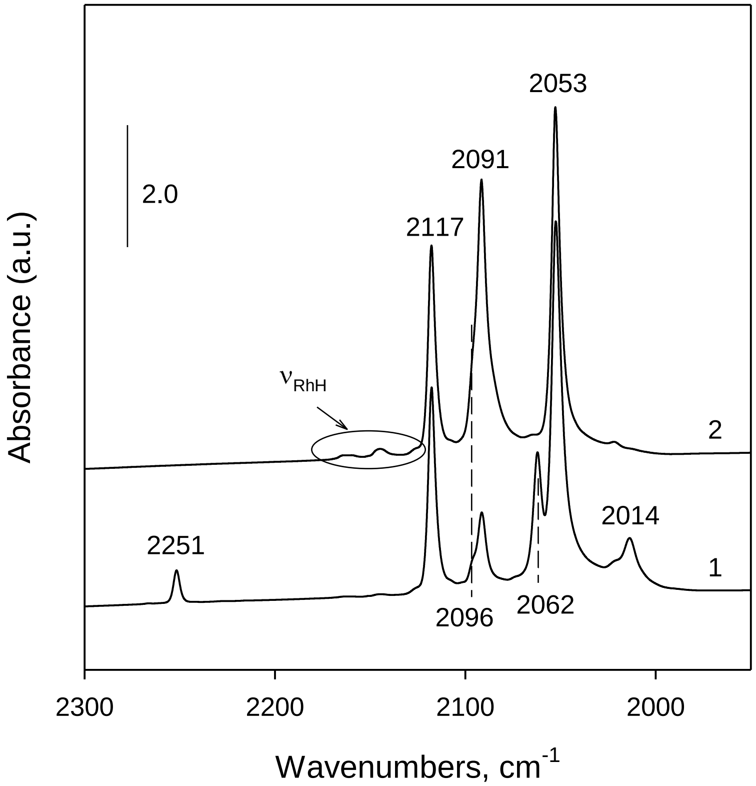

Figure 2.11 FTIR spectra of the surface species formed after (1) treatment of the $Rh(CO)(H)_x$/HY30 sample with N_2 at room temperature for 12 h and (2) subsequent treatment with H_2 at room temperature for 5 min.

Finally, when the $Rh(CO)(H)_x$/HY30 sample was exposed to the flow of C_2H_4 at room temperature, the v_{RhH} (2170-2115 cm^{-1}) and v_{CO} (2100-2080 cm^{-1}) stretching vibrations characteristic of $Rh(CO)(H)_x$ species disappeared immediately from the spectrum. Simultaneously, a relatively strong band appeared at 2053 cm^{-1} and the resulting spectrum was identical to that shown in Fig. 2.1 (spectrum 2) for the $Rh(CO)(C_2H_4)$ species. This result indicates that the $Rh(CO)(H)_x$ complexes were selectively converted into $Rh(CO)(C_2H_4)$. To further investigate this reaction, a larger amount of $Rh(CO)(H)_x$/HY30 was loaded into a reactor system, the sample was exposed to a 1% C_2H_4/He mixture, and the effluent was analyzed by mass spectrometry. A sharp C_2H_6 signal (m/z=30) appeared immediately after exposure of the sample to C_2H_4, while no H_2 signal (m/z=2) was observed. This result shows that C_2H_4 does not simply displace hydride ligands in the $Rh(CO)(H)_x$ complexes, but rather reacts with them to form C_2H_6 species, which are then released into the gas phase. We can further infer that this reaction is catalyzed by the Rh cations and rapidly proceeds to completion, leaving coordinatively unsaturated Rh(CO) complexes on the surface when all hydride ligands are consumed. These unsaturated Rh complexes readily coordinate C_2H_4 from the gas phase to form more stable $Rh(CO)(C_2H_4)$ species. Overall, these results demonstrate the high reactivity of the hydride ligands in $Rh(CO)(H)_x$ complexes towards C_2H_4 and show that the conversion of $Rh(CO)(H)_x$ into $Rh(CO)(C_2H_4)$ species is reversible.

2.4.5 THERMAL STABILITY OF $Rh(CO)(H_x)$ SPECIES

Difference spectra of the HY zeolite-supported $Rh(CO)(H)_x$ species collected during thermal treatment under the flow of He are shown in Fig. 2.12. As can be seen in these spectra, the characteristic vibrations of the $Rh(CO)(H)_x$ complexes in the v_{RhH} and v_{CO} regions declined in intensity as the temperature was increased and disappeared from the spectra at approximately 130°C. Simultaneously, two strong bands, assigned to the $Rh(CO)_2$ species, appeared in the v_{CO} region at 2117 and 2053 cm^{-1}, the intensity of which reached a maximum when the Rh(CO)$(H)_x$ bands were no longer evident in the spectra. In addition, a relatively weak band assigned to Rh(CO) species developed at 2014 cm^{-1}, but its intensity declined substantially at temperatures above 120°C. These results suggest that the hydride ligands are removed from the Rh(CO)$(H)_x$ complexes with increasing temperature. Since no gas phase CO was detected during this process, we can postulate that a Rh(CO) species are also formed during dehydrogenation. Since such Rh(CO) species are coordinatively unsaturated and reactive [142,144], redistribution of CO, leading to the formation of stable $Rh(CO)_2$ complexes, is expected in this case. Such redistribution appears to be faster at higher temperatures, as indicated by the gradual disappearance of the 2014 cm^{-1} band.

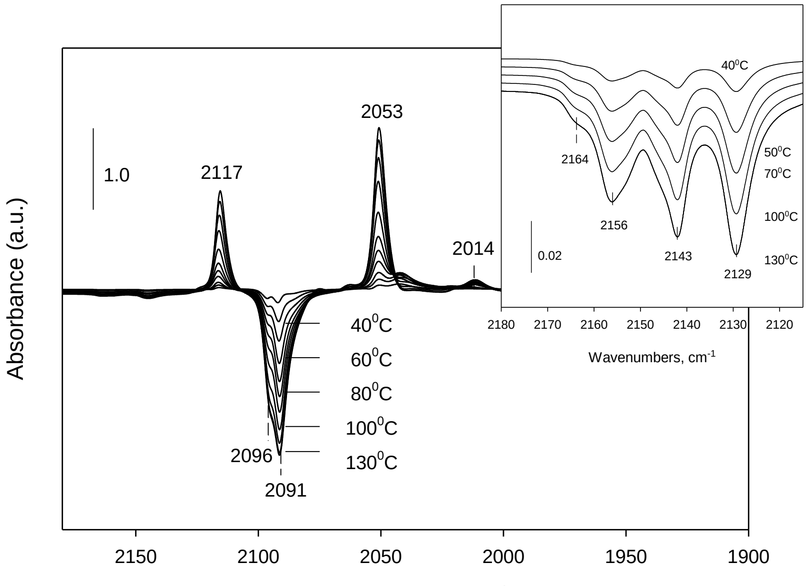

Figure 2.12 Difference FTIR spectra of the Rh(CO)$(H)_x$/HY30 sample illustrating the appearance (positive bands) and disappearance (negative bands) of different vibrations during thermal treatment under the flow of He in the 25-130°C temperature range. Insert shows corresponding changes in the ν_{RhH} region.

When the thermal treatment of the Rh(CO)(H)$_x$/HY30 sample was performed under the flow of H_2, similar changes in spectra were observed in the 25-130°C temperature range. More specifically, the ν_{CO} and ν_{RhH} bands of Rh(CO)(H)$_x$ declined in intensity, while the intensities of the ν_{CO} bands at 2117 and 2052 cm^{-1}, assigned to Rh(CO)$_2$, increased. Furthermore, the ν_{RhH} bands disappeared completely from spectra at approximately 130°C. In this case, however, the ν_{CO} band at 2092 cm^{-1} remained in the spectrum, although at a reduced intensity, and temperatures as high as 280°C were required to completely remove it (Fig. 2.13). In fact, at the same temperature (i.e., 280°C) the two Rh(CO)$_2$ ν_{CO} bands were also completely eliminated from the spectrum.

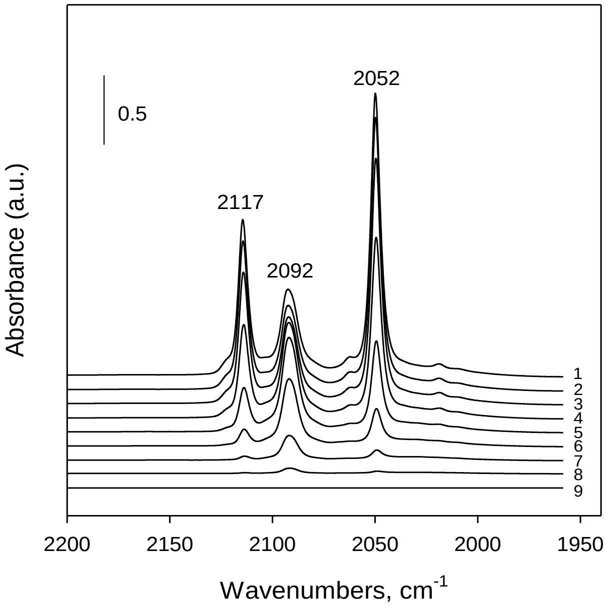

Figure 2.13 FTIR spectra in the ν_{CO} region collected during the thermal treatment of the Rh(CO)(H)$_x$/HY30 sample in H_2 at various temperatures: (1) 200°C, (2) 210°C, (3) 220°C, (4) 230°C, (5) 240°C, (6) 250°C, (7) 260°C, (8) 270°C, and (9) 280°C.

These results suggest that the overall thermal stability of the hydride ligands in the HY30 zeolite-supported $Rh(CO)(H)_x$ complexes is very similar under He and H_2 atmospheres. In both cases, the thermal decomposition of these complexes follows the same route, with the removal of the hydride ligands leading primarily to the formation of $Rh(CO)_2$ surface species. However, when the hydride ligands have been completely removed at elevated temperatures, the presence of gas phase hydrogen results in the preservation of the band at 2092 cm^{-1}. Since this band does not shift during deuterium experiments, it can be confidently assigned to v_{CO} vibrations. Moreover, this band quickly disappears when the flow of H_2 is replaced by He or when the sample is exposed to a pulse of CO.

An v_{CO} band at 2093 cm^{-1} with similar properties has been observed by Miessner in spectra of a $Rh(CO)_2$/HY sample treated with diluted H_2 in the 200-250°C temperature range and attributed to the formation of a reactive $Rh^I(CO)$ species [142]. It was suggested that these species are different from the $Rh^I(CO)$ complexes characterized by the v_{CO} band at 2014 cm^{-1} in terms of their binding to the zeolite framework. More recent results of DFT calculations reported elsewhere [143] do not support such an assignment and strongly suggest that the v_{CO} frequency at 2092 cm^{-1} most likely originates from surface Rh complexes incorporating a combination of H/CO ligands. Although with the experimental techniques used in our experiments it is difficult to prove conclusively the exact composition of these complexes, we can postulate that the v_{CO} band at 2092 cm^{-1} observed under the flow of H_2 at elevated temperatures most likely represents the same type of $Rh(CO)(H)_x$ complexes observed originally. First, the position of this band is the same as that for v_{CO} vibrations in the $Rh(CO)(H)_x$ complexes. Upon removal of the hydride ligands, one can postulate the formation of a $Rh(CO)(H_2)$ complex from Rh(CO) when gas phase H_2 is present. Such a complex is unstable-even at room temperature and could rapidly be converted to the original $Rh(CO)(H)_x$ species [176]. Therefore, one can suggest that a dynamic equilibrium should exist between $Rh(CO)(H_2)$, $Rh(CO)(H_x)$, and empty Rh(CO) sites in the presence of H_2 in the gas phase. Since the H_2 dissociation process is very fast at elevated temperatures, such an equilibrium is expected to be shifted to the direction of $Rh(CO)(H)_x$ species and empty Rh(CO) sites. At elevated temperatures, however, the desorption of hydride ligands also becomes fast. H_2 from the gas phase immediately fills vacant sites on Rh and rapidly dissociates to reform hydride ligands. We can further infer that when H_2 is present in the gas phase, the circle of such transformations occurs continuously. Unfortunately, the dynamic of this process cannot be registered by the conventional FTIR equipment because the lifetime of hydride ligands at elevated temperatures (i.e., above 130°C) is short. However, since the CO ligand remains on the Rh site during these transformations, the v_{CO} band position (i.e., 2092 cm^{-1}) could be regarded as an indicator reflecting the existence of hydride ligands with short lifetimes.

2.4.6 CATALYTIC ACTIVITY OF Rh(CO)(H_x) SPECIES

While rhodium carbonyl hydride complexes are believed to be key intermediates in hydroformylation and hydrogenation of alkenes in solutions [177-179], catalytic properties of their heterogeneous analogs remain largely unknown due to inability to selectively prepare such species on surfaces of solid supports in the past. Therefore, the selective synthesis of zeolite-grafted $Rh(CO)(H)_x$ complexes described above opens up a unique opportunity to evaluate their catalytic performance and show their importance for alkenes hydrogenation reactions.

The $Rh(CO)(H)_x$/HY30 sample was found to be active for hydrogenation of C_2H_4 even at room temperature with an initial TOF measured under differential conditions (i.e., C_2H_4 conversions below 1%) of approximately 0.05 s^{-1}. While no an induction period was observed in this case, the TOF of this sample slowly declined during 20 h on stream and leveled at 0.030 s^{-1} when steady state was reached. In contrast, when the $Rh(CO)_2$/HY30 sample was tested under similar conditions, the induction period lasting for approximately 5 h was observed. During this period of time, the TOF increased from 0 to 0.053 s^{-1} and then declined to approximately 0.036 s^{-1} during next 15 h on stream. Based on these data, we can suggest that the induction period is associated with transformation of catalytically inactive $Rh(CO)_2$ species into catalytically active $Rh(CO)(H)_x$ complexes, which are playing a key role in hydrogenation of C_2H_4. It is further evident that this transformation does not occur instantly under experimental conditions used likely due to relatively low C_2H_4 and H_2 partial pressures in the feed.

The TOF values characterizing Y zeolite-supported $Rh(CO)(H)_x$ complexes in C_2H_4 hydrogenation are consistent with results reported in literature for similar catalytic materials. For example, Liang et al. have examined C_2H_4 hydrogenation over Y zeolite-supported $Rh(C_2H_4)_2$ complexes and reported TOF of 0.022 s^{-1} for feeds containing 30 Torr H_2 and C_2H_4 [64]. Angelini et al. have reported TOF of 0.027 s^{-1} for liquid phase C_2H_4 hydrogenation over unsupported $[RhCl(C_2H_4)PiPr_3]_2$ complexes under 4 MPa of H_2 and C_2H_4 pressures [173]. Slightly higher TOF values (i.e., in the 0.01-0.9 s^{-1} range) were reported for C_2H_4 hydrogenation over MgO-supported Rh_6 clusters and feeds containing 40 Torr C_2H_4 and 80-700 Torr H_2 [180], suggesting that metal surfaces are more active in hydrogenation of alkenes than supported metal complexes. However, spectroscopic results provided herein clearly show that the ethylene hydrogenation catalytic cycle can be performed in steps over zeolite-grafted Rh complexes, with key reaction intermediates being selectively formed and characterized at each step. More data related to catalytic properties of these materials will be reported separately.

2.5 CONCLUSIONS

FTIR and EXAFS results have demonstrated that supported $Rh(CO)(C_2H_4)$ complexes can be selectively formed upon exposure of dealuminated Y zeolite-supported $Rh(CO)_2$ complexes to C_2H_4. Subsequent exposure of these $Rh(CO)(C_2H_4)$ complexes to H_2 under ambient conditions selectively yields well-defined surface $Rh(CO)(H)_x$ species. These $Rh(CO)(H)_x$ species are site-isolated and mononuclear, bound to oxygen atoms of the zeolite framework, and characterized by a set of well-defined v_{CO} and v_{RhH} bands in their FTIR spectra. They exhibit a pseudo-trigonal bipyramidal or pseudo-octahedral geometry, resulting in the presence of several structural isomers with cis and trans coordination of hydrides in respect to each other and to the CO ligand, and they are stable at room temperature under the flow of H_2 or He for an extended period of time. However, the hydride ligands in $Rh(CO)(H)_x$ can be displaced by CO or N_2 at room temperature to form $Rh(CO)_2$ and $Rh(CO)(N_2)$ complexes, although the displacement of the hydrides with N_2 is slow and non-selective. In contrast, C_2H_4 does not displace the hydride ligands but reacts with them to form C_2H_6 and an unsaturated Rh(CO) reactive intermediate. The latter readily reacts with C_2H_4 from the gas phase to form a more stable $Rh(CO)(C_2H_4)$ complex. FTIR results further show that the $Rh(CO)(H)_x$ species start decomposing at approximately 130°C by losing the hydride ligands. Subsequent rapid redistribution of CO between the unstable Rh(CO) species formed in this process leads to the formation of more stable $Rh(CO)_2$ complexes and Rh sites free of CO ligands. The two-step selective synthesis of well-defined molecular $Rh(CO)(H)_x$ complexes grafted on the surface of dealuminated Y zeolite opens up new opportunities to examine the role of single Rh sites and the resulting structure-reactivity relationships for a wide spectrum of industrially relevant catalytic applications.

2.6 ACKNOWLEDGMENTS

The authors gratefully acknowledge the University of South Carolina for partial financial support of this work (ASPIRE grant 15510-12-29499). XAS data were collected at the Stanford Synchrotron Radiation Laboratory, a national user facility operated by Stanford University on behalf of the U.S. Department of Energy, Office of Basic Energy Sciences. The assistance of the beam line staff at SSRL is gratefully acknowledged. The EXAFS data were analyzed with the XDAP software developed by XAFS Services International [148].

CHAPTER 3. HY ZEOLITE-SUPPORTED RHODIUM DICARBONYL COMPLEXES: THE EFFECT OF Si/Al RATIO

3.1 PREFACE

Fourier transform infrared (FTIR), extended X-ray absorption fine structure (EXAFS), and X-ray photoelectron spectroscopy (XPS) measurements were used to characterize the species formed after grafting of a $Rh(CO)_2(acac)$ precursor on dealuminated HY zeolites with different Si/Al ratios. The results show the formation of two types of $Rh(CO)_2$ species with characteristic v_{CO} bands at 2117/2053 and 2110/2043 cm^{-1}. Both of these species are evidently grafted to the zeolite framework and have similar structural properties. However, their thermal stabilities are different and the fraction of each species formed strongly depends on the Si/Al ratio, as zeolites with a higher Al content favor the formation of the latter species in larger amounts. Carbonyl ligands in both types of zeolite-grafted $Rh(CO)_2$ complexes are capable of reacting with gas phase C_2H_4 to form $Rh(CO)(C_2H_4)$ species. Nevertheless, the conversion rate is substantially higher for $Rh(CO)_2$ complexes with the v_{CO} bands at 2117/2053 cm^{-1}, suggesting that electronic properties of Rh sites are important for reactivity of carbonyl ligands. New results presented herein strongly suggest that the second type of $Rh(CO)_2$ species with the v_{CO} bands at 2110/2043 cm^{-1} cannot be linked to unreacted and partially reacted $Rh(CO)_2(acac)$ complexes or to the formation of $Rh(CO)_2(H_2O)_x$ species. Most likely, binding sites of different nature in dealuminated faujasites are responsible for their formation.

3.2 INTRODUCTION

The importance of rhodium carbonyl complexes and their derivatives as catalysts for a variety of industrially relevant liquid phase reactions is well documented in literature [181-183]. Since solid catalytic materials could offer significant technological advantages for many of these practical applications, substantial research efforts have been focused on finding heterogeneous analogs for them. The use of conventional metal oxides as supports led to understanding that their surfaces are nonuniform and, therefore, have a variety of binding sites with different structural and electronic properties [184,185]. As a result, metal complexes grafted on such supports could also be nonuniform in structure and composition and have different electronic properties, impacting substantially their catalytic performance [186]. In this regard, the use of zeolites as supports is more promising because these crystalline materials offer highly ordered arrays of binding sites for metal complexes and, therefore, allow to prepare catalytic materials with nearly uniform and well-defined structures.

During the past decade, a significant progress has been made toward the synthesis and understanding structural and catalytic properties of zeolite-grafted Rh carbonyl complexes [63,142]. When highly dealuminated HY zeolites with a Si/Al ratio of 30 or higher were used as supports, the synthesis of well-defined and site-isolated $Rh(CO)_2$ complexes was reported [63,189]. For example, it has been shown that $Rh(CO)_2(acac)$ complexes are capable of reacting with surfaces of dealuminated Y zeolites and this reaction leads to the displacement of the acac ligand and to the formation of site-isolated and well-defined $Rh(CO)_2$ species anchored inside the zeolite supercage [63]. These species are characterized by sharp v_{CO} bands at approximately 2117 and 2053 cm^{-1} with a FWHM of approximately 6 cm^{-1}. Such narrow v_{CO} bands are believed to signify a highly uniform nature of the grafted species formed. Based on EXAFS data and DFT calculations, it has been also suggested that such $Rh(CO)_2$ species retain their square-planar geometry upon anchoring and, in fact, two oxygen atoms located in the T4 ring of zeolite Y and coordinated to Al^{3+} cations represent binding sites for these species [63].

However, several other examples in which faujasites with lower Si/Al ratios were used as supports for $Rh(CO)_2$ complexes indicate the presence of broader v_{CO} bands often with splits, consistent with the formation of several types of rhodium dicarbonyl species. For example, Rode et al. [190] have reported two types of $Rh(CO)_2$ species in NaY (Si/Al = 2.4) with v_{CO} bands at 2111/2045 and 2097/2019 cm^{-1} and assigned them to species located inside zeolite pores and on the external surface, respectively. Likewise, Wolf et al. [189] have observed v_{CO} bands of NaY (Si/Al=2.6) and NaX (Si/Al=1.3) supported $Rh(CO)_2$ complexes at 2118/2053 cm^{-1} but also identified the second type of $Rh(CO)_2$ species on these supports with characteristic v_{CO} bands at 2099/2020 and 2096/2015 cm^{-1}, respectively. In this case, however, the authors suggested that $Rh(CO)_2$ species anchored next to zeolite framework Al atoms that isolated by one or more than one Si atoms have different fingerprints in the v_{CO} region. Furthermore, Shannon et al [191]. have examined the reaction of CO with a Rh exchanged Y zeolite (Si/Al = 2.4) and observed two types of $Rh(CO)_2$ species which were bound differently to the support. More specifically, these authors have suggested that the v_{CO} bands at 2101 and 2022 cm^{-1} represent $Rh(CO)_2$ species bound to two framework oxygen atoms, while the v_{CO} bands at 2116 and 2048 cm^{-1} represent similar species bound to one framework oxygen and one water molecule. While several other reports seem to support such an assignment [192,193], the data reported by Ben Taarit et al. [194] strongly suggest that coordination of water molecules to zeolite-grafted $Rh(CO)_2$ complexes results in a redshift of corresponding v_{CO} bands, as the v_{CO} bands at 2216/2048, 2101/2022, and 2090/2030 cm^{-1} were assigned to $Rh(CO)_2(Oz)_2$, $Rh(CO)_2(H_2O)(Oz)$, and $Rh(CO)_2(H_2O)_2$ (or $Rh(CO)_2(H_2O)(OH)$) complexes, respectively.

Unfortunately, neither of these reports was focused on the nature of different $Rh(CO)_2$ species or their reactivity. However, the origin of different $Rh(CO)_2$ complexes formed in zeolites with different Si/Al ratios is important for understanding catalytic properties of these materials. Since several factors (i.e., different binding sites, nonframework Al species, zeolite acidity, and residual water content) could have a significant impact on the reactivity of zeolite-grafted $Rh(CO)_2$ species, we have attempted to approach these issues systematically.

In this work we report structural and electronic properties of two types $Rh(CO)_2$ species formed in cages of dealuminated Y zeolites with different Si/Al ratios. FTIR, EXAFS, and XPS were used to reveal the nature of grafted complexes, their stability, and reactivity in a simple probe reaction with C_2H_4. New results presented herein strongly suggest that while dealuminated Y zeolites act as macroligands for grafted metal complexes, they have at least two different types of binding sites capable of accommodating $Rh(CO)_2$ moieties. The fraction of these sites strongly depends on the Si/Al ratio and two types of grafted $Rh(CO)_2$ complexes formed in these materials exhibit remarkably different reactivities toward C_2H_4, suggesting that the selection of zeolites as supports for molecular metal complexes should be done thoughtfully.

3.3 EXPERIMENTAL

3.3.1 REAGENTS AND MATERIALS

Dicarbonylacetylacetonato rhodium (I) $Rh(CO)_2(acac)$ (acac = $C_5H_7O_2$) (Strem, 98% purity), triethylphosphine (Strem, 99% purity), tris(2,4-dimethylphenyl)phosphine (Strem, 98% purity), anhydrous ethanol (Aldrich, 99.5 % purity), and aluminum nitrate nonahydrate (Aldrich, 99.997 % purity) were used as supplied. n-Pentane (Aldrich, 99% purity) was refluxed under N_2 in the presence of Na/benzophenone ketyl to remove traces of moisture and deoxygenated by sparging of dry N_2 prior to use. All glassware used in preparation steps was previously dried at 120°C. He, and C_2H_4 (Airgas, all UHP grade) were additionally purified prior to their use by passage through oxygen/moisture traps (Agilent) capable of removing traces of O_2 and water to 15 and 25 ppb, respectively. The γ-Al_2O_3 support was prepared by forming a paste of aluminum oxide C (Degussa) and deionized water, followed by overnight drying at 120°C, calcination at 400°C in flowing O_2 (Airgas, UHP grade) for 2 h, and then evacuation (10-3 Torr) at 400°C for 16 h. The BET surface area of the resultant material was approximately 100 m^2/g. Commercial CBV760, CBV720, and CBV600 dealuminated HY zeolites (Zeolyst International) with Si/Al atomic ratios of 30, 15, and 2.6, respectively, were calcined in flowing O_2 at 300°C for 3 h and then evacuated at 10^{-3} Torr and 300°C for 16 h. For simplicity, these zeolite supports are further denoted as HY30, HY15, and HY2.6, respectively. All treated supports were stored and handled in a glovebox (MBraun) filled with dry N_2. The residual water and O_2 concentrations in the glovebox were kept below 0.1 ppm.

3.3.2 PREPARATION OF SUPPORTED SAMPLES

The syntheses and sample transfers were performed with exclusion of air and moisture on a double-manifold Schlenk line and in a N_2-filled MBraun glove box. Supported samples were prepared by slurrying the $Rh(CO)_2(acac)$ precursor with a corresponding powder support in n-pentane under N_2 for 24 h at room temperature, followed by overnight evacuation at 25°C to remove the solvent. In each case, the $Rh(CO)_2(acac)$ precursor was added in the amount needed to yield samples containing 1 wt% Rh. The Rh weight loading was verified by inductively coupled plasma-mass spectrometry (ICP-MS) analysis (Galbraith Laboratories Inc.). The prepared samples were stored and handled in a glovebox filled with dry N_2 to prevent possible contamination and decomposition of supported species.

3.3.3 FTIR SPECTROSCOPY

A Nicolet Nexus 470 spectrometer equipped with a MCT-B detector cooled by liquid nitrogen was used to collect spectra with a resolution of 2 cm^{-1}, averaging 64 scans per spectrum. Each powder sample was pressed into a self-supported wafer with a density of approximately 20 mg/cm^2 and mounted in a home-made cell connected to a gas distribution manifold. The cell design allowed for the treatment of samples at different temperatures, while various gases flowed through the cell.

3.3.4 X-RAY ABSORPTION SPECTROSCOPY (XAS) MEASURMENTS

XAS spectra were collected at X-ray beamline 4-1 of the Stanford Synchrotron Radiation Laboratory (SSRL), Stanford Linear Accelerator Center, Menlo Park, CA. The storage ring electron energy was 3 GeV and the ring current was in the range of 495-500 mA.

XAS measurements were used to characterize the surface species formed after the impregnation of $Rh(CO)_2(acac)$ on the support. Prior to these measurements, each powder sample was pressed into a wafer inside a N_2-filled glovebox. The sample mass was calculated to give an absorbance of approximately 2.5 at the Rh K absorption edge. After the sample had been pressed, it was loaded into an EXAFS cell [145], sealed under N_2, and removed from the glovebox. The cell was evacuated at 10^{-5} Torr and aligned in the X-ray beam. The XAS data were collected at liquid nitrogen temperature in the transmission mode with a Si(220) double crystal monochromator that was detuned by 30% to minimize effects of higher harmonics in the X-ray beam. Samples were scanned at energies near the Rh K absorption edge (23220 eV). All spectra were calibrated with respect to Rh foil, the spectrum of which was collected simultaneously.

3.3.5 EXTENDED X-RAY ABSORPTION FINE STRUCTURE (EXAFS) DATA ANALYSIS

The EXAFS data were analyzed with experimentally determined reference files obtained from EXAFS data characterizing materials of known structure. The Rh–Rh and Rh–Osupport contributions were analyzed with phase shifts and backscattering amplitudes obtained from EXAFS data for Rh foil and Rh_2O_3, respectively. The Rh–C and Rh–O* contributions (where O* represents carbonyl oxygen) were analyzed with phase shift and backscattering amplitudes obtained from EXAFS data characterizing crystalline $Ru_3(CO)_{12}$, which has only terminal CO ligands. The transferability of the phase shifts and backscattering amplitudes for near neighbors in the periodic table has been justified experimentally [146]. The parameters used to extract these files from the EXAFS data are reported elsewhere [147]. The EXAFS data were extracted from the spectra with the XDAP software developed by XAFS Services International [148]. The EXAFS function for each sample was obtained from the X-ray absorption spectrum by a cubic spline background subtraction and normalized by dividing the absorption intensity by the height of the absorption edge. The final normalized EXAFS function for each sample was obtained from an average of six scans. The parameters characterizing both low-Z (O, C) and high-Z (Rh) contributions were determined by multiple-shell fitting with a maximum of 16 free parameters in r space (where r is the distance from the absorbing atom, Rh) and in k (wave vector) space over the ranges of $3.5 < k < 15.0$ Å-1 and $0.5 < r < 3.5$ Å with application of k^1 and k^3 weighting of the Fourier transform. The statistically justified number of free parameters (n), estimated from the Nyquist theorem [149,150], $n = (2\Delta k\Delta r/\pi) + 1$, where Δk and Δr are the k and r ranges used to fit the data, was approximately 23. The fit was optimized by use of a difference file technique [151,152], with phase- and amplitude-corrected Fourier transforms. Standard deviations for the various parameters were calculated with the XDAP software, as described elsewhere [153]. Systematic errors are not included in the calculation of the standard deviations. The values of the goodness of fit (ε_ν^2) were calculated with the XDAP software as outlined in the Reports on Standards and Criteria in XAFS Spectroscopy [154]. The variances in both the imaginary and absolute parts were used to determine the fit quality [155].

3.3.6 X-RAY PHOTOELECTRON SPECTROSCOPY MEASURMENTS

XPS measurements were conducted using a Kratos AXIS Ultra DLD XPS system equipped with a monochromatic Al Kα source. The system energy scale was calibrated using an Ag foil with the Ag $3d_{5/2}$ binding energy set at 368.21 ±

0.025 eV for the monochromatic Al Kα source operated at 15 keV and 120 W. The pass energy was fixed at 40 eV for the detailed scans. A charge neutralizer was used to compensate for the surface charging during the photoemission. The powder samples (approximately 5 mg) were loaded into the air-tight cell in the N_2-filled glovebox and transferred without air exposure into the UHV chamber for the XPS analysis. The C 1s signal with a binding energy of 285.0 eV was used as an internal reference for calibration of the Rh $3d_{5/2}$ and Rh $3d_{3/2}$ binding energy values. All binding energies reported in this work were measured with a precision of ±0.1 eV. XPS data were analyzed by nonlinear curve fitting using the XPSPEAK 4.1 software. In all cases, a linear-type background was subtracted from the spectra and a curve fit was performed using the minimum number of G/L-type peaks that provides a good fit. In each case the fitting routine was completed when the coefficient of determination (R^2) value was 0.98 or higher.

3.4 RESULTS AND DISCUSSION

3.4.1 DIFFERENT TYPES OF GRAFTED $Rh(CO)_2$ SPECIES

The infrared spectrum of the $Rh(CO)_2(acac)$ precursor dissolved in n-pentane exhibits two strong bands in the v_{CO} region at 2083 and 2014 cm^{-1} (Fig. 3.1) due to symmetric and asymmetric v_{CO} vibrations of carbonyl ligands, respectively. These bands are very narrow, with the FWHM values of approximately 3.5 cm^{-1}. Due to symmetrical shapes, each of these bands can be fitted with only one component to achieve the R^2 coefficient of determination on the order of 0.998 or higher. Very weak satellite bands observed in the spectrum at 2065 and 1984 cm^{-1} (Fig. 3.1) are consistent with symmetric and asymmetric ν_{CO} vibrations, respectively, of carbonyl ligands in $Rh(CO)(^{13}CO)(acac)$ complexes, which are present in trace amounts. In contrast to the crystalline form of this precursor, in which the square-planar $Rh(CO)_2(acac)$ molecules are stack to each other in such a way that the Rh atoms of neighboring molecules form pseudo-octahedral structures [163], the data of Fig. 3.1 exemplifying FTIR fingerprints of isolated and well-defined $Rh(CO)_2(acac)$ molecules existing in solution.

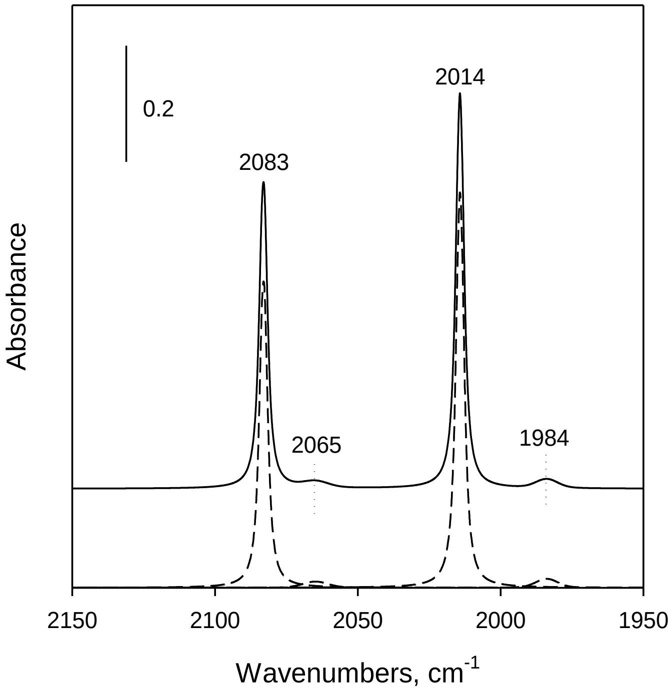

Figure 3.1 FTIR spectrum of $Rh(CO)_2(acac)$ in pentane (solid line) and deconvolution results (dashed line).

The interaction of acetylacetonate complexes of different metals, including Rh, with γ-Al_2O_3 and zeolite surfaces has been examined extensively in the past [207,209,65,60,57-59]. From these reports, it is evident that $Rh(CO)_2$(acac) readily reacts with acidic OH groups of these supports, leading to protonation and removal of the acac ligand from Rh and formation of grafted mononuclear $Rh(CO)_2$ species on the support surface. Consistent with this type of surface chemistry, FTIR data shown in Figs. 3.2 A-C provide an evidence for the formation of such surface species from the $Rh(CO)_2$(acac) precursor on HY zeolites dealuminated to various degrees. In all these spectra, the supported $Rh(CO)_2$ species can be identified by strong bands in the v_{CO} region at 2117 and 2053 cm^{-1}, originating from symmetric and asymmetric v_{CO} vibrations of carbonyl ligands, respectively.

However, the analysis of the v_{CO} bands shown in Figs. 3.2 A-C indicates that their shapes are not symmetrical due to the presence of tails at the low frequency side of each band. As the Si/Al ratio declines with increasing the number of Al atoms in the zeolite framework, the asymmetry of v_{CO} bands becomes more apparent. The spectrum of the $Rh(CO)_2$/HY2.6 sample with the largest content of Al (Si/Al=2.6) exhibits very strong tails (Fig. 3.2 C) and credibly shows that several types of grafted $Rh(CO)_2$ species are formed. Deconvolution results shown in Fig. 3.2 C as dotted lines confirm this point, as two different types of Rh dicarbonyl species can be clearly identified. The first type of $Rh(CO)_2$ species is characterized by a pair of sharp and strong v_{CO} bands at 2117 and 2053 cm^{-1}, while broader and less intense bands at 2110 and 2043 cm^{-}

[1] represent the second type of Rh dicarbonyl species. The appearance of the latter species in spectra of $Rh(CO)_2$/HY30 and $Rh(CO)_2$/HY15 is less apparent (Figs. 3.2 A and B). However, acceptable fits with R^2 coefficients of determination above 0.95 can be obtained for these two samples only when two components per each ν_{CO} band are included in the fit. Based on these deconvolution results (Figs. 3.2 A and B, dotted lines), it is evident that two different types of Rh dicarbonyl species are also present in these samples.

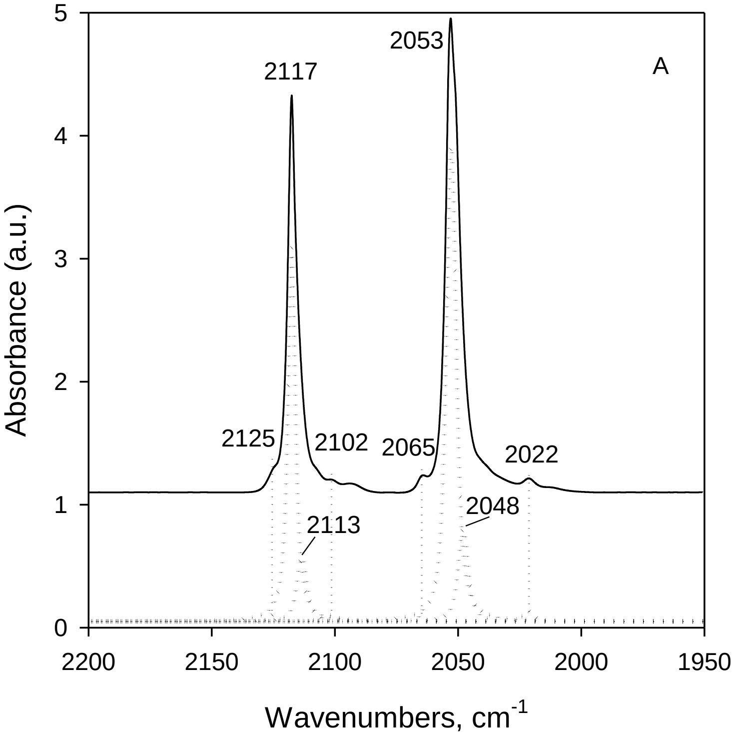

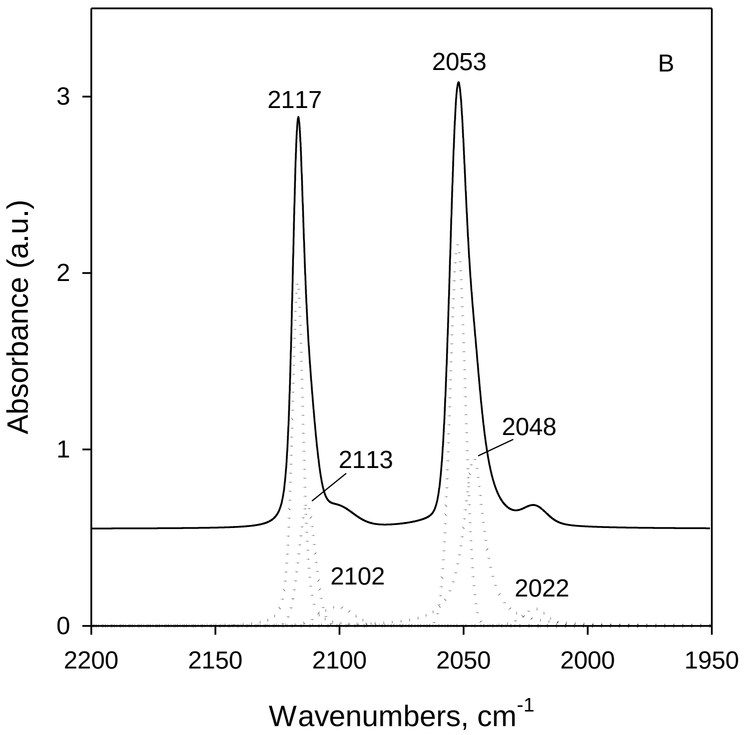
B
Absorbance (a.u.)
Wavenumbers, cm-1
2117
2053
2113
2048
2102
2022
0
1
2
3
2200
2150
2100
2050
2000
1950

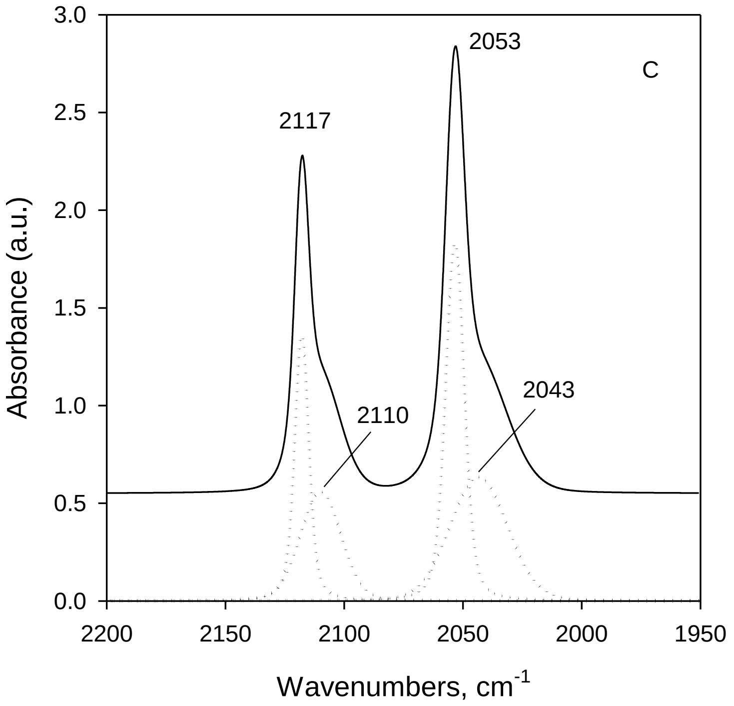
C
Absorbance (a.u.)
Wavenumbers, cm-1
2117
2053
2110
2043
0.0
0.5
1.0
1.5
2.0
2.5
3.0
2200
2150
2100
2050
2000
1950

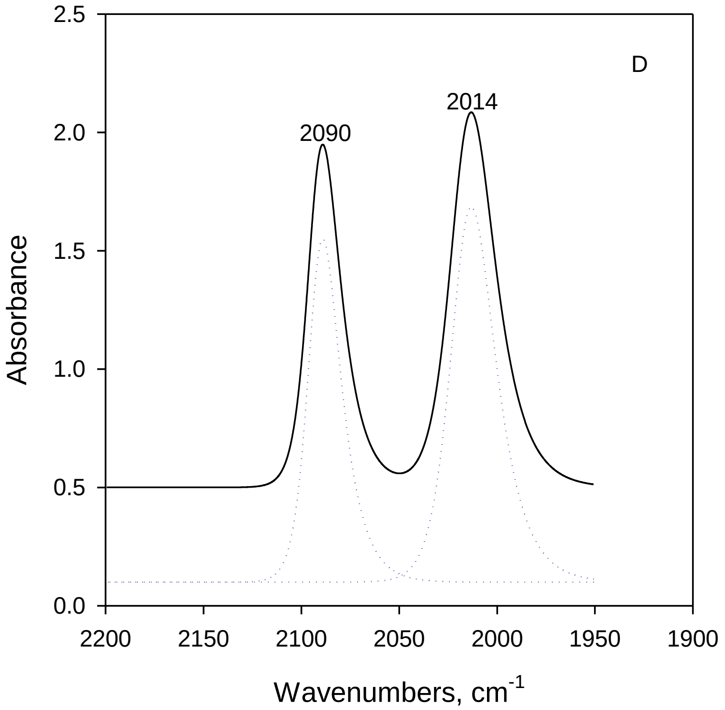

Figure 3.2 FTIR spectra in the v_{CO} region of (A) $Rh(CO)_2$/HY30, (B) $Rh(CO)_2$/HY15, (C) $Rh(CO)_2$/HY2.6, and (D) $Rh(CO)_2/\gamma\text{-}Al_2O_3$ samples (solid lines) and deconvolution results (dotted lines).

Deconvolution results summarized in Table 3.1 for all zeolite-based samples examined lead to several conclusions. Regardless of the zeolite used as a support, both types of detected $Rh(CO)_2$ species are nearly identical in terms of the split between symmetric and asymmetric v_{CO} vibration modes and C-Rh-C angles, which were calculated from I_{sym}/I_{asym} ratios, as reported elsewhere [125]. Moreover, these split and angle parameters characteristic of zeolite-grafted $Rh(CO)_2$ species closely resemble those of $Rh(CO)_2$(acac) in solution (Table 3.1), indicating that the replacement of acac ligands by the zeolite support does not affect substantially the geometry of $Rh(CO)_2$ moieties. The comparison of the v_{CO} bands of zeolite-grafted $Rh(CO)_2$ species (Figs. 3.2 A-C) and $Rh(CO)_2$(acac) complexes in solution (Fig. 3.1) clearly shows that oxygen atoms in the zeolite framework are more electronegative than those in the acac ligand, as the v_{CO} bands of grafted $Rh(CO)_2$ species are substantially shifted to the region of high frequencies in the former case. This result is consistent with previous literature reports [166], implying that Rh atoms in zeolite-grafted $Rh(CO)_2$ species are more electron deficient than those in free $Rh(CO)_2$(acac) complexes. Such differences in electronic properties of Rh are expected to have an effect on the chemical properties of carbonyl ligands, especially when the zeolite support acts as a macro ligand for grafted species [216]. As far as the comparison between two types of zeolite-grafted $Rh(CO)_2$ species is concerned, there is a measurable difference in the position of v_{CO} bands of these complexes on all zeolites used as supports (Table 3.1), suggesting that Rh atoms in these species are not identical in terms of their electronic properties, which could also affect the reactivity of carbonyl ligands in such species.

Table 3.1 Parameters of v_{CO} bands observed in FTIR spectra of various samples.

Sample	Band position, cm^{-1}	FWHM, cm^{-1}	Split (v_s–v_{as}), ^{a} cm^{-1}	C-Rh-C angle, deg	Relative fraction, %	Suggested species/remarks
$Rh(CO)_2$/HY 30	2117 2053	3.6 4.8	64	96	83	grafted $Rh(CO)_2$
	2113 2048	4.8 4.8	65	94	17	grafted $Rh(CO)_2$
$Rh(CO)_2$/HY 15	2117 2053	5.1 7.3	64	94	60	grafted $Rh(CO)_2$
	2113 2048	7.7 9.9	65	95	40	grafted $Rh(CO)_2$
$Rh(CO)_2$/HY 2.6	2117 2053	7.1 9.3	64	99	50	grafted $Rh(CO)_2$
	2110 2043	20.2 28.5	67	94	50	grafted $Rh(CO)_2$
$Rh(CO)_2$/γ-Al_2O_3	2090 2014	20.0 27.2	76	98	-	grafted $Rh(CO)_2$
$Rh(CO)_2$(acac) in pentane	2083 2014	3.5 3.4	69	97	-	complex in solution

[a]The “s” and “as” refer to symmetric and asymmetric vibrations, respectively.

It is further evident that the v_{CO} bands assigned to type I $Rh(CO)_2$ species (i.e., 2117 and 2053 cm^{-1}) are identical for all three zeolites used. While the same conclusion can be extended to type II $Rh(CO)_2$ species (v_{CO} bands at 2113 and 2048 cm^{-1}) formed in the case of dealuminated Y zeolites with Si/Al ratios of 30 and 15, a small shift of these bands to the low frequency region was observed when a zeolite with the Si/Al ratio of 2.6 was used as a support (Table 3.1). Since this shift is only marginal, one can infer that the Si/Al ratio in the range of 2.6-30 does not influence substantially the v_{CO} vibrational frequency of HY zeolite-grafted rhodium dicarbonyl species.

However, the data summarized in Table 3.1 for the $Rh(CO)_2$/HY30 sample show that relative fractions of type I and type II $Rh(CO)_2$ species formed in this sample are 83 and 17%, respectively. In the case of the $Rh(CO)_2$/HY15 sample, type I and II species constitute 60 and 40% of Rh dicarbonyls, respectively, while they are formed in equal fractions in the $Rh(CO)_2$/HY2.6 sample. These data clearly show the more Al atoms in the zeolite framework the larger fraction of type II $Rh(CO)_2$ species is formed.

Finally, both types of zeolite-grafted $Rh(CO)_2$ species exhibit the highest degree of uniformity in the case of the $Rh(CO)_2$/HY30 sample, as their v_{CO} bands are very narrow with FWHM values closely resembling those of $Rh(CO)_2$(acac) complexes in solution (Table 3.1). As the Si/Al ratio was decreased to 15, the width of v_{CO} bands was increased for both types of zeolite-grafted $Rh(CO)_2$

species. However, all of them still remain to be relatively uniform with a FWHM below 10 cm^{-1}. In the case of the $Rh(CO)_2$/HY2.6 sample, a FWHM of type I species is below 10 cm^{-1}, while v_{CO} bands of type II species are substantially broader (average FWHM of approximately 24 cm^{-1}). This comparison clearly shows that type I zeolite-grafted $Rh(CO)_2$ species are not affected substantially by Si/Al ratios, but type II species are very sensitive to the presence of Al in the zeolite framework.

For comparison, when $Rh(CO)_2$ complexes were grafted on the γ-Al_2O_3 surface, the v_{CO} bands of these species were observed at 2090 and 2014 cm^{-1} (Fig. 3.2 D), resembling those of $Rh(CO)_2$(acac) complexes in n-pentane solution (Table 3.1). In contrast to the case of dealuminated HY zeolites, this result suggests that the γ-Al_2O_3 support does not affect substantially electronic properties of Rh in grafted $Rh(CO)_2$ species. While the C-Rh-C angle characterizing γ-Al_2O_3-grafted $Rh(CO)_2$ species is similar to that of zeolite-grafted complexes (Table 3.1), the v_{CO} bands are evidently wider with an average FWHM of approximately 24 cm^{-1}, indicating that γ-Al_2O_3-grafted $Rh(CO)_2$ complexes are non-uniform in nature.

3.4.2 THERMAL STABILITY OF GRAFTED $Rh(CO)_2$ SPECIES

To examine how stable the supported Rh dicarbonyl species of both types are, FTIR spectra were collected during exposure of the $Rh(CO)_2$/HY2.6 sample with the largest fraction (i.e., 50%) of type II Rh dicarbonyl species to different temperatures under the flow of He. During these measurements, the sample was heated at a rate of 3°C/min to a desired temperature and held at this temperature until no changes in the v_{CO} region were observed. The deconvolution procedure was applied to each resulting spectrum to accurately quantify each type of $Rh(CO)_2$ species and determine how much of these species remained in the sample at each temperature. Results summarized in Fig. 3.3 show that the fraction of $Rh(CO)_2$ species with v_{CO} bands at 2117 and 2053 cm^{-1} (type I) remains nearly unchanged, as the temperature was increased from 25 to 150°C. At higher temperatures, accelerated removal of CO ligands was observed, as the fraction of type I species dropped to approximately 20% at 300°C and temperatures higher than 350°C were required to complete the decarbonylation process.

In contrast, the $Rh(CO)_2$ species with v_{CO} bands at 2110 and 2043 cm^{-1} (type II) loose CO ligands with increasing temperature in a much faster fashion, as approximately 47 and 90% of such species were removed at 100 and 250°C, respectively (Fig. 3.3). When the temperature was further increased to 300°C, the decarbonylation process was nearly completed for this type of species, since v_{CO} bands assigned to them were no longer evident in the spectrum. These data provide a solid evidence that two types of HY zeolite-grafted $Rh(CO)_2$ complexes exhibit substantially different thermal properties, with the type I being more stable among them.

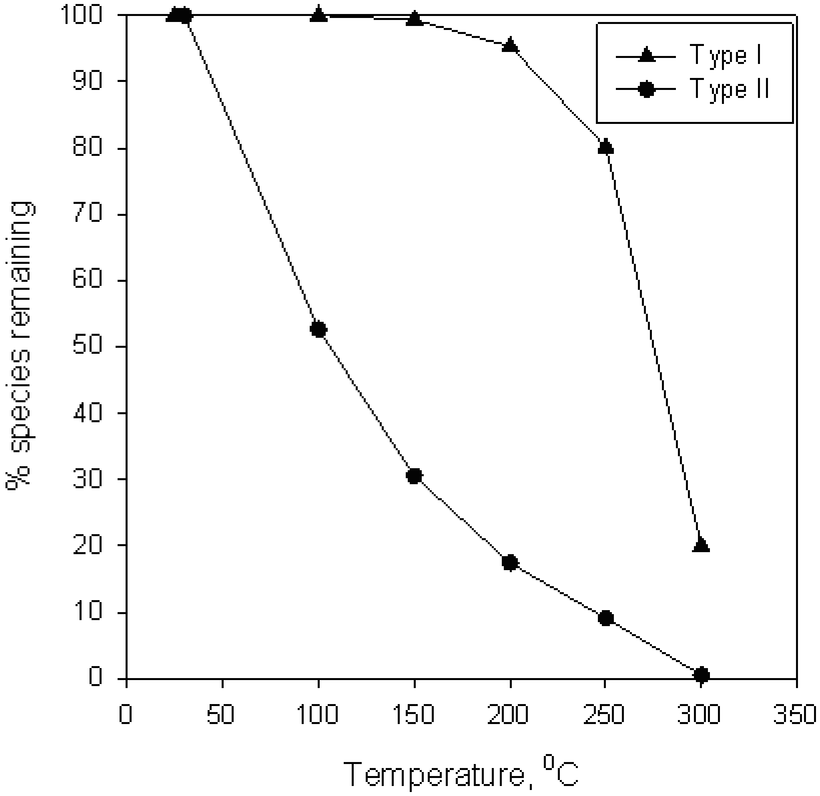

Figure 3.3 Percent of Rh dicarbonyls remaining on the surface of $Rh(CO)_2$/HY2.6 during thermal treatments with He at different temperatures: (▲) type I (ν_{CO} at 2117/2053 cm^{-1}) and (●) type II (ν_{CO} at 2110/2043 cm^{-1}) species.

When similar experiments were performed with the $Rh(CO)_2/\gamma\text{-}Al_2O_3$ sample, only 85% of grafted $Rh(CO)_2$ species remain intact in the 25-100°C range of temperatures (Fig. 3.4). At temperatures above 100°C, the removal of carbonyl ligands occurs in a linear fashion and no such species remain on the surface at 300°C.

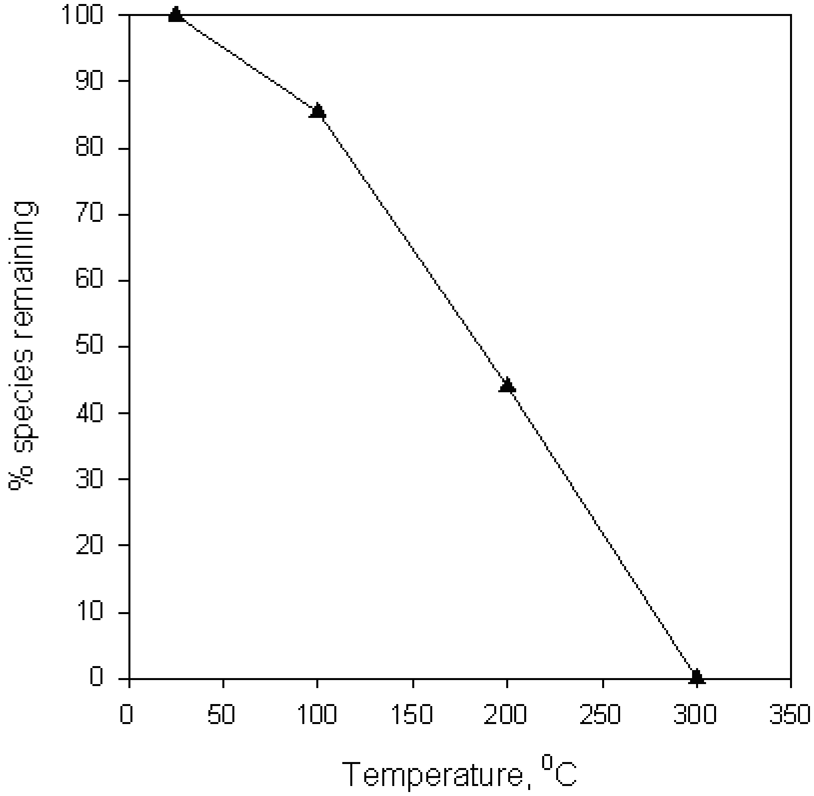

Figure 3.4 Percent of Rh dicarbonyls remaining on the surface of $Rh(CO)_2/\gamma$-Al_2O_3 during thermal treatments with He at different temperatures.

3.4.3 STRUCTURAL PROPERTIES OF GRAFTED $Rh(CO)_2$ SPECIES

EXAFS data collected for $Rh(CO)_2(acac)$ complexes grafted on the surface of γ-Al_2O_3 and HY zeolites with different Si/Al ratios are summarized in Table 3.2. Consistent with previous literature reports [63,217], these data provide a solid evidence for the formation of site-isolated $Rh(CO)_2$ species in all samples examined. For example, the absence of Rh–Rh contributions in EXAFS spectra points to the mononuclear character of Rh surface species formed and the presence of two CO ligands per each Rh atom (evidenced by Rh–C and

Rh–O* contributions with average coordination numbers of approximately 2 at average bond distances of 1.83 and 2.97 Å, respectively) confirms that these mononuclear complexes are dicarbonyls. Furthermore, these structural parameters are consistent with the crystal structure of the $Rh(CO)_2(acac)$ precursor in which the Rh–C and Rh–O* bond distances for two carbonyl ligands attached to Rh are 1.83 and 2.99 Å, respectively [163]. Based on these structural data and also FTIR results, indicating that the C-Rh-C angles in all grafted $Rh(CO)_2$ complexes are similar to that of the $Rh(CO)_2(acac)$ precursor in solution (Table 3.1), we can infer that the facile substitution of the acac ligand by the support takes place upon grafting, so that the structure of the $Rh(CO)_2$ moieties remains essentially unchanged.

The Rh-support interactions in all samples examined are evidenced by the presence of Rh–O_s contributions at an average bond distance of approximately 2.14 Å (Table 3.2). While this distance is entirely consistent with those reported in literature for zeolite- or metal oxide-supported complexes of different transition metals [63,65,59], it is substantially longer than that (i.e., 2.04 Å) between Rh and two oxygen atoms of the acac ligand in the $Rh(CO)_2(acac)$ precursor [163], confirming the replacement of the acac ligand by zeolite or γ-Al_2O_3 supports upon grafting. An average Rh–O_s coordination number was found to be approximately 2 for all zeolite-supported samples examined. Similar to the case of the acac ligand, this result indicates that zeolite supports with different Si/Al ratios are capable of chelating $Rh(CO)_2$ moieties and acting as bidentate ligands. In contrast, when γ-Al_2O_3 was used as a support, an average Rh–O_s coordination number was found to be 3.3 (Table 3.2). The larger Rh–O_s coordination number shows more complex binding of $Rh(CO)_2$ moieties to the surface of this support, which is amorphous and structurally non-uniform. However, this result is completely consistent with other literature reports demonstrating that the $\{OAl\}_3$ units on the γ-Al_2O_3 surface are primarily involved in coordination of metal carbonyl complexes [218,219,146], implying that grafted $Rh(CO)_2$ moieties could be located at the hollow sites between three oxygen anions of the support [218].

Furthermore, the Rh–O_l contributions at distances in the 2.76-2.81 Å range were consistently detected in EXAFS spectra of all samples examined (Table 3.2). While such contributions were routinely reported for metal complexes grafted on metal oxide surfaces [59], assignments for Rh neighbors located at such long distances in zeolite structures are less straightforward. For the case of dealuminated Y zeolites, DFT calculations reported elsewhere [63] predict coordination of $Rh(CO)_2$ moieties near Al cations of the zeolite framework with expected Rh–Al distances of 2.8 Å. Upon treatment of experimental EXAFS spectra for zeolite-supported Rh complexes, such contributions were often included in a fitting routine and average coordination numbers and distances reported for them were found to be in the 0.6-1.3 and 2.74-3.39 Å range, respectively [63,217,62]. However, it was also recognized that coordination numbers and distances reported for the Rh–Al contributions were determined with rather low confidence. In contrast, structural parameters reported elsewhere for Mo [222] and Pt [223] clusters and highly dispersed particles formed in various zeolites do not include metal-Al contributions but report metal-$O_{support}$

contributions at distances larger than 2.60 Å, which represent oxygen atoms in the zeolite framework. Consistent with these latter reports, optimal structural parameters for all zeolite-supported samples reported herein were obtained when Rh–O_l contributions were included in the fit. Regardless of such an assignment, it is evident that backscatterers located at such long distances are not bound to Rh by chemical bonds and, therefore, could have no direct influence on electronic and chemical properties of grafted $Rh(CO)_2$ species.

While structural data presented here confirm the formation of well-defined and site-isolated $Rh(CO)_2$ species in cages of zeolites, they also point to nearly identical structures formed in each case and do not allow to distinguish between two types of $Rh(CO)_2$ species, which are evidently present in these samples based on FTIR results. It is possible, that these two types of $Rh(CO)_2$ species could have only marginal differences in their structures, which cannot be resolved in average data provided by this technique. Alternatively, one can also suggest that both types of $Rh(CO)_2$ species could have structurally identical binding sites but oxygen atoms in such sites could exhibit different electronic properties. The presence of such binding sites would explain FTIR and EXAFS data discussed above.

Table 3.2 EXAFS structural parameters characterizing surface species formed from the $Rh(CO)_2(acac)$ precursor on different supports.

Support	Shell	*N*	*R* (Å)	$\Delta\sigma^2$ (Å^2)	ΔE_0 (eV)	ε_v^2	k^1-variances (%)	
							Im.	Abs.
HY30 [a]	Rh–Rh	--	--	--	--	1.4	0.4	0.2
	Rh–C*	2.0	1.84	0.00280	10.0			
	Rh–O*	2.3	2.99	0.00218	-7.2			
	Rh–$O_{support}$							
	Rh–O_S	2.3	2.13	0.00051	0.3			
	Rh–O_l	1.9	2.75	0.00018	-6.2			
HY15 [a]	Rh–Rh	--	--	--	--	1.8	0.6	0.2
	Rh–C*	1.9	1.84	0.00211	10.0			
	Rh–O*	2.3	2.99	0.00258	-7.3			
	Rh–$O_{support}$							
	Rh-O_S	2.4	2.13	0.00074	-0.6			
	Rh-O_l	2.0	2.75	0.00105	-6.1			
HY3 [a]	Rh–Rh	--	--	--	--	1.6	0.5	0.2
	Rh–C*	1.9	1.84	0.00203	10.0			
	Rh–O*	2.2	2.99	0.00241	-7.4			
	Rh–$O_{support}$							
	Rh-O_S	2.4	2.13	0.00084	-0.6			
	Rh-O_l	1.9	2.76	0.00039	-6.4			
Al_2O_3 [a]	Rh–Rh	--	--	--	--	2.1	0.8	0.7
	Rh–C*	1.6	1.84	0.00519	10			
	Rh–O*	2.1	2.96	0.0039	6			
	Rh–$O_{support}$							
	Rh-O_S	3.3	2.13	0.00755	-2.7			
	Rh-O_l	3	2.81	0.00471	-9.1			

Standard deviations in fits: N ± 20%, R ± 1%, $\Delta\sigma^2$ ± 10%, ΔE_0 ± 10%. N, coordination number; R, distance between absorber and backscatterer atoms; $\Delta\sigma^2$, Debye-Waller factor relative to the Debye-Waller factor of the reference compound; ΔE_0, inner potential correction accounting for the difference in the inner potential between the sample and the reference compound; ε_v^2, goodness of fit; the superscript * refers to carbonyl ligands. [a] R-space fit ranges $3.5 < k < 15.0$ Å^{-1} and $0.5 < r < 3.5$ Å; 23 allowed fitting parameters.

3.4.4 ELECTRONIC PROPERTIES OF GRAFTED $Rh(CO)_2$ SPECIES

XPS measurements were used to determine electronic properties of zeolite- and γ-Al_2O_3-grafted $Rh(CO)_2$ complexes and results are summarized in Fig. 3.5 and Table 3.3. Spectra collected for the $Rh(CO)_2$/HY30 sample show relatively sharp Rh $3d_{5/2}$ and $3d_{3/2}$ peaks (FWHM of 2.4 eV) at binding energies of 308.8 and 313.5 eV, respectively. An identical set of Rh 3d peaks was observed for the $Rh(CO)_2$/HY15 sample characterized by a Si/Al ratio of 15. However, when the $Rh(CO)_2$/HY2.6 sample with a Si/Al ratio of 2.6 was analyzed, Rh $3d_{5/2}$ and $3d_{3/2}$ peaks were found to be wider (FWHM of 2.7 eV) and corresponding binding energies lower (i.e., 308.5 and 313.2 eV, respectively). Even more broader Rh $3d_{5/2}$ and $3d_{3/2}$ peaks were observed in the case of $Rh(CO)_2$/γ-Al_2O_3 sample at binding energies of 307.9 and 312.8 eV, respectively, matching those of the $Rh(CO)_2$(acac) crystalline precursor (Table 3.3). Consistent with several literature reports [218,224-226], Rh $3d_{5/2}$ and $3d_{3/2}$ peaks observed in all these cases can be assigned to cationic $Rh^{\delta+}$ (δ~1) species. However, a measurable decrease in Rh 3d core level binding energies (~0.3 eV) with an increase in the Al content shows that the effective overall charge of Rh cations is somewhat different from sample to sample.

To better understand these data, the O 1s region of XPS spectra was also examined. Results collected for zeolite-supported samples show that the O 1s core level binding energy shifts from 532.8 to 531.8 eV, as the Si/Al ratio decreases from 30 to 2.6 and peaks become broader (Table 3.3). In the case of the γ-Al_2O_3-supported sample, the O 1s peak was found to be relatively wide

(FWHM of 2.5 eV) with a binding energy of 530.7 eV, which is substantially lower than that in all dealuminated Y zeolite-based samples. This result shows that oxygen atoms on the γ-Al_2O_3 surface are more electron reach as compared to those located in the zeolite framework.

As far as the comparison between zeolite-based samples is concerned, it is evident that the Al content in the zeolite framework affects significantly electronic properties of oxygen atoms associated with Al, as O 1s binding energies decline for approximately 1 eV when the Si/Al ratio decreases from 30 to 2.6 (Table 3.3). Moreover, since changes in Rh 3d core level binding energies characterizing zeolite-grafted $Rh(CO)_2$ species are similar to those observed in the O 1s region, we can conclude that electron accepting properties of oxygen atoms associated with framework Al affect electronic properties of Rh species substantially [227,228]. This conclusion is consistent with previous literature reports indicating that such oxygen atoms represent binding sites for $Rh(CO)_2$ species [63].

Table 3.3 XPS data characterizing surface species formed by adsorption of the $Rh(CO)_2(acac)$ precursor on different HY zeolites and γ-Al_2O_3.

Sample	Rh $3d_{5/2}$, eV	FWHM, eV	Rh $3d_{3/2}$, eV	FWHM, eV	O 1s, eV	FWHM, eV
$Rh(CO)_2$/HY30	308.8	2.4	313.5	2.4	532.8	1.7
$Rh(CO)_2$/HY15	308.8	2.4	313.6	2.4	532.6	1.8
$Rh(CO)_2$/HY2.6	308.5	2.7	313.2	2.7	531.8	2.4
$Rh(CO)_2$/γ-Al_2O_3	307.9	2.9	312.8	2.9	530.7	2.5
$Rh(CO)_2(acac)$	307.8	3.1	312.5	3.1	-	-

Overall, XPS results presented herein show that both the acac ligand and γ-Al_2O_3 support have quite similar electron withdrawing properties, as Rh 3d core level binding energies characterizing the $Rh(CO)_2(acac)$ precursor and γ-Al_2O_3-grafted $Rh(CO)_2$ species were found to be nearly identical (Table 3.3). In contrast, HY zeolite-grafted $Rh(CO)_2$ species exhibit substantially higher Rh 3d binding energies, indicating that dealuminated zeolites are stronger electron acceptors. This conclusion is further reinforced by FTIR results (section 1) that show v_{CO} bands of zeolite-supported $Rh(CO)_2$ species in the range of higher frequencies. Therefore, electronic properties of oxygen atoms associated with Al sites seem to explain the observed differences in electronic properties of $Rh(CO)_2$ species grafted on different supports.

However, expected differences in electronic properties of two types of zeolite-grafted $Rh(CO)_2$ species are not apparent from XPS results. Symmetrical shapes of Rh 3d peaks (Fig. 3.5) do not substantiate their deconvolution with several components, especially when FWHM parameters of these peaks are in the range of values typically reported in the literature [225,230]. This further suggests that differences in electronic properties of grafted $Rh(CO)_2$ species could be relatively small and difficult to resolve from spectra collected on a conventional XPS equipment. At the same time, we infer that broadening of the Rh 3d peaks could be an indicator of such species, the presence of which in each sample examined is established with high confidence from more sensitive FTIR measurements.

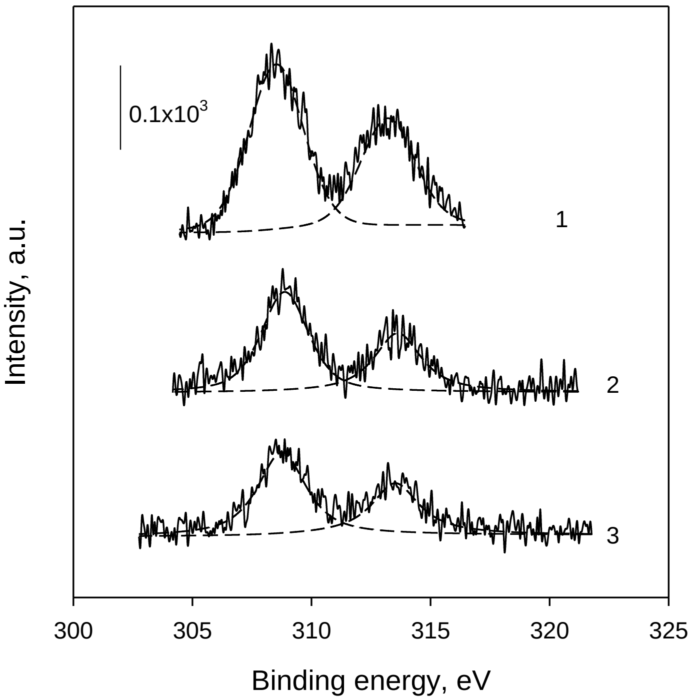

Figure 3.5 XPS spectra of the Rh 3d region (solid line) and deconvolution results (dashed line) of (1) $Rh(CO)_2$/HY2.6, (2) $Rh(CO)_2$/HY15, and (3) $Rh(CO)_2$/HY30 samples.

3.4.5 NATURE OF GRAFTED $Rh(CO)_2$ SPECIES

While differences in structure and electronic properties of binding sites in the zeolite framework could be responsible for the appearance of two types of $Rh(CO)_2$ species, the analysis of literature reports suggests that some other factors may be involved. For example, it was suggested that v_{CO} bands of $Rh(CO)_2$ species located on external zeolite surfaces are redshifted as compared to those of encaged complexes [62,190]. Since Al atoms in the zeolite framework could be isolated from each other by one or more Si atoms, it was also suggested that $Rh(CO)_2$ complexes anchored to such structurally different Al sites have different fingerprints in the v_{CO} region [189]. Several other explanations associated with physisorbed $Rh(CO)_2$(acac) complexes, incomplete removal of acac ligands upon anchoring, and coordination of water molecules directly to $Rh(CO)_2$ species can be also found in the literature [62,191,194]. To examine if any of these factors can potentially contribute to the appearance of two types of HY zeolite-grafted $Rh(CO)_2$ complexes, additional experiments were performed.

3.4.5.1 INTERACTION OF ZEOLITE-GRAFTED $Rh(CO)_2$ SPECIES WITH PHOSPHINES

It is well known that carbonyl ligands of the $Rh(CO)_2$(acac) precursor readily react with phosphines in solution to produce partially or fully substituted derivatives, depending on the phosphine nature and reaction conditions used [234]. During such substitution reactions, the formal oxidation state of Rh^+ species does not change and Rh-phosphine complexes formed retain the square planar geometry. Since carbonyl ligands in supported $Rh(CO)_2$ complexes are also capable of reacting with phosphines, it had been suggested that such reactivity can be used to distinguish between surface and encaged $Rh(CO)_2$ species, as sufficiently large phosphines are not capable of penetrating inside zeolite cages and, therefore, can react only with $Rh(CO)_2$ complexes located on the external surface [190]. The same methodology was used in this work to determine if any zeolite-grafted $Rh(CO)_2$ complexes could be located on the zeolite exterior.

Experiments were performed with triethylphsophine $P(C_2H_5)_3$ and tris(2,4-dimethylphenyl)phosphine $P[C_6H_3(CH_3)_2]_3$ complexes having molecular dimensions of 6.97 and 11.7 Å, respectively [235,236]. Among these complexes, only $P(C_2H_5)_3$ can fit into the 7.4 Å aperture of HY zeolites. As expected, when grafted $Rh(CO)_2$ complexes were treated with $P(C_2H_5)_3$, v_{CO} bands assigned to dicarbonyl species disappeared, while a new v_{CO} band at 1993 cm^{-1} appeared in spectra of all zeolite-based samples examined (Fig. 3.6 shows an example of such changes for the $Rh(CO)_2$/HY30 sample). This result confirms the reactivity of zeolite-grafted $Rh(CO)_2$ species toward phosphines and the changes observed in the v_{CO} region are consistent with the formation of $Rh(CO)(P(C_2H_5)_3)$ complexes, which exhibit only one v_{CO} vibration. Such a conversion of surface species resembles closely the reaction of $Rh(CO)_2(acac)$ with different phosphines in solution to yield $Rh(CO)(PR_3)(acac)$ complexes [177].

In contrast, when the $P[C_6H_3(CH_3)_2]_3$ complex with larger dimensions was used to treat zeolite-grafted $Rh(CO)_2$ species, no changes in intensity of the v_{CO} bands of Rh dicarbonyl species were observed and additional v_{CO} bands did not appear in the spectra, regardless of the zeolite used. This result unambiguously shows that all grafted $Rh(CO)_2$ complexes are located inside zeolite pores and, therefore, are inaccessible for this bulky phosphine. Consequently, we can conclude with confidence that neither type of zeolite-grafted $Rh(CO)_2$ species detectable by FTIR can be assigned to species formed on the external zeolite surfaces. This conclusion if further reinforced by DFT calculations [63], demonstrating that the majority of energetically preferable binding sites for $Rh(CO)_2$ complexes are located inside supercages of faujasites.

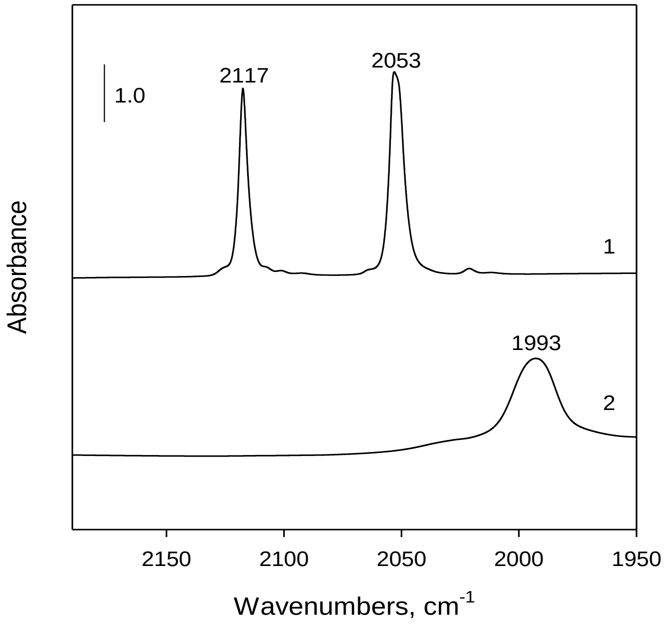

Figure 3.6 FTIR spectra in the ν_{CO} region of (1) $Rh(CO)_2$/HY30 and (2) the same sample treated with $P(C_2H_5)_3$.

3.4.5.2 INTERACTION OF $Rh(CO)_2$(acac) SPECIES WITH ZEOLITES

It is quite possible that incomplete removal of the acac ligand during grafting $Rh(CO)_2$(acac) complexes on HY zeolites with different Si/Al ratios could account for the presence of two sets of ν_{CO} bands from $Rh(CO)_2$ species. For example, it was reported previously [62] that the reaction of $Rh(CO)_2$(acac) with H-SSZ-42 and H-Mordenite zeolites does not proceed to completion, as ν_{CO} bands from both zeolite-grafted $Rh(CO)_2$ species and physisorbed $Rh(CO)_2$(acac) complexes were found to be present in FTIR spectra of these samples.

To identify v_{CO} bands of $Rh(CO)_2(acac)$ complexes unreacted with HY zeolites, the empty HY30 support was initially treated with an excess of acetylacetone/pentane solution at room temperature to provide the molar acetylacetone/Al ratio of approximately 1.8. Since acetylacetone forms strong chelate complexes with Al^{3+} cations [59], the intension was to block the majority of Al^{3+} sites by acetylacetone and to make them unavailable for Rh complexes. After this treatment was completed, the support was washed with a pure solvent to remove unreacted acetylacetone and the $Rh(CO)_2(acac)$ complex was impregnated on the support according to the procedure described in the preparation section. Three pairs of v_{CO} bands can be identified in the FTIR spectrum of this sample (Fig. 3.7).

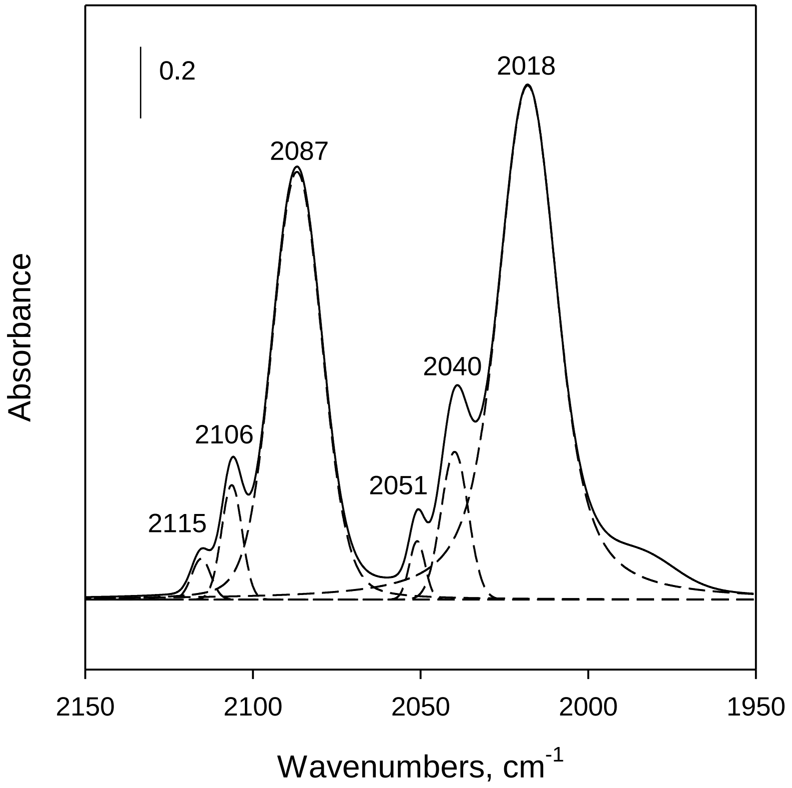

Figure 3.7 FTIR spectra in the v_{CO} region (solid line) and deconvolution results (dashed line) of the sample prepared by impregnation of $Rh(CO)_2(acac)$ on the HY30 support pretreated with acetylacetone.

Relatively strong v_{CO} bands at 2087 and 2018 cm^{-1} can be assigned to physisorbed $Rh(CO)_2(acac)$ complexes, since the position of these bands is similar to that of $Rh(CO)_2(acac)$ in pentane solution (Table 3.1). The v_{CO} bands at 2106 and 2040 cm^{-1} can be attributed to surface complexes in which acac ligands are only partially displaced from Rh, while the pair of bands at 2115 and 2051 cm^{-1} represents $Rh(CO)_2$ species grafted to the zeolite framework. As expected, deconvolution results further show that physisorbed $Rh(CO)_2(acac)$

complexes constitute the majority (approximately 88%) of all surface species formed, while partially reacted $Rh(CO)_2(acac)$ and grafted $Rh(CO)_2$ species are present only in small amounts, as their fractions in the sample do not exceed 9 and 3%, respectively.

The same set of bands was observed when crystalline $Rh(CO)_2(acac)$ was carefully mixed with the empty HY30 support without solvents being present to produce a physical mixture containing approximately 5 wt.% Rh (Table 3.4). In this case, however, the fraction of physisorbed $Rh(CO)_2(acac)$ complexes was less significant (approximately 46%), while greater amounts of partially reacted $Rh(CO)_2(acac)$ (approximately 25%) and grafted $Rh(CO)_2$ species (approximately 29%) were formed. From this result, it is evident that a significant portion of $Rh(CO)_2(acac)$ complexes was capable of penetrating into zeolite pores upon mixing and grinding of these solid materials and reacting with the zeolite framework since none of Al sites were blocked in this case. It is further notable that the reaction between $Rh(CO)_2(acac)$ complexes and the support accelerates at higher temperatures. For example, the fraction of grafted $Rh(CO)_2$ species increased from 29 to 97%, as the temperature was increased from 25 to 200°C (Table 3.4). The fraction of unreacted $Rh(CO)_2(acac)$ complexes decreased from 46 to 25%, as the temperature was increased 100°C, and no such species were evident at higher temperatures. In contrast, the fraction of partially reacted $Rh(CO)_2(acac)$ complexes slightly increased at 50°C, remained nearly unchanged at 100°C, and declined significantly at higher temperatures when unreacted complexes completely disappeared (Table 3.4). As expected, this pattern clearly demonstrates an intermediate character of partially reacted $Rh(CO)_2(acac)$ species.

Overall, the data presented herein allow to identify precisely the v_{CO} bands of unreacted and partially reacted $Rh(CO)_2(acac)$ complexes and show nearly quantitative transformations between them and grafted $Rh(CO)_2$ species. Furthermore, since the v_{CO} bands of partially reacted $Rh(CO)_2(acac)$ complexes (i.e., 2106 and 2040 cm^{-1}, Table 3.4) closely resemble those of type II species (i.e., 2113 and 2048 cm^{-1}, Fig. 3.2A), incomplete displacement of acac ligands from Rh could reasonably explain the appearance of the latter species in spectra of all samples examined. However, a further comparison of thermal properties of partially reacted $Rh(CO)_2(acac)$ complexes and type II $Rh(CO)_2$ species suggests that this is not the case, as the latter species undergo decarbonylation in the 25-200°C temperature range (Fig. 3.3) but the former ones are evidently converted into $Rh(CO)_2$ species grafted to the zeolite framework (Table 3.4).

Table 3.4 FTIR bands in the v_{CO} region characterizing surface species formed by mixing of crystalline $Rh(CO)_2(acac)$ with dry HY30 zeolite.

v_{CO} bands positions, cm^{-1}	Treatment temperature/relative fraction of species (%)					Suggested surface species
	25°C	50°C	100°C	150°C	200°C	
2115 2051	29	30	45	82	97	grafted $Rh(CO)_2$
2106 2040	25	31	30	18	3	partially reacted $Rh(CO)_2(acac)$
2089 2023	46	39	25	-	-	physisorbed $Rh(CO)_2(acac)$

3.4.5.3 INTERACTION OF ZEOLITE-GRAFTED $Rh(CO)_2$ COMPLEXES WITH H_2O

While aqua complexes of Rh are well known in solution chemistry and some of these complexes with carbonyl ligands are even capable of catalyzing a water gas shift reaction [238-242], a limited information related to interactions of H_2O molecules with supported Rh carbonyl complexes is available. It has been reported that water facilitates reductive carbonylation of zeolite- and alumina-supported $Rh(CO)_2$ species at elevated temperatures to yield $Rh_6(CO)_{16}$ or $Rh_4(CO)_{12}$ clusters [243-245]. At room temperature, however, this reaction does not proceed with measurable rates and $Rh(CO)_2(H_2O)_x$ complexes are formed instead of Rh clusters [246,247].

To determine the location of v_{CO} bands characterizing $Rh(CO)_2(H_2O)_x$ complexes and understand if these complexes could represent type II species, several additional experiments were performed. In the first set, HY2.6 and HY30 supports were pretreated under vacuum in the 100-400°C range of temperatures to remove zeolite-trapped water molecules to a different extent. As expected, the presence substantial amounts of water in the samples treated at 100°C is evidenced by infrared bands at approximately 3500 and 1630 cm^{-1} assigned to stretching and bending vibrations, respectively, of H_2O molecules hydrogen-bonded to zeolite surfaces (spectra are not shown for brevity). As the treatment temperature was increased to 200°C, bands associated with H_2O molecules declined in intensity, while relatively weak ν_{OH} bands of acidic hydroxyls appeared in the spectra at 3630 and 3565 cm^{-1}. These bands became somewhat stronger after thermal treatments in the 300-400°C temperature range, but bending vibrations of H_2O were no longer evident in the spectra. These data are consistent with progressive desorption of water from zeolite surfaces at elevated temperatures, suggesting that the residual water content in such treated supports is significantly different. When these supports were further impregnated with $Rh(CO)_2(acac)$, type I and type II $Rh(CO)_2$ species were detected in all samples examined (Table 3.5). In all these cases, however, neither the position of ν_{CO} bands nor the fraction of species formed change substantially as a function of the pretreatment temperature. This result strongly suggests that H_2O molecules residing in zeolite pores do not promote the formation of type II $Rh(CO)_2$ species.

Table 3.5 FTIR bands in the v_{CO} region characterizing surface species formed by adsorption of the $Rh(CO)_2(acac)$ precursor on HY30 and HY2.6 zeolites treated under vacuum at different temperatures.

Sample	Support treatment conditions	v_{CO} band positions, cm^{-1}	Relative fraction, %
$Rh(CO)_2$/HY30	vacuum at 100°C	2117/2052 2112/2048	85 15
	vacuum at 200°C	2117/2051 2112/2048	84 16
	vacuum at 300°C	2117/2053 2113/2048	83 17
	vacuum at 400°C	2117/2051 2112/2048	79 21
$Rh(CO)_2$/HY2.6	vacuum at 100°C	2117/2052 2109/2045	54 46
	vacuum at 200°C	2117/2053 2109/2043	46 54
	vacuum at 300°C	2117/2053 2110/2043	50 50
	vacuum at 400°C	2117/2052 2109/2042	42 58

In the second set of experiments, the $Rh(CO)_2$/HY30 sample with the smallest fraction of type II species originally formed (Fig. 3.2 A) was exposed to wet He feeds and significant changes in FTIR spectra were observed (Fig. 3.8). With 2.5 Torr H_2O in the He feed, two sets of v_{CO} bands can be clearly identified in the spectrum at 2117-2053 cm^{-1} and 2112-2046 cm^{-1}. When the H_2O partial pressure was increased to 3.1 Torr, the v_{CO} bands at 2117-2053 cm^{-1} declined in intensity, while those at 2112-2046 cm^{-1} shifted to 2110-2043 cm^{-1} and grew in intensity. Simultaneously, a new set of v_{CO} bands appeared at 2094-2025 cm^{-1}. The latter two sets of v_{CO} bands continue to shift toward low frequencies and grow in intensity with H_2O partial pressures (Fig. 3.8).

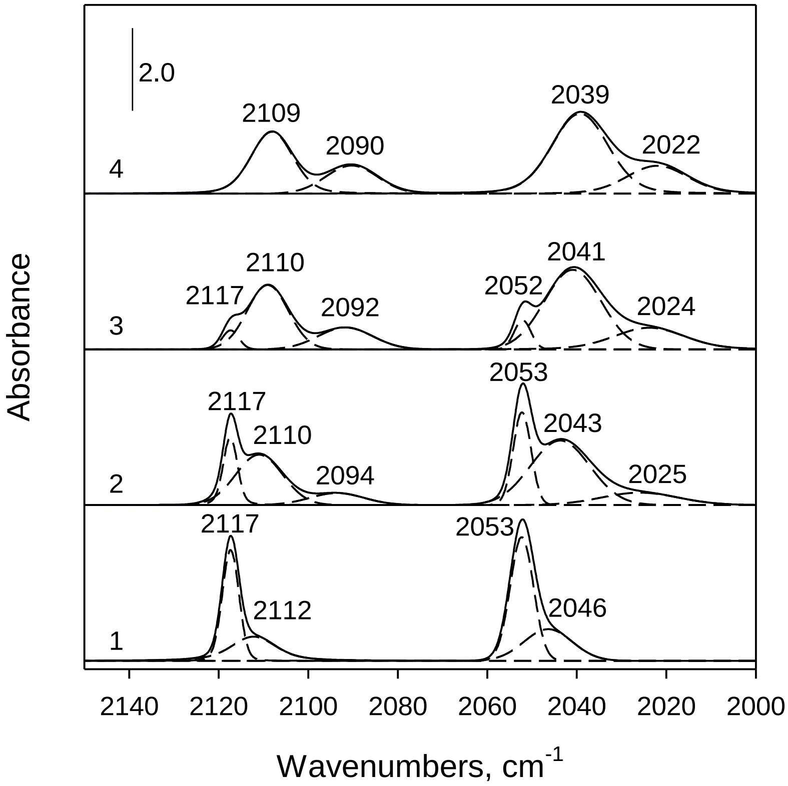

Figure 3.8 FTIR spectra in the v_{CO} region (solid line) and deconvolution results (dashed line) of $Rh(CO)_2$/HY30 exposed to H_2O/He feeds with different H_2O partial pressures: (1) 2.5 Torr, (2) 3.1 Torr, (3) 5.2 Torr, and (4) 8.6 Torr.

Deconvolution results summarized in Fig. 3.9 for all experimental conditions examined further suggest that the bands at 2109-2039 cm^{-1} and 2090-2022 cm^{-1} are formed at the expense of those at 2117-2053 cm^{-1}. This transformation is completed when 8.6 Torr H_2O is present in the feed, as the latter bands are no longer evident in the spectra. Therefore, these two sets of v_{CO} bands (i.e., at 2109-2039 cm^{-1} and 2090-2022 cm^{-1}) can be assign to different $Rh(CO)_2(H_2O)_x$ complexes, which are formed from grafted $Rh(CO)_2$ species in the presence of H_2O in a gas phase. An overall surface concentration of such species strongly depends on the H_2O partial pressure and their formation is further evident from specific deformation vibrations of H_2O molecules. For example, the $\delta(H_2O)$ region shown in Fig. 3.10 for the same set of spectra exhibits a relatively complex band structure, consistent with the presence of two components at 1630 and 1619 cm^{-1} with intensities highly dependent on the H_2O partial pressure. The former band originates from H_2O molecules adsorbed in zeolite pores and not interacting directly with Rh sites, while the latter one represents H_2O molecules specifically bound to Rh [248]. It is important to emphasize that the band at 1619 cm^{-1} does not appear in spectra of $Rh(CO)_2$/HY30 under dry conditions, but it emerges immediately when H_2O is present in the He feed. An average number of H_2O molecules coordinated to each Rh site can be roughly estimated from the integral intensity of this band, as reported elsewhere [248]. The estimate performed for the spectrum collected with 8.6 Torr H_2O in the feed shows an average H_2O/Rh ratio of 1.4, consistent with the formation of approximately 60% $Rh(CO)_2(H_2O)$ and 40% $Rh(CO)_2(H_2O)_2$

complexes under these conditions. Furthermore, these percentages closely resemble those of v_{CO} bands at 2109-2039 cm^{-1} and 2090-2022 cm^{-1} (i.e., 60 and 40%, respectively) in the same spectrum. Based on all above and assuming that molar absorption coefficients of carbonyl ligands in various $Rh(CO)_2(H_2O)_x$ complexes are not substantially different, we can assign with confidence v_{CO} bands at 2109-2039 cm^{-1} to $Rh(CO)_2(H_2O)$ and those at 2090-2022 cm^{-1} to $Rh(CO)_2(H_2O)_2$ complexes.

When a wet feed was replaced with dry He, v_{CO} bands assigned to $Rh(CO)_2(H_2O)_x$ species gradually disappeared and those assigned to $Rh(CO)_2$ complexes reappeared in the spectrum. Consistent with previous literature reports [247], this result demonstrates that transformations between $Rh(CO)_2$ and $Rh(CO)_2(H_2O)_x$ species are completely reversible. Even though the v_{CO} bands characterizing $Rh(CO)_2(H_2O)$ complexes overlap with those of type II species, it is evident that these complexes cannot be linked to each other since significant partial pressures of water are required to form $Rh(CO)_2(H_2O)$ species.

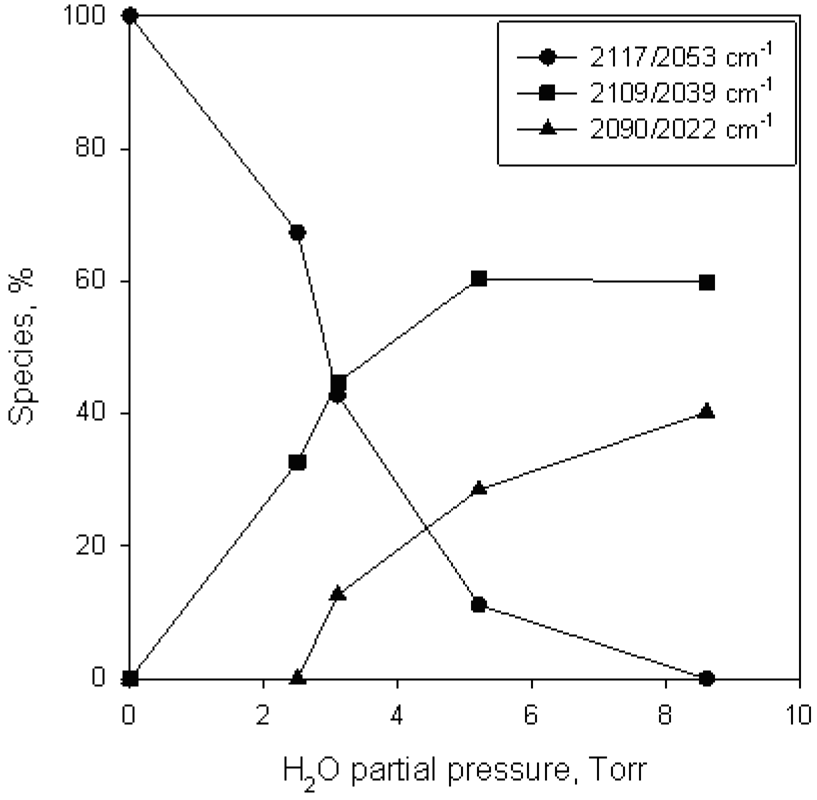

Figure 3.9 Percent of species with characteristic ν_{CO} bands at 2117/2053 cm^{-1} (●), 2109/2039 cm^{-1} (■), and 2090/2022 cm^{-1} (▲) formed after exposure of $Rh(CO)_2$/HY30 to H_2O/He feeds with different H_2O partial pressures.

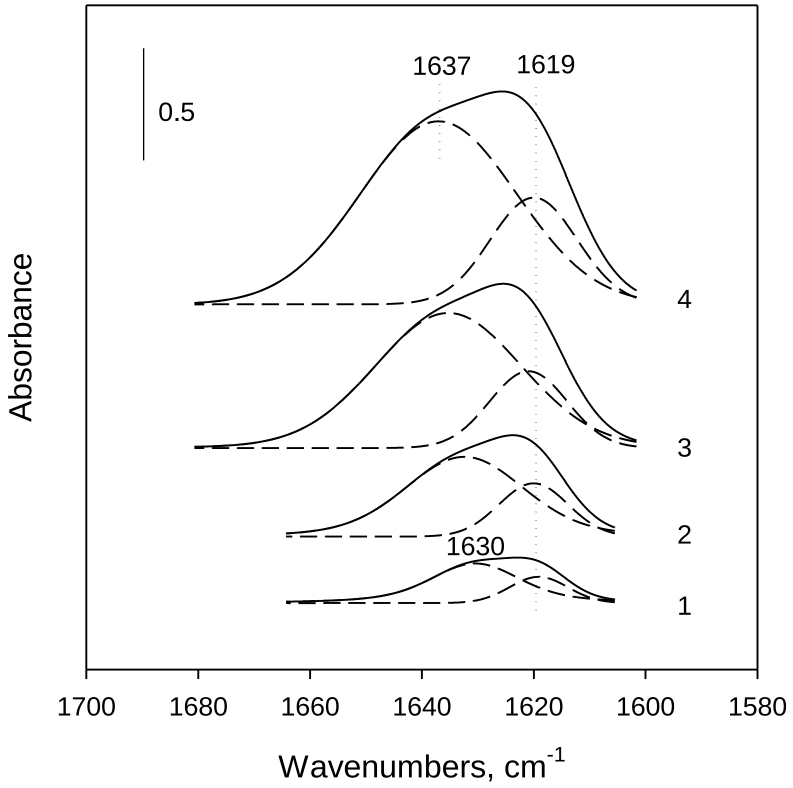

Figure 3.10 FTIR spectra in the δ(H_2O) region (solid line) and deconvolution results (dashed line) of $Rh(CO)_2$/HY30 exposed to H_2O/He feeds with different H_2O partial pressures: (1) 2.5 Torr, (2) 3.1 Torr, (3) 5.2 Torr, and (4) 8.6 Torr.

3.4.5.4 ROLE OF ALUMINUM SPECIES

Results described so far show the absence of $Rh(CO)_2$ species on external zeolite surfaces and demonstrate that properties of partially reacted $Rh(CO)_2(acac)$ and $Rh(CO)_2(H_2O)_x$ complexes are quite different from those of type II $Rh(CO)_2$ species. All these allow us to suggest that binding sites of different nature in the zeolite framework are most likely responsible for the appearance of different $Rh(CO)_2$ species and several literature examples seem to support this suggestion.

For example, it has been reported that the adsorption of CO at low temperature over NaY and NaX zeolites leads to multiple v_{CO} bands, which were explained by different coordination of Na^+ cations to the zeolite framework [249,250]. DFT calculations reported elsewhere [251] for the same supports further suggest that Na cations preferentially interact with the oxygen atoms connected to aluminum in six-rings of the zeolite framework. Since the negative charge density of oxygen atoms in a ring increases with Al content, the strength of the electric field induced on Na^+ cations by neighboring oxygen atoms increases as well. This affects the electronic state of Na^+ cations and their positions in respect to the six-ring plane, leading to a split of the CO frequency upon adsorption on Na^+ [251]. It is quite possible that the same phenomenon takes place with HY zeolite-grafted $Rh(CO)_2$ complexes, as the FTIR results clearly show the existence of two types of grafted species with fractions highly dependent on the Al content.

Furthermore, it is also possible that nonframework aluminum species formed during dealumination of zeolites could participate in anchoring at least some $Rh(CO)_2$ complexes, leading to a split of v_{CO} bands. Nonframework aluminum species are often classified as condensed and noncondensed in nature [252,253]. The former type of species is usually associated with small Al_2O_3 clusters located on external zeolite surfaces [254]. The nature of noncondensed extraframework aluminum is not fully understood but Al^{3+}, $Al(OH)^{2+}$, $Al(OH)_2^+$, $Al(OH)_3$, and AlOOH species are among possible suggested structures [252]. Such species are assumed to be highly dispersed and bound to oxygen atoms of the framework aluminum by strong electrostatic interactions [255-257]. In fact, the presence of nonframework octahedral Al in dealuminated HY30, HY15, and HY2.6 zeolites has been confirmed by ^{27}Al MAS NMR and results suggest that the fraction of these species increases with the Al content [254]. The same NMR results also show that besides well-established signals from framework tetrahedral and nonframework octahedral Al species at 60 and 0 ppm, respectively, additional Al species contribute to ^{27}Al MAS NMR spectra of these supports at 30 ppm. While the nature of these additional Al species is under extensive discussion [259-261], it is evident that their fraction also increases with Al content [254]. Since our data show a similar pattern for zeolite-grafted $Rh(CO)_2$ complexes associated with type II species, we can further infer that both nonframework octahedral Al species and Al species of unknown nature could account for their appearance.

To verify this suggestion, a HY30 zeolite was impregnated with appropriate amounts of $Al(NO_3)_3 \cdot 9H_2O$ in ethanol to yield supports containing 2 and 5 wt.% Al. The intension was to create different concentrations of nonframework Al species in this highly dealuminated HY zeolite and determine if the fraction of type II $Rh(CO)_2$ species correlates with their content. The resulting supports were calcined at 300°C to decompose the Al precursor and treated under vacuum at the same temperature for 16 h. XRD spectra collected for these modified supports were found to be identical to that of original HY30 (data are not shown for brevity), suggesting that Al species added to this support are in a highly dispersed state rather than in a form of a bulk Al_2O_3 phase. When the $Rh(CO)_2$(acac) precursor was further impregnated from n-pentane on these modified supports to attain 1 wt.% Rh loadings and FTIR spectra were collected, a deconvolution procedure was used in each case to accurately quantify different types of $Rh(CO)_2$ species formed. Results summarized in Table 3.6 clearly show that the fraction of $Rh(CO)_2$ species with v_{CO} bands at 2113/2048 cm^{-1} increases, while that of species with v_{CO} bands at 2117/2053 cm^{-1} decreases in a linear fashion with the loading of extra Al species. Realizing that the observed change ratio is not 1:1 and the presence at least some Al species on external zeolite surfaces of these materials is highly possible due to the preparation procedure used, the result obtained still strongly suggests that nonframework Al species in dealuminated HY zeolites could also bind $Rh(CO)_2$ complexes and be responsible for the observed split of v_{CO} frequencies. However, more efforts are required to determine precisely the specific nature of nonframework Al species involved.

Table 3.6 Fractions of grafted $Rh(CO)_2$ species formed by adsorption of $Rh(CO)_2$(acac) on the HY30 support loaded with extra Al species.

Loading of extra Al species, wt.%	Si/Al ratio	Fraction of $Rh(CO)_2$ species, %	
		2117/2053 cm^{-1}	2113/2048 cm^{-1}
none	30.0	83.0	17.0
2.0	12.6	77.5	22.5
5.0	6.8	69.8	30.2

3.4.5.5 REACTIVITY OF GRAFTED $Rh(CO)_2$ COMPLEXES

It has been shown previously that $Rh(CO)_2$(acac) complexes in solution readily react with C_2H_4 at room temperature to yield $Rh(CO)(C_2H_4)$(acac) species [161]. The same facile C_2H_4/CO substitution reaction is also well documented for zeolite-grafted $Rh(CO)_2$ species [217]. We have used this reaction as a convenient probe to determine differences in reactivity of various zeolite-grafted $Rh(CO)_2$ complexes. While the $Rh(CO)(C_2H_4)$ complexes finally formed exhibit only one v_{CO} vibration at 2053 cm^{-1} that overlaps with asymmetric v_{CO} vibrations of $Rh(CO)_2$ species [217], changes in intensity of corresponding symmetric v_{CO} bands of $Rh(CO)_2$ species allow us to determine precisely the extent of their conversion into $Rh(CO)(C_2H_4)$ complexes. Moreover, since this substitution reaction is very fast over all $Rh(CO)_2$/HY samples, the most accurate data can be obtained only for the $Rh(CO)_2$/HY2.6 material with the largest fraction of type II $Rh(CO)_2$ species initially formed.

Results shown in Fig. 3.11 (curves 2 and 3) for this sample indicate that after 50 seconds of C_2H_4 exposure approximately 13 and 50 % of type I (the v_{CO} band at 2117 cm^{-1}) and type II (the v_{CO} band at 2110 cm^{-1}) $Rh(CO)_2$ species remained unconverted, respectively. Type I $Rh(CO)_2$ complexes completely disappeared after 300 seconds of C_2H_4 exposure, while approximately 16 % of type II species still remained unconverted at this point. These data clearly show that two types of zeolite-grafted $Rh(CO)_2$ complexes are not identical in terms of their chemical properties, as carbonyl ligands in type I $Rh(CO)_2$ species exhibit higher reactivities toward C_2H_4. Since the v_{CO} bands characterizing type II $Rh(CO)_2$ complexes are redshifted relative to those of type I species in spectra of all samples examined (Fig. 3.2), it is evident that Rh atoms associated with the former type of species are more electron rich. This further implies that oxygen atoms in the zeolite framework associated with each type of $Rh(CO)_2$ species are not identical in terms of their electronegativity and, therefore, can alter differently electronic properties of Rh atoms. It is expected that the gain in Rh electron density will enhance the transfer of Rh 3d electrons onto π* molecular orbitals of CO ligands, leading to weaker C=O and stronger Rh-CO bonds [262,263]. Since electron rich metal sites typically promote CO dissociation but not CO substitution reactions [262], we can further infer that variations in electron density of Rh sites and, therefore, in strength of Rh-CO bonds in two types of zeolite-grafted $Rh(CO)_2$ species could be accountable for differences observed in their

C_2H_4/CO substitution activities. Similar experiments performed with the $Rh(CO)_2$/γ-Al_2O_3 sample seem to support this suggestion, as the v_{CO} bands of $Rh(CO)_2$ species were observed at very low frequencies (i.e., 2090 and 2014 cm^{-1}) and their C_2H_4/CO substitution activity was very low as well (Fig. 3.11, curve 1).

To explore this point further, additional experiments with the $Rh(CO)_2$/HY30 sample pretreated in NH_3 were performed. NH_3 is a strong Lewis base that readily forms complexes with Rh in solution [264,265]. Therefore, our intention was to modify the coordination environment of grafted $Rh(CO)_2$ species with NH_3 and examine the reactivity of species thus formed with C_2H_4. Since the fraction of type II $Rh(CO)_2$ species initially formed in this sample is relatively low (Table 3.1), no distinctions between different types of $Rh(CO)_2$ species were made in this set of measurements for the sake of simplicity.

When the $Rh(CO)_2$/HY30 sample was exposed to a 1 % NH_3/He mixture for 3 min, significant changes in the v_{CO} region were observed. The v_{CO} bands at 2117 and 2053 cm^{-1} assigned to $Rh(CO)_2$ species disappeared from a spectrum, while a new pair of v_{CO} bands appeared at 2110 and 2048 cm^{-1} (Fig. 3.12).

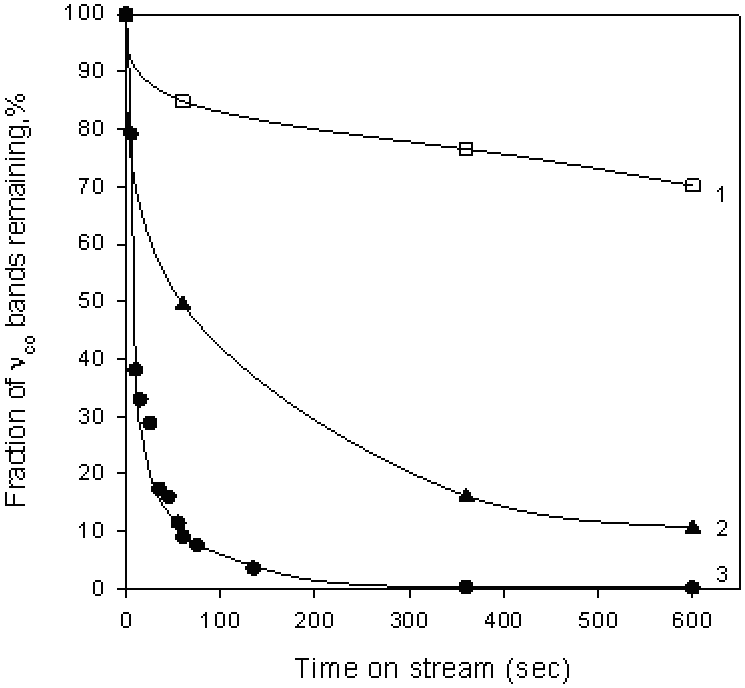

Figure 3.11 Fractions of ν_{CO} bands remaining in spectra of (1) $Rh(CO)_2/\gamma$-Al_2O_3 (□-2090 cm^{-1}) and (2, 3) $Rh(CO)_2$/HY2.6 (▲- 2110 cm^{-1}; ●- 2117 cm^{-1}) samples after exposure to C_2H_4 as a function of time on stream.

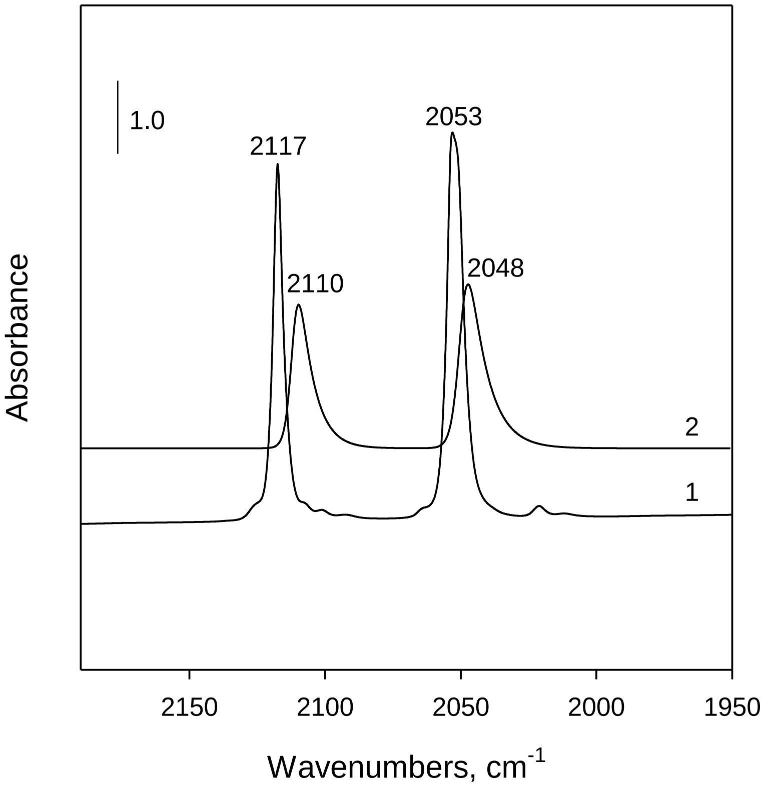

Figure 3.12 FTIR spectra in the ν_{CO} region of (1) $Rh(CO)_2$/HY30 and (2) $Rh(CO)_2$/HY30 pretreated in a 1 % NH_3/He mixture for 3 min.

While the reduced intensity of these new bands could be related to partial decarbonylation of grafted $Rh(CO)_2$ species or changes in absorption coefficients of carbonyl ligands during such a treatment, the changes observed in the ν_{CO} region alone are short of any hints clarifying whereabouts of NH_3 species. It is quite possible that NH_3 coordinates directly to $Rh(CO)_2$ species by replacing the support oxygen atoms at the metal-support interface or alternatively coordinates to Al atoms in the zeolite framework and influences the electronic properties of Rh indirectly. In any case, the position of these new ν_{CO} bands and the split between them (i.e., 62 cm^{-1}) are consistent with the presence of Rh dicarbonyl species with different electronic properties (i.e., electron rich) in the NH_3 modified sample. Such modified Rh dicarbonyls were found to be substantially less reactive toward C_2H_4 than original $Rh(CO)_2$ complexes (Fig. 3.13). Consistent with other data reported herein, this result confirms one more time that the electronic properties of Rh atoms in surface complexes affect substantially the reactivity of carbonyl ligands. Furthermore, results presented here for zeolite- and γ-Al_2O_3-grafted $Rh(CO)_2$ complexes provide unambiguous evidence that each of these supports acts as a macro ligand to Rh species, inducing significant changes in reactivity of supported complexes.

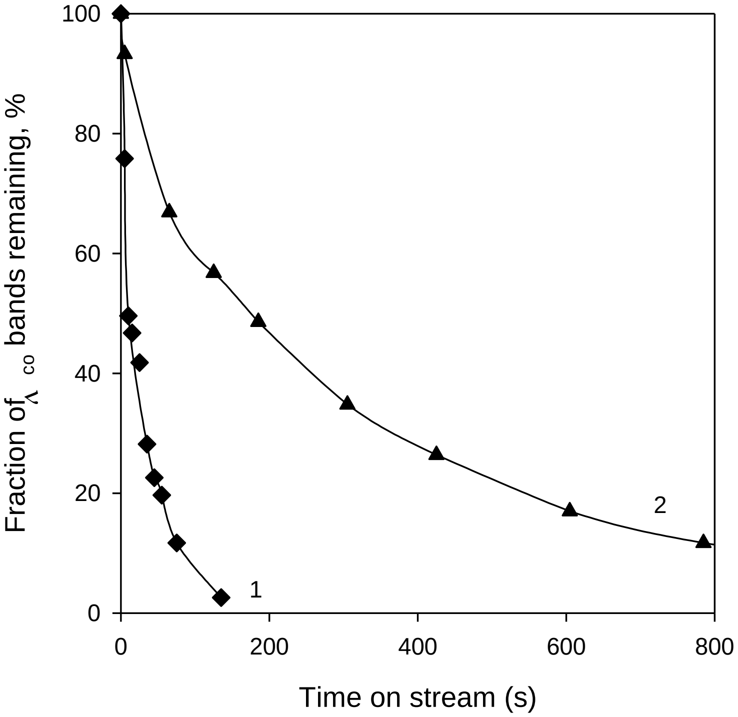

Figure 3.13 Fractions of the ν_{CO} band at 2117 cm^{-1} remaining in spectra of (1) $Rh(CO)_2$/HY30 and (2) $Rh(CO)_2$/HY30 pretreated in a 1 % NH_3/He mixture for 3 min samples after exposure to C_2H_4 as a function of time on stream.

Finally, the suggested inference of stronger Rh-CO bonds in type II $Rh(CO)_2$ complexes clearly does not correlate with the thermal properties of these species (see section 2 for details). While our data do not allow to resolve this issue, we can speculate that properties of the specific binding sites in the zeolite framework accommodating these species could provide more clues related to such a discrepancy. However, much more efforts are required to determine the nature and properties of such binding sites.

3.5 CONCLUSIONS

Experimental results presented here demonstrate the formation of two different types of grafted $Rh(CO)_2$ complexes when dealuminated HY zeolites with various Si/Al ratios are used as supports. Type I species are characterized by the v_{CO} bands at 2117/2053 cm^{-1}, while those at 2110/2043 cm^{-1} represent type II species. The Si/Al ratio in the range of 2.6-30 does not influence substantially the v_{CO} vibrational frequencies of these species. However, the fraction of each species formed strongly depends on this ratio, as supports with a higher Al content favor the formation of type II species in larger amounts. Our results further show that both types of $Rh(CO)_2$ complexes are located within zeolite pores and Rh atoms in such complexes have a similar coordination environment but slightly different electronic properties, as the v_{CO} bands of type II species appear at lower frequencies. As a result, these two types of zeolite-grafted $Rh(CO)_2$ complexes are not identical in terms of their chemical properties, as carbonyl ligands in type I species exhibit higher reactivities toward C_2H_4. Experiments with the $Rh(CO)_2$/HY30 sample pretreated in NH_3 reinforce this point and further show that that electronic properties of Rh atoms in surface complexes affect substantially the reactivity of carbonyl ligands.

Furthermore, our results strongly suggest that the second type of $Rh(CO)_2$ species formed in all samples examined cannot be linked to unreacted and partially reacted $Rh(CO)_2(acac)$ complexes or to the formation of $Rh(CO)_2(H_2O)_x$ species, since both of these latter species have different properties or require quite special conditions for their formation. Most likely, the existence of two types of zeolite-grafted $Rh(CO)_2$ complexes could be related to the different nature of binding sites existing in dealuminated faujasites, as both nonframework Al species and a different distribution of Al in the zeolite framework could account for their appearance to some extent. While stronger experimental tools are obviously required to prove this point, the existence of zeolite-grafted $Rh(CO)_2$ complexes with remarkably different reactivities of carbonyl ligands strongly suggests that properties of supports that are used for grafting molecular metal complexes should not be overlooked.

3.6 ACKNOWLEDGENETS

The authors thank Dr. Shuguo Ma for the assistance with X-ray Photoelectron Spectroscopy (XPS) measurements. XAS data were collected at the Stanford Synchrotron Radiation Laboratory, a national user facility operated by Stanford University on behalf of the U.S. Department of Energy, Office of

Basic Energy Sciences. The assistance of the beam line staff at SSRL is gratefully acknowledged. The EXAFS data were analyzed with the XDAP software developed by XAFS Services International [148].

CHAPTER 4. ETHYLENE HYDROGENATION AND ETHYLENE DIMERIZATION USING HY ZEOLITE-SUPPORTED RHODIUM DICARBONYL COMPLEXES: ROLE OF THE SUPPORT AND COMPLEX COORDINATON ENVIROMENT ON CATALYTIC ACTIVITY

4.1 PREFACE

HY Zeolite-supported mononuclear $Rh(CO)_2$ complexes were shown to be active in ethylene hydrogenation and ethylene dimerization at ambient conditions. The role of the support as a macroligand was found to be crucial for catalytic properties of supported carbonyl complexes. More specifically, Al_2O_3-supported catalyst does not favor formation of rhodium carbonyl hydride species and it is virtually inactive in hydrogenation and dimerization reactions. Activity measurements performed on HY zeolite-supported catalyst at 76-608 Torr of H_2 and 38 -152 Torr of C_2H_4 revealed strong dependence of hydrogenation and dimerization kinetics on partial pressure of hydrogen while obtained activity trends suggested that both reactions involve same intermediate. Catalytic functions of HY zeolite surface in ethylene dimerization are discussed in a light of new data demonstrating cooperation between mononuclear rhodium complexes and acid hydroxyl sites of the zeolite support in C-C bond formation process. Finally, it is shown that dimerization pathway can be completely suppressed by modifying rhodium coordination environment in supported complexes with “bulky” ligands.

4.2 INTRODUCTION

Supported metal complexes received significant attention in literature due to their growing importance as potential analogues of their homogeneous counterparts known for remarkable activity and selectivity [266,167,268]. Such species are considered molecular in nature often allowing for same reactivity patterns as exhibited by their precursor complexes in solution. Recent developments in understanding of structure and catalytic properties of grafted organometallic fragments made it possible to approach one of the “Holy Grails” of heterogeneous catalysis – precise control of catalyst selectivity on a molecular/atomic level [269-271]. Such principle is widely implemented for homogeneous catalysts (i.e. hydroformylation Rh catalysts etc.) where steric and electronic effects induced by spectator ligands on active complex have profound influence on products distribution [272,177,274,275].

It was demonstrated that some anchored complexes not only retain their molecular nature but their ligands gain significant reactivity [217,22,278], therefore, it should be possible to modify coordination environment of supported species and, thus, tune catalyst selectivity in a reaction of interest. In case of heterogeneous catalyst, however, support could significantly impact the surface chemistry of grafted species (or supported particles) influencing their properties [270,216] and, in some cases, contribute to catalysis by offering active sites (i.e. Bronsted, Lewis acid sites) for the reaction of interest as well as for side reactions [280,281]. Thus, one of the major challenges when using molecular engineering to improve performance of heterogeneous catalyst is to resolve roles of support and a supported complex. To approach this problem we decided to choose of one the most studied reaction – olefins hydrogenation and relatively well understood catalytic system – HY zeolite supported rhodium dicarbonyl complexes.

Olefins hydrogenation by supported complexes is one of the most thoroughly investigated reactions and, simultaneously, one of the simplest to approach. Starting from early reports by Wilkinson demonstrating activity of $RhCl(PPh_3)_3$ in olefin hydrogenation in liquid phase [282], there have been numerous attempts to synthesize single-site hydrogenation catalysts by immobilizing Rh complexes on silica [283,284], alumina, zeolites [284], and polymer films [285].

In most latest reports Gates and coworkers demonstrated that Y zeolite supported $Rh(C_2H_4)_2$ complexes exhibit activity not only in ethylene hydrogenation but also in ethylene dimerization into butenes [286,287].The authors emphasized that selectivity for ethane hydrogenation could be boosted by converting Rh complexes into small Rh clusters prior to reaction or, alternatively, by supporting $Rh(C_2H_4)_2$ species on a surface with enhanced electron donating properties such as MgO [287]. It was proposed that the mechanism of butenes formation involves ethylene interaction with both the rhodium centre and the acidic Si-OH-Al sites. However, the role and location of Al sites and –OH groups associated with them were not clarified [286,287].

In our previous communication [288] we showed that Y zeolite-supported $Rh(CO)_2$ species are also active in ethylene hydrogenation primary due to the formation of key intermediates - $Rh(CO)(H)_x$ complexes under the reaction conditions. In this work we will further explore activity of $Rh(CO)_2$ species in both ethylene hydrogenation and ethylene dimerization reactions. Also, herein, for the first time, we will show that selectivity of ethylene hydrogenation can be tuned by modifying coordination environment of supported $Rh(CO)_2$ species exemplifying the validity of truly molecular engineering approach to heterogeneous catalysis.

4.3 EXPERIMENTAL

4.3.1 REAGENTS AND MATERIALS

Dicarbonylacetylacetonato rhodium (I) $Rh(CO)_2(acac)$ (acac = $C_5H_7O_2$) (Strem, 98% purity) was used as supplied. n-Pentane (Aldrich, 99% purity) and Tetrahydrofuran (Aldrich, >99.9 %) were refluxed under N_2 in the presence of Na/benzophenone ketyl to remove traces of moisture and deoxygenated by sparging of dry N_2 prior to use. All glassware used in preparation steps was previously dried at 120°C. He, H_2 and C_2H_4 (Airgas, all UHP grade) were additionally purified to their use by passage through oxygen/moisture traps (Agilent) capable of removing traces of O_2 and water to 15 and 25 ppb, respectively. CBV760, CBV720, and CBV600 dealuminated HY zeolites (Zeolyst International) with Si/Al atomic ratios of 30, 15, and 2.6, respectively, were calcined in flowing O_2 at 300°C for 3 h and then evacuated at 10^{-3} Torr and

300°C for 16 h. For simplicity, these zeolite supports are further denoted as HY30, HY15, and HY2.6, respectively. All treated supports were stored and handled in a glovebox (MBraun) filled with dry N_2. The residual water and O_2 concentrations in the glovebox were kept below 0.1 ppm. Potassium dicyanoaurate (Strem, 99 % purity), Chlorotrimethylsilane (Aldrich, > 99.9 % purity) were used as supplied (Strem). Ethanol anhydrous (Aldrich, > 99.5 % purity) was also used as received.

4.3.2 PREPARATION OF SUPPORTED SAMPLES

The syntheses and sample transfers were performed with exclusion of air and moisture on a double-manifold Schlenk line and in a N_2-filled MBraun glove box. Supported samples were prepared by slurrying the $Rh(CO)_2(acac)$ precursor with a corresponding powder support in n-pentane under N_2 for 24 h at room temperature, followed by overnight evacuation at 25°C to remove the solvent. In each case, the $Rh(CO)_2(acac)$ precursor was added in the amount needed to yield samples containing 1 wt% Rh. The Rh weight loading was verified by inductively coupled plasma-mass spectrometry (ICP-MS) analysis (Galbraith Laboratories Inc.).

Reaction between $[Au(CN)_2]^-$ species and HY30-supported $Rh(CO)_2$ complexes was performed in Schlenk flask with exclusion of air and moisture. Initially, the powder sample ~ 1 g ($Rh(CO)_2$ on HY30) was loaded in a glovebox in a sealed flask. Subsequently, anhydrous ethanol was added with a syringe to cover the solid material followed by dropwise addition of $K[Au(CN)_2]$ solution in ethanol while the mixture was stirring. After reaction was complete (the mixture turned color to bright reddish) ethanol was removed by decantation and the resulted slurry was washed 3 times with 50 ml of fresh ethanol to remove unreacted $K[Au(CN)_2]$ species. Finally, the solid was dried under the vacuum and transferred into a glovebox. All prepared samples were stored and handled in a glovebox filled with N_2 to prevent possible contamination and decomposition of supported species.

4.3.3 FTIR SPECTROSCOPY

A Nicolet Nexus 470 spectrometer equipped with a MCT-B detector cooled by liquid nitrogen was used to collect spectra with a resolution of 2 cm^{-1}, averaging 64 scans per spectrum. Each powder sample was pressed into a self-supported wafer with a density of approximately 20 mg/cm^2 and mounted in a home-made cell connected to a gas distribution manifold. The cell design allowed for the treatment of samples at different temperatures, while various gases flowed through the cell.

4.3.4 X-RAY ABSORPTION SPECTROSCOPY (XAS) MEASURMENTS

XAS spectra were collected at X-ray beamline 4-1 of the Stanford Synchrotron Radiation Laboratory (SSRL), Stanford Linear Accelerator Center, Menlo Park, CA. The storage ring electron energy was 3 GeV and the ring current was in the range of 345-350 mA.

XAS measurements were used to characterize the surface species formed after the reaction of HY30 zeolite-supported $Rh(CO)_2$ complexes and $[Au(CN)_2]^-$ species. Prior to these measurements, each powder sample was pressed into a wafer inside a N_2-filled glovebox. The sample mass was calculated to give an absorbance of approximately 2.5 at the Rh K and Au LIII absorption edges. After the sample had been pressed, it was loaded into an EXAFS cell [145], sealed under N_2, and removed from the glovebox. The cell was evacuated at 10^{-5} Torr and aligned in the X-ray beam. The XAS data were collected at liquid nitrogen temperature in the transmission mode with a Si(220) double crystal monochromator that was detuned by 30% to minimize effects of higher harmonics in the X-ray beam. Samples were scanned at energies near the Rh K (23220 eV) and Au LIII (11919 eV) absorption edges. All spectra were calibrated with respect to Rh foil or Au foil, the spectrum of which was collected simultaneously.

4.3.5 EXTENDED X-RAY ABSORPTION FINE STRUCTURE (EXAFS) DATA ANALYSIS

The EXAFS data were analyzed with experimentally determined reference files obtained from EXAFS data characterizing materials of known structure. The Rh–Osupport and Rh–C contributions were analyzed with phase shifts and backscattering amplitudes obtained from EXAFS data for Rh_2O_3 and $Ru_3(CO)_{12}$ (which has only terminal CO ligands), respectively. EXAFS data characterizing crystalline $K[Au(CN)_2]$ were used to obtain phase shift and backscattering amplitudes of Au–C and Au–N contributions (where N represents cyanide nytrogen). The phase shifts and backscattering amplitudes representing Rh-Rh, Au-Au shells were calculated from the structural parameters characterizing rhodium and gold foils, respectively. The transferability of the phase shifts and backscattering amplitudes for near neighbors in the periodic table has been justified experimentally [146]. The parameters used to extract these files from the EXAFS data are reported elsewhere [147]. The EXAFS data were extracted from the spectra with the XDAP software developed by XAFS Services International [148]. The EXAFS function for each sample was obtained from the X-ray absorption spectrum by a cubic spline background subtraction and normalized by dividing the absorption intensity by the height of the absorption edge. The final normalized EXAFS function for each sample was obtained from an average of six scans. The parameters characterizing both low-Z (O, C, N) and high-Z (Rh, Au) contributions were determined by multiple-shell fitting with a maximum of 16 free parameters in r space (where r is the distance from the absorbing atom, Rh or Au) and in k (wave vector) space over the ranges of $3.5 < k < 15.0$ Å-1 and $0.5 < r < 3.5$ Å with application of k^1 and k^3 weighting of the Fourier transform. The statistically justified number of free parameters (n), estimated from the Nyquist theorem [149,150], $n = (2\Delta k\Delta r/\pi) + 1$, where Δk and Δr are the k and r ranges used to fit the data, was approximately 23. The fit was optimized by use of a difference file technique [151,152], with phase- and amplitude-corrected Fourier transforms. Standard deviations for the various parameters were calculated with the XDAP software, as described elsewhere [153]. Systematic errors are not included in the calculation of the standard deviations. The values of the goodness of fit (ε_v^2) were calculated with the XDAP software as outlined in the Reports on Standards and Criteria in XAFS Spectroscopy [154]. The variances in both the imaginary and absolute parts were used to determine the fit quality [155].

4.3.6 X-RAY PHOTOELECTRON SPECTROSCOPY MEASURMENTS

XPS measurements were conducted using a Kratos AXIS Ultra DLD XPS system equipped with a monochromatic Al Ka source. The binding energy is calibrated using an Ag foil with Ag3d$_{5/2}$ set at 368.21 ± 0.025 eV for the monochromatic Al X-ray source. The monochromatic Al Ka source was operated at 15 keV and 120 W. The pass energy was fixed at 40 eV for the detailed scans. A charge neutralizer (CN) was used to compensate for the surface charge. The powder samples (approximately 5 mg) were loaded into the air-tight cell in the N2-filled glovebox. The sample was then transferred without air exposure into the UHV chamber for the XPS analysis. The C1s signal with a binding energy of 285.0 eV was used as an internal reference for calibration of the Rh 3d$_{5/2}$ and Rh 3d$_{3/2}$ binding energy values. All binding energies reported in this work were measured with a precision of ±0.1 eV. XPS data were analyzed by nonlinear curve fitting using the XPSPEAK software version 4.1. In all cases, a linear-type background was subtracted from the spectra and a curve fit was performed using the minimum number of G/L-type peaks that provides a good fit.

In each case the fitting routine was completed when the coefficient of determination (R^2) value was 0.98 or higher.

4.4 RESULTS AND DISCUSSION

4.4.1 ACTIVITY OF HY30-SUPPORTED $Rh(CO)_2$ COMPLEXES IN ETHYLENE HYDROGENATION AND DIMERIZATION

Site-isolated rhodium dicarbonyl complexes supported on HY zeolites posses of rich surface chemistry allowing for selective synthesis of $Rh(CO)(C_2H_4)$ and $Rh(CO)(H)_x$ species [288]. Formation of stable rhodium carbonyl hydride complexes which are viewed as important intermediates in olefin hydrogenation in liquid phase motivated us to investigate catalytic activity of supported analogs. Initial results presented by our group [288] indicate that regardless of the complex structure i.e. weather $Rh(CO)_2$ or $Rh(CO)(H)_x$ are used, the rate of ethane formation at the maximum activity is virtually identical suggesting that Rh hydrides could be formed in-situ during the reaction (the transient period was observed in case of $Rh(CO)_2$ species). It is remarkable that ethane is not the only product formed. Butenes were also detected in a gas phase revealing significant capacity of rhodium carbonyl complexes to promote ethylene dimerization reaction. Results of the typical experiment performed at 608 Torr of H_2 and 76 Torr of C_2H_4 at ambient conditions show rates of ethane, butene-1, cis-2-butene and trans-2-butene formation with time on stream (TOS) (Fig 4.1). These data indicate remarkable activity of the catalyst towards C-C bond formation and, moreover, the overall rate of butenes formation exceeds ethane formation rate after approximately 3 h. Although ability of HY zeolite-supported $Rh(C_2H_4)_2$ complexes to promote ethylene hydrogenation and ethylene dimerization reactions was thoroughly described in literature [286,287], the fact that $Rh(CO)_2$ species are capable of facilitating similar transformation is somewhat unexpected. More specifically, it was reported that poisoning of Rh sites with CO results in almost complete catalyst deactivation towards formation of butenes [287].

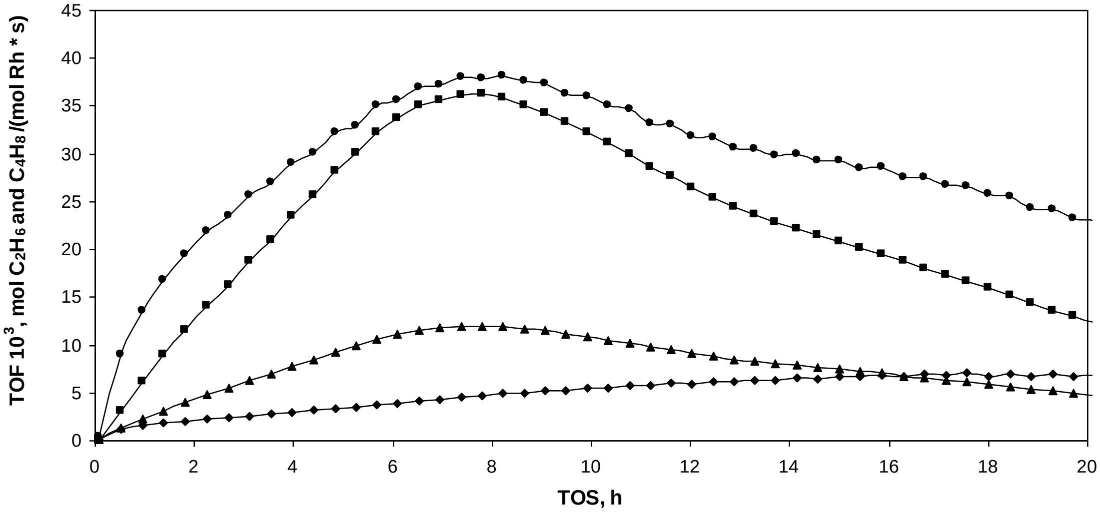

Figure 4.1 Rates (Turn Over Frequencies) of Ethane (●), Trans-2-Butene (■), Cis-2-Butene (▲), and Butene-1 (♦) formation with Time on Stream (TOS) for $Rh(CO)_2$/HY30 at 76 Torr of C_2H_4 and 608 Torr of H_2 at ambient conditions.

Mechanism of ethylene hydrogenation over $Rh(CO)_2$ species was already discussed by our group [288]. In brief, it is suggested that at the first stage one of the CO ligands in $Rh(CO)_2$ complex is substituted with ethylene yielding $Rh^I(CO)(C_2H_4)$ species. The following transformation implies oxidative addition of hydrogen and formation of formally 18-electron $Rh^{III}(CO)(C_2H_4)(H)_2$ complexes which rapidly undergo hydride ligand migration giving $Rh^{III}(CO)(C_2H_5)(H)$ structures. The subsequent reductive elimination of ethane from such surface species yields coordinatively unsaturated and highly reactive 14-electron $Rh^{I}(CO)$ complexes which immediately coordinate ethylene from a gas phase closing up the catalytic cycle. In contrast to hydrogenation, the mechanistic aspects of ethylene dimerization involving rhodium dicarbonyls are not obvious and have not been discussed. The closest analog to such species reported in literature with substantial activity in butenes formation are HY zeolite-supported $Rh(C_2H_4)_2$ complexes which are proposed to operate via bifunctional mechanism which involve Rh sites and Brønsted acid sites of the zeolite support [286]. In the following sections we will give an insight into catalytic performance of rhodium dicarbonyls in ethylene hydrogenation and dimerization reactions, attempt to clarify the role and functions of the support during the catalysis and, most importantly, suggest ways to tune selectivity of ethylene transformations.

4.4.2 COMPARISON OF HY AND Al_2O_3-SUPPORTED $Rh(CO)_2$ COMPLEXES ACTIVITY IN ETHYLENE HYDROGENATION

The importance of the support as a macroligand affecting properties and reactivity of supported complexes was widely discussed in literature [300-302,112-114]. We note that support effect is magnified when atomically dispersed metals or small metal clusters are used as active sites [112,345]. It is the understanding of this property of supported catalysts which evolved throughout the years of research and led to the development of “support as a ligand” concept [114,345].

It was shown, for instance, that temperature of CO ligand hydrogenation when using immobilized $Rh(CO)_2$ species as catalysts depends on the support and it decreases in the following order NaX < Al_2O_3 < NaY < TiO_2 which is consistent with decreasing of electron accepting properties of supports [113]. It is remarkable, that when highly dispersed Rh clusters were used, CO hydrogenation activity varied over 200-fold dependent upon the support (SiO_2, $A1_2O_3$, MgO, CeO_2 and TiO_2 were used) [112]. In another work it was demonstrated that activity of low nuclearity supported Rh clusters (2-4 atoms in size) in 1,3-butadiene hydrogenation is biased to electronic properties of the support and exceptional selectivity to 1-butene was obtained on MgO which possesses of significantly higher electron-donating properties than zeolite Y [302].

In order to investigate the effect of the support on activity of $Rh(CO)_2$ species in ethylene hydrogenation, we compared catalytic performance of Al_2O_3 and HY30 supported complexes. It is recognized that the key intermediates responsible for catalytic activity of HY zeolite-supported $Rh(CO)_2$ species in ethylene hydrogenation are $Rh(CO)(H)_x$ complexes which can be synthesized selectively on zeolite surface via sequence of C_2H_4-H_2 reactions [288]. Interestingly, similar transformations performed with Al_2O_3-supported $Rh(CO)_2$ complexes does not result in the formation of $Rh(CO)(H)_x$ species.

FTIR spectra in CO stretching region of the initial $Rh(CO)_2/Al_2O_3$ sample exhibits two bands at 2090 cm^{-1} and 2014 cm^{-1} characterizing symmetric and asymmetric vibrations of CO ligands, respectively, with an average FWHM of approximately 24 cm^{-1} Fig. 4.2, A. The infrared peaks of HY30-supported $Rh(CO)_2$ species are extremely narrow with FWHM of about 6 cm^{-1} suggesting their high structural uniformity with v(CO) bands located at 2117 cm^{-1} and 2051 cm^{-1}. We note that EXAFS measurements confirmed the presence of site-isolated $Rh(CO)_2$ species on both supports [303]. Such a significant difference in positions of v(CO) peaks is a first indication of quite different properties of Al_2O_3 and HY zeoltie as ligands and, more specifically, it reveals stronger electron-accepting properties of zeolite oxygen atoms.

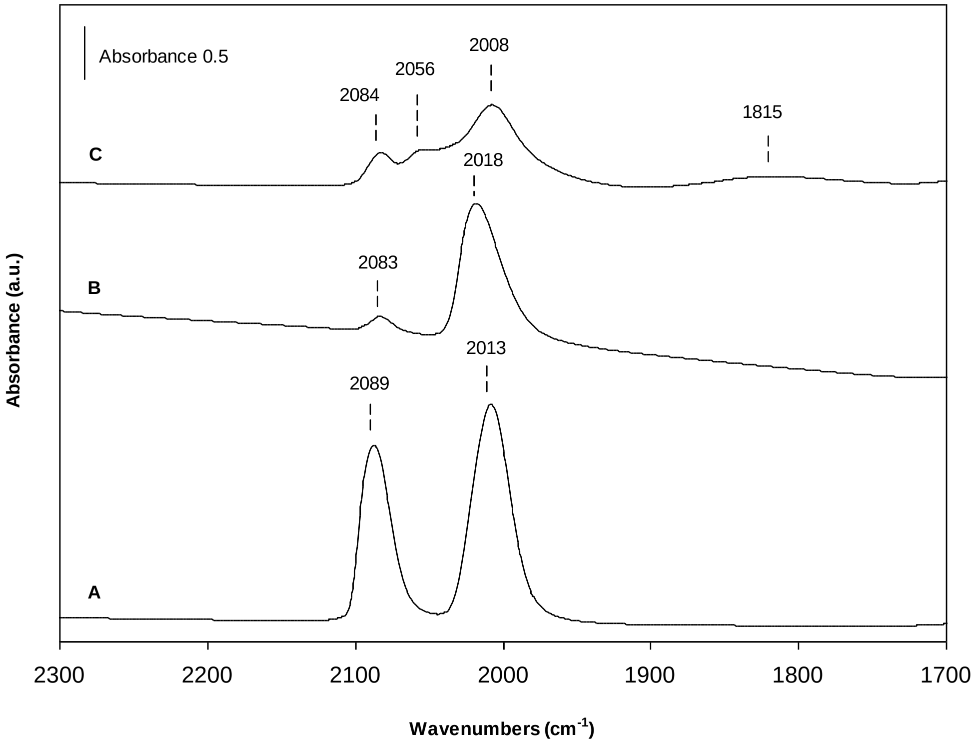

Figure 4.2 FTIR spectra in the v_{CO} region of $Rh(CO)_2/\gamma\text{-}Al_2O_3$ (A) in He (B) after exposure to C_2H_4 for 10 h (C) after exposure to H_2 for 30 min.

When $Rh(CO)_2/Al_2O_3$ sample was exposed to stream of ethylene for 10 hours (followed by helium purge), the band at 2090 cm^{-1} lost about 90 % of its initial intensity and shifted to 2083 cm^{-1} while the band at 2014 cm^{-1} broadened and slightly blueshifted to 2018 cm^{-1} Fig. 4.2,B. Simultaneously, weak features appeared at 3075, 3057, 3010, and 2978 cm^{-1} characterizing v(CH) vibrations of ethylene π bonded to Rh center. In contrast, in case if $Rh(CO)_2$/HY30 sample ethylene pulse of only 3 minutes was sufficient to remove 97 % of 2117 cm^{-1} band intensity and no shift of the $v_{as}(CO)$ peak at 2052 cm^{-1} was detected. Consistent with the presence of ethylene ligand on Rh, the bands in v(C–H) region were also identified although at slightly different positions: 3094, 3070, 3021, and 2986 cm^{-1}. These data suggest that ethylene exposure to $Rh(CO)_2$ species results in its coordination on Rh site yielding $Rh(CO)(C_2H_4)$ complexes. We note that for both supports C_2H_4/CO substitution was reversible, i.e. pulse of CO led to immediate reappearance of bands characterizing initial $Rh(CO)_2$ complexes indicating that CO affinity to Rh is very high regardless of the support.

It was discussed in our previous communication that HY30 supported $Rh(CO)(C_2H_4)$ complexes can be converted into stable $Rh(CO)(H)_x$ species in hydrogen flow [288]. More specifically, this transformation is accompanied by evolution of a strong band at 2091 cm^{-1} and weak features at 2170-2120 cm^{-1} region in FTIR spectrum characterizing v(CO) and v(Rh-H) vibrations in the rhodium carbonyl hydride complexes, respectively. In contrast, exposure of Al_2O_3-supported $Rh(CO)_2(C_2H_4)$ species to hydrogen for 60 minutes led to the appearance of bands at 2056 cm^{-1} and 1815 cm^{-1} with no peaks evolving in

2100-2200 cm^{-1} region Fig. 4.2,C. Simultaneously, weak features in v(CH) region disappeared from the spectrum and ethane was detected in a gas phase with mass-spectrometry suggesting that observed changes are associated with hydrogenation of ethylene ligands into ethane. This result clearly indicates that unlike in case of zeolite-supported sample, rhodium hydrides species are not formed. The bands at 2050-2070 cm^{-1} and 1800-1900 cm^{-1} region were previously reported in literature and are normally assigned to carbonyl groups linearly and bridged bound to metallic rhodium species, respectively [112-114]. We also note that similar bands evolved in the spectrum when Al_2O_3-supported $Rh(CO)_2$ complexes were heated in H_2 to 100 ºC (2053 cm^{-1}, 1830 cm^{-1}) . We propose that at this temperature rhodium dicarbonyls become mobile and aggregate into rhodium particles (but temperature is not high enough for carbonyls to fully react).

We exclude formation of $Rh_4(CO)_{12}$ and $Rh_6(CO)_{16}$ clusters under given conditions (after C_2H_4-H_2 sequence) for several reasons. First, FTIR signatures of these species supported on alumina have four bands with at least one band located in 2080 cm^{-1} region: 2083s, 2060ms, 2004s, and 1802w ($Rh_6(CO)_{16}/Al_2O_3$) and 2383s, 2058ms, 2032s, and 2002w cm^{-1} ($Rh_4(CO)_{12}/Al_2O_3$) [345]. Second, Rh/CO ratios in $Rh_6(CO)_{16}$ and $Rh_4(CO)_{12}$ complexes are 0.375 and 0.333, respectively, which is lower than in $Rh(CO)_2/Al_2O_3$ sample indicating that there are not enough CO molecules on the surface to form Rh4 or Rh6 carbonyl clusters. Finally, formation of small metallic rhodium aggregates (not Rh4 or Rh6 clusters) from alumina supported $Rh(CO)_2$

species was reported by Wovchko et al when they investigated transformations of these complexes in hydrogen atmosphere under the UV light [304]. Therefore, we infer that, unlike in case of HY zeolite, alumina facilitates aggregation of Rh species upon consecutive exposure of $Rh(CO)_2$ complexes to C_2H_4 and H_2. However, it can be suggested that transient formation of alumina-supported $Rh(CO)(H)_x$ species occur since ethylene hydrogenation into ethane could only proceed via intermediate formation of hydrides but the former complexes are not stabilized by the support and immediately recombine into Rh aggregates.

We propose that among key factors contributing to different surface chemistry of rhodium species on alumina and HY zeolite are metal oxidation state in supported complexes and structure of the support surface. FTIR data and XPS measurements [303] show that Rh formally more electron positive when supported on HY zeolite than on alumina. As a result, we expect less backbonding (donation of electron density from filled d orbitals of Rh to empty antibonding orbitals of CO) occurring in case of zeolite-supported $Rh(CO)_2$ species and, consequently, weaker Rh-C bond (more liable) if compared to Al_2O_3-anchored rhodium carbonyl complexes. Besides, we propose that remarkable stability of HY zeolite-supported $Rh(CO)(H)_x$ complexes could be related to Si/Al ratio in the framework. More specifically, it is known that excess negative charge around isolated Al sites of the zeolite framework is the primary reason for the coordination of $Rh(CO)_2$ fragment to such sites [63]. These sites do not exist on alumina where surface is relatively energetically homogeneous favoring Rh migration under the reducing conditions.

Such different surface chemistry of rhodium complexes on alumina and dealuminated zeolite has drastic impact on catalytic performance of these materials. Fig. 4.3 demonstrates activity of HY30 and Al_2O_3 supported samples in ethylene hydrogenation with time on stream (TOS). HY30-supported sample has an induction period of a bout 6 hours associated with C_2H_4/CO exchange with TOF reaching about 0.04 s^{-1} after that period. In contrast, Al_2O_3-supported sample exhibits virtually no activity with TOF being nearly 0.003 s^{-1} after 20 h on stream. This result confirms the key role of Y zeolite-supported $Rh(CO)_2(H)_x$ complexes in ethylene hydrogenation suggesting that these species are intermediates in this reaction.

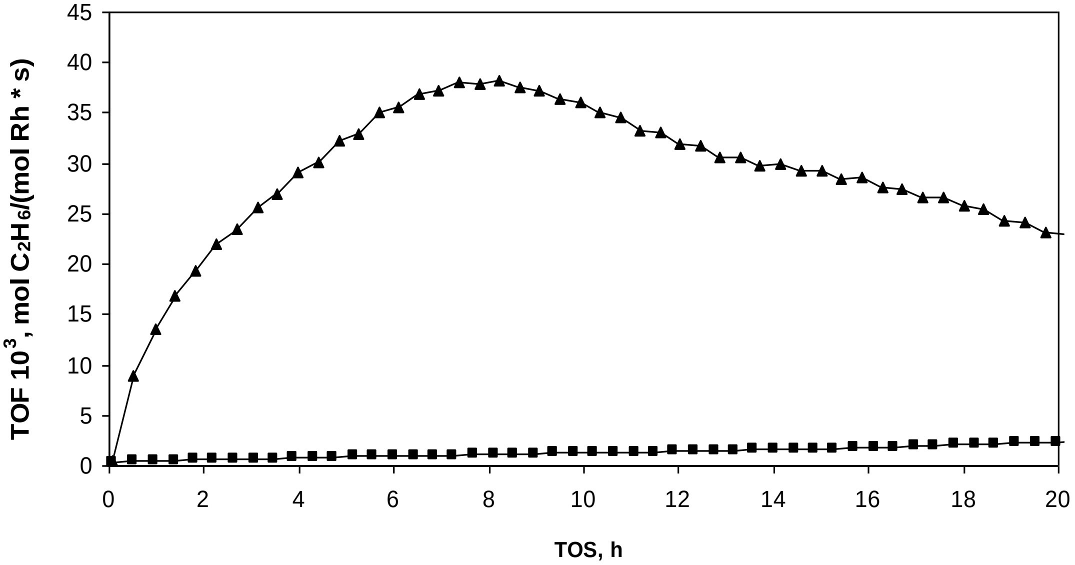

Figure 4.3 Rates (Turn Over Frequencies) of Ethane formation with Time on Stream (TOS) for $Rh(CO)_2$/HY30 (▲),$Rh(CO)_2$/γ-Al_2O_3 (■) at 76 Torr of C_2H_4 and 608 Torr of H_2 at ambient conditions.

4.4.3 KINETICS OF ETHYLENE HYDROGENATION AND DIMERIZATION BY HY30 ZEOLITE-SUPPORTED $Rh(CO)_2$ COMPLEXES

It was reported in literature that HY zeolite-supported $Rh(C_2H_4)_2$ complexes active not only in ethylene hydrogenation but also show remarkable activity in ethylene dimerization into n-butenes [286,287]. Same authors noted that poisoning of Rh sites with CO results in almost complete catalyst deactivation towards formation of butenes [287]. However, since we demonstrated that HY zeolite-supported $Rh(CO)_2$ species are active in ethylene hydrogenation (via formation of $Rh(CO)(H)_x$ complexes), it is of particular interest to understand weather same complexes could promote ethylene dimerization. In order to explore activity of HY zeolite-supported $Rh(CO)_2$ in these reactions we performed set of experiments with varying partial pressures of H_2 and C_2H_4. In the first series of experiments C_2H_4 partial pressure was kept at 76 Torr while H_2 partial pressure was varied in the 76-608 Torr range. Results presented herein Fig. 4.4 clearly demonstrate significant increase in a rate of ethane formation (TOF) with H_2 partial pressure. Linearization of these data with respect to maximum TOF yields first order dependence towards partial pressure of H_2 which is consistent with most kinetic data published on ethylene hydrogenation catalyzed by homogeneous complexes of rhodium [305,306].

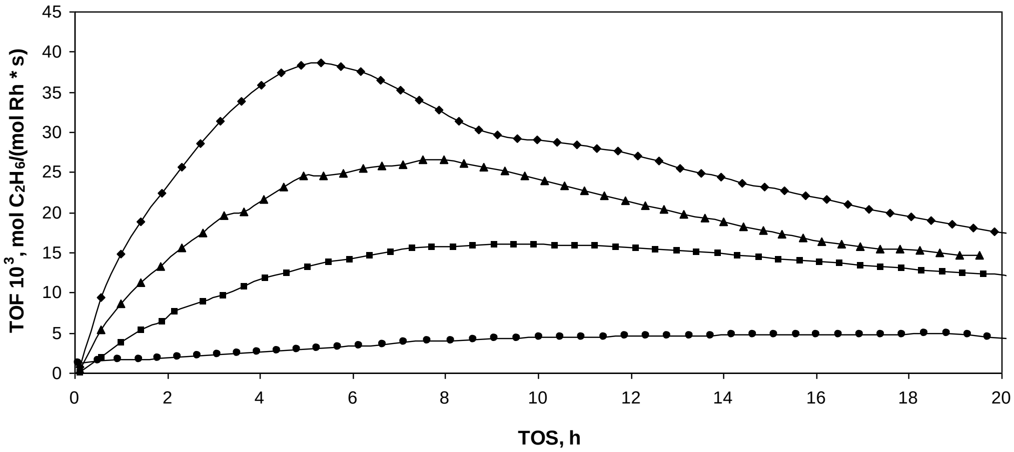

Figure 4.4 Rates (Turn Over Frequencies) of Ethane formation with Time on Stream (TOS) for Rh(CO)$_2$/HY30 at 76 Torr of C_2H_4 and different partial pressures of H_2: 76 Torr (●) 228 Torr (■) 380 Torr (▲) 608 Torr (♦).

We note that rates of butenes formation (trans-2-butene, cis-2-butene, 1-butene) were also consistently increasing with H_2 partial pressure suggesting participation of hydrogen (i.e. hydrides) in ethylene dimerization mechanism (Figs. 4.5-4.7). Reaction order of ethylene dimerization with respect to partial pressure of hydrogen was estimated to be approximately 1.2. (using TOF of total C4 formation: butene-1, cis-2-butene, and trans-2-butene). Since hydrogen is not consumed in dimerization, this is remarkable result clearly pointing out to the mechanism involving hydride transfer and not to metallocycle type mechanism for ethylene oligomerization [307]. The mechanistic aspects of ethylene dimerization will be discussed later in a text. Interestingly, except small induction period in the experiment at 76 Torr H_2 and 76 Torr C_2H_4, the rates of ethylene dimzerization were always higher than rates of ethylene hydrogenation regardless of hydrogen partial pressure. In experiments at 228, 380, 608 Torr of

H_2 the ratio between those rates reached 2 and was gradually declining to value of about 1.5 with TOS (Fig. 4.8). We also note very similar trends in formation of ethane, trans-2-butene and cis-2-butene but quite different in case of butene-1 (Figs. 4.5-4.7). This observation suggests that Rh site could be involved in isomerization of the butene-1 or, in other words that ethylene hydrogenation and n-butenes isomerization reactions are parallel. However, this conclusion is rather tentative since Bronsted acid sites of zeolite are known to promote the later transformation as well.

Finally, we note a slight decline from the equilibrium in butenes composition and, in particular, in trans-2-butene and cis-2-butene concentrations (Fig. 4.9). Cis/trans isomers ratio at 76 Torr of H_2 goes from about 1.4 to 0.43 during the experiment which is slightly higher than in case of 228, 380, 608 Torr of H_2. Since the equilibrium ratio between these isomers at 25 ºC is 0.29 [341], we infer that at H_2 - C_2H_4 partial pressures higher than stechiometric isomerization into cis- and trans- isomers is close to equilibrium. The observed deviation from equilibrium composition of isomers with TOS is most likely due to catalyst deactivation or, more specifically, it is a result of active sites blockage with long chain oligomers. It was reported in literature that transition metal cations exchanged zeolites are active enough in 1-butene isomerization to yield equilibrium composition of n-butenes [308].

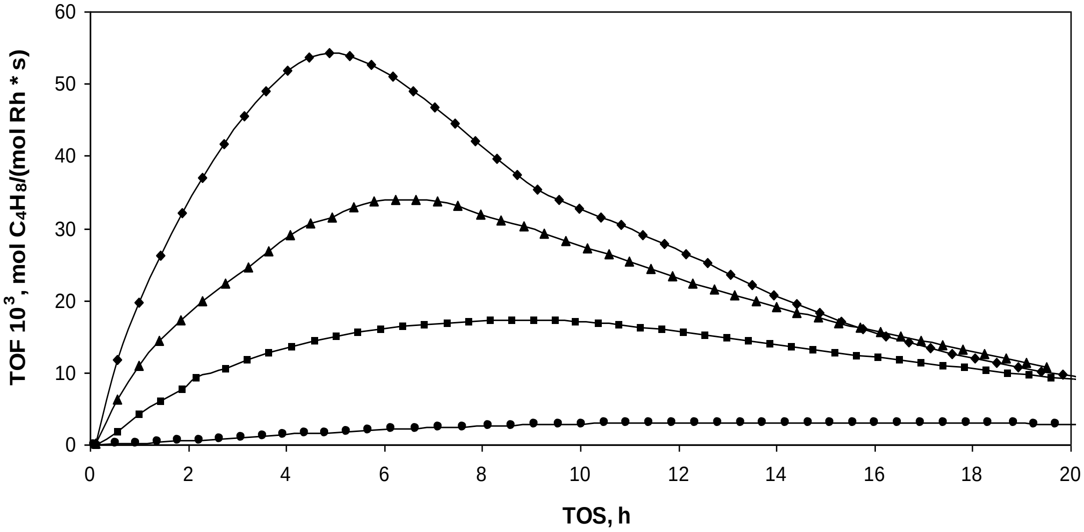

Figure 4.5 Rates (Turn Over Frequencies) of Trans-2-Butene formation with Time on Stream (TOS) for Rh(CO)$_2$/HY30 at 76 Torr of C_2H_4 and different partial pressures of H_2: 76 Torr (●) 228 Torr (■) 380 Torr (▲) 608 Torr (♦).

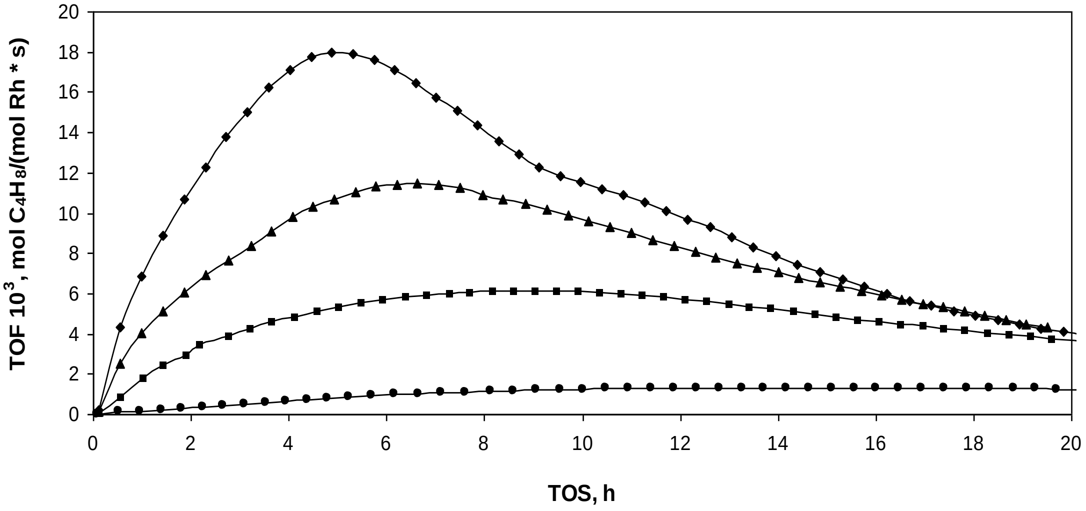

Figure 4.6 Rates (Turn Over Frequencies) of Cis-2-Butene formation with Time on Stream (TOS) for Rh(CO)$_2$/HY30 at 76 Torr of C_2H_4 and different partial pressures of H_2: 76 Torr (●) 228 Torr (■) 380 Torr (▲) 608 Torr (♦).

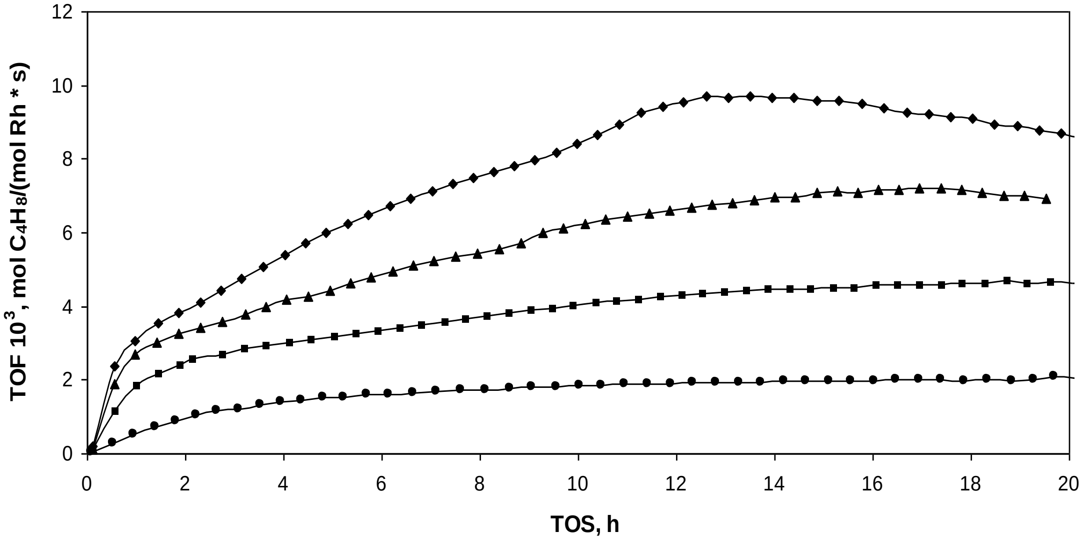

Figure 4.7 Rates (Turn Over Frequencies) of Butene-1 formation with Time on Stream (TOS) for $Rh(CO)_2$/HY30 at 76 Torr of C_2H_4 and different partial pressures of H_2: 76 Torr (●) 228 Torr (■) 380 Torr (▲) 608 Torr (♦).

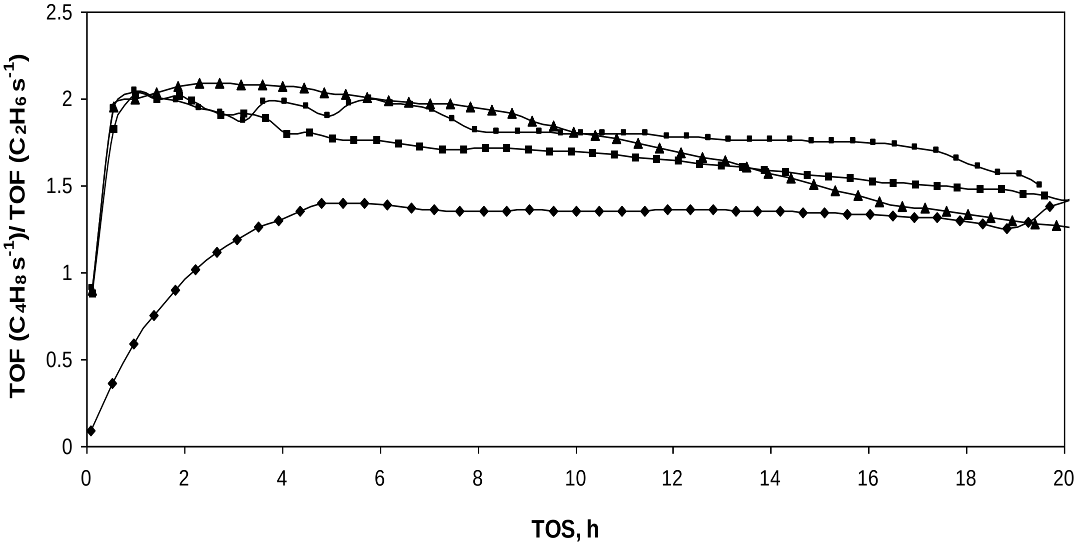

Figure 4.8 Ratio of Ethane and Butenes formation rates with Time on Stream (TOS) for $Rh(CO)_2$/HY30 at 76 Torr of C_2H_4 and different partial pressures of of H_2: 76 Torr (●) 228 Torr (■) 380 Torr (▲) 608 Torr (♦).

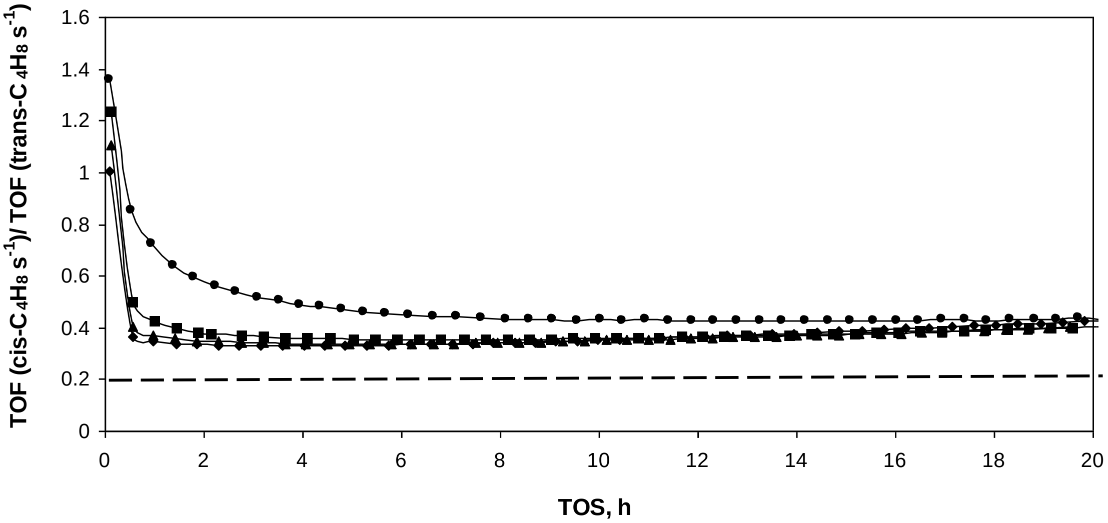

Figure 4.9 Ratio of Cis-2-Butene and Trans-2-Butene formation rates with Time on Stream (TOS) for $Rh(CO)_2$/HY30 at 76 Torr of C_2H_4 and different partial H_2: 76 Torr (●) 228 Torr (■) 380 Torr (▲) 608 Torr (♦).

In the second set of experiments H_2 partial pressure was kept at 608 Torr and C_2H_4 partial pressure was varied in 38 – 152 Torr range. Results presented in Fig. 4.10 indicate that C_2H_4 concentration influences ethylene hydrogenation but also catalyst deactivation rates. The ethane formation TOF curves have maximums which become more distinct and appear earlier in time as ethylene concentration increases. We suggest that these peaks arise due to several simultaneously occurring processes. The first one is CO/C_2H_4 substitution which explains the transient period when activity increases during the first 3-4 hours of the reaction. This statement was confirmed in a separate experiment when $Rh(CO)(H)_x$ species were formed on a surface before reaction was started and no transient period was observed. The rate of CO/C_2H_4 substitution depends on ethylene partial pressure and it is reflected in slightly shifted in time TOF peaks maxima. The second process is catalyst deactivation which is proposed to be due to formation of long chain oligomers blocking the active sites. Considering the ethane concentrations at top of these peaks, the observed reaction order with respect to ethylene partial pressure was found approximately 0.7. This value is less than 1 which is normally reported for ethylene kinetics in homogeneous catalysis [305,306] indicating that kinetics over supported catalyst is more complex.

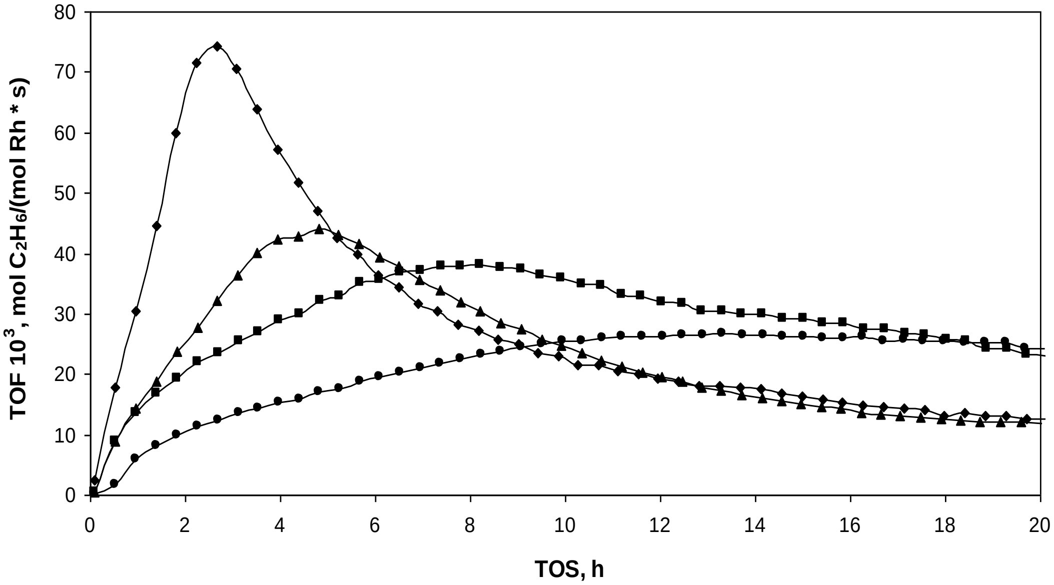

Figure 4.10 Rates (Turn Over Frequencies) of Ethane formation with Time on Stream (TOS) for $Rh(CO)_2$/HY30 at 608 Torr of H_2 and different partial pressures of C_2H_4: 38 Torr (●) 76 Torr (■) 114 Torr (▲) 152 Torr (♦).

We note that rates of ethylene dimzerization are more sensitive to ethylene partial pressure than rates of ethylene hydrogenation. The ratio between rates of formation of C4 olefins and ethane increases with ethylene partial pressure approaching the value of 3 at 152 Torr of ethylene (Fig. 4.14). The reaction order of ethylene dimerization with respect to partial pressure of ethylene was found to be approximately 1.2.

We also observed very similar activity patterns for the formation of ethane, cis-2-butene and trans-2-butene, which in this case were even more pronounced than in case of experiments with varying hydrogen partial pressures (Figs. 4.10-4.12). Butenes composition was close to equilibrium regardless of ethylene partial pressure for the first 4 hours of TOS when cis-2-butene/trans-2-butene ratio was approximately 0.33 (equilibrium is 0.29) (Fig. 4.15). After this time period, the ratio began to deviate and increase with increase of ethylene partial pressure clearly pointing out to positive influence of ethylene pressure on catalyst deactivation rates.

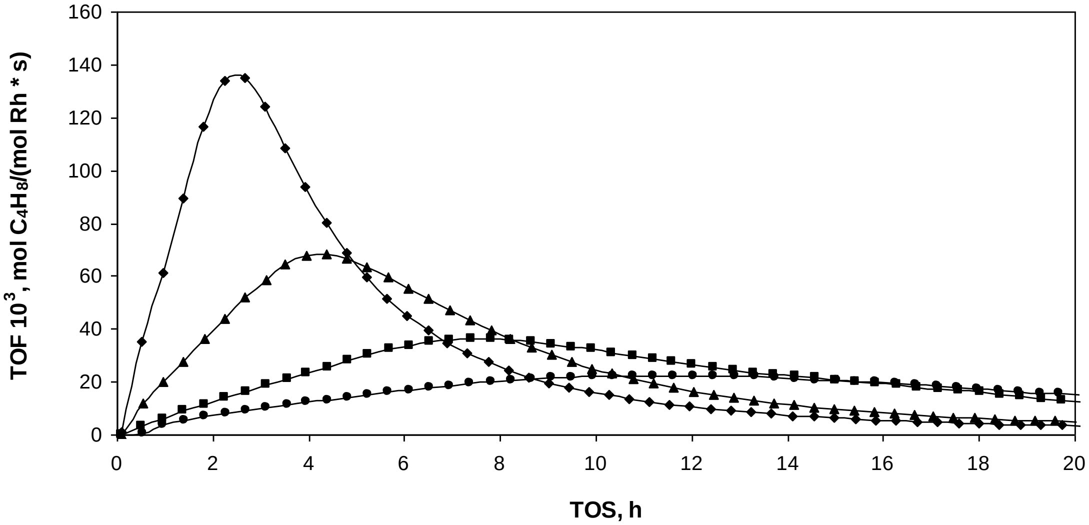

Figure 4.11 Rates (Turn Over Frequencies) of Trans-2-Butene formation with Time on Stream (TOS) for $Rh(CO)_2$/HY30 at 608 Torr of H_2 and different partial pressures of C_2H_4: 38 Torr (●) 76 Torr (■) 114 Torr (▲) 152 Torr (♦).

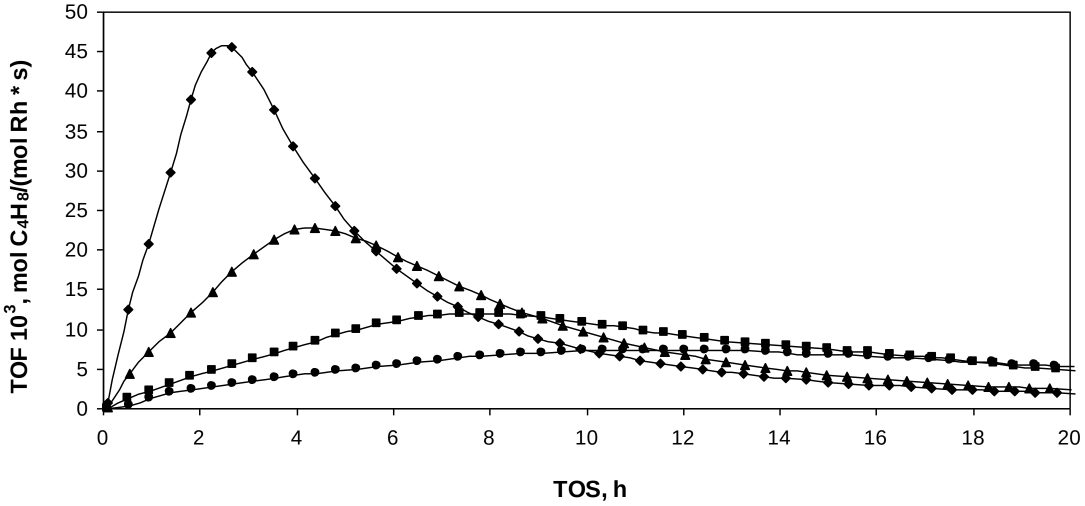

Figure 4.12 Rates (Turn Over Frequencies) of Cis-2-Butene formation with Time on Stream (TOS) for $Rh(CO)_2$/HY30 at 608 Torr of H_2 and different partial pressures of C_2H_4: 38 Torr (●) 76 Torr (■) 114 Torr (▲) 152 Torr (♦).

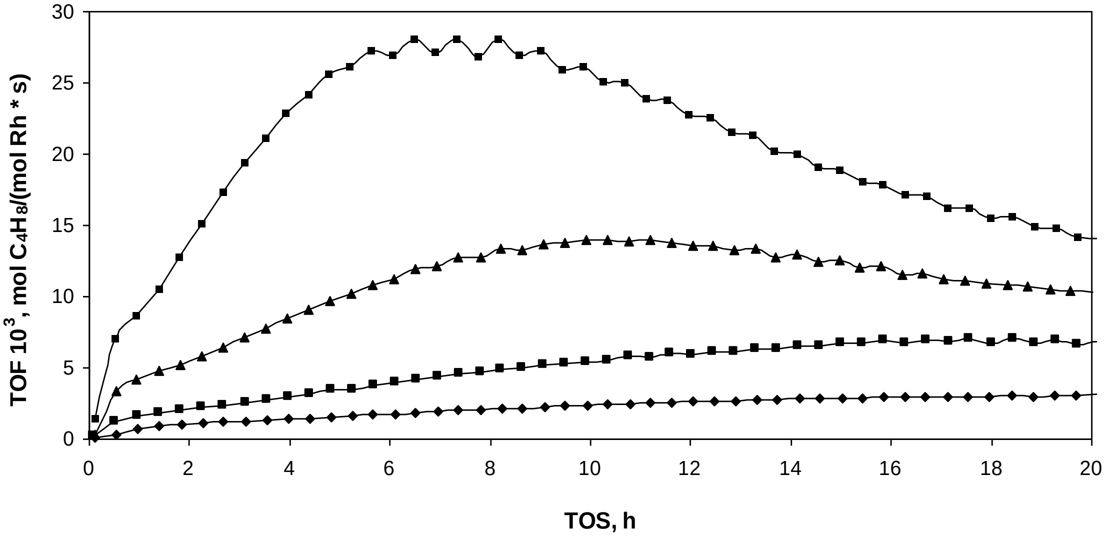

Figure 4.13 Rates (Turn Over Frequencies) of Butene-1 formation with Time on Stream (TOS) for $Rh(CO)_2$/HY30 at 608 Torr of H_2 and different partial pressures of C_2H_4: 38 Torr (●) 76 Torr (■) 114 Torr (▲) 152 Torr (♦).

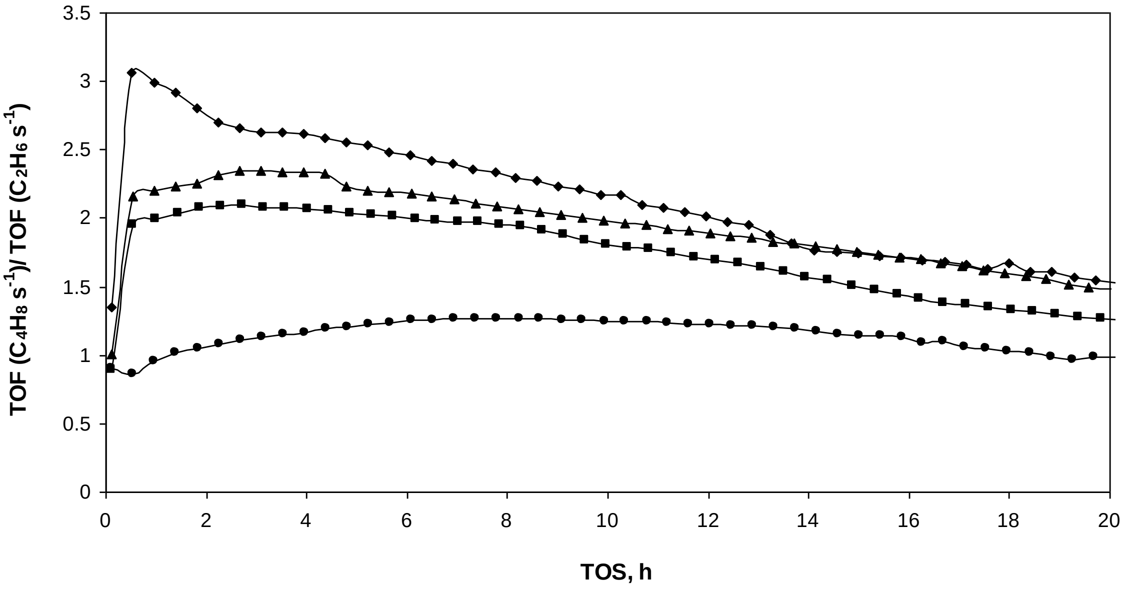

Figure 4.14 Ratio of Ethane and Butenes formation rates with Time on Stream (TOS) for $Rh(CO)_2$/HY30 at 608 Torr of H_2 and different partial pressures of C_2H_4: 38 Torr (●) 76 Torr (■) 114 Torr (▲) 152 Torr (♦).

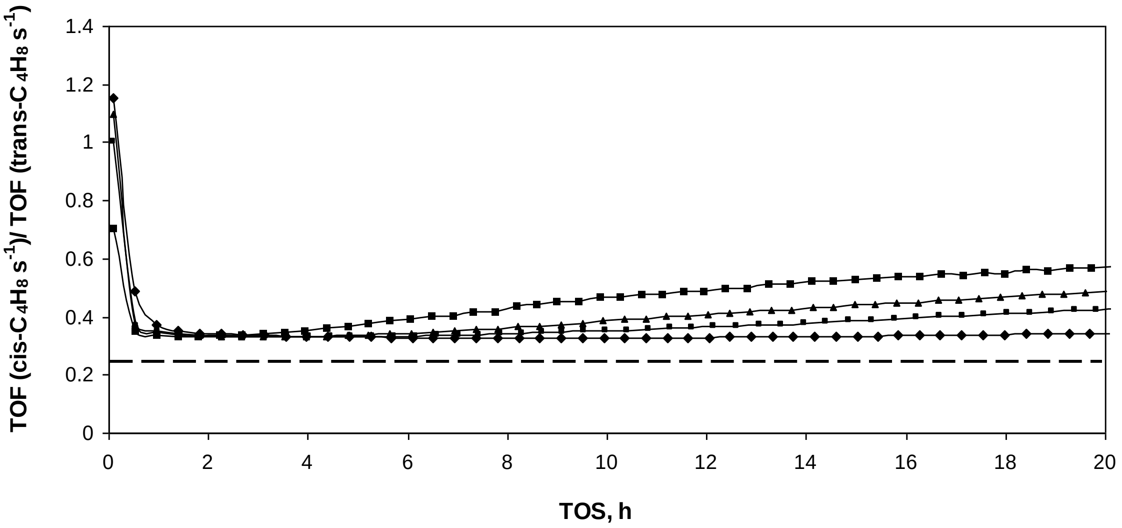

Figure 4.15 Ratio of Cis-2-Butene and Trans-2-Butene formation rates with Time on Stream (TOS) for $Rh(CO)_2$/HY30 at 608 Torr of H_2 and different partial pressures of C_2H_4: 38 Torr (●) 76 Torr (■) 114 Torr (▲) 152 Torr (♦).

4.4.4 MECHANISM OF ETHYLENE HYDROGENATION AND DIMERIZATION BY HY30 ZEOLITE-SUPPORTED $Rh(CO)_2$ COMPLEXES

Etyhlene dimerization over zeolites has been well-investigated [309-311]. The mechanism is believed to involve Bronsted or Lewis acid sites and generally considered as sequence of the following elementary steps: coordination of olefin to the active site, protonation of olefin and formation of alkylcarbenium ion, addition of second olefin (chain propagation) to alkylcarbenium ion, and deprotonation [312]. Two types of mechanisms were proposed which consider formation of either carbenium ion of alkoxy structure [312]. However, our experiments as well as literature reports suggest that at ambient conditions HY zeolites have negligible activity in this reaction [286,287,313]. Thus, observed activity should be ascribed either to rhodium complexes alone or a joint action of rhodium complexes and acidic active sites on zeolite surface. The oligomerization of olefins using metal complexes in solution also received significant attention [307,314]. The commercial process of ethylene dimerization into butene-1 currently utilizes a combination of triethylaluminum and titanium or zirconium alkoxides $Ti(OAr)_4/AlEt_3$ catalyst functioning trough the metallacyclic mechanism which does not require external source of protons [315,316]. Rhodium compounds are also known to promote this reaction with most focus of the research in this direction being on rhodium halide complexes [317]. It is suggested that bis(ethylene) complex of monovalent rhodium (i.e. $Rh_2Cl_2(C_2H_4)_2$ or $Rh(C_2H_4)_2(acac)$) is converted by reaction with HCl into an ethylrhodium(III) which further coordinates second ethylene molecule yielding a butyl fragment [317].

It was proposed by Serna et al, while investigating mechanism of ethylene dimerization over HY-supported $Rh(C_2H_4)_2$ species, that only one of ethylene ligands on Rh centre is engaged in reaction while another ligand is converted into ethyl group and present as spectator [286,287].The second ethylene that participates in a reaction is proposed to coordinate to -OH group associated with Al atom (bridging –OH groups) in the vicinity of Rh site. It is important to note that this mechanism does not imply formation of carbenium ions (i.e. protonation of either of two participating ethylenes) and hydrogen is thought to spill on a surface to replenish protons in –OH groups of Al-OH-Si moieties removed upon complex immobilization which involved in a catalytic cycle as a binding sites for second ethylene molecule (one is activated on Rh center) [287]. The role and type of these Al sites that give rise to acidic –OH groups involved in a reaction are not clear. Author suggested that Al-OH-Si moiety could be the same as one responsible for complex binding or originate from neighboring Al sites.

We note that our catalytic system is structurally very similar to one described by Serna et al with the only difference that CO ligand instead of ethyl group is present as a spectator. This inference is evidenced by very similar reaction rates found in this work and reported by Serna et al. However, such a strong dependence of dimerization kinetics on hydrogen partial pressure raises the question regarding the role of hydrogen in this process. More specifically, it is not clear weather its role is limited to interaction with surface hydroxyls (spillover) [287] or it is needed to produce rhodium ethyl species which could further be converted into ethane (hydrogenation pathway) or interact with second ethylene molecule to yield C4 chain (dimerization pathway). As we pointed out above, the closest analog to our supported catalyst are rhodium ethylene halide complexes which require proton source to operate [317]. In fact, the catalytically active species $[Rh(C_2H_4)_2(Cl)_2]^-$ are isoelectronic (i.e. also 16 electron species) to $Rh(C_2H_4)_2(acac)$ and to supported $Rh(C_2H_4)$ complexes (since zeolite surface is considered as 3 electron donor in this case) indicating electronic and structural similarity between supported and unsupported complexes. Considering significant dependence of C4 olefins formation rate on partial pressure of hydrogen and the fact that dimerization according to beta-hydrogen transfer route (with participation of hydride ligand) is known for rhodium complexes in solution [317], we could assume similar mechanism for supported complexes.

This alternative mechanism which we have to consider does not involve participation of ethylene molecule adsorbed on acid –OH group in dimerization catalysis but implies coordination of additional ethylene ligand to Rh center. In this case the complex has to retain 16 electrons configuration in order for dissociative addition of hydrogen to occur. We note that zeolite surface is regarded as 3 electron donor implying that metal interacts with one frame oxygen atom via covalent bond (contributing 1 electron to total electron count) and with –OH group via dative bond (contributing 2 electrons to total electron count). The dative bond is originating from the donation of lone electrons pair on oxygen of the –OH group to Rh and considered to be labile. According to the proposed pathway, additional ethylene molecule enters Rh coordination environment and essentially occupies coordination space which previously has been filled by the –OH group. At the next step dissociative addition of hydrogen occurs yielding $Rh^{III}(CO)(C_2H_4)_2(H)_2$ species and raising the total electron count up to 18 electrons. The following migration of hydride leads to the formation of ethyl group giving 16-electron $Rh^{III}(CO)(C_2H_5)(C_2H_4)(H)$ complex. Formation of C4 chain occurs via insertion of ethylene into Rh-C_2H_5 bond resulting in formation of $Rh^{III}(CO)(C_4H_7)(H)$ species. Since ethylene ligand is now converted vacating a coordination space on Rh and the formal electron count dropped to 14 electrons (which is nonstable electron configuration), we propose that at this stage –OH group recoordinates to metal raising the total electron count to 16 electrons. Finally, beta-elimination of hydrogen from butyl ligand yields butene-1 coordinated to Rh center in π mode which subsequently evolves in a gas phase leaving Rh^{III} $(CO)(H)_2$ complexes.

We note that this is a tentative mechanism which is alternative to one proposed by Serna et al and it does not involve surface –OH groups as active sites for dimerization catalysis. In order to clarify the reaction mechanism and, in particular, role of -OH groups we performed experiments when amount of acidic hydroxyls exposed to gas phase ethylene was varied. This can be done in two ways: either by using HY zeolites with different Si/Al ratios (which automatically implies different hydroxyls coverage) at constant Rh loading (1 wt %) or use same HY zeolite (HY30) and immobilize different amount of $Rh(CO)_2$ complexes (anchoring mechanism implies consumption of one acidic –OH group per one $Rh(CO)_2(acac)$ molecule reacted).

4.4.5 ETHYLENE HYDROGENATION AND DIMERIZATION WITH HY15 AND HY2.6 ZEOLITE-SUPPORTED $Rh(CO)_2$ COMPLEXES

Characterization of samples obtained after interaction of $Rh(CO)_2(acac)$ with zeolites having Si/Al ratio of 2.6 (HY2.6) and 15 (HY15) was already reported by our group [303]. We showed that although supported $Rh(CO)_2$ complexes are structurally identical, two types of binding sites for $Rh(CO)_2$ species are present which were suggested to be due to different Al types/Al distribution in these zeolites. Catalytic tests were performed at 608 Torr of H_2 and 76 Torr of C_2H_4 at ambient conditions and revealed striking differences in activity of these materials in ethylene hydrogenation (Fig. 4.16). HY2.6 supported sample exhibited a sharp spike in ethane and butenes formation rates with a maximum at approximately 30 minutes TOS followed by a rapid decline in activity. In case of HY15 supported sample the TOF maximum appeared at about 2.2 hours with a following moderate decline. We note that at maximum activity HY2.6 and HY15 supported rhodium species showed reaction rates 7.2 and 3.2 times higher than HY30 supported, respectively.

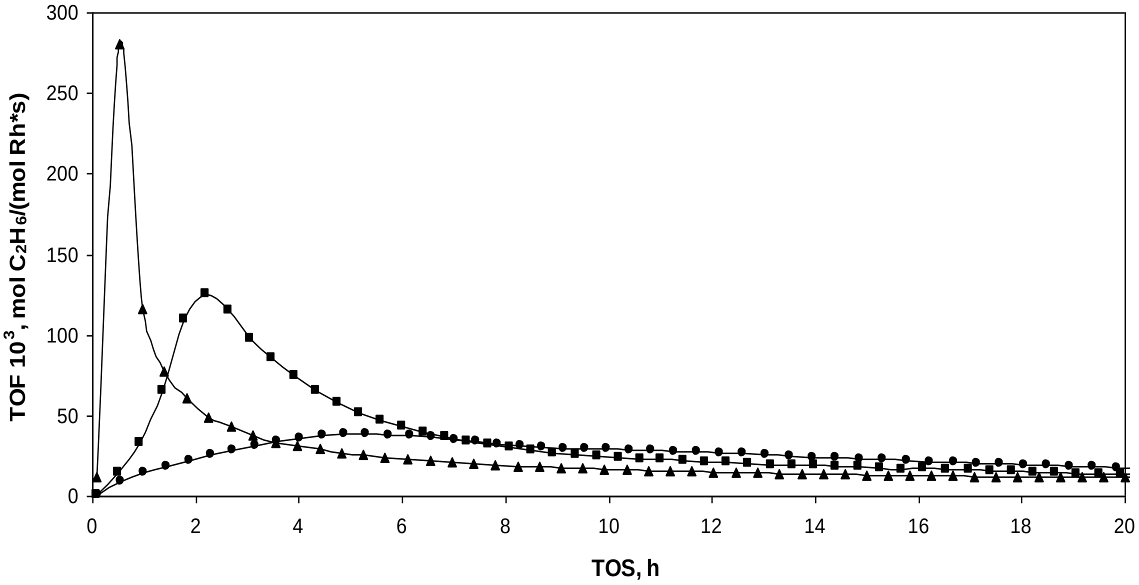

Figure 4.16 Rates (Turn Over Frequencies) of Ethane formation with Time on Stream (TOS) for $Rh(CO)_2$/HY30 (●), $Rh(CO)_2$/HY15 (■), $Rh(CO)_2$/HY2.6 (▲) at 608 Torr of H_2 and 76 Torr of C_2H_4.

It is remarkable that catalysts activity towards formation of Butenes follow the same trends as formation of ethane suggesting that both reactions probably involve same active site and both are affected by same factors (Fig. 4.17). Consistent with our previous observations, butenes composition close to equilibrium achieved only at early stages of the reaction, namely, before maximum activity is reached and deactivation started to prevail (Fig. 4.18). FTIR spectra in v(CH) region collected on used samples show substantial difference in amount of accumulated hydrocarbons (Fig. 4.19). More specifically, the integrated intensities of v(CH) bands in case of HY2.6-based samples is significantly higher than on HY15, HY30-supported materials suggesting that Al rich zeolite promotes formation of oligomers which is consistent with observed deactivation patterns.

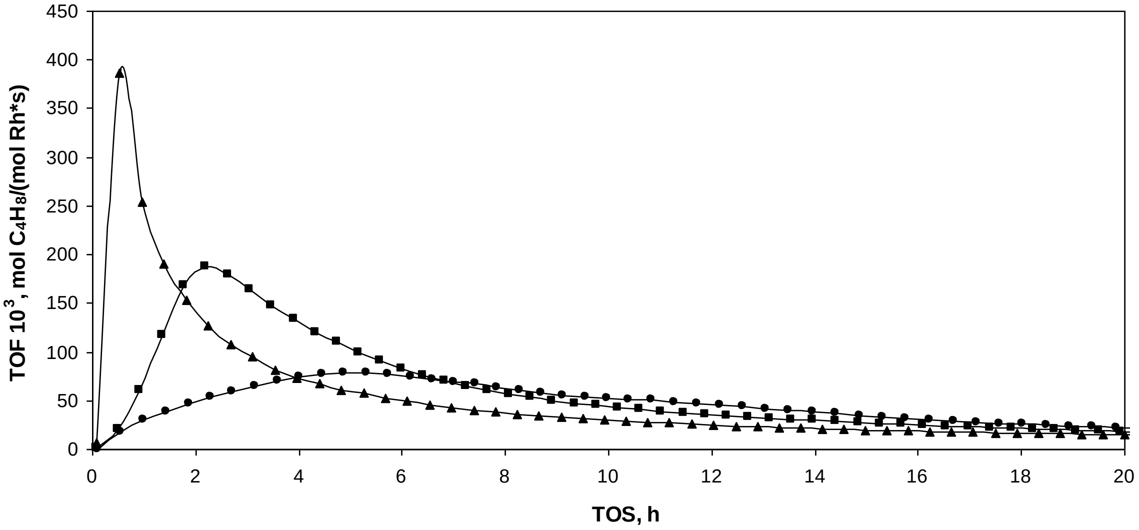

Figure 4.17 Rates (Turn Over Frequencies) of Butenes (Trans-2-butene, Cis-2-butene. Butene-1) formation with Time on Stream (TOS) for Rh(CO)$_2$/HY30 (●), Rh(CO)$_2$/HY15 (■), Rh(CO)$_2$/HY2.6 (▲) at 608 Torr of H_2 and 76 Torr of C_2H_4.

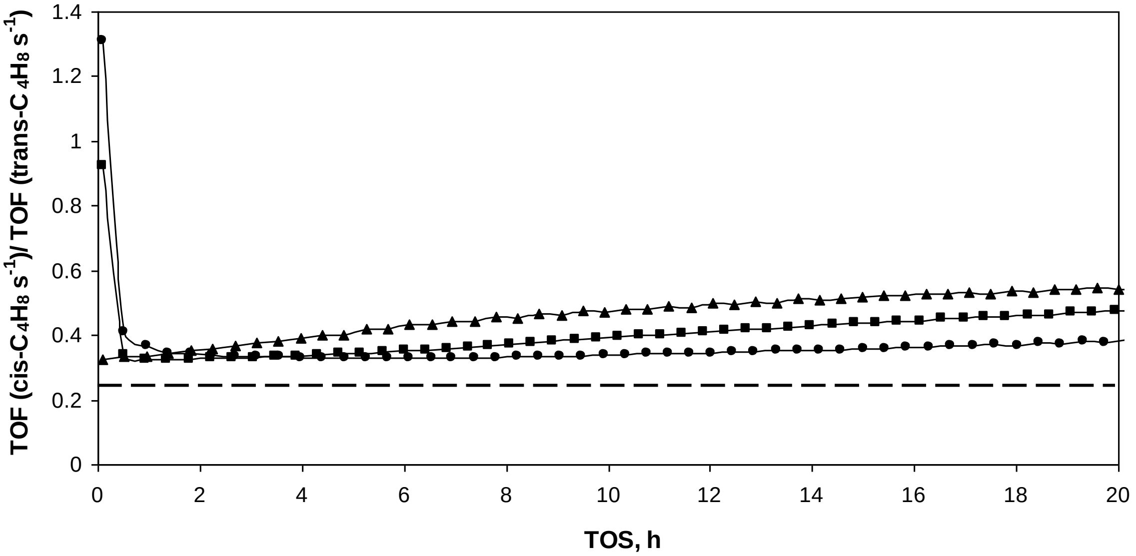

Figure 4.18 Ratio of Cis-2-Butene and Trans-2-Butene formation rates with Time on Stream (TOS) for Rh(CO)$_2$/HY30 (●), Rh(CO)$_2$/HY15 (■), Rh(CO)$_2$/HY2.6 (▲) at 608 Torr of H_2 and 76 Torr of C_2H_4.

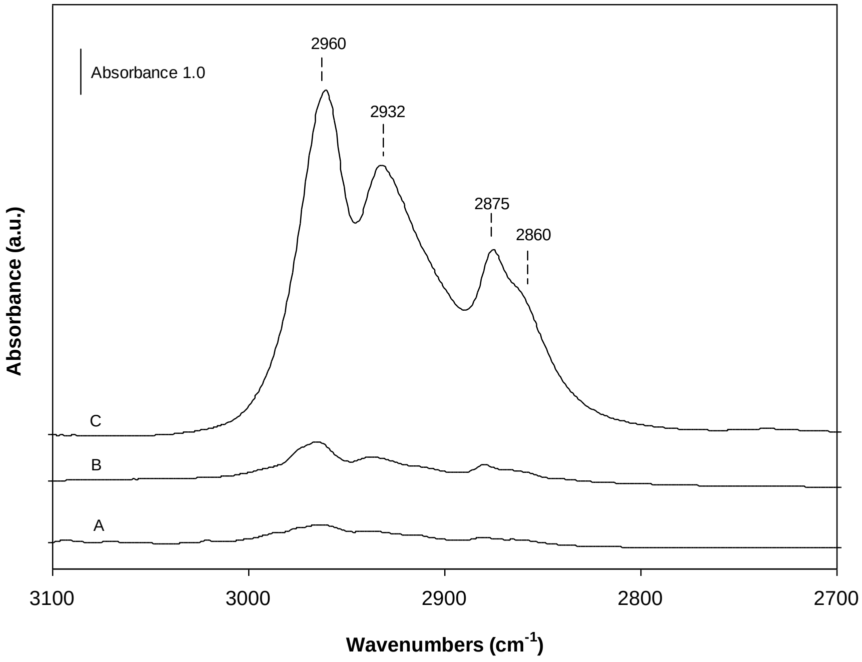

Figure 4.19 FTIR spectra in the v_{CH} region of $Rh(CO)_2$/HY30 (A), $Rh(CO)_2$/HY15, and $Rh(CO)_2$/HY2.6 (C) after reaction: 608 Torr of H_2 and 76 Torr of C_2H_4 for 20 h.

Such a significant difference in activities of HY zeolite-supported $Rh(CO)_2$ complexes exhibited in the initial period of the reaction is of particular interest. Since experimental conditions and metal loading were kept the same in these experiments, the observed difference in activity should be associated with different amount of –OH groups. The alternative explanation of this effect could be a change of active site structure (i.e. rhodium clustering).

In order to investigate weather rhodium aggregation is responsible for a boost in HY2.6 and HY15 based catalysts activity we performed XPS characterization of samples before and after reaction. XPS results for fresh $Rh(CO)_2$ complexes supported on HY30, HY15, and HY2.6 indicated Rh 3d binding energy of 308.8 eV, 308.8 eV, and 308.5 eV (Table 4.1), respectively, corresponding to rhodium in +1 oxidation state which is consistent with most literature reports [218,224,225]. XPS data on samples after reaction showed no evidence of Rh species with binding energy below 308.3 eV suggesting that rhodium clustering is unlikely. Although we admit that formation of cationic Rh6 and/or Rh4 clusters could be a possibility (especially in case of Al reach supports such HY2.6), literature data suggest that the drop in the Rh 3d binding energy a of approximately 0.7 eV should be expected for $Rh(CO)_2$ to Rh4/Rh6 transformation [322]. Besides, exposure of a used samples to a pulse of CO results in immediate reappearance of v(CO) bands with same integrated intensity as initial $Rh(CO)_2$ complexes regardless of a support indicating that structurally Rh sites remained unaltered. Although we do recognize that oxidative disruption of small Rh clusters with CO could occur, experiments with CO adsorption on Y zeolite-supported Rh clusters characterized by N_{Rh-Rh} = 4.6 revealed no evidence of this process taking place to a measurable extend [288]. (also consistent with literature data)

Table 4.1 XPS data characterizing $Rh(CO)_2$ species supported on HY30, HY15, and HY2.6 zeolties after reaction in 608 Torr H_2, 76 Torr C_2H_4 for 20 h.

Sample	Rh $3d_{5/2}$, eV	FWHM, eV	Rh $3d_{3/2}$, eV	FWHM, eV
$Rh(CO)_2$/HY30	308.4	2.1	313.1	2.1
$Rh(CO)_2$/HY15	308.5	1.8	313.2	1.8
$Rh(CO)_2$/HY2.6	308.7	2.2	313.4	2.2

Thus, increased activity of HY15 and HY2.6 based materials should be attributed to the influence of the support. We note the striking similarities between plots showing rates of ethane formation (as well as trans- and cis-2-butene) in experiments with HY30 supported rhodium complexes performed at 607 Torr of H_2 and different C_2H_4 partial pressures (38 -152 Torr) and experiments carried out at 607 Torr of H_2/76 C_2H_4 with HY15 and HY2.6 supported samples. One of the possible explanations for these data could be a purely kinetic factor of surface concentration of ethylene. Interaction of ethylene with Bronsted acid sites of zeolites is well-known and often reported as first step in ethylene dimerization mechanism over zeolties [312,323]. Thus, one can assume that concentration of ethylene on the surface could be varied by either changing partial pressure of ethylene in a gas phase or by changing number of surface binding sites – hydroxyl groups. If ethylene coverage at giving experimental conditions is not full (and we assume that at low partial pressure of ethylene this holds true) than the reaction rate (dimerization) should be defined by proximity of acid sites to Rh centers (-OH groups density) and partial pressure of ethylene in a gas phase. In case of HY30 zeolite, there is only about 1 Al atom and, thus, only 1 –OH group per supercage [254]. The Rh loading of 1 wt% allows only for 1 Rh per 8 supercages making the probability of close location of Rh to a –OH group in case of HY30 small. In case of HY15 and HY2.6 materials, there are approximately 2 and 6 Al atoms per supercage [254], respectively, making the likehood of close proximity of Rh and Brønsted acid site higher.

Finally, we have to acknowledge the possible effect of extraframework Al species (EFAL). It is proposed that up to 50 % of Al atoms in HY2.6 zeolite are nonframework and exist as EFAL species [254] which could serve as binding sites for supported $Rh(CO)_2$ complexes [303]. Although the exact role of EFAL species in catalytic performance of supported Rh complexes in hydrogenation and/or dimerization reaction is not clear, it is reported that Y zeolites with high EFAL content greatly enhance hydrogen transfer reactions (H/D exchange etc) at elevated temperatures [254,325,326]. One of the proposed explanations attributes this effect to so called “superacidity” of bridging Al-OH-Si hydroxyls due to close proximity of these sites to the the extraframework AlOH species (Lewis acid sites) [327]. However, since all our experiments were conducted at ambient conditions, we consider such effects negligible.

One of the ways to understand weather Brønsted –OH groups are responsible for enhanced activity of HY2.6 supported sample is to make them inaccessible for ethylene molecules, i.e. to block them with another more strongly binding adsorbate. This can be done by using water as it was reported that water and ethylene compete for Brønsted acid sites and physisorbed water prevents the adsorption of the olefin [328]. The ultimate condition that has to be met in this case is that water must not interact with Rh sites and we showed previously that, unless water is present in a gas phase, it does not coordinate to Rh species [303]. In order to prepare samples with different water content, the HY2.6 zeolite was subject to pretreatments at deferent calcination temperatures before $Rh(CO)_2$ complexes were immobilized on its surface (100, 200, 300 and 400 °C).

FTIR spectrum characterizing sample treated at 100 °C revealed the presence substantial amounts of water as evidenced by infrared bands at approximately 3500 and 1630 cm^{-1} assigned to stretching and bending vibrations, respectively, of H_2O molecules hydrogen-bonded to zeolite –OH groups (Figs. 4.20,4.21). The sample treated at 200 °C showed significant decline in intensity of bands characterizing H_2O while new features emerged at 3630 and 3565 cm^{-1} designating acidic hydroxyls. Finally, samples after thermal treatments in the 300-400 °C temperature range revealed no evidence of surface-bound H_2O.

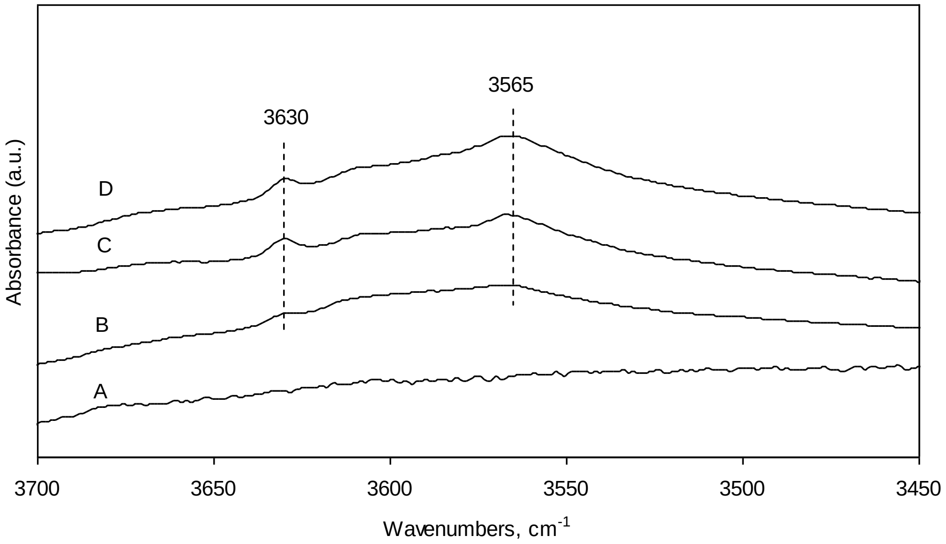

Figure 4.20 FTIR spectra in the v_{OH} region of $Rh(CO)_2$/HY2.6 sample obtained by reaction of $Rh(CO)_2$(acac) with HY2.6 zeolite calcined at 100 °C (A), 200 °C (B), 300 °C (C), and 400 °C (D).

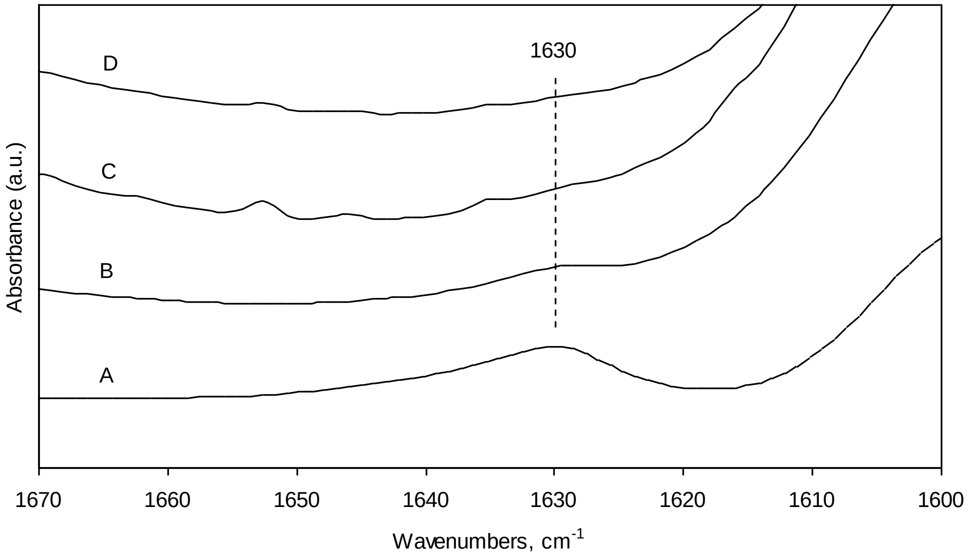

Figure 4.21 FTIR spectra in the δ_{H_2O} region of $Rh(CO)_2$/HY2.6 sample obtained by reaction of $Rh(CO)_2$(acac) with HY2.6 zeolite calcined at 100 °C (A), 200 °C (B), 300 °C (C), and 400 °C (D).

Catalytic performance of those materials measured at 607 Torr of H_2/76 C_2H_4 is presented in Figs. 4.22-4.25. These data indicate that there is about 30 % drop in ethane formation rate at maximum activity for sample treated at 100 °C if compared to samples calcined 200 °C, 300 °C, and 400 °C and deactivation patterns for all four samples are very similar. There is also relatively small decrease in activity towards trans-2-butene and cis-2-butene formation (Figs. 4.23,4.24) and virtually no change in TOF of butene-1 formation for H_2O rich sample (100 °C calcined) (Fig. 4.25). These results are certainly not conclusive but suggest that blocking of Brønsted acid sites with water does influence the catalyst activity in both ethylene hydrogenation and dimerization reactions although the effect is relatively small.

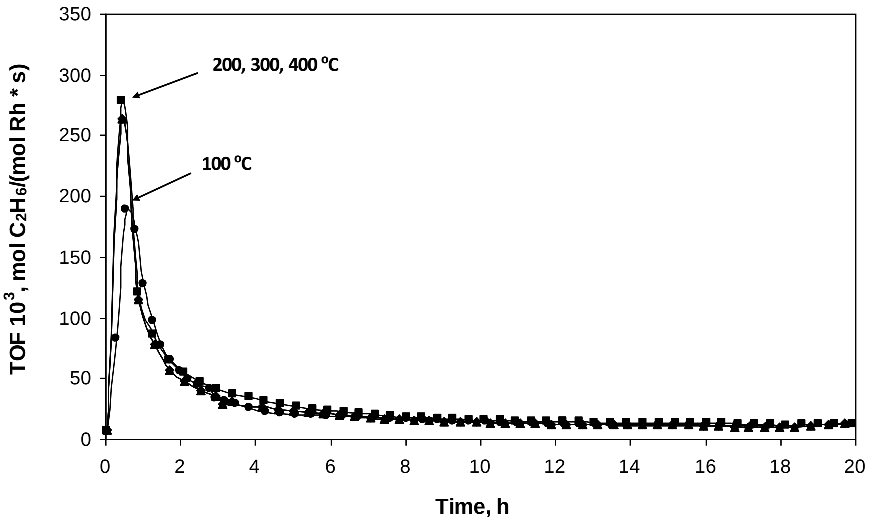

Figure 4.22 Rates (Turn Over Frequencies) of Ethane formation with Time on Stream (TOS) for Rh(CO)$_2$/HY2.6 sample obtained by reaction of Rh(CO)$_2$(acac) with HY2.6 zeolite calcined at 100 °C (●), 200 °C (■), 300 °C (▲), and 400 °C (♦).

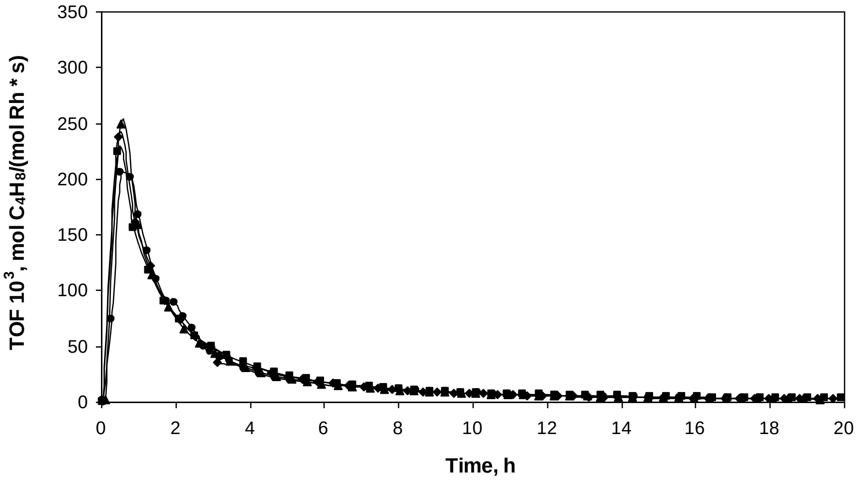

Figure 4.23 Rates (Turn Over Frequencies) of Trans-2-butene formation with Time on Stream (TOS) for Rh(CO)$_2$/HY2.6 sample obtained by reaction of Rh(CO)$_2$(acac) with HY2.6 zeolite calcined at 100 °C (●), 200 °C (■), 300 °C (▲), and 400 °C (♦).

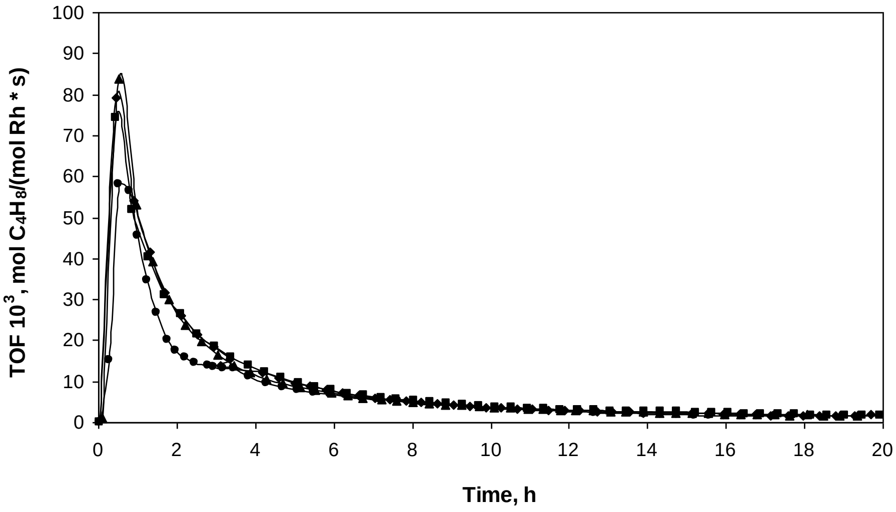

Figure 4.24 Rates (Turn Over Frequencies) of Cis-2-butene formation with Time on Stream (TOS) for $Rh(CO)_2$/HY2.6 sample obtained by reaction of $Rh(CO)_2$(acac) with HY2.6 zeolite calcined at 100 °C (●), 200 °C (■), 300 °C (▲), and 400 °C (♦).

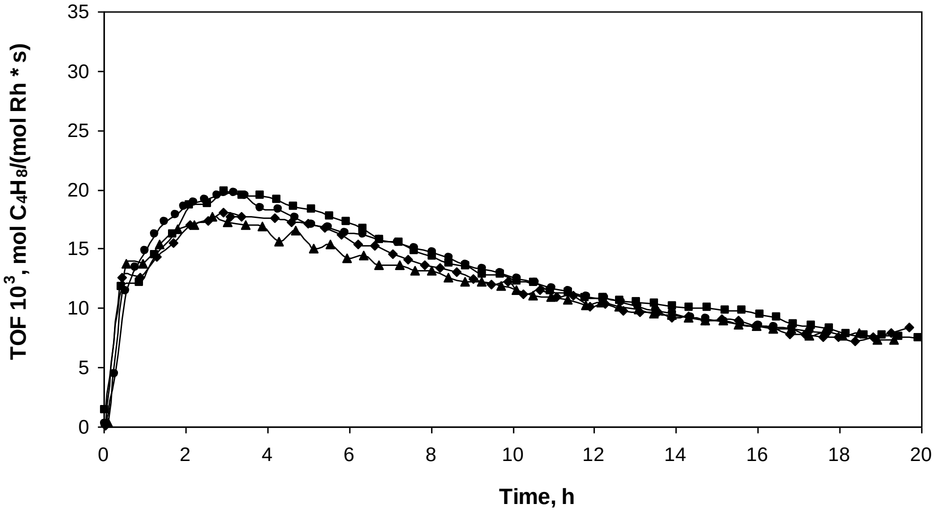

Figure 4.25 Rates (Turn Over Frequencies) of Butene-1 formation with Time on Stream (TOS) for $Rh(CO)_2$/HY2.6 sample obtained by reaction of $Rh(CO)_2$(acac) with HY2.6 zeolite calcined at 100 °C (●), 200 °C (■), 300 °C (▲), and 400 °C (♦).

4.4.6 ETHYLENE HYDROGENATION AND DIMERIZATION WITH HY30 ZEOLITE-SUPPORTED $Rh(CO)_2$ COMPLEXES WITH DIFFERENT Rh LOADINGS

The alternative way to vary amount of acidic hydroxyls which could serve as binding sites for ethylene molecules and participate in dimerization catalysis is to immobilize different amount of $Rh(CO)_2(acac)$ complexes. We note that protonation of “acac” ligand by the bridging –OH group is a primary pathway for complex immobilization implying that each zeolite has a certain chemisorption capacity. In order to reveal the maximum Rh uptake when complexes are still covalently bound to the surface, IR measurements of samples prepared by interaction of HY zeolite with different amount of $Rh(CO)_2(acac)$ were conducted. We used zeolite with the lowest Al content in a framework (HY30) where limiting chemisorption capacity is expected at reasonably low Rh loadings.

FTIR spectra in v(CO) region for samples with 1, 2, 3 and 4 % wt of Rh are presented in Fig. 4.26. For samples with 1 and 2 % wt of Rh only bands at 2117 and 2053 cm^{-1} are observed suggesting the presence of anchored $Rh(CO)_2$ species. As Rh loading was increased to 3 and then to 4 % wt, two new band pairs appeared in spectra. More specifically, for the sample with 3 % wt of Rh the bands at 2107, 2039 cm^{-1} and 2093, 2025 cm^{-1} were detected indicating partially reacted and unreacted $Rh(CO)_2(acac)$ complexes. Similar features were observed for the sample with 4 % wt loading (2105, 2038 cm^{-1} and 2090, 2024 cm^{-1}), in this case however intensities of bands at 2090 and 2024 cm^{-1} characterizing physisorbed $Rh(CO)_2(acac)$ complexes are increased. These results suggest that the maximum capacity of HY30 zeolite towards chemisorption of precursor complexes is somewhere between 2 and 3 % wt and, therefore, the following catalytic testing was performed for the sample with 2 % wt Rh loading. Catalyst activity in both ethylene hydrogenation and ethylene dimerization was evaluated at 76 Torr of C_2H_4 and 608 Torr of H_2 at ambient conditions. Fig. 4.27 compares activities of HY30 supported $Rh(CO)_2$ species at 1 % and 2 % wt Rh loadings and indicates that the rate of ethane formation experienced about 50 % drop as Rh loading increased from 1 to 2 % wt. Similar picture was observed for the rate of butenes formation (butene-1, trans-2-butene and cis-2-butene) (Fig. 4.28) suggesting that both processes are essentially coupled and confirming our inference that they most likely proceed through the same intermediate. We note that the observed behavior is consistent with activities detected for $Rh(CO)_2$ complexes supported on HY zeolites with different Si/Al ratios but, in fact, demonstrates the reverse trend - decrease in the rate of dimerization with decrease of acidic hydroxyls coverage. Such a strong dependence of the dimerization rate on the amount of surface –OH groups points out to the key role of these sites in dimerization catalysis.

In summary, we can conclude that ethylene dimerization involves both Rh complexes and –OH groups of the zeolite as active sites. This mechanism is broadly consistent with the reaction pathway proposed in literature, however, unlike literature reports our data suggest participation of rhodium hydride species in dimerization reaction. Moreover, both ethylene hydrogenation and dimerization seem to be coupled and involve same intermediate.

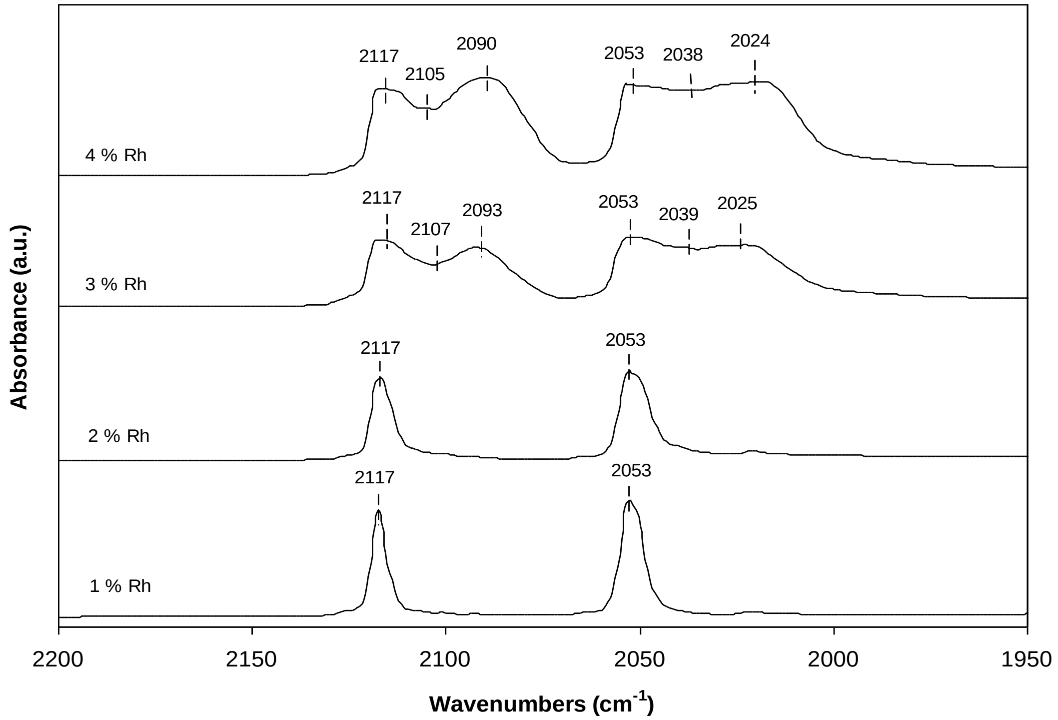

Figure 4.26 FTIR spectra in the v_{CO} region of $Rh(CO)_2$/HY30 at different Rh loading: 1, 2, 3, and 4 %wt.

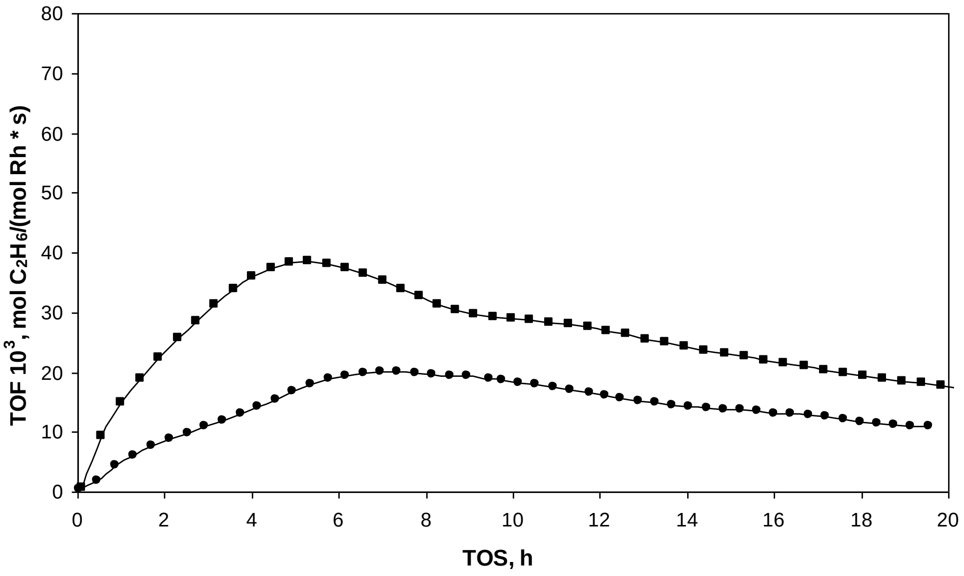

Figure 4.27 Rates (Turn Over Frequencies) of Ethane formation with Time on Stream (TOS) for $Rh(CO)_2$/HY30 with 1 % wt Rh (●), 2 % wt Rh (■) at 608 Torr of H_2 and 76 Torr of C_2H_4.

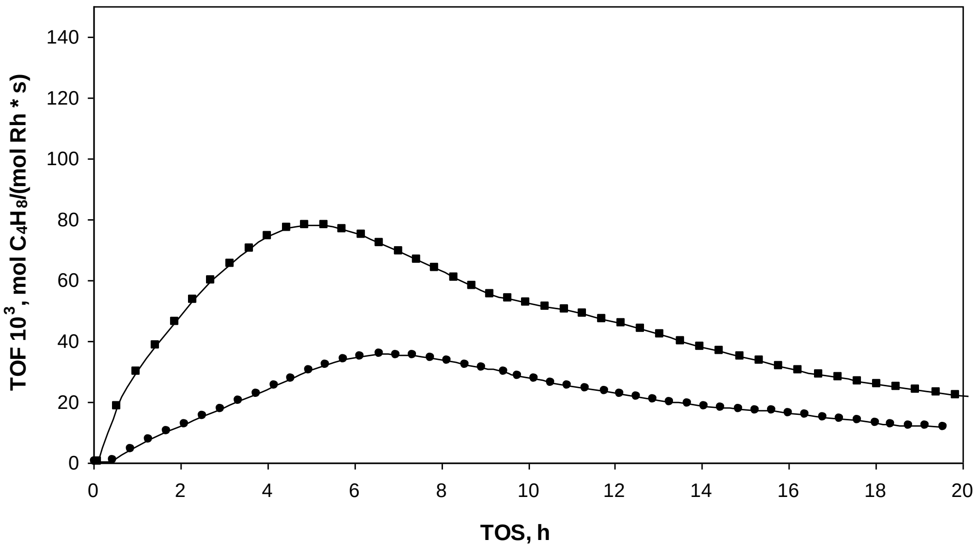

Figure 4.28 Rates (Turn Over Frequencies) of Butenes (Trans-2-butene, Cis-2-butene, Butene-1) formation with Time on Stream (TOS) for $Rh(CO)_2$/HY30 with 1 % wt Rh (●), 2 % wt Rh (■) at 608 Torr of H_2 and 76 Torr of C_2H_4.

4.4.7 TUNING SELECTIVITY OF ETHYELENE HYDROGENATION/DIMERIZATION USING HY30 ZEOLITE-SUPPORTED $Rh(CO)_2$ COMPLEXES

Tuning the selectivity of chemical reaction promoted by homogeneous catalyst is normally achieved by modifying electronic and/or steric properties of a metal complex [272,177,274,275]. This implies detailed understanding of a reaction mechanism and reactivity of modified catalyst. The mechanism of ethylene dimerization discussed above suggests cooperative action of Rh complex and neighboring –OH group implying that both sites have to be located in close proximity to each other.

One of the approaches which could be used to “shut down” the dimerization is to create a sterical hindrance which would prevent interaction of ethylene adsorbed on –OH group with the Rh center. This can be done by introducing new ligands in supported rhodium complexes, preferably, bulk. Such ligand has to be chemically inert and have a chemical bond with Rh strong enough so not to dissociate (detach) during the reaction. However, complex has to retain reactivity and remain active towards hydrogen activation. One of the good candidates on this role is the dicyanoaurate anion, $[Au(CN)_2]^-$ which has been extensively used in synthesis of cyano-bridged heterometallic coordination polymers [329-332]. In synthesis of such materials $[Au(CN)_2]^-$ building block acts as a bridging ligand between transition metal cations and allows for the construction of bimetallic materials with no direct metal-metal interaction [329]. Those materials are stable due to remarkable properties of nitrogen atom of –CN group which acts as strong Lewis base allowing for relatively strong M-N= bonds. Since HY zeoltie supported $Rh(CO)_2$ complexes were shown to react with weak Lewis bases such as H_2O and NH_3, [303] it is reasonable to assume that it should react with stronger bases such as $[Au(CN)_2]^-$. Finally, it is remarkable that CN group has very distinct signature in FTIR spectrum which is very sensitive to its chemical environment allowing for easy discrimination between different structures involving this functional group [330,334].

It is important to note that no reaction occurred between the precursor complex $Rh(CO)_2(acac)$ and $[Au(CN)_2]^-$ ions in a liquid phase (evidenced by FTIR) suggesting that “acac” ligand has to be displaced from Rh in order to enable coordination of $[Au(CN)_2]^-$ groups. In contrast, when same reaction was performed with HY30 supported $Rh(CO)_2$ complexes (Rh/Au = 1/1 mol), the support immediately turned color from pale white to bright reddish. FTIR spectrum of a sample after reaction revealed that v(CO) bands became broader (FWHM = 15) and redshifted to 2102 cm^{-1} and 2043 cm^{-1} (relatively to v(CO) bands in a sample before the reaction) (Fig. 4.29). Besides, the new strong feature appeared at 2193 cm^{-1} designating v(CN) vibration of CN groups in -Au-CN-Rh- fragments. We note that this band is clear indication of bridging CN groups and it is normally used in literature as a major evidence of a formation of cyano-bridged bimetallic structures [329,330]. In a separate experiment when we took excess of $[Au(CN)_2]^-$ with respect to Rh (Rh/Au = 1/2 mol), the bands at 2145 cm^{-1} and 2139 cm^{-1} appeared in FTIR spectrum which we attributed to v(CN) vibrations in unreacted $[Au(CN)_2]^-$ complexes adsorbed on zeolite surface (confirmed in a separate experiment when $[Au(CN)_2]^-$ was adsorbed on a bare zeolite) (Fig. 4.30). FTIR spectrum of $K[Au(CN)_2]$ in KBr exhibits one strong feature at 2142 cm^{-1} characterizing v(CN) vibration which is consistent with literature reports [333-335]. The observed split of this band into two features when $[Au(CN)_2]^-$ species adsorbed on zeolite could be indicative of slightly different adsorption sites of $[Au(CN)_2]^-$ in a framework. This result confirms that the Rh/Au mole ratio in a supported species is likely to be 1/1.

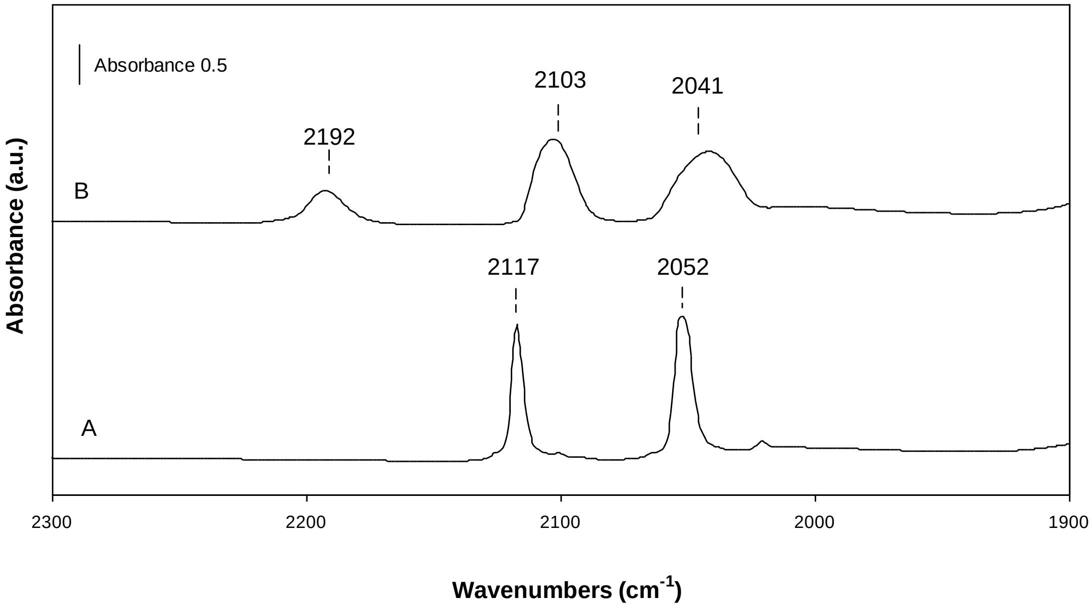

Figure 4.29 FTIR spectra in the v_{CO} region of $Rh(CO)_2$/HY30 (A), $Rh(CO)_2$-$Au(CN)_2$/HY30 (Rh/Au = 1/1 mol) (B) samples.

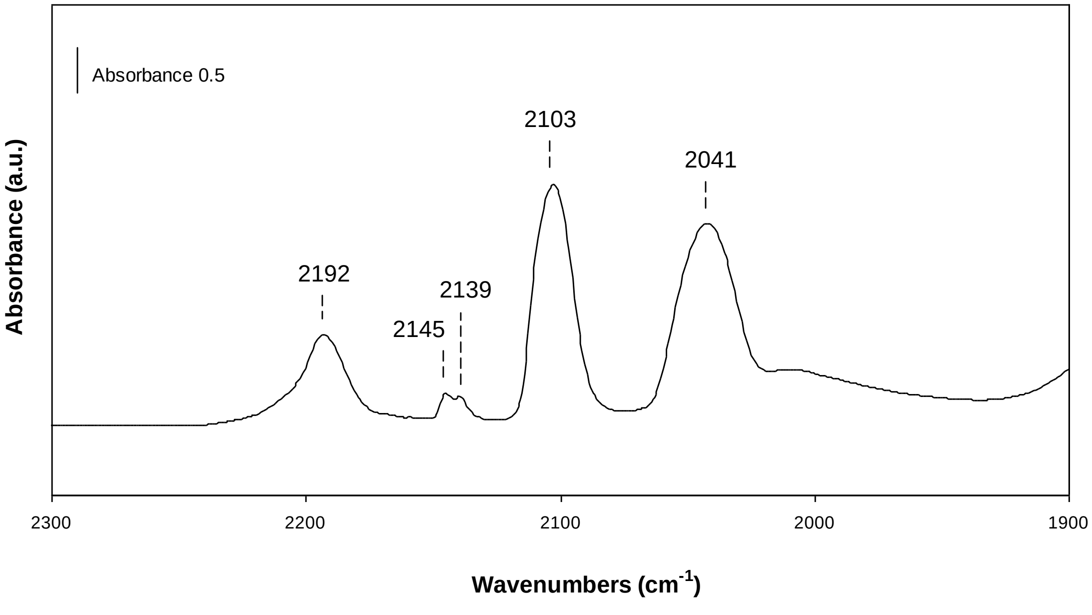

Figure 4.30 FTIR spectra in the v_{CO} region of $Rh(CO)_2$-$Au(CN)_2$/HY30 (Rh/Au = 1/2 mol) sample.

The EXAFS data collected at the Rh K edge and Au LIII edge (Table 4.2) for sample after reaction provide a basis for estimating the structure of surface species formed. Rh K edge EXAFS data revealed Rh-C contribution with an average coordination number of 1.6 at a bonding distance of 1.83 Å suggesting the presence of two carbonyl groups on Rh site after the reaction. We observe slight shortening of Rh-C bonds if compared to the initial HY supported $Rh(CO)_2$ complex where Rh-C was found to be 1.84 Å. The change in a bond length could be a result of increased backbonding from Rh center to π* antibonding orbitals of CO ligands. In fact, excessive electronic density on Rh site (compared to initial $Rh(CO)_2$ species) is evidenced by a redshift of carbonyl bands in FTIR spectrum. Nevertheless, we do recognize that the accuracy in bond length measurement with EXAFS (0.02 Å) does not allow to be certain regarding the influence of electronic effects. We also detected a new contribution originally absent in spectra of the sample before the reaction. The backscatter was identified as nitrogen atom with an average coordination number of 2 at 1.94 Å. Metal-support interface was characterized by Rh-O contribution with coordination number of about 1.3 at a distance of 2.02 A. This result indicates changes in Rh-zeolite binding mode after reaction suggesting detachment of one of zeolite oxygens upon coordination of $[Au(CN)_2]^-$ groups. The EXAFS data collected at Au LIII edge showed the presence of Au-C and Au-N contributions with average coordination numbers of 2.4 and 2.3 at average distance of 2.12 Å and 3.28 Å, respectively. This result suggests the presence of two –CN groups on Au atom and fully consistent with crystallographic parameters reported for $[Au(CN)_2]^-$ (Au-

C at 2.11 A and Au-N at 3.27 A) [336]. Interestingly, we did not detect Au-O contributions (neither short nor long oxygens) indicating that Au does not directly interact with oxygens of zeolite framework. We note that no oxygen neighbors in close proximity to Au sites were found in EXAFS spectra of the sample obtained after $[Au(CN)_2]^-$ adsorption on HY30 zeolite without Rh complexes. We infer that this could be due to anionic nature of gold cyanide species which unlike cations (i.e. Rh^I) tend to repel from atoms with high electronegativity i.e. oxygen atoms. Instead, the possible locations of such complexes could be associated with Lewis sites of zeolite such as framework or extraframework Al atoms. Nevertheless, further research is needed to clarify the binding site of such species on a zeolite. We emphasize that no Rh-Au clusters were formed during the reaction as evidenced by the complete absence of the Rh–Au contributions in EXAFS spectra. Thus, our EXAFS data is consistent with FTIR results and strongly suggest that -Au-CN-Rh-NC-Au- type structures are formed.

Table 4.2 EXAFS structural parameters characterizing surface species formed after the reaction of HY30-supported Rh(CO)$_2$ complexes with [Au(CN)$_2$]$^-$ species (Rh/Au = 1/1 mol).

Support	Shell	*N*	*R* (Å)	Δσ^2 (Å^2)	Δ*E*$_0$ (eV)	ε_v^2	*k*^{1}-variances (%)	
							Im.	Abs.
Rh K	Rh–Rh	--	--	--	--	1.8	3.6	3.3
	Rh–C	1.6	1.83	0.00121	10.0			
	Rh–N*	2	1.94	0.00085	-8.7			
	Rh–O$_{support}$							
	Rh–O$_S$	1.3	2.02	0.00740	3.1			
	Rh–Al	2.25	2.81	0.00587	-4.5			
Au LIII	Au–Au	--	--	--	--	2.5	1.5	1.9
	Au–C*	2.4	2.12	0.00128	0.1			
	Au–N*	2.3	3.28	0.00051	-0.7			
	Au–O$_{support}$							
	Au–O$_S$	--	--	--	--			
	Au–Al	--	--	--	--			
[Au(CN)$_2$]$^-$ [336]	Au–Au	--	--	--	--	--	--	--
	Au–C*	2	2.11	--	--			
	Au–N*	2	3.27	--	--			

Standard deviations in fits: N ± 20%, R ± 1%, Δσ^2 ± 10%, ΔE$_0$ ± 10%. N, coordination number; R, distance between absorber and backscatterer atoms; Δσ^2, Debye-Waller factor relative to the Debye-Waller factor of the reference compound; ΔE$_0$, inner potential correction accounting for the difference in the inner potential between the sample and the reference compound; ε_v^2, goodness of fit; the superscript * refers to carbonyl ligands. ^{a} R-space fit ranges $3.5 < k < 15.0$ Å^{-1} and $0.5 < r < 3.5$ Å; 23 allowed fitting parameters.

The question that has to be clarified is weather these structures are formed inside the zeolite cages or they reside on the outer surface of zeolite. In order to reveal the location of -Rh-NC-Au- species, XPS measurements were conducted. Surface concentration of rhodium in $Rh(CO)_2$/HY30 samples before and after interaction with $[Au(CN)_2]^-$ species could be estimated by relating the integrated area of Rh $3d_{5/2}$ band to the area of Si 2p peak (Rh/Si ratio) in correspondent samples. It was found that Rh/Si ratio increased almost five-fold (from 0.031 to 0.157) after HY30 supported $Rh(CO)_2$ complexes reacted with $[Au(CN)_2]^-$ species indicating that significant fraction of -Rh-NC-Au- structures are primary located on the outer surface of zeolite. Although this finding could partly explain changes in Rh-zeolite interface which were observed with EXAFS for gold-modified sample, further investigation is needed to clarify possible binding mode of Rh to the support in -Rh-NC-Au- species. We also would like to point out that since bridging –OH groups are located inside zeolite supercages, their contribution to catalysis in case of zeolite-supported -Rh-NC-Au- species which mostly reside on the outer surface could be small.

Finally, Energy-dispersive X-ray spectroscopy (EDX) was used to probe spatial distribution of Rh and Au atoms in a sample after the reaction (Fig. 4.31). demonstrates results obtained from EDX spectra collected on zeolite slab of about 300 nm long. It is evident that Rh and Au distributions in the slab are almost identical and, in fact, completely overlap suggesting that these elements are chemically bound and located next to each other on the surface.

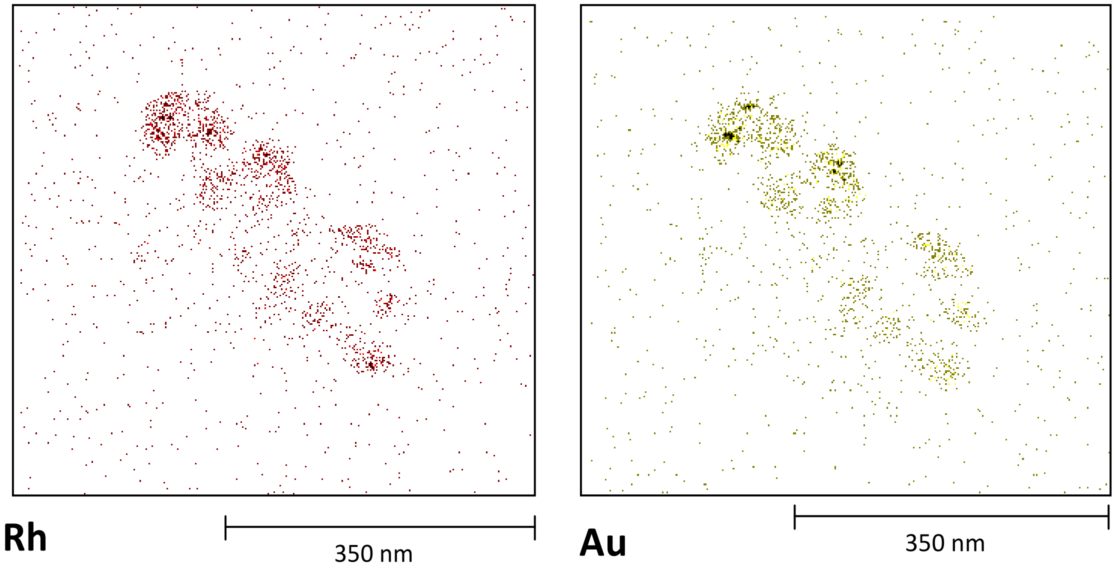

Figure 4.31 EDX mapping of $Rh(CO)_2$-$Au(CN)_2$/30□(Rh/Au = 1/1 mol) sample.

Catalytic performance of both modified and unmodified samples was evaluated at 607 Torr of H_2 and 76 Torr of C_2H_4 at ambient conditions. We note that $[Au(CN)_2]^-$ adsorbed on HY30 zeolite surface exhibits no activity in neither ethylene hydrogenation nor ethylene dimerization reactions. The data presented in Fig. 4.32 demonstrate that modified sample maintained activity in ethylene hydrogenation although the induction period is significantly longer than for $Rh(CO)_2$/HY30. However, most importantly, we observed absolutely no activity in ethylene dimerization reaction (Fig. 4.33) indicating that the proposed concept of “selective blocking” of coordination sites on Rh with bulky ligand could be valid. We emphasize that at this point it is difficult to discriminate between possible effects of acidic hydroxyl groups which can not contribute to the dimerization activity if major fraction of -Rh-NC-Au- species are on the outer surface and the effect of -NC-Au- ligands present on Rh sites preventing interaction of ethylene molecules with rhodium ethyl species.

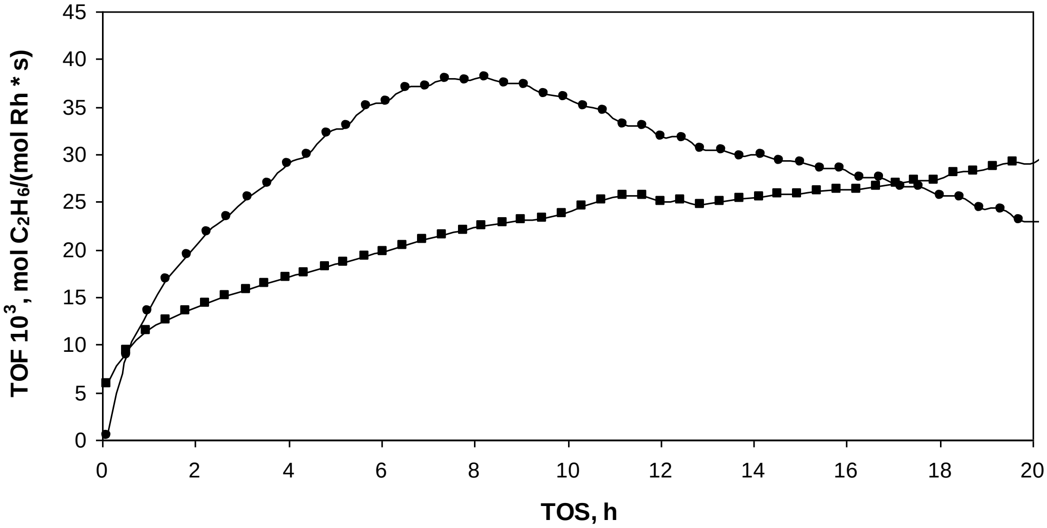

Figure 4.32 Rates (Turn Over Frequencies) of Ethane formation with Time on Stream (TOS) for $Rh(CO)_2/HY30$ (●) and $Rh(CO)_2-Au(CN)_2/HY30$ (Rh/Au = 1/1 mol) (■) at 608 Torr of H_2 and 76 Torr of C_2H_4.

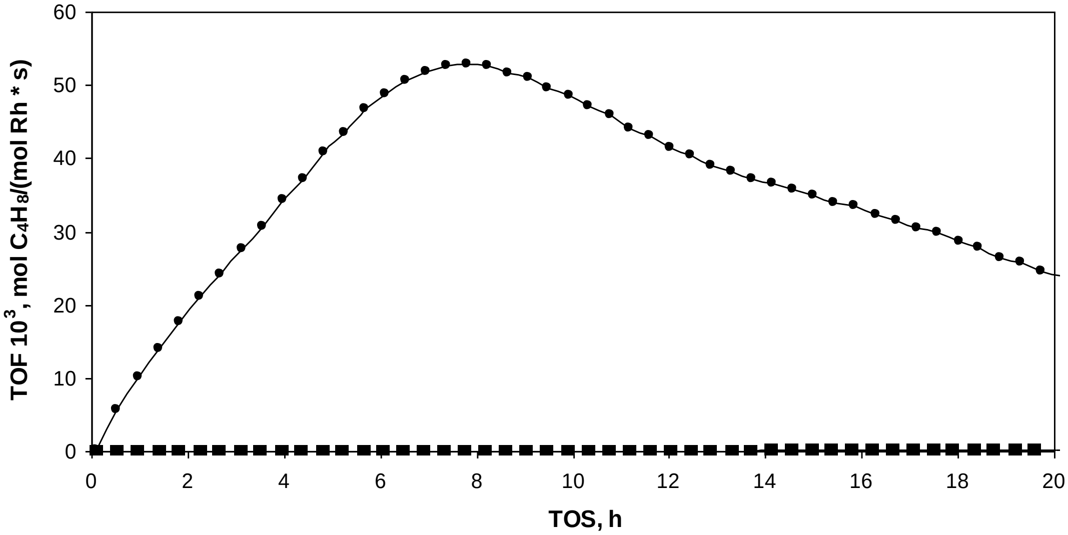

Figure 4.33 Rates (Turn Over Frequencies) of Butenes formation with Time on Stream (TOS) for $Rh(CO)_2/HY30$ (●) and $Rh(CO)_2-Au(CN)_2/HY30$ (Rh/Au = 1/1 mol) (■) at 608 Torr of H_2 and 76 Torr of C_2H_4.

4.5 CONCLUSIONS

HY zeolite-grafted rhodium carbonyl complexes are active in both ethylene hydrogenation and dimerization at ambient conditions with the latter process being approximately 2.5 times faster at partial pressures of H_2 (76-608 Torr) and C_2H_4 (38 -152 Torr) used. The results presented herein show that support is of crucial importance in defining catalytic functions of supported rhodium carbonyl complexes. More specifically, HY zeolite and Al_2O_3-supported rhodium species exhibit very different surface chemistry and, as a result, different catalytic properties which are proposed to be due substantially different electron withdrawing properties of these supports. Activity measurements revealed that Al_2O_3-anchored $Rh(CO)_2$ complexes are inactive in ethylene hydrogenation and dimerization. Kinetic data acquired on HY zeolite-supported catalyst indicated that hydrogenation and dimerization processes are essentially coupled and revealed strong dependence of ethane and butenes formation rates on partial pressure of hydrogen (1 and 1.2 order, respectively) suggesting that both reactions involve rhodium hydrides species as intermediates. The role of the support in dimerization mechanism was investigated in experiments where amount of acidic –OH groups available for ethylene adsorption was varied. These results conclusively demonstrated that zeolite surface is involved in C-C bond formation reaction and confirmed the concept reported earlier in literature regarding the bifunctional performance of HY zeolite-supported rhodium species in ethylene dimerization. Finally, we demonstrated that catalytic activity of HY zeolite-supported $Rh(CO)_2$ complexes can be tuned by modifying their coordination environment. It was shown that reaction between supported rhodium dicarbonyls and $[Au(CN)_2]^-$ species leads to the formation of chain type Au-CN-$Rh(CO)_2$-NC-Au- structures which retain activity in ethylene hydrogenation but fully inactive in dimerization reaction.

4.6 ACKNOWLEDGENETS

XAS data were collected at the Stanford Synchrotron Radiation Laboratory, a national user facility operated by Stanford University on behalf of the U.S. Department of Energy, Office of Basic Energy Sciences. The assistance of the beam line staff at SSRL is gratefully acknowledged. The EXAFS data were analyzed with the XDAP software developed by XAFS Services International [148].

CHAPTER 5. NO REDUCTION WITH CO USING HY ZEOLITE-SUPPORTED RHODIUM DICARBONYL COMPLEXES: GIVING AN INSIGHT INTO THE STRUCTURE SENSETIVITY

5.1 PREFACE

Activity of $Rh(CO)_2$ complexes supported on HY zeolites with Si/Al ratio of 30 and 2.6 in NO reduction with CO reaction was investigated. Facile exchange between CO and NO ligands occurred at ambient conditions but no activity towards formation of N_2, N_2O and CO_2 was observed. Significant difference in catalytic performance of both samples was observed at elevated temperatures. When temperature was increased to 270 ºC, induction period in about 145 minutes was detected for HY2.6 supported sample when NO conversion increased from approximately 9 % to 100 % while HY30 anchored $Rh(CO)_2$ species remained inactive. In-situ Fourier transform infrared (FTIR) and High resolution transition microscopy (HRTEM) measurements revealed that the transient period is associated with decomposition of $Rh(CO)_2/Rh(NO)_2$ complexes and formation of rhodium particles. These data unambiguously demonstrated that mononuclear $Rh(CO)_2/Rh(NO)_2$ species which are stabilized by HY30 zeolite under the reaction conditions do not promote NO reduction with CO but conglomerate of Rh atoms is needed to initiate the catalytic cycle.

5.2 INTRODUCTION

Regulations of motor vehicle exhaust emissions impose strict requirements concerning the abatement of nitrogen oxides (NO_x) and CO [347,348]. Currently, removal of harmful components in an automotive exhaust is achieved by using Three Way Catalyst (TWC) containing precious metals (Rh, Pt, Pd) as active components [349-351]. Rhodium is essential constitute of such catalytic systems due to its remarkable activity in NO reduction with CO or hydrocarbons [350]. CO-NO reaction over rhodium catalysts has been subject to extensive research for more than two decades with a primary emphasis on its mechanistic aspects [352-354].Although the reaction mechanism is found to be relatively simple occurring via few elementary steps [355-357], design of optimal catalyst is still a challenge due to structure-sensitive nature of CO-NO transformation on rhodium surfaces [358-363].

More specifically, surface-science studies combined with kinetic data analysis from single-crystal surfaces revealed that reaction rates as well as selectivity towards nitrogen formation depend on the density of rhodium atoms in the top-most layer of exposed rhodium surface. (i.e. N_2 selectivity increase in the order: Rh(111) > Rh(100) > Rh(110)) [364,365]. This result is generally explained by steric hindrance of NO dissociation elementary step implying that more open surfaces favor higher N atoms coverages [364]. In reality, however, the picture is more complex since unlike flat single crystals studies under the UHV conditions, surface chemistry of the actual supported catalyst is complicated by such effects as adsorbate-adsorbate lateral interactions, adsorption of species on different sites (i.e. edges, steps, kinks etc.), and contribution of the support [366,367]. Besides, supported metal nanoparticles exhibit several low index faces (i.e. (111), (100) etc.) with their contribution to total exposed metal surface area being dependent on the crystalline size and since activity of those faces are different, they contribute differently to the measured reaction rate [361]. Nevertheless, it is generally established that for supported catalysts rate of NO-CO reaction increases with rhodium particle size with most reports covering 1-7 nm size range [360,362,363].

The question that remains open and still matter of debate in literature is weather single Rh ion could catalyze NO-CO reaction. Supported single-site catalysts have been an area of interest for researchers for several reasons [368,369,278]. First, such materials offer higher concentration of exposed surface sites than conventional supported catalysts which could be principal for industrial applications. Second, these sites are uniform in composition providing opportunities for more selective catalysis. The first indication that Rh complex is capable to promote nitric oxide reduction with carbon monoxide came from work of Meyer and Eisenberg who showed that $[RhCl_2(CO)_2]^-$ complexes in liquid phase are capable to facilitate NO-CO reaction yielding N_2O and CO_2 at ambient conditions [370]. Supported analogs of these species were investigated by Iizuka et al who suggested that Y-zeolite immobilized $Rh(CO)_2$ and $Rh(NO)_2$ species could be involved in reduction of NO by CO at 135 ºC with key intermediate defined as $[Rh(CO)_2(NO)]^+$ [371]. Cannon et al discussed reactivity of silica-bound $Rh(CO)_2$ complexes towards nitric oxide and concluded that interaction of these species with NO at 100 ºC results in a formation rhodium-oxygen adduct (i.e. supposingly $Rh(O)_2$) on a surface and evolution of CO_2 and N_2 in a gas phase [372]. In contrast, Almusaiteer et al. observed no gaseous products other than CO after the reaction between alumina-supported $Rh(CO)_2$ complexes and NO at 300 ºC but detected $Rh(NO)_2$ and $[Rh(NO)]^+$ species on a surface which indicated that simple substitution occurred [373]. They proposed that in order to initiate and sustain NO–CO redox reaction cycle, $Rh(CO)_2$ complexes and metallic Rh crystallites have to coexist. More specifically, the latter species are responsible for CO activation while the former act as NO dissociation sites and supply active oxygen atoms for the reaction. Besides, it was found that composition of surface species (i.e. $Rh(CO)_2$, $Rh\text{-}NO^+$, $Rh^0\text{-}CO$ etc.) formed under the reaction conditions is governed by temperature and reactant partial pressures and formation of $Rh(CO)_2$ species is favored at low temperatures (below light-off) and high NO/CO ratios [374].

Thus, reviewed results indicate some discrepancy regarding the role and functions of $Rh(CO)_2$ species in NO-CO reaction. In order to clarify these aspects, we used well-defined site-isolated $Rh(CO)_2$ complexes immobilized into zeolite Y framework. As it was shown previously, such materials could serve as model catalysts to demonstrate reactivity and catalytic properties of isolated $Rh(CO)_2$ complexes [63,288]. We utilized FTIR, STEM, and XPS techniques as well as activity measurements in order to reveal catalytic functions of single-site rhodium complexes in NO-CO reaction and clarify structure-catalytic properties relationships. The results presented herein demonstrate that single-site

$Rh(CO)_2/Rh(NO)_2$ complexes are not responsible for the observed activity and conglomerate of rhodium atoms (i.e. Rh^0 sites) are required to initiate the reaction.

5.3 EXPERIMENTAL

5.3.1 REAGENTS AND MATERIALS

Dicarbonylacetylacetonato rhodium (I) $Rh(CO)_2(acac)$ (acac = $C_5H_7O_2$) (Strem, 98% purity) was used as supplied. n-Pentane (Aldrich, 99% purity) and Tetrahydrofuran (Aldrich, >99.9 %) were refluxed under N2 in the presence of Na/benzophenone ketyl to remove traces of moisture and deoxygenated by sparging of dry N_2 prior to use. All glassware used in preparation steps was previously dried at 120°C. He, 1 % CO balance He and 1 % NO balance He (Airgas, all UHP grade) were additionally purified to their use by passage through oxygen/moisture traps (Agilent) capable of removing traces of O_2 and water to 15 and 25 ppb, respectively. CBV760 and CBV600 dealuminated HY zeolites (Zeolyst International) with Si/Al atomic ratios of 30 and 2.6, respectively, were calcined in flowing O_2 at 300°C for 3 h and then evacuated at 10-3 Torr and 300°C for 16 h. For simplicity, these zeolite supports are further denoted as HY30 and HY2.6, respectively. All treated supports were stored and handled in a glovebox (MBraun) filled with dry N_2. The residual water and O_2 concentrations in the glovebox were kept below 0.1 ppm.

5.3.2 PREPARATION OF SUPPORTED SAMPLES

The syntheses and sample transfers were performed with exclusion of air and moisture on a double-manifold Schlenk line and in a N_2-filled MBraun glove box. Supported samples were prepared by slurrying the $Rh(CO)_2(acac)$ precursor with a corresponding powder support in n-pentane under N_2 for 24 h at room temperature, followed by overnight evacuation at 25°C to remove the solvent. In each case, the $Rh(CO)_2(acac)$ precursor was added in the amount needed to yield samples containing 1 wt% Rh. The Rh weight loading was verified by inductively coupled plasma-mass spectrometry (ICP-MS) analysis (Galbraith Laboratories Inc.). All prepared samples were stored and handled in a glovebox filled with N_2 to prevent possible contamination and decomposition of supported species.

5.3.3 FTIR SPECTROSCOPY

A Nicolet Nexus 470 spectrometer equipped with a MCT-B detector cooled by liquid nitrogen was used to collect spectra with a resolution of 2 cm^{-1}, averaging 64 scans per spectrum. Each powder sample was pressed into a self-supported wafer with a density of approximately 20 mg/cm^2 and mounted in a home-made cell connected to a gas distribution manifold. The cell design allowed for the treatment of samples at different temperatures, while various gases flowed through the cell.

5.3.4 X-RAY ABSORPTION SPECTROSCOPY (XAS) MEASURMENTS

XAS spectra were collected at X-ray beamline 4-1 of the Stanford Synchrotron Radiation Laboratory (SSRL), Stanford Linear Accelerator Center, Menlo Park, CA. The storage ring electron energy was 3 GeV and the ring current was in the range of 345-350 mA.

XAS measurements were used to characterize the surface species formed after the thermal treatments of HY30 zeolite-supported $Rh(CO)_2$ complexes. Prior to these measurements, each powder sample was pressed into a wafer inside a N_2-filled glovebox. The sample mass was calculated to give an absorbance of approximately 2.5 at the Rh K absorption edge. After the sample had been pressed, it was loaded into an EXAFS cell [145], sealed under N_2, and removed from the glovebox. The cell was evacuated at 10^{-5} Torr and aligned in the X-ray beam. The XAS data were collected at liquid nitrogen temperature in the transmission mode with a Si(220) double crystal monochromator that was detuned by 30% to minimize effects of higher harmonics in the X-ray beam. Samples were scanned at energies near the Rh K (23220 eV) absorption edge. All spectra were calibrated with respect to Rh foil, the spectrum of which was collected simultaneously.

5.3.5 EXTENDED X-RAY ABSORPTION FINE STRUCTURE (EXAFS) DATA ANALYSIS

The EXAFS data were analyzed with experimentally determined reference files obtained from EXAFS data characterizing materials of known structure. The Rh–Osupport and Rh–C contributions were analyzed with phase shifts and backscattering amplitudes obtained from EXAFS data for Rh_2O_3 and $Ru_3(CO)_{12}$ (which has only terminal CO ligands), respectively. The phase shifts and backscattering amplitudes representing Rh-Rh shell was calculated from the structural parameters characterizing rhodium foil. The transferability of the phase shifts and backscattering amplitudes for near neighbors in the periodic table has been justified experimentally [146]. The parameters used to extract these files from the EXAFS data are reported elsewhere [147]. The EXAFS data were extracted from the spectra with the XDAP software developed by XAFS Services International [148]. The EXAFS function for each sample was obtained from the X-ray absorption spectrum by a cubic spline background subtraction and normalized by dividing the absorption intensity by the height of the absorption edge. The final normalized EXAFS function for each sample was obtained from an average of six scans. The parameters characterizing both low-Z (O, C) and high-Z (Rh) contributions were determined by multiple-shell fitting with a maximum of 16 free parameters in r space (where r is the distance from the absorbing atom, Rh or Au) and in k (wave vector) space over the ranges of $3.5 < k < 15.0$ Å-1 and $0.5 < r < 3.5$ Å with application of k^1 and k^3 weighting of the Fourier transform. The statistically justified number of free parameters (n), estimated from the Nyquist theorem [149,150], $n = (2\Delta k\Delta r/\pi) + 1$, where Δk and Δr are the k and r ranges used to fit the data, was approximately 23. The fit was optimized by use of a difference file technique [151,152], with phase- and amplitude-corrected Fourier transforms. Standard deviations were calculated with the XDAP software, as described elsewhere [153]. Systematic errors are not included in the calculation of the standard deviations. The values of the goodness of fit (ε_v^2) were calculated with the XDAP software as outlined in the Reports on Standards and Criteria in XAFS Spectroscopy [154]. The variances in both the imaginary and absolute parts were used to determine the fit quality [155].

5.3.6 X-RAY PHOTOELECTRON SPECTROSCOPY MEASURMENTS

XPS measurements were conducted using a Kratos AXIS Ultra DLD XPS system equipped with a monochromatic Al Kα source. The system energy scale was calibrated using an Ag foil with the Ag $3d_{5/2}$ binding energy set at 368.21 ± 0.025 eV for the monochromatic Al Kα source operated at 15 keV and 120 W. The pass energy was fixed at 40 eV for the detailed scans. A charge neutralizer was used to compensate for the surface charging during the photoemission. The powder samples (approximately 5 mg) were loaded into the air-tight cell in the N_2-filled glovebox and transferred without air exposure into the UHV chamber for the XPS analysis. The C 1s signal with a binding energy of 285.0 eV was used as an internal reference for calibration of the Rh $3d_{5/2}$ and Rh $3d_{3/2}$ binding energy values. All binding energies reported in this work were measured with a precision of ±0.1 eV. XPS data were analyzed by nonlinear curve fitting using the XPSPEAK 4.1 software. In all cases, a linear-type background was subtracted from the spectra and a curve fit was performed using the minimum number of G/L-type peaks that provides a good fit. In each case the fitting routine was completed when the coefficient of determination (R^2) value was 0.98 or higher.

5.4 RESULTS AND DISCUSSION

5.4.1 INTERACTION OF HY ZEOLITE-SUPPORTED $Rh(CO)_2$ COMPLEXES WITH NO

Reaction of $Rh(CO)_2(acac)$ with HY zeolites results in site-isolated $Rh(CO)_2$ complexes anchored to zeolite framework. In our earlier communication we reported that, in fact, two types of binding sites for $Rh(CO)_2$ species exist in dealuminated Y zeolites with relative fraction of these sites being function of Al content [303]. More specifically, HY30-supported $Rh(CO)_2$ complexes are characterized by FTIR bands at 2117, 2053 cm^{-1} and 2113, 2048 cm^{-1} with the relative fraction of these species of 83 % and 17 %, respectively. As zeolite Si/Al ratio decreases to 2.6, the fraction of Type I sites drops to 50 % with positions of correspondent features being the same while features characterizing Type II species appear at slightly lower wavenumers: 2110 and 2043 cm^{-1}.

Exposure of HY30-supported sample to a pulse of 1 % NO in helium for 30 sec resulted in immediate disappearance of carbonyl bands and formation of new features at 1854 cm^{-1} and 1780 cm^{-1} assigned to symmetric and asymmetric vibrations of nitrosyl ligands in $Rh(NO)_2$ species (conversion of rhodium carbonyl to rhodium nitrosyl complexes is accompanied by the change of a zeolite color from pale white to purple) (Fig. 5.1). This result is consistent with literature reports suggesting similar FTIR signature for rhodium dinitrosyl species [375]. Analysis of FTIR spectrum in v(NO) region did not allow to distinguish two types of $Rh(NO)_2$ complexes with substantial level of confidence.

Similarly, interaction of HY2.6-supported $Rh(CO)_2$ complexes with 1 % NO in helium yields two intense bands in the v(NO) region centered at 1857 cm^{-1} and 1781 cm^{-1}. Deconvolution of this spectrum reveals two weak features at 1849 cm^{-1} and 1762 cm^{-1} suggesting that NO/CO substitution occurred on both types of surface sites (Fig. 5.2). We note that reactivity of two types of sites towards reaction with NO is different, more specifically, if 1 % NO exposure is performed in 10 sec pulses mode, Type I $Rh(CO)_2$ complexes react first (in other words, these sites could be almost selectively “titrated” with NO leaving only Type II $Rh(CO)_2$ species on the surface). Mass spec analysis of the effluent gas during NO exposure for both samples (HY30 and HY2.6-supported) revealed no other products (i.e. CO_2, N_2O and N_2) than CO suggesting that no reaction between NO and CO takes place at room temperature. We also did not observe formation of any mixed $Rh(CO)_x(NO)_y$ type complexes which were previously indicated as potential active sites for NO-CO reaction. Finally, it is remarkable that CO/NO substitution on HY zeolite-supported Rh complexes is fully reversible and even traces of CO introduced into the cell (5 Torr) result in a immediate reappearance of $Rh(CO)_2$ complexes.

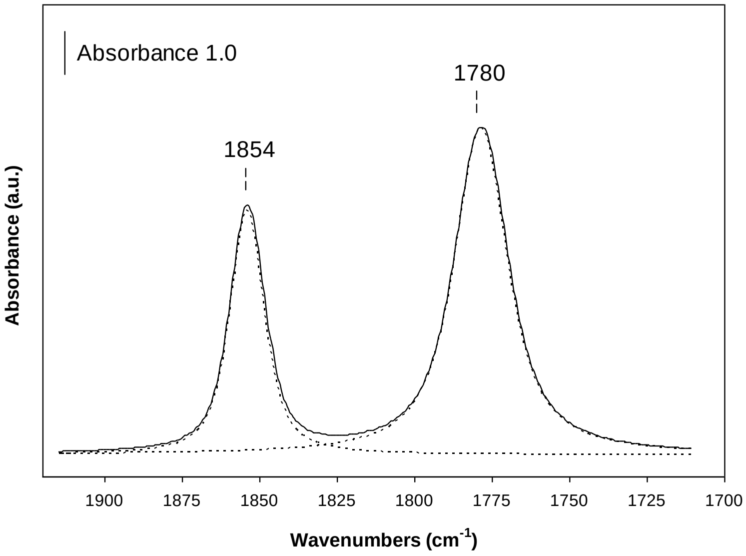

Figure 5.1 FTIR spectrum in the ν_{NO} region of $Rh(CO)_2$/HY30 sample after exposure of 1 % NO/He for 1 minute at ambient conditions.

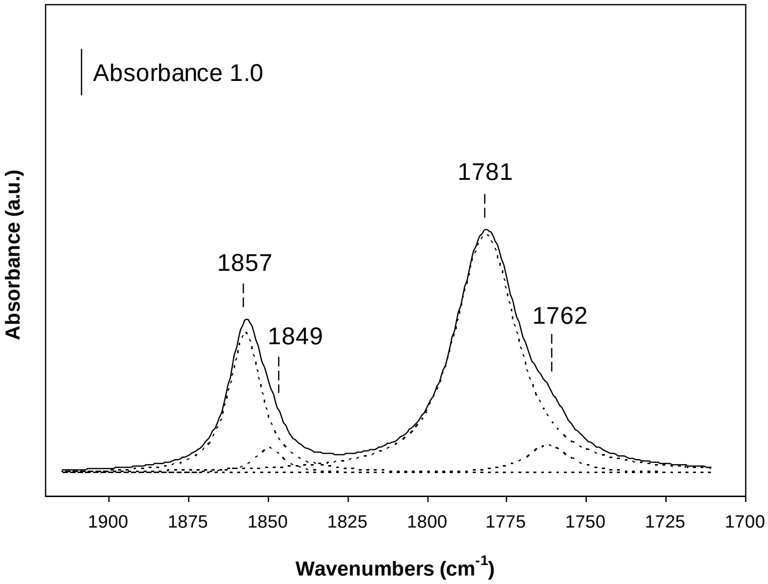

Figure 5.2 FTIR spectrum in the ν_{NO} region of $Rh(CO)_2$/HY2.6 sample after exposure of 1 % NO/He.

5.4.2 THERTHERMAL STABILITY OF HY ZEOLITE-SUPPORTED $Rh(CO)_2$ COMPLEXES

Since HY zeolite-supported complexes do not exhibit activity in NO-CO reaction at ambient conditions, experiments at elevated temperatures were conducted. However, prior to performing such experiments one has to define range of temperatures when structural integrity of initial $Rh(CO)_2$ complexes is preserved. Thermal stability of HY30 and HY2.6-supported rhodium dicarbonyls in helium was investigated at 100 - 400 °C.

IR spectra in the CO region recorded during the thermal treatments of HY30-supported $Rh(CO)_2$ sample in flowing He are presented in Fig. 5.3. This result shows that up to 200 °C, neither intensity nor integrated area of v(CO) bands undergo any detectable changes suggesting that $Rh(CO)_2$ complexes remain fully intact. However, we note that close analysis of FTIR spectrum in v(CO) region for sample treated at 100 °C in He indicated that Type II species diminished at this temperature. At 300 °C v(CO) bands loose about 30 % of their intensity indicating that decarbonylation occurred to certain extend and, finally, at 400 °C carbonyl ligands were completely removed.

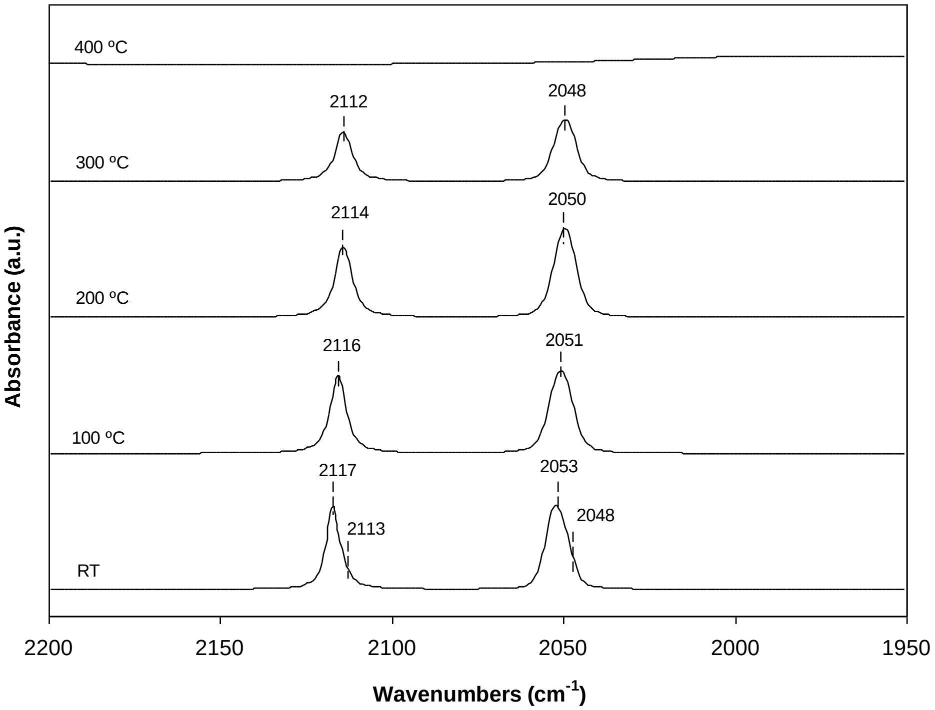

Figure 5.3 FTIR spectra in the v_{CO} region of $Rh(CO)_2$/HY30 sample after treatment in He for 1 h at different temperatures.

EXAFS data collected at Rh K-edge in the same temperature range is fully consistent with FTIR data and support conclusions stated above (Table 5.1). The results characterizing $Rh(CO)_2$/HY30 sample treated in He at 100 °C and 200 ºC revealed no Rh–Rh contributions pointing out to the mononuclear character of Rh surface species. The presence of two carbonyl ligands per each Rh atom was designated by Rh–C and Rh–O* contributions with average coordination numbers of approximately 2 at average bond distances of 1.83 (200 °C) and 2.97 Å (200 °C), respectively. Metal-supported interface was characterized by the presence of $Rh–O_S$ contributions at an average bond distance of approximately 2.14 Å (100 °C) and 2.13 (200 °C) with coordination number nearly 2. When temperature was further raised to 300 °C, some changes in structural parameters of $Rh(CO)_2$ surface complexes were observed. Although Rh-Rh contribution was not detected suggesting that rhodium species remain mononuclear, Rh–C and Rh–O* coordination numbers dropped to 0.5 and 0.6 (at bond distances 1.82 Å and 3.02 Å, respectively) indicating that partial decarbonylation of supported complexes occurred. The Rh-support interactions were not altered significantly and were designated by $Rh–O_s$ contributions with an average coordination number of 1.7 at a bond distance of approximately 2.17 Å. Finally, at 400 ºC complete destruction of rhodium surface complexes occurred as evidenced by the appearance of Rh-Rh contribution with average coordination of 5.3 at a bond distance of about 2.65 Å.

FTIR data characterizing $Rh(CO)_2$/HY2.6 sample treated in He at elevated temperatures show that thermal stability of Type I and Type II species on this support is significantly different (Fig. 5.4). More specifically, 47 % of Type II complexes are removed already at 100 °C as evidenced by the reduced intensity of correspondent ν(CO) bands. Further increase of a temperature to 200 °C resulted in decarbonylation of 80 % of Type II species while intensity of ν(CO) bands characterizing Type I complexes was essentially unchanged. Rapid decarbonylation of both types of species was observed at 300 ºC when only approximately 20 % of Type I species remained on a surface and this process was completed at 400 °C.

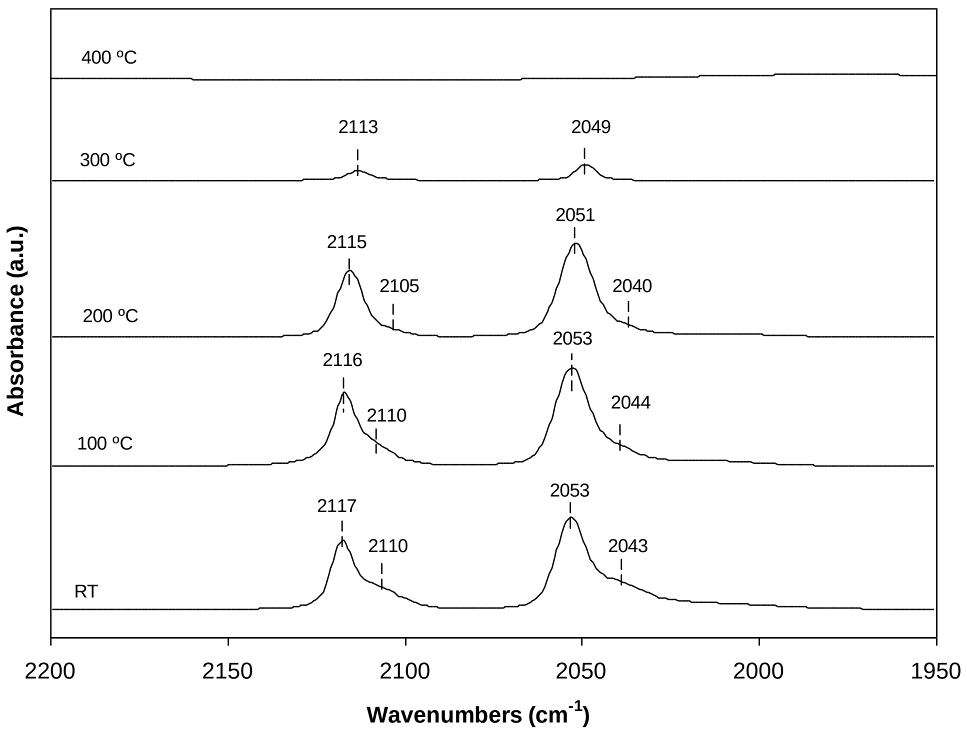

Figure 5.4 FTIR spectra in the v_{CO} region of $Rh(CO)_2$/HY2.6 sample after treatment in He for 1 h at different temperatures.

EXAFS data obtained on HY2.6-supported $Rh(CO)_2$ complexes are complementary to FTIR results (Table. 5.2). Although some fraction of Type II species was thermally decomposed at 100 °C, rhodium species are confirmed to remain mononuclear as evidenced by the absence of Rh–Rh contribution. $Rh(CO)_2$ moiety is retained as indicated by Rh–C and Rh–O* contributions with average coordination numbers 1.9 and 2.2 at bonding distances of 1.84 Å and 3 Å, respectively. The complex is interacting with on average two oxygens of the support as designated by Rh–O_S contribution with coordination number 2.1 at 2.16 Å. The structural parameters of HY2.6-supported complexes did not change significantly when temperature was further raised to 200 °C. Two carbonyl ligands were still present on Rh sites (Rh–C and Rh–O* contributions were characterized by coordination numbers of 1.9 and 2.2 at bonding distances of 1.84 Å and 3 Å, respectively) and Rh atoms in each complex were bonded to two support oxygen atoms as shown by the Rh-O_s contribution with coordination number being nearly 2. This result is consistent with FTIR data which indicate that Type I rhodium dicarbonyls constitute majority of surface species at this temperature. In contrast to the HY30-supported sample, rhodium species on HY2.6 zeolite did not retain mononuclear structure at 300 °C, but aggregated into relatively small rhodium clusters as evidenced by Rh-Rh contribution with coordination number approximately 5.1. The agglomeration processes proceeded further at 400 °C when Rh-Rh contribution was found to be on average 8.8.

Thus, FTIR and EXAFS results suggest that decarbonylation of supported $Rh(CO)_2$ species begin in a relatively narrow temperature window from 200 to 300 °C. These data also indicate that Al content of a zeolite does affect the thermal stability of supported complexes and Al rich support clearly favor decomposition and subsequent aggregation of rhodium species.

Table 5.1 EXAFS structural parameters characterizing $Rh(CO)_2$/HY30 catalyst treated in He for 1 h at different temperatures.

Support	Shell	*N*	*R* (Å)	$\Delta\sigma^2$ (Å^2)	ΔE_0 (eV)	ε_v^2	k^1-variances (%)	
							Im.	Abs.
100 °C	Rh–Rh	--	--	--	--	3.6	3.4	5
	Rh–C*	2.1	1.83	0.00256	10			
	Rh–O*	2	2.99	0.00164	10			
	Rh–$O_{support}$							
	Rh–O_s	2.4	2.14	0.00299	-1.8			
	Rh–O_l	2.1	2.77	-0.0055	-7.3			
200 °C	Rh–Rh	--	--	--	--	3.4	2.4	3.5
	Rh–C*	2.1	1.83	0.00382	10			
	Rh–O*	1.9	2.97	0.00052	10			
	Rh–$O_{support}$							
	Rh–O_s	2.3	2.13	0.00122	-0.6			
	Rh–O_l	2.1	2.76	-0.00568	-9.1			
300 °C	Rh–Rh	--	--	--	--	4.4	1.9	2.9
	Rh–C*	0.5	1.82	-0.00318	10			
	Rh–O*	0.6	3.02	-0.00073	0.72			
	Rh–$O_{support}$							
	Rh–O_s	1.8	2.17	-0.00173	-5.2			
	Rh–O_l	2.4	2.79	-0.00396	-10			
400 °C	Rh–Rh	5.3	2.65	0.00752	7.7			
	Rh–C*	--	--	--	--			
	Rh–O*	--	--	--	--			
	Rh–$O_{support}$							
	Rh–O_s	--	--	--	--			
	Rh–O_l	--	--	--	--			

Standard deviations in fits: N ± 20%, R ± 1%, $\Delta\sigma^2$ ± 10%, ΔE_0 ± 10%. N, coordination number; R, distance between absorber and backscatterer atoms; $\Delta\sigma^2$, Debye-Waller factor relative to the Debye-Waller factor of the reference compound; ΔE_0, inner potential correction accounting for the difference in the inner potential between the sample and the reference compound; ε_v^2, goodness of fit; the superscript * refers to carbonyl ligands. ^{a} R-space fit ranges 3.5< k < 15.0 Å^{-1} and 0.5< r < 3.5 Å; 23 allowed fitting parameters.

Table 5.2 EXAFS structural parameters characterizing Rh(CO)$_2$/HY2.6 catalyst treated in He for 1 h at different temperatures.

Support	Shell	*N*	*R* (Å)	$\Delta\sigma^2$ (Å^2)	ΔE_0 (eV)	ε_ν^2	k^1-variances (%)	
							Im.	Abs.
100 °C	Rh–Rh	--	--	--	--	8	2.1	3.1
	Rh–C*	1.9	1.84	0.0015	10.0			
	Rh–O*	2.2	3.00	0.00261	10.0			
	Rh–O$_{\text{support}}$							
	Rh–O$_{\text{S}}$	2.1	2.16	0.00192	-3.0			
	Rh–O$_{\text{l}}$	2.4	2.80	-0.00384	-10.0			
200 °C	Rh–Rh	--	--	--	--	7.1	1.8	2.6
	Rh–C*	1.8	1.84	0.00335	10.0			
	Rh–O*	2.2	2.99	0.00397	9.2			
	Rh–O$_{\text{support}}$							
	Rh–O$_{\text{S}}$	2.1	2.16	0.00142	-3.1			
	Rh–O$_{\text{l}}$	2.3	2.81	-0.00262	-10.0			
300 °C	Rh–Rh	5.1	2.68	0.00207	5.1		13.4	30.3
	Rh–C*	--	--	--	--			
	Rh–O*	--	--	--	--			
	Rh–O$_{\text{support}}$							
	Rh–O$_{\text{S}}$	--	--	--	--			
	Rh–O$_{\text{l}}$	--	--	--	--			
400 °C	Rh–Rh	8.8	2.68	0.00273	6.4		6.6	9.6
	Rh–C*	--	--	--	--			
	Rh–O*	--	--	--	--			
	Rh–O$_{\text{support}}$							
	Rh–O$_{\text{S}}$	--	--	--	--			
	Rh–O$_{\text{l}}$	--	--	--	--			

Standard deviations in fits: *N* ± 20%, *R* ± 1%, $\Delta\sigma^2$ ± 10%, ΔE_0 ± 10%. *N*, coordination number; *R*, distance between absorber and backscatterer atoms;

$\Delta\sigma^2$, Debye-Waller factor relative to the Debye-Waller factor of the reference compound; ΔE_0, inner potential correction accounting for the difference in the inner potential between the sample and the reference compound; ε_v^2, goodness of fit; the superscript * refers to carbonyl ligands. [a] *R*-space fit ranges 3.5< k < 15.0 $Å^{-1}$ and 0.5< r < 3.5 Å; 23 allowed fitting parameters.

5.4.3 ACTIVITY OF HY ZEOLITE-SUPPORTED $Rh(CO)_2$ COMPLEXES IN NO-CO REACTION AT ELEVATED TEMPERATURES

Since zeolite-supported $Rh(CO)_2$ species do not exhibit activity in NO-CO reaction at ambient conditions, catalysts performance was evaluated at elevated temperatures. In order to reveal the temperature when catalysts start to exhibit activity, we conducted experiments in tubular plug flow reactor with 1000 ppm NO and 1000 ppm CO feed when the temperature was ramped with 10-15 ºC increment while products were analyzed on-line with a GC. We found that activities of HY30 and HY2.6-supported samples are very different. More specifically, the latter sample starts to show activity at 270 ºC while former is virtually inactive at this temperature. In order to compare both samples in a reaction while avoiding complications associated with possible structural changes of supported complexes during the heating in NO/CO mixture, we performed experiments when both samples were preheated to 270 ºC in He. Catalytic results presented in Figs. 5.5,5.6 demonstrate that HY2.6-supported catalyst exhibit induction period, more specifically, NO conversion increased from about 9 % to 100 % in 145 minutes. CO conversion started at about 4.9 % and leveled-off at roughly 80 % during the same time period. Finally, selectivity towards N_2 formation did not change substantially with TOS and was found at about 55 % throughout the experiment. In contrast, HY30-supported sample has no activity in the reaction at this temperature. When answering the question what is the primary reason for such different performance of both catalysts, one has to confirm that initial state of rhodium species (prior to reaction) on both supports is the same.

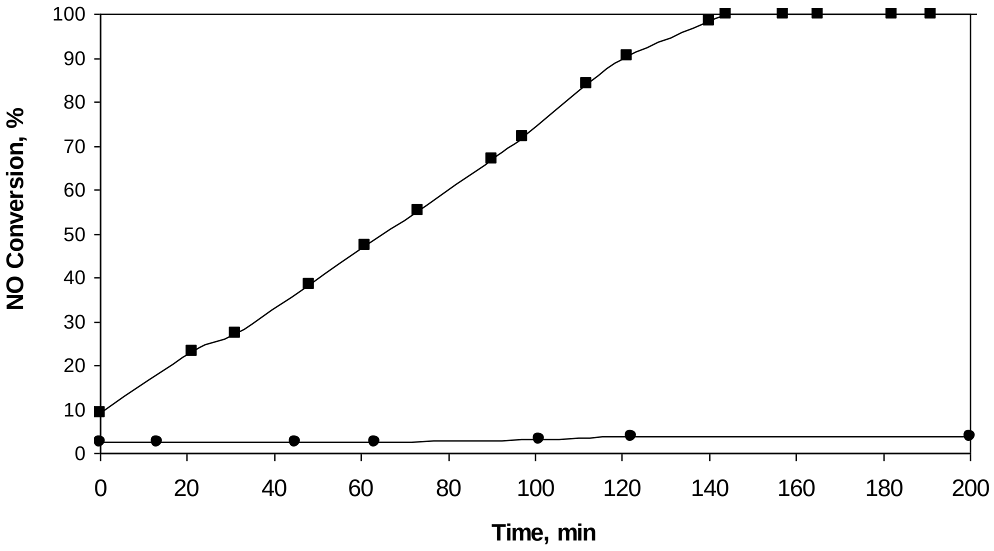

Figure 5.5 NO conversion with time for $Rh(CO)_2$/HY30 (●) and $Rh(CO)_2$/HY2.6 (■) samples during NO/CO reaction at 1000 ppm NO, 1000 ppm CO, 270 ºC.

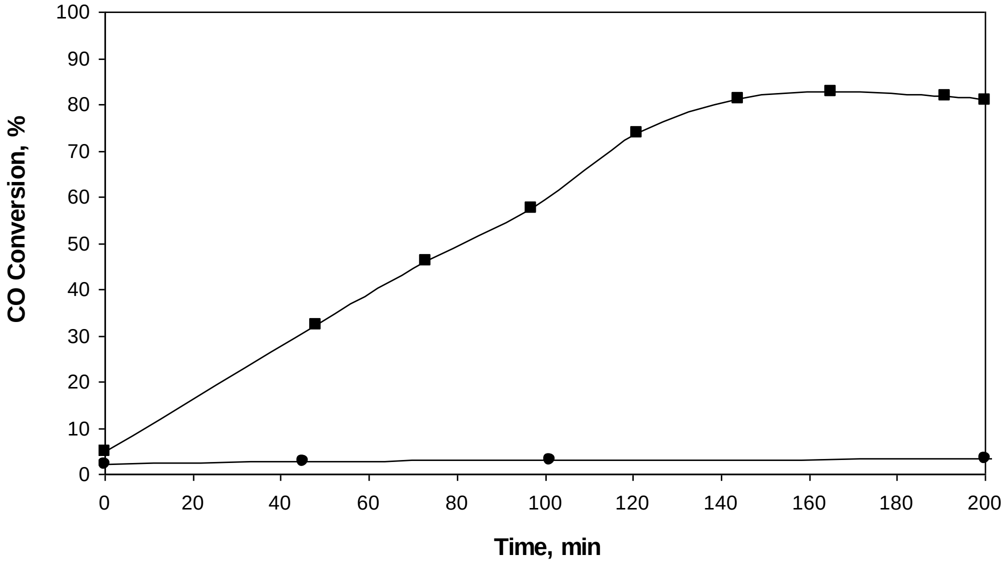

Figure 5.6 CO conversion with time for $Rh(CO)_2$/HY30 (●) and $Rh(CO)_2$/HY2.6 (■) samples during NO/CO reaction at 1000 ppm NO, 1000 ppm CO, 270 ºC.

EXAFS and FTIR data reported above indicate that substantial decarbonylation occurs in He at 300 ºC while at 200 ºC rhodium dicarbonyl species are fully intact. In order to determine weather supported $Rh(CO)_2$ complexes retain structural integrity at 270 ºC (before reaction starts), EXAFS measurements were performed. EXAFS data reordered at Rh K edge for $Rh(CO)_2$/HY30 sample which was heated in He to 270 ºC and kept for 1 hour at this temperature showed that rhodium dicarbonyl species are intact and, in contrast to sample treated at 300 ºC, no evidences of partial decarbonylation was revealed (Table 5.3, A). More specifically, Rh–C and Rh–O* contributions were characterized by coordination numbers of 1.9 and 1.7 at bonding distances of 1.83 Å and 2.97 Å, respectively. Rh atom in each complex was still bound to roughly two oxygens of support ($Rh\text{-}O_s$ coordination number is 2.2) suggesting that metal-support interface is also unaltered. We note that FTIR data not only confirm the presence rhodium dicarbonyls species at 270 ºC on the surface of the support but also suggest that their concentration did not change upon heating. (based on the integrated intensities of the correspondent v(CO) bands)

EXAFS measurements conducted on $Rh(CO)_2$/HY2.6 sample treated in similar way showed no Rh-Rh contribution indicating that rhodium aggregation did not occur (or, at least, did not occur to measurable extend) (Table 5.3, B). Rh–C and Rh–O* contributions were indentified with coordination numbers of 1.6 and 1.5, respectively pointing out to the presence of on average 2 carbonyl groups per one Rh atom. Metal-support interactions were also found essentially unchanged. It is important to emphasize that Type II species which initially account for almost 50 % of rhodium dicarbonyls on HY2.6 surface fully disappear at 270 ºC as indicated by FTIR spectrum. Besides, by comparing integrated intensities of Type I complexes in a sample at ambient temperature and after heating to 270 ºC, one can observe 44 % increase in the latter case (at T=270 ºC). Although the exact fate of rhodium carbonyls associated with Type II binding sites is not clear, we could infer based on this result that at least some fraction of them could be converted into Type I complexes at elevated temperatures.

Table 5.3 EXAFS structural parameters characterizing $Rh(CO)_2$/HY30 (A) $Rh(CO)_2$/HY2.6 (B) catalyst treated in He at 270 ºC for 1 h.

(A)

Support	Shell	*N*	*R* (Å)	$\Delta\sigma^2$ (Å^2)	ΔE_0 (eV)	ε_v^2	k^1-variances (%)	
							Im.	Abs.
270 ºC	Rh–Rh	--	--	--	--	2.7	2.4	3.5
	Rh–C*	1.9	1.84	0.00312	10			
	Rh–O*	1.7	2.97	0.00042	9.5			
	Rh–O$_{support}$							
	Rh–O$_s$	2.3	2.13	0.00029	-0.4			
	Rh–O$_l$	2.1	2.76	-0.00505	-8.9			

(B)

Support	Shell	*N*	*R* (Å)	$\Delta\sigma^2$ (Å^2)	ΔE_0 (eV)	ε_v^2	k^1-variances (%)	
							Im.	Abs.
270 ºC	Rh–Rh	--	--	--	--	10.6	3.3	4.9
	Rh–C*	1.6	1.83	0.00087	6.9			
	Rh–O*	2.2	2.97	0.004	7.6			
	Rh–O$_{support}$							
	Rh–O$_s$	2.1	2.16	0.00157	-6.9			
	Rh–O$_l$	2.2	2.79	-0.00246	-10			

Thus, rhodium species on both HY30 and HY2.6 supports remain mononuclear at the moment before NO and CO reagents are introduced into the reactor. In order to further understand the nature of different catalytic properties of these materials, we performed in-situ FTIR measurements under the reaction conditions.

FTIR spectra in the v(CO) and v(NO) region of HY30-supported sample before and right after introduction of 1000 ppm of NO and 1000 ppm of CO (balance He) mixture into the IR cell is presented in Fig. 5.7 Exposure to reactants immediately resulted in a decrease of v(CO) bands intensities and appearance of a new doublet at 1855 cm^{-1} and 1780 cm^{-1} indicating formation of $Rh(NO)_2$ complexes on the surface. Based on the integrated intensities of carbonyl features (before and after sample contact with reactants) we infer that the surface composition of rhodium dicarbonyls and dinitrosyls is correspondent to gas phase ratio of CO/NO concentrations and approximately constitute 50/50 % ratio. Similar picture in the first moments of the reaction was observed for HY2.6-supported sample. Both rhodium dicarbonyls and dinotrosyls were found to coexist on the surface. We emphasize that no bands were detected which could be indicative of mixed $Rh(CO)_x(NO)_y$ complexes on HY30 and HY2.6.

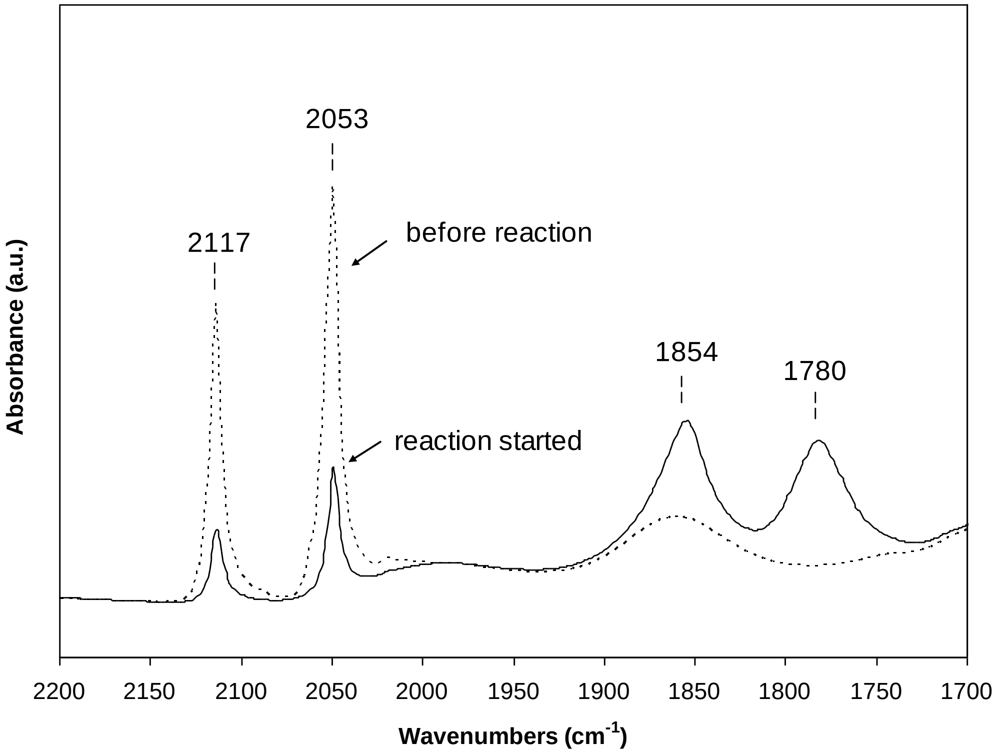

Figure 5.7 FTIR spectra in the v_{CO} and v_{NO} regions of $Rh(CO)_2$/HY2.6 sample in He (before reaction) and when 1000 ppm NO 1000 ppm CO was introduced into the cell (reaction started) at 270 ºC.

The striking difference in the surface chemistry between HY30 and HY2.6-supported samples could be revealed if difference spectra are plotted in time. More specifically, the spectrum collected right after reactants were introduced into the cell was subtracted from each consecutive spectrum collected every 5 minutes. Results presented in Figs. 5.8, 5.9 show spectacular difference in reactivities of HY30 and HY2.6-supported rhodium species. It is evident that bands at 2117 cm^{-1}, 2053 cm^{-1} and 1855 cm^{-1} and 1780 cm^{-1}, designating

$Rh(CO)_2$ and $Rh(NO)_2$ complexes, respectively, are rapidly loosing intensity with time in case of HY2.6-supported catalyst but remain unchanged in case of HY30-supported sample. Interestingly, disappearance of bands characterizing dicarbonyl and dinitrosyl species on the surface of HY2.6 zeolite was not accompanied by the evolution of any new features suggesting that these complexes are not converted into new intermediates but most likely decompose. Considering the literature reports which suggest that at elevated temperature CO could act as reducing agent [376-378], we propose that the major reason of decomposition of HY2.6-supported complexes could be their aggregation into rhodium particles. In order to understand weather rhodium aggregation is responsible for the induction period in the activity of the catalyst and observed changes in FTIR spectra, used samples (after the reaction) were analyzed with Scanning Transmission Electron Microscopy.

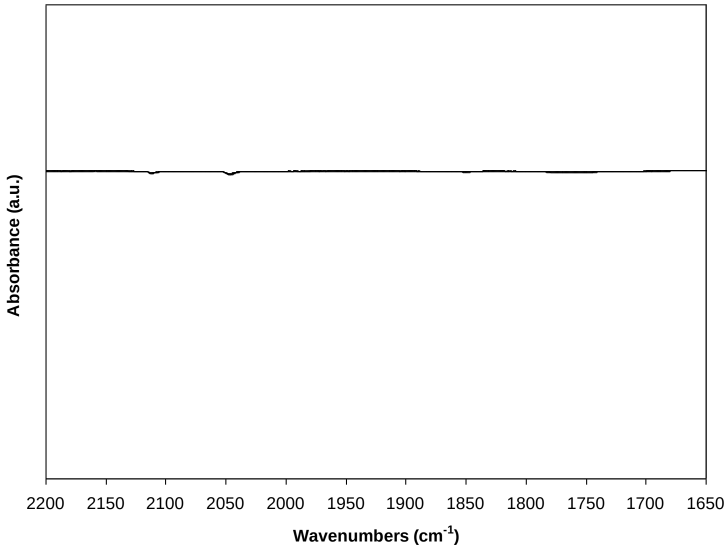

Figure 5.8 FTIR difference spectra in the v_{CO} and v_{NO} regions of $Rh(CO)_2$/HY30 sample collected during the reaction 200 min in 1000 ppm NO, 1000 ppm CO at 270 ^oC.

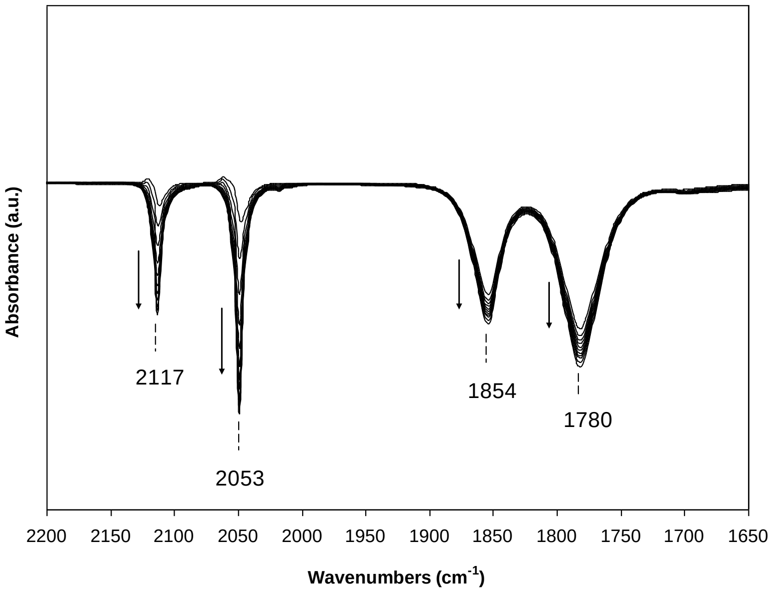

Figure 5.9 FTIR difference spectra in the v_{CO} and v_{NO} regions of $Rh(CO)_2$/HY2.6 sample collected during the reaction 200 min in 1000 ppm NO, 1000 ppm CO at 270 ºC.

Representative HRTEM images presented in Fig. 5.10 demonstrate that no particles of measurable size (resolution 1 Å) were formed on the surface of used HY30-supported sample while multiple particles were detected on the surface of HY2.6 zeolite after the reaction. The histogram of particle sizes distribution indicates that most of particles are in the range of 6 – 8 nm with the mean particle size approximately 7.2 Å. (Fig. 5.11) These results are consistent with FTIR data and suggest that decomposition of rhodium dicarbonyl and dinatrosyl complexes under the reaction conditions in case of HY2.6-supported catalyst is associated with rhodium aggregation. Therefore, we infer that the primary reason for such different catalytic activity of HY30 and HY2.6 supported samples is different structure of active sites on these supports. Reported data clearly suggest that Al content in HY zeolite framework has crucial influence on stability of supported rhodium species.

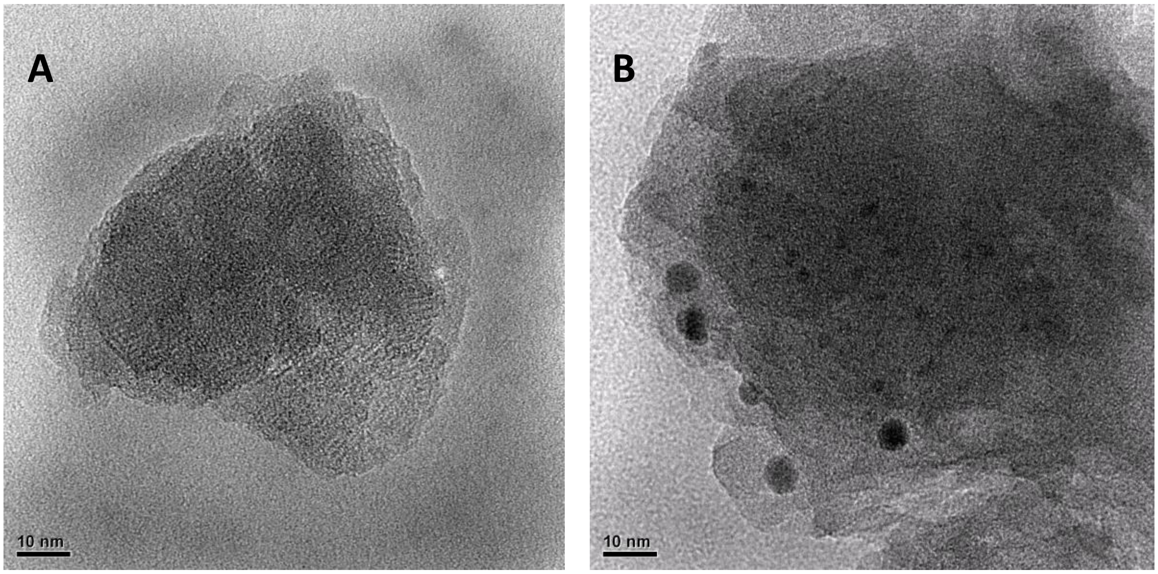

Figure 5.10 HRTEM images of used Rh(CO)$_2$/HY30 (A) and Rh(CO)$_2$/HY2.6 (B) samples (after reaction in 1000 ppm NO, 1000 ppm CO at 270 ºC for 200 min).

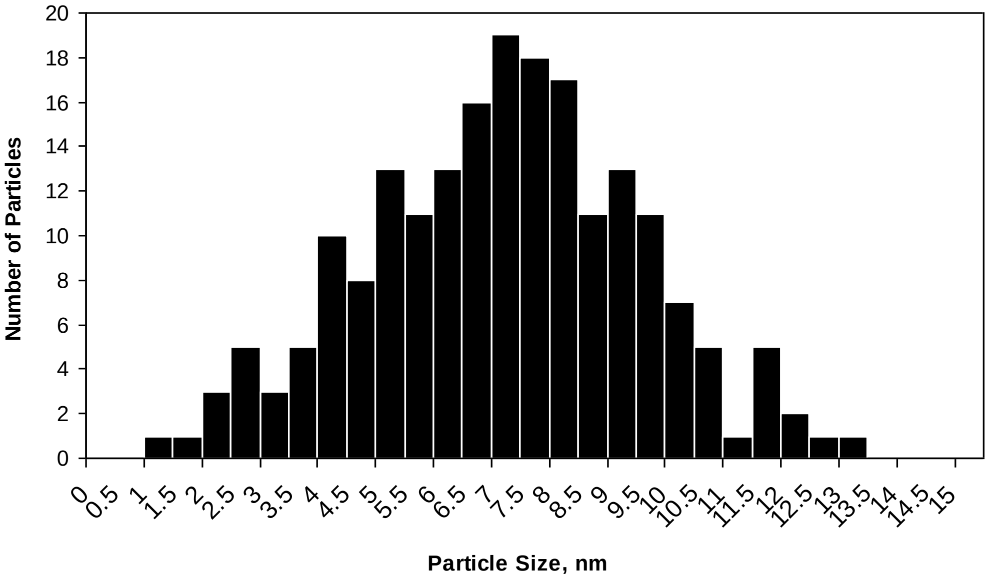

Figure 5.11 Particle size distribution histogram (175 particles counted) obtained from HRTEM measurements of used Rh(CO)$_2$/HY2.6 sample (after reaction in 1000 ppm NO, 1000 ppm CO at 270 ºC for 200 min).

Highly dealuminated zeolite (HY30) stabilizes rhodium complexes in mononuclear state even under reaction conditions at 270 ºC while Al rich zeolite clearly promotes rhodium agglomeration. One of the reasons that could explain these effects is inhomogeneous distribution of rhodium species in HY zeolite with high framework Al content. It is recognized that $Rh(CO)_2$ complexes find binding sites next to framework Al atoms due to excessive electronegativity of adjacent oxygens [63]. Increasing of amount of such Al sites ultimately leads to situation when instead of well spatially isolated binding sites for rhodium complexes, we have arrays of Al atoms which could be relatively close to each other reducing diffusion limitations for rhodium atoms under the reaction conditions. Alternatively, we have to acknowledge that HY2.6 zeolite initially has two types of binding sites for $Rh(CO)_2$ complexes where the second type is supposingly being associated with extraframework Al species [303]. Although we showed that $Rh(CO)_2$ species related to these sites posses of significantly different thermal stability and suggested that conversion of type II into type I species could occur upon heating, we can not exclude possibility that at least fraction of rhodium species experienced complete decarbonylation (during heating in He to 270 ºC) and remained “naked” on a surface before reaction was started. Such species are not stabilized by CO ligands and more likely to undergo agglomeration functioning as “seeds” for growing rhodium particles in the first moments of reaction.

One of the most obvious conclusions following our results is that single-site $Rh(CO)_2$/$Rh(NO)_2$ complexes do not promote NO reduction with CO. This inference contradict the work of Izuka et al who suggested that $Rh(CO)_2$/$Rh(NO)_2$ could be involved in catalytic cycle [372]. However, we note that the initial state of active sites (i.e., rhodium carbonyls) in our experiments and in experiments reported by Izuka et al is different. More specifically, this group reported two pairs of v(CO) bands characterizing $Rh(CO)_2$ complexes on the catalyst surface prior to the reaction (i.e., 2115 cm^{-1}, 2050 cm^{-1} and 2110 cm^{-1}, 2030 cm^{-1}) which could be indicative of rhodium species on inner and outer surface of zeolite while in our work it was shown that all Rh species are located in inner cavities. Homogeneous composition of supported rhodium carbonyls is important when investigating the active site structure since different reactivity and different surface chemistry could be reasonably expected on outer and inner zeolite surface.

Additionally, the sample was subject to high temperature pretreatment (350 ^oC for 3 h in vacuum) which do not exclude formation of small rhodium aggregates. Thus, the observed catalytic activity could be associated with NO–CO redox reaction cycle when Rh^0 and $Rh^{\delta+}$ species coexist on the surface. This scenario seems to be the most probable in our case as well. XPS measurements carried out on a used HY2.6 supported sample revealed both oxidized and reduced Rh species on the surface (Table 5.4). Although the nature of oxidized Rh species is not clear, it is evident that metallic rhodium sites are needed to promote NO/CO reaction. It is generally accepted that dissociation or recombination of NO molecules on the metallic surface are major pathways leading to adsorbed O atoms which further interact with adsorbed CO molecules yielding CO_2 [356] It is important to point out that CO molecules could be activated on rhodium particles where they present as linearly bound CO or on single rhodium sites where gem-dicorbonyl binding mode is preferential. In the latter case, however, $Rh(CO)_2$ complexes have to be in a close proximity to rhodium agglomerates where NO dissociation/recombination takes place. Thus, our data do not allow to differentiate between different mechanistic routes of NO/CO reaction, but clearly show that HY zeolite-supported single-site rhodium complexes do not facilitate reaction due to inability of these sites to dissociate/recombine NO molecules.

Table 5.4 XPS data characterizing $Rh(CO)_2$/HY2.6 sample before (fresh) and after (used) in CO/NO reaction (1000 ppm NO, 1000 ppm CO at 270 ºC for 200 min).

Sample	Rh $3d_{5/2}$, eV	FWHM, eV	Rh $3d_{3/2}$, eV	FWHM, eV
fresh	308.5	2.7	313.2	2.7
used	308.6	2.3	313.3	2.3
	307	1.4	311.7	1.4

5.5 CONCLUSIONS

Activity of HY30 (Si/Al =30) and HY2.6 (Si/Al=2.6) zeolite-supported single-site $Rh(CO)_2$ complexes in NO reduction with CO was investigated. At ambient conditions no reaction was observed between NO and CO but, instead, facile CO/NO ligands exchange occurred as evidenced by Fourier transform infrared spectroscopic (FTIR) and mass spectrometric measurements. When temperature was raised to 270 ºC, HY2.6 supported sample exhibited the transient period of about 145 minutes when NO conversion increased from approximately 9 % to 100 % while HY30 supported Rh species remained non-active at these conditions. In-situ FTIR measurements showed that the induction period in case of HY2.6 supported sample is associated with decomposition of $Rh(CO)_2$/$Rh(NO)_2$ complexes while these species were found fully intact on the surface of HY30 based sample under the reaction conditions. High resolution transition microscopy (HRTEM) experiments performed on used samples showed that rhodium particles were formed on the surface of HY2.6 zeolite (mean particle size 7.3 nm) and no particles were detected in case of HY30 support. These results clearly demonstrated that mononuclear single-site zeolite-anchored $Rh(CO)_2$/$Rh(NO)_2$ complexes do not facilitate NO reduction with CO and group of rhodium atoms (i.e., cluster, particle) is required to initiate and sustain NO/CO catalytic transformations. It is proposed that the major reason for the observed effects is inability of mononuclear rhodium species to dissociate/recombine NO molecules.

5.6 ACKNOWLEDGENETS

The authors gratefully acknowledge Clemson Electron Microscopy Laboratory and Dr. Haijun Qian for the help with High Resolution Transmisson Electron Microscopy (HRTEM) measurements. XAS data were collected at the Stanford Synchrotron Radiation Laboratory, a national user facility operated by

Stanford University on behalf of the U.S. Department of Energy, Office of Basic Energy Sciences. The assistance of the beam line staff at SSRL is gratefully acknowledged. The EXAFS data were analyzed with the XDAP software developed by XAFS Services International [148].

CHAPTER 6. CONCLUSIONS

Development of new efficient heterogeneous alternatives to highly active homogeneous catalysts has been an area of extensive research in both academic and industrial environments. Remarkable progress achieved in this direction indicated that supported single-site metal complexes are very promising materials with properties similar to their homogeneous counterparts. Among other complexes, rhodium carbonyls are especially important due to versatility of their catalytic implications and exceptional activity in a liquid phase. Although numerous attempts have been made to synthesize analogs of such species on solid supports, their surface chemistry remains unclear. We used HY zeolite-supported mononuclear rhodium dicarbonyl complexes and attempted to gain fundamental molecular level understanding of reactivity of their ligands, pathways of ligands catalytic transformations and effects of the support.

In Chapter 2, synthesis and characterization of dealuminated Y zeolite-supported well-defined rhodium monocarbonyl hydride species was performed. It was demonstrated that supported $Rh(CO)(C_2H_4)$ complexes are formed upon exposure of $Rh(CO)_2$ species to C_2H_4 at ambient conditions. These $Rh(CO)(C_2H_4)$ complexes can be selectively converted into mononuclear surface $Rh(CO)(H)_x$ species in H_2 flow. Structural characterization revealed that

$Rh(CO)(H)_x$ complexes are bound to two oxygen atoms of the zeolite framework and assume pseudo-trigonal bipyramidal or pseudo-octahedral geometry. Hydride ligands were found very reactive and can be displaced by CO or N_2 resulting in well-defined $Rh(CO)_2$ and $Rh(CO)(N_2)$ complexes. Additionally, it was shown that $Rh(CO)(H)_x$ complexes can function as active sites for ethylene hydrogenation reaction. More specifically, C_2H_4 reacts with hydride ligands to form ethane and unsaturated Rh(CO) species which interact with gas-pahse C_2H_4 yielding stable $Rh(CO)(C_2H_4)$ complexes.

In Chapter 3, effect of the support on reactivity of anchored $Rh(CO)_2$ was examined. The results indicated that two different types of grafted $Rh(CO)_2$ complexes can be obtained when dealuminated HY zeolites with various Si/Al ratios are used as supports. The Al content in a framework was found to have pronounced influence on the relative fractions of these species on the surface.

Experiments confirmed that neither water present in zeolites nor partially reacted precursor $Rh(CO)_2$(acac) complexes are responsible for the formation of different types of $Rh(CO)_2$ species. It was suggested that the existence of two types of zeolite-grafted $Rh(CO)_2$ complexes could be associated with the different nature of binding sites in dealuminated faujasites (i.e., nonframework Al species and a different distribution of Al in the zeolite framework). Although Rh atoms in both types of $Rh(CO)_2$ species have similar coordination environment, they were shown to posses slightly different electronic properties. As a result, these complexes exhibit different reactivities in a simple CO/C_2H_4 probe reaction. Alternatively, it was revealed that chemical properties of $Rh(CO)_2$ species can be altered when they coordinate strong electron donor ligands such as NH_3. These results clearly demonstrated that support acts as a ligand influencing electronic properties of Rh atoms in mononuclear complexes and, consequently, their reactivities.

In Chapter 4, catalytic activity of supported $Rh(CO)_2$ complexes in ethylene hydrogenation and ethylene dimerization reactions was investigated. The results confirmed the crucial role of the support in catalysis. More specifically, it was found that HY zeolite-grafted rhodium carbonyl complexes are active in both ethylene hydrogenation and dimerization at ambient conditions while Al_2O_3 supported species exhibits no activity. Kinetic data complimented by FTIR spectroscopy results revealed that when HY zeolite is used as a support hydrogenation and dimerization processes are coupled and probably involve same surface species as intermediates. Furthermore, it was demonstrated that acidic hydroxyl groups present on the zeolite surface cooperate with grafted rhodium species in C-C bond formation mechanism confirming the bifunctional properties of the catalyst. Finally, by taking advantage of the molecular nature of HY zeolite-supported $Rh(CO)_2$ complexes, we showed that selectivity of the catalyst in ethylene hydrogenation/dimerization reactions can be tuned by blocking available coordination sites on Rh. This was achieved by performing surface reaction between rhodium dicarbonyls and $[Au(CN)_2]^-$ species which resulted in the formation of chain type Au-CN-$Rh(CO)_2$-NC-Au- structures. The modified catalyst retained activity in ethylene hydrogenation but was found fully inactive in dimerization reaction.

In Chapter 5, catalytic properties of HY zeolite-supported $Rh(CO)_2$ complexes in NO-CO reaction were explored. At room temperature CO/NO ligands exchange occurred and no activity towards formation of CO_2, N_2, or N_2O was observed. When temperature was raised to 270 ºC (rhodium carbonyls are still mononuclear at this temperature), catalytic properties were found to be highly affected by the Al content in the HY zeolite framework. Sample prepared by anchoring $Rh(CO)_2$ species on Al rich zeolite (Si/Al = 2.6) showed a transient period in activity in about 145 minutes when NO conversion increased from approximately 9 % to 100 % while dealuminated zeolite-supported rhodium species were fully inactive. *In situ* FTIR experiments and HRTEM measurements of used materials indicated that the observed transient period is associated with Rh aggregation and the actual active site for NO/CO reaction involves a metallic surface. Thus, single-site Rh complexes which are stabilized on dealuminated HY zeolite even at elevated temperatures were found unable to promote NO/CO reaction confirming the structure-sensitive character of NO/CO transformation.

REFERENCES

[1] R.I. Wijngaarden, K.R. Westerterp, A. Kronberg, “Industrial Catalysis: Optimizing Catalysts and Processes”, WILEY-VCH, Weinheim, 1998.

[2] C.H. Bartholomew, R.J. Farrauto, “Fundamentals of Industrial Catalytic Processes”, WILEY-INTERSCIENCE, Hoboken, New Jersey, 2006.

[3] D.J. Adams, P.J. Dyson and S.J. Taverner, Chemistry in Alternative Reaction Media, John Wiley & Sons Ltd, Chichester, 2004.

[4] Shang-Tian Yang, Hesham El Enshasy, Nuttha Thongchul, Bioprocessing Technologies in Biorefinery for Sustainable Production of Fuels, Chemicals, and Polymers, John Wiley & Sons Inc, Hoboken, 2013

[5] H. Sugiyama, F. Uemura, N. Yoneda, T. Minami, T. Maejima, K. Hamato, Japan Patent 235250 (1997).

[6] D.J. Cole-Hamilton, Science 299 (2003) 1702.

[7] J.M. Fraile, J.I. Garcia, C.I. Herrerias, J.A.M. and E. Pires, Chemical Society Reviews 2009 (38) 695.

[8] A. Choplin, F. Quignard, Coordination Chemistry Reviews 178–180 (1998) 1679.

[9] G.A. Ozin, C. Gil, Chemical Reviews 89 (1989) 1749.

[10] S.M.C. Neiva, J.A.V. Santos, J.C. Moreira, Y. Gushikem, H. Vargas, D.W. Franco, Langmuir 9 (1993) 2982.

[11] J.C. Hicks, B.A. Mullis, C.W. Jones, Journal of American Chemical Society 129 (2007) 8426.

[12] J.F. Dıaz, K.J. Balkus, Journal of Chemical Materials 9 (1997) 61.

[13] P. Sutra, D. Brunel, Chemical Communications (1996) 2485.

[14] P. Hernan, C. del Pino, E. Ruiz-Hitzky, Chemical Materials 4 (1992) 49.

[15] A.M. Liu, K. Hidajat, S. Kawi, Journal of Molecular Catalysis A: Chemical 168 (2001) 303.

[16] H. Zhao, J. Peng, M. Cai, Catalysis Letters 142 (2012) 138.

[17] Y. I. Yermakov, B. N. Kuznetsov, V. A. Zakharov, "Catalysis by Supported Complexes", Elsevier, Amsterdam, 1981.

[18] H. C. Foley, S. J. DeCanio, K. D. Tau, K. J. Chao, J. H. Onuferko, Cecil Dybowski, B. C. Gates, Journal of the American Chemical Society 105 (1983) 3074.

[19] P. Dufour, C. Houtman, C.C. Santini, C. Ndez, J.M. Basset, L.Y. Hsuf, S.G. Shore, Journal of the American Chemical Society 114 (1992) 4248.

[20] M.D. Ward, J.J. Schwartz, Journal of Molecular Catalysis 11 (1981) 397.

[21] M.D. Ward, J.J. Schwartz, Journal of the American Chemical Society 103 (1981) 5253.

[22] S.L. Scott, M. Szpakowicz, A. Mills, C.C. Santini, Journal of the American Chemical Society 120 (1998) 1883.

[23] W.A. Herrmann , A.W. Stumpt, T. Priermeier, S. Bogdanovic, V. Dufaud, J.-M. Basset, Angewandte Chemie International Edition 35 (1997) 2803.

[24] F. Blanc, M. Chabanas, C. Coperet, B. Fenet, E. Herdweck, Journal of Organometallic Chemistry 690 (2005) 5014.

[25] Q. Yang , C. Coperet, C. Li, J.-M. Basset, New Journal of Chemistry 27 (2003) 319.

[26] M. Chabanas, C. Coperet, J.-M. Basset, Chemistry - A European Journal 9 (2003) 971.

[27] X. Solans-Monfort, E. Clot, C. Coperet, O. Eisenstein, Organometallics 24 (2005) 1586.

[28] X. Solans-Monfort, J.-S. Filhol, C. Coperet, O. Eisenstein, New Journal of Chemistry 30 (2006) 842.

[29] E. Le Roux, M. Taoufik, M. Chabanas, D. Alcor, A. Baudouin, C. Coperet, J. Thivolle - Cazat, J.-M. Basset, A. Lesage, S. Hediger, L. Emsley, Organometallics 24 (2005) 4274.

[30] E. Le Roux, M. Taoufik, C. Coperet, A. de Mallmann, J. Thivolle-Cazat, J.-M. Basset, B.M. Maunders, G.J. Sunley, Angewandte Chemie International Edition 44 (2005) 6755.

[31] E. Le Roux, M. Taoufik, A. Baudouin, C. Coperet, J. Thivolle-Cazat, J.-M. Basset, B.M. Maunders, G.J. Sunley, Advanced Synthesis & Catalysis 349 (2007) 231.

[32] L. Lefort, M. Chabanas, O. Maury, D. Meunier, C. Coperet, J. Thivolle-Cazat, J.-M. Basset, Journal of Organometallic Chemistry 593 - 594 (2000) 96.

[33] V. Dufaud, G.P. Niccolai, J. Thivolle-Cazat, J.-M. Basset, Journal of the American Chemical Society 117 (1995) 4288.

[34] V. Vidal, A. Theolier, J. Thivolle-Cazat, J.-M. Basset, J. Corker, Journal of the American Chemical Society 118 (1996) 4595.

[35] C. Rosier, G.P. Niccolai, J.-M. Basset, Journal of the American Chemical Society 119 (1997) 12408.

[36] F. Bini, C. Rosier, R.P. Saint-Arroman, E. Neumann, C. Dablemont, A. de Mallmann, F. Lefebvre, G.P. Niccolai, J.-M. Basset, M. Crocker, J.K. Buijink, Organometallics 25 (2006) 3743.

[37] U. Romano, Gicrnale di Chimica Industriale 83 (2001) 30.

[38] J. Corker, F. Lefebvre, C. Lecuyer, V. Dufaud, F. Quignard, A. Choplin, J. Evans, J.-M. Basset, Science 271 (1996) 966.

[39] F. Rascon, R. Wischert, C. Coperet, Chemical Science 2 (2011) 1449.

[40] M. Chabanas, A. Baudouin, C. Copeeret, J.-M. Basset, Journal of the American Chemical Society 123 (2001) 2062.

[41] M. Chabanas, A. Baudouin, C. Copeeret, J.-M. Basset, W. Lukens, A. Lesage, S. Hediger, L. Emsley, Journal of the American Chemical Society 125 (2003) 492.

[42] A.Rost, H. Schneider, J.P. Zoller, W.A. Herrmann, F.E. Kuhn, Journal of Organometallic Chemistry 690 (2005) 4712.

[43] P. Van Der Voort, M.B. Mitchell, E.F. Vansant, M.G. White, Interface Science 179 (1997) 5.

[44] K. Nakamoto, A.E. Martell, Journal of Chemical Physics 32 (1960) 588.

[45] M. Mikami, I. Nakagawa, T. Shimanouchi, Spectrochimica Acta 23A (1967) 1037.

[46] H. Junge and H. Musso, Spectrochimica Acta 24A (1968) 1219.

[47] I. Jonas, B. Norden, Spectrochimica Acta 32A (1976) 427.

[48] B. Vlckova, B. Strauch, M. Horak, Collection of Czechoslovak Chemical Communications 50 (1985) 306.

[49] J.A. Bertrand, J.A. Kelley, Inorganica Chimica Acta 4 (1970) 203.

[50] K.E. Lawson, Spectrochimica Acta 17 (1961) 248.

[51] J.C. Kenvin, Ph.D. Thesis, Georgia Institute of Technology (1991).

[52] P. Van Der Voort, K. Possemiers, E.F. Vansant, Journal of the Chemical Society Faraday Transactions 5 (1996) 843.

[53] S.N.R. Rao, E. Waddell, M.B. Mitchell, M.G. White, Journal of Catalysis 163 (1996) 176.

[54] M.B. Mitchell, V.R. Chakravarthy, M.G. White, Langmuir 10 (1994) 4523.

[55] J.C. Kenvin, M.G. White, “Preparation and Characterization of Supported Mononuclear Metal Complexes as Model Complexes” 198th ACS National Meeting, Miami Beach, FL, 1989.

[56] J.C. Kenvin, M.G. White, M.B. Mitchell, “Hydrogen Bonding of Mononuclear Metal Complexes to Cab-O-Sil”, 200th ACS National Meeting, Washington, D.C., 1990.

[57] J.C. Kenvin, M.G. White, M.B. Mitchell, Langmuir 7 (1991) 1198.

[58] M. Baltes, O. Collart, P. Van Der Voort, E.F. Vansant, Langmuir 15 (1999) 5841.

[59] J. Guzman, B.C. Gates, Langmuir 19 (2003) 3897.

[60] I. Ogino, B.C. Gates, Journal of the American Chemical Society 130 (2008) 13338.

[61] I. Ogino, B.C. Gates, Journal of Physical Chemistry C 114 (2010) 2685.

[62] I. Ogino, C.-Y. Chen, B.C. Gates, Dalton Transactions 39 (2010) 8423.

[63] J.F. Goellner, B.C. Gates, G.N. Vayssilov, N. Rosch, Journal of the

American Chemical Society 122 (2000) 8056.

[64] A.J. Liang, V.A. Bhirud, J.O. Ehresmann, P.W. Kletnieks, J.F. Haw, B.C. Gates, Journal of Physical Chemistry B 109 (2005) 24236.

[65] A. Uzun, V.A. Bhirud, P.W. Kletnieks, J.F. Haw, B. C. Gates Journal of Physical Chemistry C 111 (2007) 15064.

[66] Z. Huang, M. Brookhart, A.S. Goldman, S. Kundu, A. Ray, S.L. Scott, B. C. Vicente, Advanced Synthesis & Catalysis, 351 (2009) 188.

[67] C. Johannes, Catalysis Today 51 (1999) 289.

[68] B.C. Vicente, R.C. Nelson, A.W. Moses, S. Chattopadhyay, S.L. Scott, Journal of Physical Chemistry C 115 (2011) 9012.

[69] G.-J. Li, T. Fujimoto, A. Fukuoka, M. Ichikawa, Studies in Surface Science and Catalysis 75 (1993), 1607.

[70] K.K. Bania, R.C. Deka, Journal of Physical Chemistry C 115 (2011) 9601.

[71] Tierney J. P., Lidstrom P. Eds “Microwave Assisted Organic Synthesis” Blackwell Publishing and CRC Press: Oxford, U.K. and Boca Raton, FL, 2005.

[72] A. Corma, H. Garcia, European Journal of Inorganic Chemistry (2004) 1143.

[73] N. Herron, Inorganic Chemistry 25 (1986) 4714.

[74] L. Gaillion, N. Sajot, F. Bedioui, J. F. Devynck, K.J. Balkus Jr, Journal of Electroanalytical Chemistry 345 (1993) 157.

[75] C. Bowers, P.K. Dutta, Journal of Catalysis 122 (1990) 271.

[76] K.J. Balkus Jr, A.A. Welch, B.E. Gnade, Zeolites 19 (1990) 722.

[77] S. Kowalak, R.C. Weiss, K.J. Balkus Jr, Journal of the Chemical Society Chemical Communications (1991) 57.

[78] D.E. De Vos, E.J.P. Feijen, R.A. Schoonheydt, P.A. Jacobs, Journal of the American Chemical Society 116 (1994) 4146.

[79] T. Joseph, D. Srinivas, C.S. Gopinath, Halligudi, Catalysis Letters 83 (2002) 209.

[80] K.K. Bania, R.C. Deka, Journal of Physical Chemistry C 117 (2013) 11663.

[81] Y.Y. Zakharov, B.V. Romanovsky, Vestnik Moskovskogo Universiteta, Seriya 2: Khimiya 18 (1977) 142.

[82] B.V. Romanovsky, A.G. Gabrielov, Journal of Molecular Catalysis 74 (1992) 293.

[83] K.J. Balkus Jr, I.P Ferraris, Journal of Physical Chemistry 94 (1990) 8019.

[84] M. Ichikawa, L. F. Rao, N. Kosugi, A. Fukuoka, Journal of the Chemical Society Faraday Transactions 87 (1989) 232.

[85] G.C. Shen, A. Liu, M. Ichikawa, Journal of the Chemical Society, Faraday Transactions 94 (1998) 1353.

[86] G. J. Li, T. Fujimoto, A. Fukuoka, M. Ichikawa, Journal of the Chemical Society, Chemical Communications (1991) 1337.

[87] N. Herron, G.D. Stucky, C.A. Tolman, Inorganica Chimica Acta 100 (1985) 135.

[88] G.C. Chen, T. Shdo, M. Ichikawa, Journal of Pbs. Chemistry 100 (1996) 16947.

[89] R. Raja, P. Ratnasamy, Applied Catalysis A: General 158 (1997) L7.

[90] M. Ichikawa, Advances in Catalysis (1992) 283.

[91] A. Kulkarni, R.J. Lobo-Lapidus, B.C. Gates, Chemical Communications 46 (2010) 5997.

[92] Y. Okamoto, A. Maezawa, H. Kane, T. Imanaka, Journal of the Chemical Society, Chemical Communications (1988) 380.

[93] C.-F. Cheng, J. Klinowski, Journal of the Chemical Society, Faraday Transactions 92 (1996) 289.

[94] C.-F. Cheng, H. He, W. Zhou, J. Klinowski, J.A. Sousa Goncalves, L.F. Gladden, Journal of Physical Chemistry 100 (1996) 390.

[95] Z.Y. Yuan, S.H. Liu, T.H. Chen, J.Z. Wang, H.X. Li, Journal of the Chemical Society, Chemical Communications (1995) 973.

[96] N.-Y. He, S.-L. Bao, Q.-H. Xu, Studies in Surface Science and Catalysis 105 (1997) 85.

[97] A. Corma, M.T. Navarro, J. Perez-Pariente, Journal of the Chemical Society, Chemical Communications (1994) 147.

[98] A. Corma, M.T. Navarro, J. Perez-Pariente, F. Sanchez, Studies in Surface Science and Catalysis 84 (1994) 69.

[99] O. Franke, J. Rathouski, G. Schulz-Ekloff, J. Starek, Z. Zukal, Studies in Surface Science and Catalysis 84 (1994) 77.

[100] K.M. Reddy, I.L. Moudrakovski, A. Sayari Studies in Surface Science and Catalysis 98 (1995) 19.

[101] A. Sayari, V.R. Karra, J.S. Reddy, I.L. Moudrakovski, Materials Research Society Symposium Proceedings 371 (1995) 81.

[102] K.M. Reddy, I. Moudrakovski, A. Sayari, Journal of the Chemical Society, Chemical Communications (1994) 1059.

[103] Z. Luan, J. Xu, H. He, J. Klinowski, L. Kevan, Journal of Physical Chemistry 100 (1996) 19595.

[104] S. Gontier, A. Tuel, Applied Catalysis A: General 143 (1996) 125.

[105] A. Tuel, S. Gontier, R. Teissier, Journal of the Chemical Society, Chemical Communications (1996) 651.

[106] T.K. Das, K. Chaudari, A.J. Chandwadkar, S. Sivasanker, Journal of the Chemical Society, Chemical Communications (1995) 2495.

[107] J.M. Thomas, J.C. Hernandez-Garrido, R.G. Bell, Topics in

Catalysis 52 (2009)1630.

[108] R. Raja In: Harris KDM, Edwards PP (eds) “Turning points in solid state, materials and surface science”. RSC, Cambridge, 2008, 623.

[109] S.O. Lee, R. Raja, K.D.M. Harris, J.M. Thomas, B.F.G. Johnson, G. Sankar, Angewandte Chemie International Edition 42 (2003) 1520.

[110] R. Raja, J.M. Thomas, Solid State Sciences 8 (2008) 326.

[111] A.C. Yang, C.W. Garald, Journal of Physical Chemistry 61 (1957) 1504.

[112] J.T. Yates, T.M. Duncan, S.D. Worley, R.W. Vaughan, Journal of Chemical Physics 70 (1979) 1219.

[113] J.T. Yates, T.M. Duncan, R.W. Vaughan, Journal of Chemical Physics 71 (1979) 3908.

[114] R.R. Cavanagh, J.T. Yates, Journal of Chemical Physics 74 (1981) 4150.

[115] M. Primet, Journal of the Chemical Society Faraday Transactions 74 (1978) 2570.

[116] M. Primet, E. Garbowski, Chemical Physics Letters 72 (1980) 472.

[117] M. Primet, J.C. Vedrine, C. Naccache, Journal of Molecular Catalysis 411 (1978) 4.

[118] H.F.J. Van’t Bilk, J.B.A.D. Van Zon, T. Hulzinga, J.C. Vis,

D.C. Konigsberger, R. Prins, Journal of Physical Chemistry 87 (1983) 2264.

[119] E.A. Hyde, R. Rudhow, C.H. Rochester, Journal of the Chemical Society, Faraday Transactions 79 (1983) 2405.

[120] F. Solymosi, A. Erdohelyi, T. Bansagi, Journal of the Chemical Society Faraday Transactions 77 (1981) 2645.

[121] S.D. Worley, C.A. Rice, G.A. Mattson, C.W. Curtis, J.A. Guln, A.R. Tarrer, Journal of Physical Chemistry 86 (1982), 2714.

[122] H. Arai, H. Tominaga, Journal of Catalysis 43 (1976) 131.

[123] D.J.C. Yates, L.L. Murrell, E.B. Prestridge, Journal of Catalysis 57 (1979) 41.

[124] A. Erdöhelyi, F. Solymosi, Journal of Catalysis 84 (1983) 446.

[125] H. Miessner, I. Burkhardt, D. Gutschick, A. Zecchina, C.Morterra, G. Spoto, Journal of the Chemical Society, Faraday Transactions 85 (1989) 2113.

[126] I. Burkhardt, D. Gutschick, U. Lohse, H. Miessner, Journal of the Chemical Society, Chemical Communications (1987) 291.

[127] R. V. Chaudhari, Topics in Catalysis 55 (2012) 439.

[128] K. Riener, M. Högerl, P. Gigler, F. E. Kühn, ACS Catalysis 2 (2012) 613.

[129] D.K. Dutta, B. Deb, Coordination Chemistry Reviews 255 (2011) 1686.

[130] G.P. Chiusoli, P.M. Maitlis (Eds.), Metal-catalysis in Industrial Organic Processes, RSC Publishing, Cambridge, 2006.

[131] T.W. Bell, D. M. Haddleton, A. McCamley, M. G. Partridge, R. N. Perutz, H. J. Willner, Journal of the American Chemical Society 112 (1990) 9212.

[132] T.M. Douglas, S. K. Brayshow, R. Dallanegra, G. Kociok-Köhn, S. A. Macgregor, G. L. Moxham, A. S. Weller, T. Wondimagegn, P. Vadivelu, Chemistry - A European Journal 14 (2008) 1004.

[133] A.M. Trzeciak, J. J. Ziółkowski, Journal of Organometallic Chemistry 429 (1992) 239.

[134] T. Yoshida, D. L. Thorn, T. Okano, J. A. Ibers, S. Otsuka, Journal of the American Chemical Society 101 (1979) 4212.

[135] D.Y. Zhao, D. Goldfarb, Journal of Chemical Society, Chemical Communications (1995) 875.

[136] S.D. Worley, G. A. Mattson, R. Caudill, Journal of Physical Chemistry 87 (1983) 1671.

[137] M.A. Henderson, S.D. Worley, Jornal of Physical Chemistry 89 (1985) 1417.

[138] M.L. McKee, C.H. Dai, S.D. Worley, Journal of Physical Chemistry 92 (1988) 1056.

[139] X. Wang, L. Andrews, Journal of Physical Chemistry A 106 (2002) 3706.

[140] T. Iizuka, Y. Tanaka, Journal of Catalysis 70 (1981) 449.

[141] T. Iizuka, Y. Tanaka, K. Tanabe, Journal of Catalysis 76 (1982) 1.

[142] H. Miessner, Journal of the American Chemical Society 116 (1994) 11522.

[143] G.N. Vayssilov, N. Rösch, Journal of the American Chemical Society 124 (2002) 3783.

[144] X. Wang, E.A. Wovchko, Journal of Physical Chemistry B 109 (2005) 16363.

[145] R. E. Jentoft, S. E. Deutsch, B. C. Gates, Review of Scientific Instruments 67 (1996) 2111.

[146] F.B.M. Duivenvoorden, D.C. Koningsberger, Y.S. Uh, B.C. Gates, Journal of the American Chemical Society 108 (1986) 6254.

[147] W. F. Weber, B. C. Gates, Journal of Physical Chemistry B 101 (1997) 10423.

[148] M. Vaarkamp, J.C. Linders, D.C. Koningsberger, Physica B 209 (1995) 159.

[149] E. A. Stern, Physical Review B 48 (1993) 9825.

[150] E.O. Brigham, The Fast Fourier Transform, Prentice Hall, Englewood Cliffs, NJ, 1974.

[151] P.S. Kirlin, F.B.M. van Zon, D. C. Koningsberger, B. C. Gates, Journal of Physical Chemistry 94 (1990) 8439.

[152] J.B.A.D. van Zon, D. C. Koningsberger, H.F.J. van’t Blik, D.E. Sayers, Journal of Chemical Physics 82 (1985) 5742.

[153] M. Vaarkamp, Ph.D. Thesis, Eindhoven University, The Netherlands, 1993.

[154] F. W. Lytle, D. E. Sayers, E. A. Stern, Physica B 158 (1988) 701.

[155] D.C. Koningsberger, B.L. Mojet, G.E. van Dorssen, D.E. Ramaker, Topics in Catalysis 10 (2000) 143.

[156] X. Yuan, S. Bi, Y. Ding, L. Liu, M. Sun, Journal of Organometallic Chemistry 695 (2010) 1576.

[157] H. Miessner, Journal of Chemical Society, Chemical Communications (1994) 927.

[158] A.J. Liang, B.C. Gates, Journal of Physical Chemistry C 112 (2008) 18039.

[159] A.J. Liang, R. Craciun, M. Chen, T.G. Kelly, P.W. Kletnieks, J.F. Haw, D. A. Dixon, B. C. Gates, Journal of the American Chemical Society 131 (2009) 8480.

[160] C.C. Santini , S.L. Scott, J.-M.Basset. Joumal of Molecular Catalysis A: Chemical 107 (1996) 263.

[161] D. Moigno, B. Callejas-Gaspar, J. Gil-Rubio, H. Werner, W. Kiefer, Journal of Organometallic Chemistry 661 (2002) 181.

[162] J. Zhang, X.-Z. Sun, M. Poliakoff, M. W. George, Journal of Organometallic Chemistry 678 (2003) 128.

[163] F. Huq, A. C. Skapski, Journal of Crystal and Molecular Structure 4 (1974) 411.

[164] H.E. Fischer, S.A. King, J.B. Miller, J.Y. Ying, J.B. Benziger, J. Schwartz, Inorganic Chemistry 30 (1991), 4403.

[165] M. Bühl, M. Håkansson, A. H. Mahmoudkhani, L. Öhrström, Organometallics 19 (2000) 5589.

[166] I. Ogino, B. C. Gates, Journal of Physical Chemistry C 114 (2010) 8405.

[167] J.C. Fierro-Gonzalez, S. Kuba, Y. Hao, B.C. Gates, Journal of Physical Chemistry B 110 (2006) 13326.

[168] H.Werner, M. Bosch, M.E. Schneider, C. Hahn, F. Kukla, M. Manger, B. Windmüller, B. Weberndörfer, M. Laubender, Journal of Chemical Society, Dalton Transactions (1998) 3549.

[169] L. Vaska, Journal of the American Chemical Society 88 (1966) 4100.

[170] A. Vigalok, Y. Ben-David, D. Milstein, Organometallics 15 (1996) 1839.

[171] M.J. Ingleson, S.K. Brayshaw, M.F. Mahon, G.D. Ruggiero, A.S. Weller, Inorganic Chemistry 44 (2005) 3162.

[172] C. Bianchini, C. Mealli, M. Peruzzini, F. Zanobini, Journal of the American Chemical Society 109 (1987) 5548.

[173] A. Angelini, M. Aresta, A. Dibenedetto, C. Pastore, E. Quaranta, M.R. Chierotti, R. Gobetto, I. Papai, C. Graiff, A. Tiripicchio, Dalton Transactions (2009) 7924.

[174] G. Kubas, C. J. Unkefer, B. I. Swanson, E. Fukushima, Journal of the American Chemical Society 108 (1986) 7000.

[175] B. Rybtchinski, Y. Ben-David, D. Milstein, Organometallics 16 (1997) 3786.

[176] G. J. Kubas, Proceedings of National Academy of Sciences USA 104 (2007) 6901.

[177] A.A. Oswald, D.E. Hendriksen, R.V. Kastrup, E.J. Mozeleski, Advances in Chemistry Series 230 (1992) 395.

[178] M. Sparta, K.J. Børve, V.R. Jensen, Journal of the American Chemical Society 129 (2007) 8487.

[179] F. H. Jardine, Polyhedron 1 (1982) 569.

[180] A. M. Argo, B. C. Gates, Journal of Physical Chemistry B 107 (2003) 5519.

[181] D. Evans, J.A. Osborn, G. Wilkinson, Journal of Chemical Society (1968) 3133.

[182] R. Franke, D. Selent, A. Börner, Chemical Reviews 112 (2012) 5675.

[183] R.E. Harmon, S.K. Gupta, D.J. Brown, Chemical Reviews 73 (1973) 21.

[184] A.Yu. Stakheev, L.M. Kustov, Applied Catalysis A 188 (1999) 3.

[185] V.E. Henrich, Reports on Progress in Physics 48 (1985) 1481.

[186] G.A. Somorjai, J.Y. Park, Angewandte Chemie International Edition 47 (2008) 9212.

[187] R. Petroff Saint-Arroman, M. Chabanas, A. Baudouin, C. Coperet, J.-M. Basset, A. Lesage, L. Emsley, Journal of the American Chemical Society 123 (2001) 3820.

[188] F. Blanc, C. Coperet, J. Thivolle-Cazat, J.-M. Basset, A. Lesage, L. Emsley, A. Sinha, R.R. Schrock, Angewandte Chemie International Edition 45 (2006) 1216.

[189] H.E. Maneck, D. Gutschick, I. Burkhardt, B. Luecke, H. Miessner, U. Wolf, Catalysis Today 3 (1988) 421.

[190] E.J. Rode, M.E. Davis, B.E. Hanson, N. Rosch, Journal of Catalysis 96 (1985) 574.

[191] R.D. Shannon, J.C. Vedrine, C. Naccache, F. Lefebvre, Journal of Catalysis 88 (1984) 431.

[192] T.T.T Wong, A.Yu. Stakheev, W.M.H. Sachtler, Journal of Physical Chemistry 96 (1992) 7733.

[193] H. Miessner, D. Gutschick, H. Ewald, H. Muller, Journal of Molecular Catalysis 36 (1986) 359.

[194] F. Lefebvre, P. Gelin, B. Elleuch, Y. Diab, Y. Ben Taarit, Studies in Surface Science and Catalysis 18 (1984) 257.

[195] J.P. Fackler, Progress in Inorganic Chemistry 7 (1966) 361.

[196] F.R. Clarke, J.F. Stienback, W.F. Wagner, Journal of Inorganic and Nuclear Chemistry 26 (1964) 1311.

[197] S. Ooi, Q. Fernando, Chemical Communications (1967) 532.

[198] J.A.R. van Veen, P.C. De Jong-Versloot, G.M.M. van Kessel, F.J. Fels, Thermochimica Acta 152 (1989) 359.

[199] J.P. Boitiaux, J. Cosyns, M. Derrier, G. Leger, Hydrocarbon Processing (1985) 51.

[200] A.D.K. Logan, K. Sharoudi, A.K. Datye, Journal of Physical Chemistry 95 (1991) 5568.

[201] B.M. Weckhunsen, R. Ramachandra Rao, J. Pelgrims, R.A. Schoonheydt, P. Bodart, G.Debras, O. Collart, P. Van Der Voort, E.F. Vansant, Chemistry - A European Journal 6 (2006) 2060.

[202] P. Van Der Voort, R. van Welzenis, M. de Ridder, H. H. Brongersma, M. Baltes, M. Mathieu, P.C. van de Ven, E.F. Vansant, Langmuir 18 (2002) 4420.

[203] I.V. Babitch, Plyuto, P. Van Der Voort, E.F. Vansant, Journal of Colloid Interface Science 189 (1997) 144.

[204] I.V. Babitch, Y.V. Plyuto, P. Van Der Voort, E.F. Vansant, Journal of Chemical Society, Faraday Transactions 93 (1997) 3191.

[205] R.G. Pearson, H.B. Gray, F. Basolo, Journal of the American Chemical Society 82 (1960) 787.

[206] F. Basolo, H.B. Gray, R.G. Pearson, Journal of the American Chemical Society 82 (1960) 4200.

[207] J.A.R.van Veen, G. Jonkers, W.H. Hesselink, Journal of Chemical Society, Faraday Transactions 85 (1989) 389.

[208] H.B. Gary, R.J. Olcott, Inorganic Chemistry 1 (1961) 481.

[209] P. Van Der Voort, M.B. Mitchell, E.F. Vansant, M.G. White, Interface Science 5 (1997) 169.

[210] R. Selke, M. Capka, Journal of Molecular Catalysis 63 (1990) 319.

[211] M. Mazzei, W. Marconi and M. Riocci, Journal of Molecular Catalysis 9 (1980) 381.

[212] Y. Traa, D. M. Murphy, R. D. Farley and G. J. Hutchings, Physical Chemistry Chemical Physics 3 (2001) 1073.

[213] S. Taylor, J. Gullick, P. McMorn, D. Bethell, P. C. Bullman Page, F. E. Hancock, F. King and G. J. Hutchings, Journal of Chemical Society, Perkin Transactions 2 (2001) 1714.

[214] P. Piaggio, P. McMorn, D. Murphy, D. Bethell, P. C. Bullman Page, F. E. Hancock, C. Sly, O. J. Kerton and G. J. Hutchings, Journal of Chemical Society, Perkin Transactions 2 (2000) 2008.

[215] S. Luo, J. Li, L. Zhang, H. Xu, J. Cheng, Chemistry - A European Journal 14 (2008) 1273.

[216] J. Lu, P. Serna, B.C. Gates, ACS Catalysis 1 (2011) 1549.

[217] A.J. Liang, R. Craciun, M. Chen, T.G. Kelly, P.W. Kletnieks, J.F. Haw, D.A. Dixon, B.C. Gates, Journal of the American Chemical Society 131 (2009) 8460.

[218] H.F.J. van't Blik, J.B.A.D. van Zon, T. Huizinga, J.C. Vis, D.C. Koningsberger, R.J. Prins, Journal of the American Chemical Society 107 (1985) 3139.

[219] S.E. Deutsch, J.-R. Chang, B.C. Gates, Langmuir 9 (1993) 1284.

[220] R. Selke, Journal of Molecular Catalysis 37 (1986) 227.

[221] P. Barbaro, Chemistry - A European Journal 12(2006) 5666.

[222] O. Wang, D. Sayers, M. Huang, C. Yuan, S. Wei, "EXAFS Studies of Mo-Y Zeolite Catalysts", Symposium on catalysis in fuel processing, San-Francisco, 1992.

[223] Y.Ji, A.M.J. van der Eerden, V. Koot, P.J. Kooyman, J.D. Meeldijk, B.M. Weckhuysen, D.C. Koningsberger, Journal of Catalysis 234 (2005) 376.

[224] M. Kawai, M. Uda, M. Ichikawa, Journal of Physical Chemistry 89 (1985) 1654.

[225] M.A. Baltanas, J.H. Onuferko, S.T. McMillan, J.R. Katzers, Journal of Physical Chemestry 91 (1987) 3772.

[226] Y. Okamoto, N. Ishida, T. Imanaka, S.J. Teranishi, Journal of Catalysis 58 (1979) 82.

[227] Y. Okamoto, N. Ishida, T. Imanaka, S. Teranishi, Journal of Catalysis 112 (1988) 427.

[228] J.Z. Shyu, E.T. Skopinski, J.G. Goodwin, A. Sayari, Applied Surface Science 21 (1985) 297.

[229] H.N. Flach, I. Grassert, G. Oehme, M. Capka, Colloid and Polymer Science 274 (1996), 261.

[230] G. Yuan, Y. Chen, R. Chen, Chinesse Journal of Polymer Science 7 (1989) 219.

[231] A. Michrowsak, K. Menneke, U. Kuntz, A. Kirschning, K. Grela, Journal of the American Chemical Society 128 (2006) 13261.

[232] P. Barbaro, C. Bianchini, G. Giambastiani, W. Oberhauser, L. Morassi Bonzi, F. Rossi, V. Dal Santo, Dalton Transactions (2004) 1783.

[233] R. Selke, Journal of Organometallic Chemistry 370 (1989), 241.

[234] A.M. Trzeciak, J.J. Ziolkowski, S. Aygen, R. Van Eldik, Journal of Molecular Catalysis 34 (1986) 337.

[235] S. Otto, A.J. Muller, Acta Crystallographica 57 (2001) 1405.

[236] W.L. Davis, A. Muller, Acta Crystallographica 68 (2012) 1563.

[237] M. Ooe, M. Murata, A. Takahama, T. Mizugaki, K. Ebitani, K. Kaneda, Chemistry Letters 32 (2003) 692.

[238] G. Gascon, M.C. Ortega, J.D. Suarez, A.J. Pardey, C. Longo, Reaction Kinetics Catalysis Letters 94 (2008) 85.

[239] C.-H. Cheng, D.E.Hendriksen, R. Eisenberg, Journal of the American Chemical Society 99 (1977) 2791.

[240] L. Dadci, H. Elias, U. Frey, A. Hornig, U. Koelle, A.E. Merbach, H. Paulust, J.S. Schneider, Inorganic Chemistry 34 (1995) 306.

[241] U. Kölle, R. Görissen, T. Wagner, Chemische Berichte 128 (1995) 911.

[242] S.F. Lincoln, D.T. Richens, A.G. Sykes, "Metal Aqua Ions" Comprehensive Coordination Chemistry II Volume 1, 515.

[243] P. Gelin, C. Naccache, Y. Ben Taarit, Pure & Applied Chemistry 60 (1988) 1315.

[244] G. Bergeret, P. Gallezot, P. Gelin, Y. Ben Taarit, F. Lefebvre, C. Naccache, R.D. Shannon, Journal of Chemistry 104 (1987) 279.

[245] A.K. Smith, F. Huguws, A. Theolier, J.-M. Basset, R. Ugo, G.M. Zanderighi, J.L. Bilhou, V. Bilhou-Bougnal, W.F. Graydon, Inorganic Chemistry 18 (1979) 3104.

[246] J.L. Robbins, Journal Physical Chemistry 90 (1986), 3381.

[247] E. Ivanova, K. Hadjiivanov, Physical Chemistry Chemical Physics 5 (2003) 655.

[248] K. Gora-Marek, Vibrational Spectroscopy 58 (2012) 104.

[249] S. Huber, H. Knozinger, Journal of Chemical Society, Faraday Transactions 94 (1998) 2047.

[250] S. Huber, H. Knozinger, Applied Catalysis A: General 181 (1999) 239.

[251] G.N. Vayssilov, M. Staufer, T. Belling, K.M. Neyman, H. Knozinger, N. Rosch, Journal of Physical Chemistry B 103 (1999) 7920.

[252] J. Scherzer, ACS Symposium Series 248 (1984) 157.

[253] R.D. Shannon, K.H. Gardner, R.H. Staley, G. Bergeret, P. Gallezot, A. Auroux, Journal of Physical Chemistry 89 (1985) 4778.

[254] M.J. Remy, D. Stanica, G. Poncelet, E.J.P. Feijen, P.J. Grobet, J.A. Martens, P.A. Jacobs, Journal of Physical Chemistry 100 (1996) 12440.

[255] J.A. van Bokhoven, A.L. Roest, D.C. Koningsberger, J.T. Miller, G.H. Nachtegaal, A.P.M. Kentgens, Journal of Physical Chemistry B 104 (2000) 6743.

[256] D.L. Bhering, A. Ramirez-Solis, C.J.A. Mota, Journal of Physical Chemistry B 107 (2003) 4342.

[257] J. Jiao, J. Kanellopoulos, W. Wang, S.S. Ray, H. Foerster, D. Freude, M. Hunger, Physical Chemistry Chemical Physics 7 (2005) 3221.

[258] D. de Groot, B. F. M. de Waal, J. N. H. Reek, A. P. H. J. Schenning, P. C. J. Kamer, E. W. Meijer, P. W. N. M. van Leeuwen, Journal of the American Chemical Society 123 (2001) 8453.

[259] G.J. Ray, A. Samoson, Zeolites 13 (1993) 410.

[260] A. Samoson, E. Lippmaa, G. Engelhardt, U. Lohse, H.G. Jerschkewitz, Chemical Physics Letters 88 (1985) 589.

[261] A. Zsigmond, S. Undrala, F. Notheisz, A. Szöllsy, J. Bakos, Applied Catalysis A: General 303 (2006) 29.

[262] F. Sette, J. Stöhr, E.B. Kollin, D.J. Dwyer, J.L. Gland, J.L. Robbins, A.L. Johnson, Physical Review Letters 54 (1985) 935.

[263] R.K. Hocking, T.W. Hambley, Organometallics 26 (2007) 2815.

[264] S.P. Khranenko, E.A. Bykova, A.V. Alexeyev, A.P. Tyutyunnik, S.A. Gromilov, Journal of Structural Chemistry 53 (2012) 521.

[265] R.S. Evans , E.A. Hopcus, J. Bordner, A.F. Schreiner, Journal of Crystal and Molecular Structure 3 (1973) 235.

[266] D.E. De Vos, M. Dams, B.F. Sels, P.A. Jacobs, Chemical Reviews 102 (2002) 3615.

[267] R. L. Augustine, S. K. Tanielyan, N. Mathata, Y. Gao, A. Zsigmond, H. Yang, Applied Catalysis A: General 256 (2003) 69.

[268] D.C Bailey, S.H. Langer, Chemical Reviews 81 (1981) 109.

[269] E. Gross, J. Hung-Chang Liu, F.D. Toste, G.A. Somorjai, Nature Chemistry 4 (2012) 947.

[270] D. Yardimci, P. Serna, B.C. Gates, ACS Catalysis 2 (2012) 2100.

[271] A. Salameh, A. Baudouin, J.-M. Basset, C. Coperet, Angewandte Chemie International Edition 47 (2008) 2117.

[272] P.W.N.M. Van Leeuwen, C.F. Roobeek, Journal of Organometallic Chemistry 258 (1983) 343.

[273] J. A. M. Brandts, P. H. Berben, Organic Process Research & Development 7 (2003) 393.

[274] M. Kranenburg, Y.E.M. van der Burgt, P.C.J. Kamer, P.W.N.M. van Leeuwen, K. Goubitz, J. Fraanje, Organometallics 14 (1995) 3081.

[275] J. Klosin, C.R. Landis, Accounts of Chemical Research 40 (2007) 1251.

[276] R.Augustine, S. Tanielyan, S. Anderson, H. Yang, Chemical Communications (1999) 1257.

[277] R.L. Augustine, P. Goel, N. Mahata, C. Reyes, S. K. Tanielyan, Journal of Molecular Catalysis A: Chemical 216 (2004) 189.

[278] C. Coperet, M. Chabanas, R. Petroff Saint-Arroman, J.-M. Basset, Angewandte Chemie International Edition 42 (2003) 156.

[279] C. McDonagh, P. O'Conghaile, R.J.M. Klein Gebbink, P. O'Leary, Tetrahedron Letters 48 (2007) 4387.

[280] K.G. Azzam, I.V. Babich, K. Seshan, L. Lefferts, Journal of Catalysis 25 (2007), 153.

[281] S. Liu, L. Wang, R. Ohnishi, M. Ichikawa, Journal of Catalysis 181 (1999) 175.

[282] J.F. Young, J.A. Osborne, H. Jardine, G. Wilkinson, Chemical Communication (1965) 131.

[283] K.G. Allum, R.D. Hancock, I.V. Howell, T.E. Lester, S. McKenzie, R.C. Pitkethly, P.J. Robinson, Journal of Organometallic Chemistry 107 (1976) 393.

[284] F. Sanches, M. Iglesias, A. Corma, C.J. del Pino, C. Journal of Molecular Catalalysis 70 (1991) 369.

[285] G. Strukul, M. Bonivento, M. Graziani, Inorganica Chimica Acta, 12 (1975) 15.

[286] P. Serna, B.C. Gates, Angewandte Chemie International Edition 123 (2011) 5642.

[287] P. Serna, B.C. Gates, Journal of Catalysis (2013) in press.

[288] A.D. Vityuk, O.S. Alexeev, M.D. Amiridis, Journal of Catalysis (2013) in press.

[289] F.E. Hancock, G.J. Hutchings, N.A. Caplan, Patent WO 03/018191 (2003).

[290] P. O'Leary, N.P. Krosveld, K.P. De Jong, G. van Koten, R.J.M. Klein Gebbink, Tetrahedron Letters 45 (2004) 3177.

[291] A. Crosman, W. F. Hölderich, Journal of Catalysis 232 (2005) 43.

[292] W. De Wilde, G. Peeters, J.H. Lunsford, Journal of Physical Chemistry 84 (1980) 2306 .

[293] P.P. Knops-Gerrits, C.A. Trujillo, B.Z. Zhan, X.Y. Li, P. Rouxhet, P.A. Jacobs Topics in Catalysis 3 (1996) 437.

[294] K.J.J. Balkus, A.K. Khanmamedova , K. Dixon, F. Bedioui, Applied Catalysis A: General 143 (1996) 159.

[295] A. Earnshaw, E.A. King, L.F. Larkworthy, Journal of Chemical Society A (1968) 1048.

[296] P.P. Knops-Gerrits, F. Thibault-Starzyk, P.A. Jacobs, Studies in Surface Science and Catalysis, 84 (1994) 1411.

[297] J. Lewis, F.E. Mabbs, H. Weigold, Journal of Chemical Society A (1968) 1699.

[298] J. Wöltinger, J.-E. Bäckvall, A. Zsigmond, Chemistry - A European Journal 5 (1999) 1460.

[299] C. Langham, P. Piaggio, D. Bethell, D.F. Lee, P. McMorn, P.C. Bulman Page, D.J. Willock, C. Sly, F.E. Hancock, F. King, G.J. Hutchings, Chemical Communications (1998) 1601.

[300] M. Tada, Y. Iwasawa, Journal of Molecular Catalysis A: Chemical, 204 (2003) 27.

[301] S.L. Scott, J.-M. Basset, G.P. Niccolai, C.C. Santini, J.-P. Candy, C. Lecuyer, F. Quignard, A. Choplin, New of Journal of Chemistry 18 (1994) 115.

[302] J. Guzman, B.C. Gates, B.C. Dalton Transactions (2003) 3303.

[303] A.D. Vityuk, O.S. Alexeev, M.D. Amiridis, Journal of Physical Chemistry C (2013) in press.

[304] E.A. Wovchko, J.T. Yates Jr., Journal of the American Chemical Society 117 (1995) 12557.

[305] B.R. James, G. L. Rempel, Discussion of the Faraday Society 46 (1968) 48.

[306] S.H. Straws, D. Shriver, Inorganic Chemistry 17 (1978) 3069.

[307] S. Muthukumaru Pillai, M. Ravindranathan, S. Sivaram, Chemical Reviews 86 (1986) 353.

[308] T. Yashima, Y. Ushida, M. Ebisawa, N. Hara, Journal of Catalysis 36 (1975) 320.

[309] S. Bodoardo, R. Chiappetta, F. Fajula, E. Garrone, Microporous Materials 3 (1995) 613.

[310] J.P. van den Berg, J.P. Wolthuizen, A.D.H. Clague, G.R. Hays, R. Huis, J.H.C. van Hooff, Journal of Catalysis 80 (1983) 130.

[311] C.T. O’Connor, M. Kojima, Catalysis Today 6 (1990) 329.

[312] Eric G. Derouane “Catalysts for Fine Chemical Synthesis Microporous and Mesoporous Solid Catalysts” John Wiley & Sons Ltd, 2006, 126.

[313] V.B. Kazansky, I.R. Subbotina, F.C. Jentoft, Journal of Catalysis 240 (2006) 60.

[314] A. Forestière, H. Olivier-Bourbigou, L. Saussine, Oil & Gas Science and Technology Reviews 64 (2009) 649.

[315] A.W. Al-Sa'doun, Applied Catalysis A: General 105 (1993) 1.

[316] K. Ziegler, H. Martin, U.S. Patent 2,943,125 (1960).

[317] R. Cramer, Journal of the American Chemical Society 87 (1965) 4717.

[318] C. Langham, S. Taylor, D. Bethell, P. McMorn, P.C. Bulman Page, D.J. Willock, C. Sly, F.E. Hancock, F. King, G.J. Hutchings, Journal of Chemical Society, Perkin Transactions 2 (1999) 1043.

[319] S. Taylor, J. Gullick, P. McMorn, D. Bethell, P.C. Bulman Page, F.E. Hancock, F. King, G.J. Hutchings, Journal of Chemical Society, Perkin Transactions 2 (2001) 1724.

[320] V. Parvulescu1, B.-L. Su, Catalysis Today 69 (2001) 315.

[321] K.J.J. Balkus, M. Eissa, R. Lavado, Studies in Surface Science and Catalysis 94 (1995) 713.

[322] B.G. Frederick, G. Apai, T.N. Rhodins, Journal of the American Chemical Society 109 (1987) 4797.

[323] S. Namuangruk, P. Pantu, J. Limtrakul, A European Journal of Physical Chemistry and Chemical Physics 6 (2005) 1333.

[324] K.J.J. Balkus, M. Eissa, R. Lavado, Chemical Industry 69 (1997) 363.

[325] Q.L. Wang, G. Giannetto, M. Guisnet, Journal of Catalysis 130 (1991) 471.

[326] C.J.A. Mota, R.L. Martins, L. Nogueira, W.B. Kover, Journal of Chemical Society, Faraday Transactions 90 (1994) 2297.

[327] S. Li, S.-J. Huang, W. Shen, H. Zhang, H. Fang, A. Zheng, S.-B. Liu, F. Deng, Journal of Physical Chemistry C 112 (2008) 14486.

[328] V. Bolis, J.C. Vedrine, Journal of Chemical Society, Faraday Transcactons 76 (1980) 1606.

[329] D.B. Leznoff, J. Lefebvre, Gold Bulletin 38/2 (2005) 47.

[330] C. Jobbagy, T. Tunyogi, G. Palinkas, A. Deak, Inorganic Chemistry 50 (2011) 7301.

[331] D.M. Pham, D. Rios, M.M. Olmstead, A.L. Balch, Inorganic Chimica Acta 358 (2005) 4261.

[332] A. Deak, T. Tunyogi, G. Palinkas, Journal of the American Chemical Society 131 (2009) 2815.

[333] B.M. Chadwick, S.G. Frankiss, Journal of Molecular Structure 31 (1976) 1.

[334] H.J. Llewellyn, Journal of Chemical Physics 27 (1957) 468.

[335] G. Ma, W. Yan T. Hu, J. Chen, C. Yan, H. Gao, J. Wu, G. Xua, Physical Chemistry Chemical Physics 1 (1999) 5215.

[336] A. Rosenzweig, D.T. Cromer, Acta Crystallographica 12 (1959) 709.

[337] K.J.J. Balkus, M. Eissa, R. Levado, Journal of the American Chemical Society 117 (1995) 10753.

[338] K.J.J. Balkus, A. Khanmamedova, M. Eissa, Studies in Surface Science and Catalysis 97 (1995) 189.

[339] R. Raja, P. Ratnasamy, Applied Catalysis A: General 143 (1996) 145.

[340] A. Adima, J.J.E. Moreau, M.W.C. Man, Chirality 12 (2000) 411.

[341] J.E. Kilpatrick, E.J. Prosen, K.S. Pitzer, F.E. Rossini, Journal of Research of the National Bureau of Standards 36 (1946) 559.

[342] P. Wu, M. Iwamoto, Journal of Chemical Society, Faraday Transactions, 94 (1998) 2871.

[343] A. Tuel, Zeolites, 15 (1995) 228.

[344] T. Blasco, A. Corma, M.T. Navarro, J. Perez-Pariente, Journal of Catalysis 156 (1995) 65.

[345] J. Evans, G.S. McNulty, Journal of Chemical Society Dalton Transactions (1984) 587.

[346] K.A. Koyana, T. Tatsumi, Journal of Chemical Society, Chemical Communications (1996) 145.

[347] U.S. EPA Tier 2 Standards and Limits on Gasoline Vehicles , Gateway website: http://www.dieselnet.com/standards/us/ld_t2.php; October 2013.

[348] European Union Motor vehicles with trailers: polluting emissions, Gateway website: http://europa.eu/scadplus/leg/en/lvb/l21047.htm; July 2007.

[349] K.C. Taylor, Catalysis Reviews: Science and Engineering 35 (1993) 457.

[350] M. Shelef, G.W. Graham, Catalysis Reviews: Science and Engineering 36 (1994) 433.

[351] D.N. Belton, K.C. Taylor, “Current Opinion in Solid State and Materials Science” 4 (1999) 97.

[352] A. Srinivasan, C. Depcik, Catalysis Reviews: Science and Engineering, 52 (2010) 462.

[353] A. Srinivasan, C. Depcik, Surface Review and Letters 19 (2012) 1230001.

[354] H. Hamada, M. Haneda, Applied Catalysis A: General 420-421 (2012) 1.

[355] W.C. Hecker, A.T. Bell, Journal of Catalysis 84 (1983) 200.

[356] V.P. Zhdanov, B. Kasemo, Surface Science Reports 29 (1997) 31.

[357] D.I. Kondarides, T. Chafik, X.E. Verykios, Journal of Catalysis 191 (2000) 147.

[358] A.J. Dent, J. Evans, S.G. Fiddy, B. Jyoti, M.A. Newton, M. Tromp, Angewandte Chemie International Edition 46 (2007) 5356.

[359] M.A. Newton, A.J. Dent, S.G. Fiddy, B. Jyoti, J. Evans, Journal of Materials Science 42 (2007) 3288.

[360] P. Araya, F. Gracia, J. Cortés, E.E. Wolf, Applied Catalysis B: Environmental 38 (2002) 77.

[361] V.P. Zhdanov, B. Kasemo, Catalysis Letters 81 (2002) 141.

[362] J. Cortés, P. Araya, P. Betancourt, F. Díaz, Journal of Chemical Research (2004) 68.

[363] S.H. Oh, C.C. Eickel, Journal of Catalysis 128 (1991) 526.

[364] G.S. Herman, C.H.F. Peden, S.J. Schmieg, D.N. Belton, Catalysis Letters 62 (1999) 131.

[365] C.H.F. Peden, D.N. Belton, S.J. Schmieg, Journal Catalysis 155 (1995) 204.

[366] J. Cortes, E. Valencia, Canadian Journal of Chemistry 87 (2009) 571.

[367] S.H. Oh, G.B. Fisher, J.E. Carpenter, D.W. Goodman, Journal of Catalysis 100 (1986) 360.

[368] “Supported Metal Complexes: A New Generation of Catalysts” edited by F. R. Hartley D. Reidel Publishing Company, (1985).

[369] J.M. Thomas, Proceedings of the Royal Society A 468 (2012) 1884.

[370] C.D. Meyer, R. Eisenberg, Journal of the American Chemical Society 98 (1976) 1364.

[371] T. Iizuka, J.H. Lunsford, Journal of Molecular Catalysis 8 (1980) 391.

[372] K.C. Cannon, S.K. Jo, J.M. White, Journal of the American Chemical Society 111 (1989) 5064.

[373] K.A. Almusaiteer, S.S.C. Chuang, C.-D. Tan Journal of Catalysis 189 (2000) 247.

[374] K.A. Almusaiteer, S.S.C. Chuang, Journal of Physical Chemistry B 104 (2000) 2265.

[375] H. Miessner, I. Burkhardt, D. Gutschick, A. Zecchina, C. Morterra, G. Spoto, Journal of Chemical Society, Faraday Transactions 86 (1990) 2321.

[376] F. Solymosi, T. Bansagi, E. Novak, Journal of Catalysis 112 (1988) 183.

[377] D.A. Buchanan, M.E. Hemandez, F. Solymosi, J.M. Whit, Journal of Catalysis 125 (1990) 456.

[378] E. Novak, D. Sprinceana, F. Solymosi, Applied Catalysis A 149 (1997) 89.